Wind turbine control and model predictive control for uncertain systems

Thomsen, Sven Creutz; Poulsen, Niels Kjølstad; Niemann, Hans Henrik

Publication date:
2010

Document Version
Publisher's PDF, also known as Version of record

Wind turbine control
&
model predictive control for uncertain systems

Sven Creutz Thomsen

Kongens Lyngby 2010
IMM-PHD-2010-229

Technical University of Denmark
Informatics and Mathematical Modelling
Building 321, DK-2800 Kongens Lyngby, Denmark
Phone +45 45253351, Fax +45 45882673
reception@imm.dtu.dk
www.imm.dtu.dk

IMM-PHD: ISSN 0909-3192

Summary

This thesis presents both an applied study and a theoretical study within the field of control theory. Control theory is an interdisciplinary branch between mathematics and engineering dealing with the manipulation of systems to produce a desired output.

The applied study deals with wind turbine control. Wind turbines are controlled to optimize energy extraction from the wind. This must be done while respecting physical restrictions and ensuring that loads on the wind turbine structure does not seriously reduce the lifetime of components. This poses a trade-off in the design and the wind turbine problem is hence a complex multivariable problem. In this thesis the main focus is on design of controllers which optimally attenuates the impact of the variability in the wind. The angles of the wind turbine blades have been used as the primary control variable to achieve this goal. Strategies have been studied in which the blades are controlled collectively and individually. The wind has both temporal and spatial variations with a stochastic nature. Furthermore, the wind has deterministic (or slowly varying) trends. Large parts of the thesis hence deals with developing wind models which can be used as disturbance models for controller design.

The theoretical study deals with Model Predictive Control (MPC). MPC is an optimal control method which is characterized by the use of a receding prediction horizon. MPC has risen in popularity due to its inherent ability to systematically account for time-domain constraints on signals. During the last decades several theoretical advances have been made, so that it can handle a wide variety of system structures. In this thesis, the focus is on handling uncertain linear system description. To this end the so-called Youla parameterizations have been

used. Two methods are proposed: The first method exploits the modularity of the parameterizations so that the uncertainty can be identified and the MPC controller can be reconfigured in a modular setting. The second method is a robust MPC method in which the Youla parameters are used as an integral part of the online optimization. In this way stability can be guaranteed given an assumed bound on the uncertainty.

The contributions of the thesis have been documented in a series of scientific papers. The papers form the main part of this thesis.

Resumé

Denne afhandling beskriver både et anvendt studie såvel som et teoretisk studie indenfor styringteori. Styringsteori er en krydsdeciplin mellem matematik og ingeniørvidenskab. Styringteori omhandler manipulering af systemer, således at de opfører sig på en ønsket måde.

Det anvendte studie omhandler vindmøllestyring. Vindmøller styres for at optimere energiudbyttet fra vinden. I optimeringen skal der tages hensyn til fysiske restriktioner og sikres at komponenternes livetid ikke nedsættes betydeligt som følge af overlast. Der skal derfor laves et kompromis i designet, hvilket gør vindmøllestyring til er et komplekst multivariabelt problem. Denne afhandling fokuserer primært på styringssmetoder der reducerer effekten af vindens variation. Til dette formål har den primære kontrolvariabel været vindmøllebladenes vinkel i forhold til vinden. I dette projekt er der blevet undersøgt metoder hvor vingernes vinkel er styret kollektivt såvel som individuelt. Vinden har både rumlige og tidsmæssige variationer af stokastisk natur. Derudover vil vinden udvise determiniske tendenser. En stor del af afhandlingen omhandler derfor udvikling vindmodeller der kan indarbejdes som forstyrrelsesmodeller i styringsdesign.

I det teoretiske studie har styringsmetoden Model Predictive Control (MPC) været omdrejningspunktet. MPC er en optimal styringsmetode som er karakteriseret ved anvendelsen af en vigende (receding) prediktionshorisont. MPC er steget i popularitet grundet den naturlige måde hvormed tidsdomænebegrænsninger kan inkluderes i designet. Indenfor de seneste årtier er det teoretiske grundlag for metoden blevet udvidet til at håndtere et stort spænd af systemstrukterer. I denne afhandling er der fokuseret på usikre lineære systembeskrivelser. De såkaldte Youla parameteriseringer har været benyttet til dette formål. Der foreslås to metoder: Den første metode benytter sig af parame-

teriseringernes modulariteten således at usikkerheder kan identificeres og MPC regulatoren opdateres på en modulær facon. Den anden metode er en robust MPC metode hvor parameteriseringerne er indarbejdet som en integreret del i selve MPC-optimeringen. På den måde kan stabilitet garanteres under givne antagelser på usikkerhedens størrelse.

Denne afhandlings bidrag er dokumentereret i en samling af videnskabelige artikler. Disse artikler udgør hoveddelen af afhandlingen.

Preface and acknowledgements

This thesis was prepared at the department for Informatics and Mathematical Modelling (DTU Informatik), the Technical University of Denmark (DTU) in partial fulfillment of the requirements for acquiring the PhD degree in engineering. The work was carried out in the period October 2006 - February 2010. The supervisors were Associate Professor Niels Kjølstad Poulsen (DTU Informatik) and Associate Professor Hans Henrik Niemann (DTU Elektro). The project was fully funded by a DTU scholarship.

I would like to thank my supervisors Niels Kjølstad Poulsen and Hans Henrik Niemann for advise and always being helpful. Tim Van Engelen and his group also deserve a thanks for a pleasant research stay at the Energy Research Center of the Netherlands (ECN).

I would like to thank my friends from the masters studies who likewise decided to pursue a PhD degree. Our numerous lunch meetings have always been a pleasure. A special thanks to Martin Birkelund Larsen for sharing my passion for control and for social company at conferences. I would also like to thank my fellow PhD colleagues at the Section for Mathematical Statistics for contributing to a dynamic and inspiring working environment. The research areas that fall within the section are diverse and control theory represents just a fraction. This has allowed me to gain insight into other interesting areas and has truly broadened my perspectives. I am positive that this will be beneficial to me in my future career.

Finally I would like to thank my wife Heidi for always being supportive when times where rough (well as rough as it gets in an academic environment). Also a heartfelt thanks for both marrying me and giving me a beautiful little son in the course of my PhD studies.

Lyngby, February 2010

Sven Creutz Thomsen

Papers included in the thesis

[A] Sven Creutz Thomsen, Niels Kjølstad Poulsen. A disturbance decoupling nonlinear control law for variable speed wind turbines. *In proceedings of IEEE Mediterranean conference on control and automation (Med'07)*, 2007, Athens, Greece. Published.

[B] Sven Creutz Thomsen, Hans Henrik Niemann, Niels Kjølstad Poulsen. Individual pitch control of wind turbines using local inflow measurements. *In proceedings of IFAC World Congress (IFAC'08)*, 2008, Seoul, Korea. Published.

[C] Sven Creutz Thomsen, Hans Henrik Niemann, Niels Kjølstad Poulsen. MPC for uncertain systems using the Youla parameterizations. *In proceedings of IEEE Conference on Decision and Control (CDC'08)*, 2008, Cancun, Mexico. Published.

[D] Sven Creutz Thomsen, Hans Henrik Niemann, Niels Kjølstad Poulsen. Stochastic wind turbine modeling for individual pitch control. *In proceedings of European Control Conference (ECC'09)*, 2009, Budapest, Hungary. Published.

[E] Sven Creutz Thomsen, Hans Henrik Niemann, Niels Kjølstad Poulsen. Attenuating wind turbine loads through model based individual pitch control. *In proceedings of Nordic Wind Power Conference (NWPC'09)*, 2009, Rønne, Denmark. Published.

[F] Sven Creutz Thomsen, Hans Henrik Niemann, Niels Kjølstad Poulsen. Robust stability in predictive control with soft constraints. *In proceedings of American Control Conference, ACC'10*, 2010, Baltimore, Maryland, USA. Published.

[G] Sven Creutz Thomsen, Hans Henrik Niemann, Niels Kjølstad Poulsen. Stochastic wind turbine control in multiblade coordinates. *In proceedings of American Control Conference, ACC'10*, 2010, Baltimore, Maryland, USA. Published.

[H] Sven Creutz Thomsen, Hans Henrik Niemann, Niels Kjølstad Poulsen. Robust stability in constrained predictive control through the Youla parameterizations. *International Journal on Control*, Taylor & Francis, 2010. Submitted.

[I] Sven Creutz Thomsen, Hans Henrik Niemann, Niels Kjølstad Poulsen. Pitch control in multiblade coordinates - A stochastic approach. *Wind Energy*, John Wiley & Sons, 2010. Submitted.

Contents

Papers

Chapter 1

Introduction

This thesis is divided into two main parts: (1) Wind turbine control and (2) Model predictive control (MPC) for uncertain systems. As presented in this thesis, the two subjects are unrelated.

The study on wind turbine control take various approaches. Common for all approaches is an integral incorporation of wind models in the controller design. By incorporating an internal model of the wind in a controller design it is possible to attenuate the effect of wind fluctuations. In this connection both collective pitch control and individual pitch control of the wind turbine blades are considered. Both nonlinear and linear control methods are used.

The study on MPC was commenced because of its potential use in connection with wind turbines. There are several reasons for applying MPC for wind turbine control. The main motivation is its inherent ability to systematically handle time-domain constraints on signals. Most practical problems are faced with such constraints. Examples in relation to wind turbines are limitations of pitch actuators and generator. Furthermore, MPC is an optimal control methodology which is probably more easily understood by practitioners than, e.g., $\mathcal{H}_2$ and $\mathcal{H}_\infty$ control, at least in its basic form. The study on MPC did, however, result in an interesting theoretical study rather than an applied study. The focus in the study has been on handling uncertain linear system descriptions. To this end the so-called Youla parameterizations were adopted as a tool. The proposed

MPC solutions have interesting properties and might prove to be useful for wind turbine control.

The thesis is a collection of papers written during the course of the PhD-study. The papers are attached as appendices and form the main content of this thesis. All details are to be found in these papers. The remaining part of the thesis is intended to give an overview of the subjects relevant to the contributions. Furthermore, the contributions are briefly reviewed and discussed. As the papers were written over a period of approximately three years, it is stressed that there is not necessarily consistency in notation across the different papers.

1.1 Contributions

The contributions and brief descriptions are listed in the following. The wind turbine contributions are the following:

- Development of a disturbance decoupling control law for variable speed pitch regulated wind turbines (Paper A). The control law is based on feedback linearization theory and includes an internal model of the wind in order to attenuate (ideally decouple) wind fluctuations.
- Development of a framework for using measurements of local inflow in an optimal control setup (Paper B). The wind measurements from one blade are used to estimate the wind to be experienced by the other blades.
- Derivation of a stochastic wind model which can be incorporated as an internal model for individual pitch control (Paper D). The model describes the effect of rotational sampling.
- Derivation of a stochastic wind model in multiblade coordinates which can be included as an internal model for individual pitch control in multiblade coordinates (cyclic pitch control) (Papers E, G, I). The model describes the effect of rotational sampling in multiblade coordinates.

With respect to model predictive control the contributions are the following:

- A framework for reconfiguring the MPC controller when model and prestabilizing controller is updated (Paper C). The primary and dual Youla parameter are utilized for this purpose, which leads to a modular framework.

- Development of an MPC algorithm with guaranteed stability facing models with norm bounded uncertainties (Papers F, H). The optimization problem is parameterized as a closed loop optimization problem in terms of the Youla parameter and the uncertain system description is cast in terms of the dual Youla parameter. Soft constraints are handled with the method and special situations with hard constraints.

1.2 Outline

Chapter 2 is dedicated to wind turbine control. The chapter introduces wind turbines in general and the specific type considered in this thesis. The purpose of wind turbine controllers is explained and the model elements used for controller design is described. The contributions are reviewed and discussed. Potential future research topics are proposed.

Chapter 3 is dedicated to the study on MPC. The chapter reviews the basics of MPC and the Youla parameterizations. The contributions of the thesis are reviewed and discussed. Potential future research topics are listed.

Appendices A-I are reserved for the paper contributions. The papers are inserted into the thesis in chronological order.

Chapter 2

Wind turbine control

A wind turbine is a rotating machine which converts kinetic energy of wind into mechanical energy. The name *wind turbine* implies that the mechanical energy is converted to electricity. Another common name is wind energy converter (WEC). If the mechanical energy is directly used by machinery, one would usually call it a wind mill. Whereas wind mills have been used for the last 3000 years, wind turbines date back to the late 19th century. During the period 1930-1970 a lot of advances were made both theoretically and practically. However, large scale electricity generation saw its coming with the oil crisis in the 1970s [11]. Since then wind turbines have evolved into a mature technology and the focus on wind energy and renewable energy in general is higher that ever.

Wind turbines use rotors fitted with aerodynamic blades to extract energy from the wind. The rotor rotates about either a horizontal or vertical axis - Horizontal Axis Wind Turbines (HAWT) and Vertical Axis Wind Turbines (VAWT) respectively. They both have advantages and disadvantages which favors one over the other. However, the most common type is the HAWT. A sketch of the HAWT can be seen in Fig. 2.1. It is assumed throughout this thesis that the HAWT has three blades. It consists of a vertical tower. On the tower top is a nacelle which houses a electric generator which is connected to the three bladed rotor.

Fig. 2.2 shows a sketch of a nacelle. The generator is connected to the rotor by

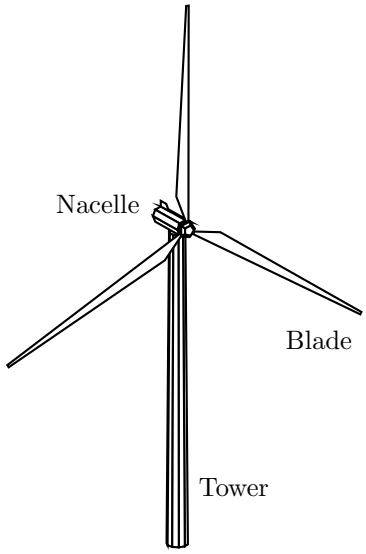

Figure 2.1: Sketch of an upwind HAWT

a shaft. Most wind turbines have a transmission which converts slow rotation of the rotor into high speed rotation.

If the wind turbine faces into the wind with the rotor in front of the nacelle the HAWT is referred to as an up-wind turbine. If it is facing in the opposite direction it is called a down-wind HAWT. The main advantage of an up-wind HAWT is the fact that it avoids the turbulence created by the tower. With

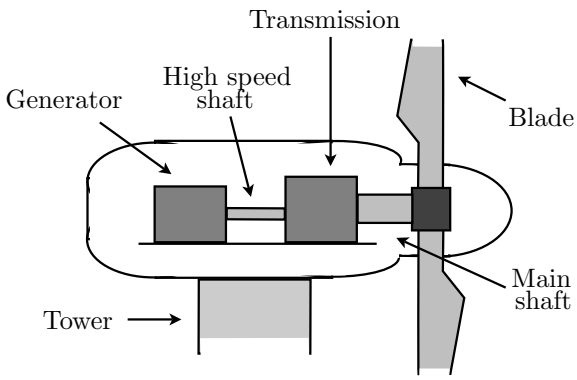

Figure 2.2: Sketch of the nacelle internals

down-wind turbines one need not worry about blades colliding with the tower.

The up-wind HAWT is the most common wind turbine structure and is the type considered in this thesis. When referring to *wind turbines* in the following, it will be an implicit reference to up-wind HAWTs.

The wind turbine contributions of this thesis are all related to wind turbine control. More specifically, controlling the pitch of the blades has been the main focus. Integral in all contributions is the incorporation of a suitable wind model such that the controller can anticipate the evolution of the wind.

A brief introduction to wind turbine control is given in Sec. 2.1. In Sec. 2.2-2.4 it is explained how the wind turbine and wind have been modeled. The contributions of the thesis are reviewed in Sec. 2.5 and discussed in Sec. 2.6. Some ideas for future developments are sketched in Sec. 2.7.

2.1 Wind turbine control

The basic purpose of a wind turbine is to extract energy from the wind. The main objective of a wind turbine controller is therefore to optimize the power extraction and to ensure that this is done safely without damaging the wind turbine. To optimize power extraction the rotor axis should naturally be oriented such that it is alligned with the wind. On small wind turbines this can be done passively if the turbine is fitted with a wind vane. On modern large wind turbines the orientation relatively to the wind (the yaw error) is controlled using servo motors based on measurements of wind direction. Yaw control is not considered in this work and in the following it is assumed that the wind turbine points into the wind.

The power extracted from wind is given by the following nonlinear function:

$$P_e = \frac{1}{2}\rho A_r {v^e}^3 C_P \tag{2.1}$$

ρ is the density of air, A_r is the rotor area, v^e is the effective wind speed and C_P is the performance coefficient of the rotor. C_P depends on the wind speed v^e, rotational speed ω_r of the rotor and the collective blade pitch angle β. On modern wind turbines the pitch of the blades can be controlled, furthermore, in case of variable speed generator, it is possible to control the rotational speed by changing the generator torque T_g (variable speed control). From a control perspective β and T_g represent the control variables and v^e is an external disturbance.

A wind turbine is designed to operate in a certain range of wind speeds. Due to limitations in generator/power-electronics, maximum energy can only be extracted up until the so-called rated wind speed v_0. Wind turbine operation is roughly divided into two regions: *Partial load* operation - below rated wind speed. *Full load* operation - above rated wind speed. This is illustrated in Fig. 2.3.

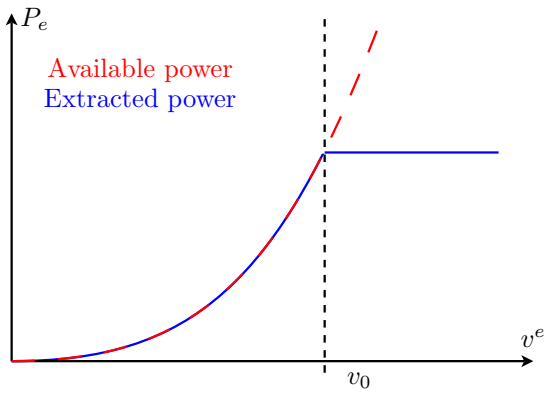

Figure 2.3: The total power available in the wind can only be extracted fully below the rated wind speed v_0

To maximize the power in the partial load region, the optimal value of the performance coefficient C_P must be tracked. At wind speeds below rated the optimal C_P is usually attained for an almost constant pitch angle. For this reason, the pitch is rarely used below rated. The generator torque T_g that leads to optimal C_p is however highly dependent on the wind speed. Consequently, T_g is the primary control variable below rated.

In full load operation, the limitations in the generator/power-electronics must be respected. The extracted power should therefore be restricted at the rated value. The usual approach is to keep the rotational speed constant and the torque constant at rated values. Pitch control provides a very effective means of adjusting the aerodynamic efficiency of the blades. Consequently, the collective blade pitch is the primary control variable for keeping the rotational speed constant. If the pitch controller is able to maintain an almost constant speed, it can be sufficient to have a constant generator torque. In general it is advantageous to control the torque as well to further optimize the produced power.

The discussion above only provides a rough sketch of the wind turbine control problem with focus restricted to that of power production. Naturally, the control problem is more colorful and complex. Additional constraints usually divide the partial-load region into further sub-regions. Furthermore, the controller should

be designed to alleviate loads on the wind turbine structure. Usual objectives are to dampen drive train torsional vibrations and tower vibrations. These objectives can be fulfilled by controlling the pitch of the blades collectively and additionally controlling the torque of the generator. The reader is referred to the following surveys for additional details [6, 37].

In this work, the focus has been on pitch control. For this reason, only the full-load region has been considered. Controlling the pitch of the blades is usually done collectively as assumed in the discussion above. Collective pitch control is a rather mature way of controlling the pitch and is widely used in practice. Researches have bben studying many different methodologies e.g. PID control [72], $\mathcal{H}_2$ and $\mathcal{H}_\infty$ [18], Model predictive control [22], linear parameter varying control [85] and nonlinear methods, such as feedback linearization [35, 68].

Due to the spatial variations in the wind field, there will be asymmetric forces at the support of the blades. It is possible to compensate for these forces by controlling the pitch of the blades individually. Individual pitch control has been given a lot of focus in recent years. Research has mainly been directed toward the framework for doing individual pitch control rather than the actual control methodology. The frameworks are usually divided into two categories: Individual pitch control [34, 62] and cyclic pitch control [7, 8, 9, 27, 57, 71]. Cyclic pitch control is characterized by the use of the so-called multiblade transformation (see Sec. 2.4).

Integral for all controllers studied in this thesis is the incorporation of a suitable wind model in the design model. If the wind model captures the structure of the wind variations, the controller can anticipate variations in the wind. Collective pitch control as well as individual pitch control have been considered. Variable speed control has also been included in some designs but has not been given special attention.

2.2 Wind turbine modeling

The wind turbine (HAWT) represents very mature technology and the basic blueprint is more or less the same for all wind turbines. It consists of tower, nacelle, and a rotor fitted with aerodynamic blades. Consequently, the mathematical models of a wind turbines will contain more or less the same elements. What will deviate are the underlying modeling principles, choice of coordinates and the complexity of the model. For example modeling flexible bodies such as blades and tower can be done with arbitrary precision, using different modeling principles and choice of coordinates.

Models of wind turbines vary in complexity depending on the use of the models. In connection with controller design one is usually not interested in detailed high order models but rather simplified models capturing the primary modes which are to be controlled. When tuning a controller for a highly detailed model, it is likely to be sensitive to modeling errors. The models used throughout this thesis are simplified models compared to the complex aeroelastic codes used for, e.g., load calculations.

The models derived in the project include dynamic descriptions of the following: Tower bending, blade bending, drive-train rotational dynamics, actuators, generator and aerodynamics. It should be noted that blade bending is not included in any of the papers associated with this thesis but is covered here for completeness. In the following, the different elements will be reviewed briefly.

2.2.1 Rotational dynamics of the drive-train

The drive-train is the combined system of generator, drive-shafts, transmission, and rotor. A schematic of the drive-train is shown in Fig. 2.4. The leftmost rotating body represents the combined inertia of all components on the rotor side of the transmission The rightmost rotating body represents the combined inertia of all components on the generator side of the transmission. The discs in the middle represent the transmission. Flexibility of the main shaft has been modeled with an equivalent spring and a damper. The drive-train system is excited by an aerodynamic torque acting on the main shaft and a generator torque on the high speed shaft. The mathematical model is a second order mass-spring-damper system. The model is quite standard and is proposed in more or less the same form in various publications e.g. [12, 38, 77].

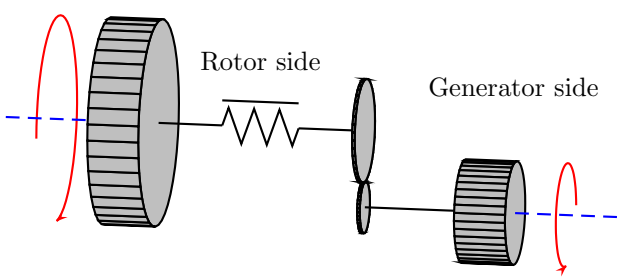

Figure 2.4: Schematic of the rotating sub-systems

2.2.2 Tower and blade bending

In the project the dynamics of blade and tower bending has been modeled as the transverse deflections of Euler-Bernoulli beams. The partial differential equation (PDE) which governs the dynamics of an Euler-Bernoulli beam is:

$$-\frac{\partial^2}{\partial x^2}\left(EI(x)\frac{\partial^2 y(x,t)}{\partial x^2}\right) + f(x,t) = m(x)\frac{\partial^2 y(x,t)}{\partial t^2} \quad , \quad 0 < x < L \tag{2.2}$$

$y(x,t)$ is the transverse deflection of the beam (at position x at time t). $f(x,t)$ is the transverse force per unit length. $m(x)$ is the mass per unit length and $EI(x)$ is the flexural rigidity. For a particular solution of (2.2) it is necessary to have two boundary conditions at each end. The boundary conditions can be derived from the following physical properties: Displacement, slope, bending, and shearing force.

A simple beam model of a blade is a clambed-free Euler-Bernoulli beam for which the boundary conditions are straight forward. A simple model of the tower is likewise a clambed-free beam but with a lumbed mass (nacelle etc.) at the free end. The boundary conditions at the free end will have a dynamic dependency on the lumbed mass. For a thorough study of the associated PDEs the reader is referred to [46, 76].

The solution to the beam equation can be found by solving the differential eigenvalue problem. However, in general the solution to (2.2) cannot be found analytically. The Rayleigh-Ritz method has been used in the project to approximate the solution. The Rayleigh-Ritz method is a variational approach to solving the differential eigenvalue problem. The n-th order approximate solution will be given by a finite sum

$$y^{(n)}(x,t) = \sum_{k=0}^{n} X_k(x) q_k(t) \tag{2.3}$$

where $X_k(x)$ is the approximate eigenfunction (shape function) of the k-th eigenmode. $q_k(t)$ is the k-th generalized coordinate. The evolution of each generalized coordinate is dictated by a linear second order ordinary differential equation (ODE). The ODEs are excited by the force $f(x,t)$ projected onto the corresponding shape functions. Since the beam dynamics is approximated by ODEs, the dynamics is easy to simulate and incorporate in a controller design.

The fundamental shape functions for a particular blade in edgewise (1. fundamental) and flapwise (1. & 2. fundamental) direction are shown in Fig. 2.5. Subscript f denotes flapwise direction and e denotes edgewise direction. The natural frequencies ω of the associated ODEs are also shown in the plot. For

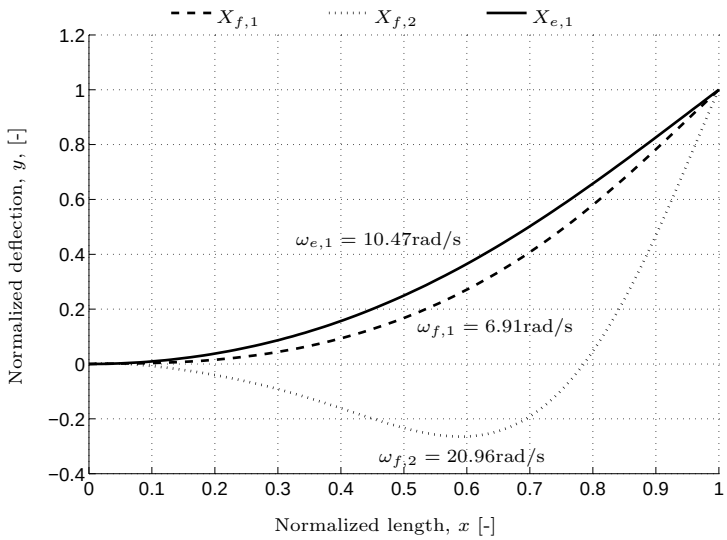

Figure 2.5: Fundamental shape functions for blade deflection in flapwise and edgewise direction.

a description of the Rayleigh-Ritz method and other approximate methods the reader is referred to [46, 76].

Similar modeling principles (although more complex) are used in, e.g., the wind turbine code FAST [26] developed by the National Renewable Energy Laboratory (NREL) in Colorado, USA.

2.2.3 Aerodynamics

To model the aerodynamics of a wind turbine one could use the simple non-linear expression in equation (2.1). This is a common approach for designing controllers. The coefficient C_p in equation (2.1) captures the aerodynamic properties of the wind turbine. C_p can be calculated, from the aerodynamic properties of the blades using blade element momentum (BEM) theory [21]. However, with C_p the wind field is only described by the effective wind speed v^e, which represents a spatial average of the whole wind field. The spatial distribution of the wind is naturally of interest in individual pitch control and when simulating a wind turbine in general. For this reason the BEM theory has been considered explicitly when modeling the aerodynamics.

BEM theory is a mixture of blade element theory and momentum theory. Blade element theory consists of breaking down the wind into small elements and determining the local forces. These forces are then integrated to obtain the total force acting on the blade. The local forces depend on the wind incident to the blade elements, however, the velocity of the incident wind will be perturbed by the rotating blades them self. Effectively, the velocity of the incident wind is decelerated and the wake of the turbine will begin to rotate (see Fig. 2.6). Momentum theory provides the additional relationships required to describe the induced velocities. The induction factors which determine the induced velocities can be calculated through an iterative algorithm [21].

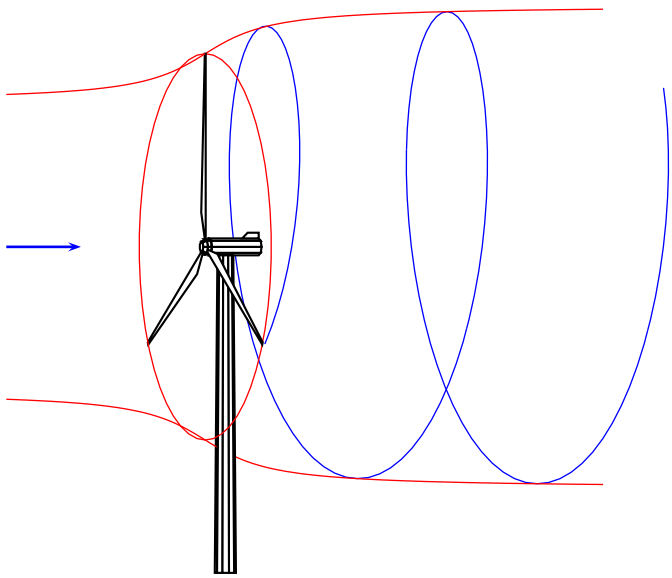

Figure 2.6: Perturbation of wind field due to wind turbine

Unsteady effects such as dynamic wake and dynamic stall [11, 21] have not been considered in this work. Consequently, the aerodynamic description is ideally represented as an algebraic (static) function. Since it is determined numerically, it will be in the form of a look-up table.

2.2.4 Pitch actuators and generator

Pitch actuators are usually complex nonlinear systems. For simplicity it has been assumed that low level loops compensate for these nonlinearities. The

actuators have simply been modeled as first order systems with appropriate time constants.

Likewise the generator model abstracts from the inner workings of the converters etc. The power produced by the generator is ideally the product of the rotational speed (high-speed shaft) and the generator torque. It is assumed that the generator torque can be controlled. A first order system relates the control demand to the actual torque.

2.2.5 Interconnection of model elements

Combining all the model elements described so far is a challenge as they consist of both rigid and flexible bodies - some in a fixed frame of reference and some in a rotating frame of reference. A systematic method for deriving the dynamic equations for the consequent multibody system is to use Lagrangian mechanics [58]. In essence, one has to set up the Lagrange equation

$$\frac{d}{dt}\left(\frac{\partial \mathcal{L}}{\partial \dot{q}_i}\right) - \frac{\partial \mathcal{L}}{\partial q_i} = Q_{i,nc} \tag{2.4}$$

where the Lagrangian $\mathcal{L}$ is the difference between the kinetic and potential energy of the total system. q_i is the i-th generalized coordinate and $Q_{i,nc}$ represents the associated non-conservative forces (e.g. external forces and forces due to damping). The generalized coordinates (degrees of freedom) q_i are assumed to be independent. If this is not the case, a solution is to include Lagrange multipliers in the equation.

2.3 Wind modeling

The wind is highly variable both temporally and spatially. The variability can be described on a wide range of scales both in time and space. In connection with wind turbine control it is sufficient to consider the temporal variability that is described on a relatively short time scale (well below 10 minutes). Wind described in this scale is referred to as the turbulent wind. Wind on a larger time scale is, e.g., considered in a supervisory controller. The main contributors to the turbulent wind is the friction with the surface and the temperature variations [11].

Two popular methods for simulating turbulence are the Sandia (Veers) method [73] and the Mann method [41]. In both methods it is assumed that time

series can be interpreted as 'space series'. The result is a tube of point wind speeds. This tube can then be propagated through the wind turbine rotor when simulating.

Both methods are very useful for detailed simulations. However, for control purposes it is not necessary to have a model which describes the entire wind field. It is advantageous to have a relatively simple wind model that adequately describes the impact of the wind on the variables of interest. When doing collective pitch control it is only of interest to know how the wind excites the rotor as a whole. Hence, a single scalar is often sufficient for describing the impact of the wind. This scalar is the previously mentioned effective wind speed v^e. This is illustrated in Fig. 2.7. The effective wind speed should capture the combined effect of the wind field and can be seen as a spatial average of the true wind field. As mentioned previously, it has been the main focus to integrate the wind model as a disturbance model in controller designs. The model hence needs to be on a differential (or difference) equation form. Several models have been used in literature to describe the effective wind, see, e.g., [12, 36, 77]). In general, the models are represented as low-pass filtered white noise.

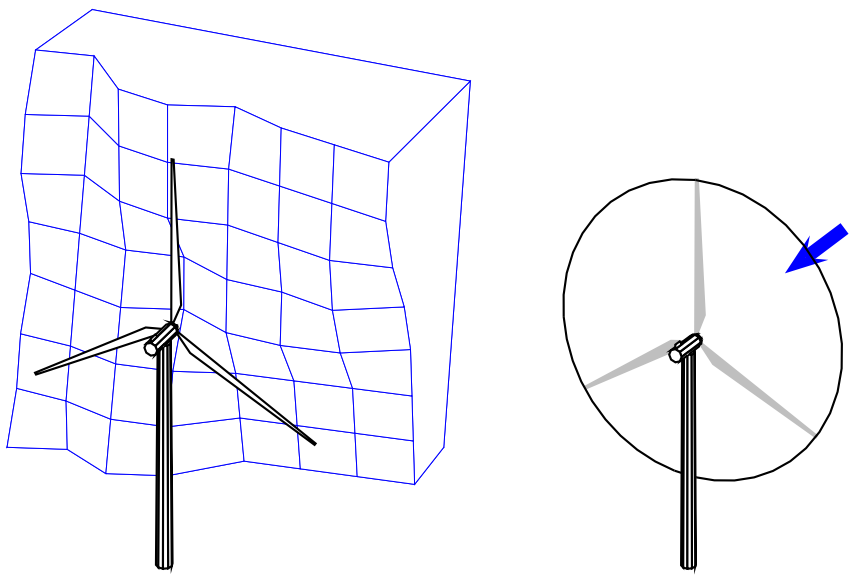

(a) Illustration of the true wind field

(b) Wind field abstraction for control - the effective wind speed

Figure 2.7: Illustration of a true wind field versus the effective wind speed

In the case of individual pitch control, the effective wind model is not sufficient

as it contains no information about the spatial properties of the wind. To induce the spatial knowledge one can consider an effective wind speed for each blade - The *blade* effective wind speed. Modeling the spectral properties of the blade effective wind speed is considered in [60] with application to load analysis. A contribution of this thesis is an extension of this model for integration in controller design.

2.4 Multiblade transformation of model

The dynamics of all blade variables (pitch, blade deflection, etc.) is usually derived in the rotating frame of the blade. The wind turbine model will consequently consist of interacting dynamics in rotating and non-rotating frames. This gives rise to an azimuth dependency in the model equations. For a linearized wind turbine model rotating at constant speed, the model will be described by time-periodic linear system. The symmetric nature of the rotor can however be exploited so that the time-periodic linear model is transformed to an equivalent time-invariant linear model. This is done by transforming all variables in rotating frame to so-called multiblade (Coleman) coordinates [14, 20, 25]. The multiblade coordinate basis is a clever representation of the blade variables in the non-rotating frame of the blade support. When the wind turbine does not rotate at a constant speed, the multiblade transformation will only attenuate the azimuth dependency.

Fig. 2.8 illustrates the multiblade coordinates in the case of edgewise blade bending. The first coordinate represents a symmetric bending of all blades. The second and third coordinate represent the projection of blade bending in the vertical and horizontal direction respectively.

The multiblade transformation has been utilized , e.g., in connection with sta-

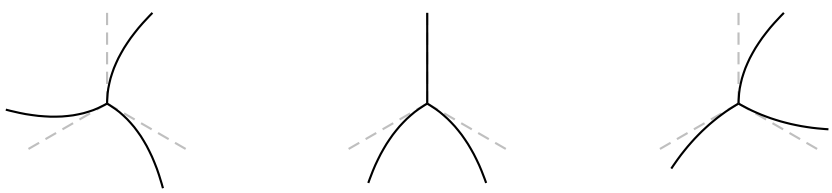

(a) Symmetric (b) 1. asymmetric (c) 2. asymmetric

Figure 2.8: Multiblade representation of edgewise blade bending

bility analysis of wind turbines in [20]. The transformation is also used for deriving time-invariant models for controller design and verification in the wind turbine code TURBU developed at the Energy Research Center of the Netherlands (ECN) [72]. This is also an approach which has been taken in this thesis.

Besides transforming the wind turbine dynamics, it is also necessary to transform the disturbances acting on the rotating blades. The wind therefore needs to be described in multiblade coordinates as well. A contribution of this thesis is the derivation of such a description.

2.5 Review of contributions

In all contributions the wind model plays a central role. Knowledge of the wind has been exploited in order to effectively attenuate fluctuations due to wind variations. The contributions are in relation to collective pitch control, individual pitch control and cyclic pitch control. The reviews in this section are divided into categories accordingly.

In the papers no distinction is made between individual pitch control and cyclic pitch control. The distinction is made here for convenience.

2.5.1 Collective pitch control

In paper A, the nonlinear control method Feedback Linearization ([24, 28, 59]) is utilized for setting up a disturbance decoupling collective pitch controller. The idea is to (ideally) decouple the wind fluctuations from the wind turbine dynamics by incorporating a stochastic model of the wind in the controller design.

The disturbance decoupling properties of feedback linearization will be explained in the following. Let the system be described by the following nonlinear state space system:

$$\dot{x} = f(x) + G(x)u + D(x)e \tag{2.5}$$

where x is the system state, u is the control input and e is the disturbance. Suppose that a diffeomorphic transformation $z = T(x)$ exists which brings the system (2.5) to the following form:

$$\dot{z}_1 = \phi(z) + \kappa(z)e \tag{2.6}$$

$$\dot{z}_2 = Az_2 + B(f_z(z) + G_z(z)u) \tag{2.7}$$

then the sub-dynamics (2.7) can be rendered linear, by choosing the control $G_z^{-1}(z)(-f_z(z)+\nu)$.

$$\dot{z}_2 = Az_2 + B\nu \tag{2.8}$$

The auxiliary signal ν is the control signal for the feedback linearized system. Since the dynamics is rendered linear, any linear control method and analysis method can be deployed for the feedback linearized system. The sub-dynamics (2.6) is denoted internal dynamics and is decoupled from the feedback linearized dynamics (2.8).

In paper A the effective wind is modeled as a linear system excited by a white noise process. It is shown in the paper that it is possible to transform an augmented system description (wind turbine and wind) to the form (2.6)-(2.7). The sub-dynamics (2.6) is in this case the wind model and (2.7) is a transformed representation of the wind turbine dynamics. The transformed model can then be feedback linearized to take the linear form (2.8) which is decoupled from the wind model.

The disturbance decoupling capabilities of feedback linearization are only valid given a perfect model and perfect state knowledge. Naturally, this is not the case for the augmented model. First of all, the wind model is an abstraction. Secondly, the states of the physical model are not necessarily available as measurements and if so, these measurements are likely noisy. A state estimator is therefore needed in the setup. The structure of the proposed controller is shown in Fig. 2.9. The design model consists of the wind turbine model aug-

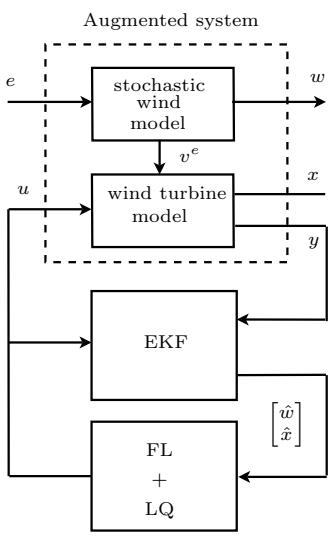

Symbol	Explanation
e	white noise
w	states of stoc. wind model
v^e	effective wind
x	states of turbine model
y	measurements
$\begin{bmatrix}\hat{w}\\ \hat{x}\end{bmatrix}$	state estimates
u	control input

Figure 2.9: Proposed nonlinear control set-up

mented with a model of the effective wind speed. The controller consists of an Extended Kalman Filter (EKF) for estimating the states and the feedback linearizing controller (FL). The FL controller uses a linear quadratic controller (LQ) for controlling the feedback linearized dynamics.

Simulations show that the controller succeeds in heavily attenuating the impact of the wind variations. In comparison with an LQ controller applied directly to the nonlinear system, a clear improvement is seen.

2.5.2 Individual pitch control

Paper B and D describe methods for modeling and incorporating the wind in an individual pitch control design. Integral in both papers is the notion of *blade effective wind speed*, however, different approaches are taken in modeling the wind. The blade effective wind speed is a generalization of the effective wind speed as it pertains to a specific blade rather than the entire rotor. In the same lines it represents a spatial average of the true wind along the span of the blade. This is illustrated in Fig. 2.10. Having a wind disturbance for each blade makes it possible to model how the wind affects the root moment of the individual blades. The root moments give rise to yaw and tilt moments at the support of the blades. The main purpose of an individual pitch controller is to minimize the asymmetric loads represented by these forces. However, it is not straightforward to target the yaw and tilt moment directly, as they have a nonlinear relation to the root moments. Instead it is proposed in paper B to target the root moment difference between the blades. If the difference is minimized so will the yaw and tilt moments be.

The approach in paper B is to use wind measurements made by sensors on an advancing blade as estimates of the wind to be observed by a trailing blade. Fig. 2.11 illustrates the idea. As examplified in the figure, the estimated wind to be

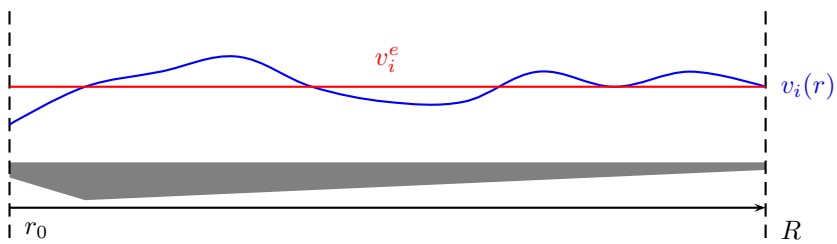

Figure 2.10: Illustration of blade effective wind speed. $v_i(r)$ is the true wind distribution along blade i. v_i^e is the corresponding blade effective wind speed.

experienced by blade 1 at time $t+1$ is the wind measured by blade 2 at time $t-3$. The wind model is hence quite trivial and merely represents the inherent time delays in the model. Simulations with an LQ controller incorporating this model indicates that the wind/disturbance model is capable of capturing the slowly varying components in the wind.

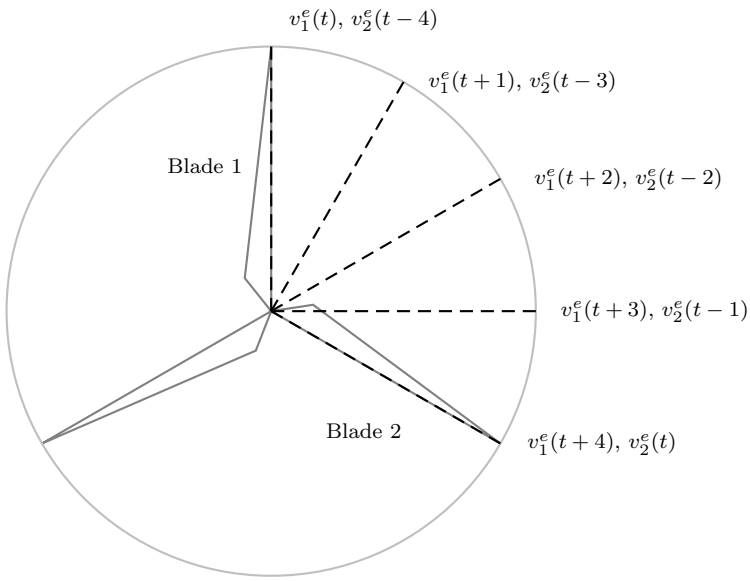

Figure 2.11: The blades enter the same spatial regions. Wind measured by an advancing blade can hence be used as an estimate for winds to be experienced by a trailing blade.

The approach in paper D has a stronger theoretical foundation. In this paper, the spectral description of the blade effective wind speed is derived based on the work in [60].

The spectral description is based on the spectral description of the point wind and the cross-spectral description between two point winds. In the derivation the rotational nature of the system is exploited. The blades will repeatedly sample the wind field (the field of point winds) as they sweep the rotor disc. Since the point winds are both correlated in space and time, the wind experienced by the blade at one sweep will be correlated with the wind experienced by the blade at preceding and subsequent sweeps. This gives rise to an interesting structure in the spectral description of the blade effective wind speed. As illustrated in Fig. 2.12 the spectral description will be dense near frequencies that are integer multiples of the rotational speed ω_r. Briefly explained, the point wind spectrum is expanded into a sum of harmonic spectra. Each bell seen in Fig.

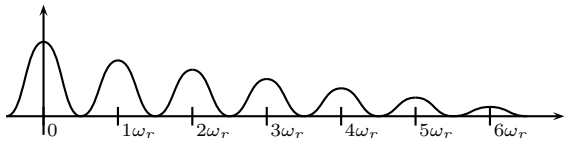

Figure 2.12: Auto spectral density of blade effective wind speed

2.12 represents a filtered harmonic. The filtering is caused by a spatial averaging effect owing to the definition of the effective wind speed. The frequency shift of the harmonics is a modulation effect which is due to the rotational sampling of the wind.

For controller design a stochastic linear system is realized with spectral properties approximating those of the wind. The stochastic system can be incorporated in a controller design as a disturbance model. Simulations with an $\mathcal{H}_2$ controller incorporating the mode in paper D illustrate the advantage of using the disturbance model.

2.5.3 Cyclic pitch control

In paper B and D, the dynamics of the rotating system and wind is described in the rotating frame of reference of the blade. In paper E,G and I, the blade effective wind description is transformed to the support frame of reference. This is done through the multiblade transformation. Having the wind model in multiblade coordinates makes it possible to include it as a disturbance model in a cyclic pitch controller design.

The advantage of controlling the turbine in multiblade coordinates is that the azimuth dependency in the model will be (nearly) cancelled. Another advantage is that the yaw and tilt moments are the multiblade equivalents of the blade root moments. Attenuating the yaw and tilt moment hence becomes a natural objective in multiblade coordinates.

The contribution of papers E,G and I is mainly the derivation of a stochastic wind model in multiblade coordinates. The wind model is a direct extension of the wind model in D. In rotating coordinates, the wind is represented by a blade effective wind speed for each blade. In multiblade coordinates there is a symmetric wind component and two asymmetric wind components. The consequent spectral description takes the form illustrated in Fig. 2.13. The spectral description of the symmetric and the asymmetric components have equivalent structures. The spectral contents is concentrated at frequencies that are integer

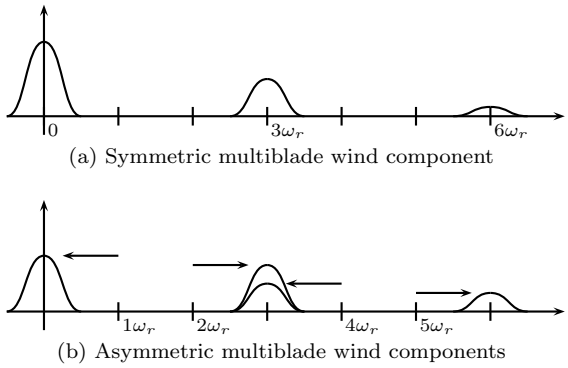

(a) Symmetric multiblade wind component

(b) Asymmetric multiblade wind components

Figure 2.13: The spectral description of the wind in multiblade coordinates

multiples of $3\omega_r$. Each component consists of a subset of the harmonics of the blade effective wind speed. However, the symmetric component does not share harmonic contents with the asymmetric components.

As for the stochastic model in paper D, the spectral properties are captured by a linear stochastic system which can be incorporated in a controller design. Simulations with $\mathcal{H}_2$ controllers show that it is easy to tune the controller to meet the desired objectives in multiblade coordinates.

Paper E and G are reduced versions of paper I. The reader is hence referred to the latter for all details.

2.6 Discussion

The disturbance decoupling method described in paper A has interesting properties but is not immediately applicable in practice. The reason is partly the rigidity of the method. Feedback linearization is a geometric control method and applicability of the method is highly dependent on the model structure. It is therefore difficult to consider more advanced wind turbine models than the one used in the paper. When simulating with more advanced models it was observed that the theoretical properties quickly deteriorated. In hindsight it is also apparent that a disturbance decoupling control law is unsuitable for wind turbine control. Decoupling the wind disturbance means that the controller should counteract the wind perfectly. Clearly, this requires a very aggressive control action which would quickly bring the life of a wind turbine to an end. A better approach would be to only decouple low frequency variations.

The individual pitch method considered in paper B introduces the appealing idea of utilizing wind measurements from the blades in the controller. The method as described in paper B is ad hoc in nature and does not take into account the stochastic nature of the wind explicitly. Its main justification is hence for attenuating variations which are relative slow compared to the rotor rotation.

The shortcomings of the wind model used in paper B are accounted for by the stochastic wind model described in paper D. Having a stochastic model of the wind makes it possible to optimize performance with respect to slow variations in the wind as well as fast variations. Although wind measurements are not utilized in paper D, they can easily be included in the framework by suitably extending the controller structure.

The stochastic model of the blade effective wind speed is arguably not the canonical way of modeling the wind if the objective is to attenuate asymmetric forces in the support of the blades. This was the motivation for shifting the entire methodology to multiblade coordinates (paper E,G and I). Collective as well as individual pitch objectives can be handled with equal ease in multiblade coordinates. The obvious advantages of the multiblade coordinates clearly outweighs the additional overhead of the multiblade transformation.

2.7 Future developments

The stochastic wind models derived in papers D,E,G and I could be used as a basis for a more general wind model. For blades with controllable variable airfoils (e.g. blades with trailing edge flaps), one needs additional resolution in the disturbance model. By extending the notion of blade effective wind speed to *blade element* effective wind speed, it is straight forward to extend the stochastic model as well - in rotating coordinates as well as multiblade coordinates. An illustration of blade element effective wind speeds is shown in Fig. 2.14. The blade element effective wind speed is a spatial average of the true wind along the element.

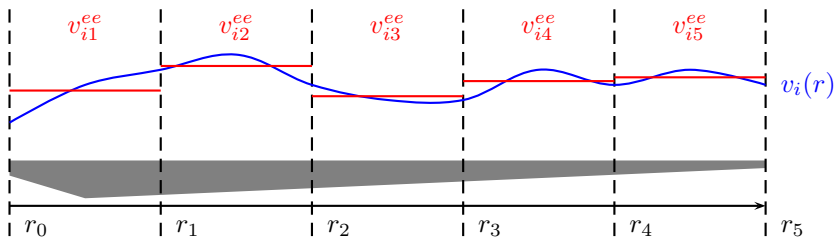

Figure 2.14: Illustration of blade element effective wind speed. $v_i(r)$ is the true wind distribution along blade i. v_{ik}^e is the corresponding blade effective wind speed for the k-th element.

Another interesting research topic would be to extend the multiblade transformation. The properties of the multiblade transformation are only perfectly valid when the rotor is rotating with a constant speed. An obvious study would be to investigate whether the transformation can be extended so that theoretical guarantees can be given for variable speed operation.

Chapter 3

MPC for uncertain systems

Model predictive control is a receding horizon methodology which has been studied intensively during the last couple of decades. The method is particularly interesting due to the fact that time-domain constraints on signals can be handeled in the framework. The appeal of the method is also largely because the basic algorithm is easy to understand and implement. Consequently, it is easily adapted by practitioners and works as an excellent educational tool.

The method has in particular found its use in the process industry. However, MPC has traditionally not been used as a direct replacement for the popular classical methods, such as PID control. Rather, it has been used to control slow dynamics, e.g., for calculating set-points for low-level controllers which are responsible for the fast dynamics. MPC requires online calculations and previously it was therefore not adequate for controlling fast dynamics. The increasing computational power of computers and the advances in optimization algorithms have, however, brought the applicability of MPC closer to applications previously only suitable for controllers designed offline.

The basic linear MPC formulation does not take into account the inherent model uncertainties whether they are due to disturbances, unmodeled dynamics or nonlinearities. In this work, suboptimal approaches have been considered for dealing with uncertainty in MPC. The focus has been on establishing ways of handling uncertainty in MPC without making the online optimization problem

deviate much from the basic algorithm. More specifically without adding an extensive online computational burden. To this end, the Youla and dual Youla parameterization of controller and system have been considered. The controller has an affine dependency on the Youla parameter. Similarly, the system has an affine dependency on the dual Youla parameter. This property makes the parameterizations advantageous in connection to, e.g., controller synthesis and system identification.

The outline of the chapter is as follows: Section 3.1 gives a basic introduction to the receding horizon methodology and a short review of advanced subjects. Section 3.2 introduces the Youla parameterizations and shows how the parameterizations can be constructed from co-prime factorizations of plant and a stabilizing controller. The contributions of this thesis are reviewed in Sec. 3.3 and discussed in Sec. 3.4. Proposals for future developments are outlined in Sec. 3.5.

3.1 Model predictive control

The origin of MPC is hard to trail. However, common for all original formulations is that they rewrite the dynamic optimization problem as a static optimization problem which is solved at every time step. The system models used in the earlier frameworks were primarily polynomial systems or impulse/step-response descriptions. The prevailing framework these days is undoubtedly the state-space formulation, which is also adopted in this thesis.

The following introduction to state-space MPC is equivalent to the presentations found in, e.g., [40, 54]. These references also include a historical overview.

3.1.1 The basic receding horizon algorithm

We consider the discrete time linear time invariant (LTI) system

$$x(k+1) = Ax(k) + Bu(k) \tag{3.1}$$

where x is the state of the system and u is the control input. The control objective at time k is to minimize the following quadratic cost:

$$J(k; x, u) = \sum_{i=k}^{N+k} \|x(i)\|_R^2 + \|u(i)\|_Q^2 \tag{3.2}$$

where $\|q\|_P^2 = q^T P q$ is the weighted two-norm and N is the prediction horizon. More specifically, at sample-time k the input sequence $\{u(k),\ u(k+1),\ \ldots,\ u(k+N)\}$ that minimizes the cost (3.2) is calculated. The first element $u(k)$ is actuated. The prediction horizon is shifted forward at every sample (see Fig. 3.1), consequently it is termed a receding horizon methodology.

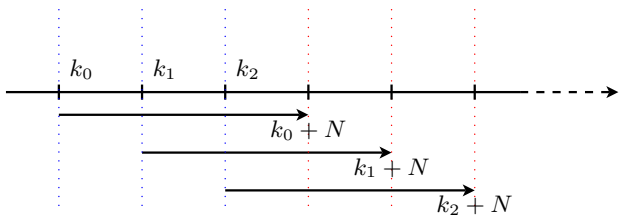

Figure 3.1: Illustration of receding horizon

Minimizing the cost (3.2) with respect to u and the restriction of the dynamics (3.1) is a dynamic optimization problem. However, the trick used in MPC is to rewrite the problem as a static optimization problem. To this end the cost-function is written explicitly as a function of the state-evolution and control-decisions:

$$J(k; X, U) = X(k)^T \mathcal{Q} X(k) + U(k)^T \mathcal{R} U(k) \tag{3.3}$$

where

$$X(k) = \begin{bmatrix} x(k) \\ x(k+1) \\ \vdots \\ x(k+N) \end{bmatrix},\ U(k) = \begin{bmatrix} u(k) \\ u(k+1) \\ \vdots \\ u(k+N) \end{bmatrix} \tag{3.4}$$

$$\mathcal{Q} = \begin{bmatrix} Q & 0 & \cdots & 0 \\ 0 & Q & \cdots & 0 \\ \vdots & \vdots & \ddots & \vdots \\ 0 & 0 & \cdots & Q \end{bmatrix},\ \mathcal{R} = \begin{bmatrix} R & 0 & \cdots & 0 \\ 0 & R & \cdots & 0 \\ \vdots & \vdots & \ddots & \vdots \\ 0 & 0 & \cdots & R \end{bmatrix} \tag{3.5}$$

The relation between the state evolution and the control decision over the prediction horizon is:

$$X(k) = \mathcal{A} x(k) + \mathcal{B} U(k) \tag{3.6}$$

where

$$\mathcal{A} = \begin{bmatrix} I \\ A \\ A^2 \\ \vdots \\ A^N \end{bmatrix}, \ \mathcal{B} = \begin{bmatrix} 0 & 0 & 0 & \cdots & 0 \\ B & 0 & 0 & \cdots & 0 \\ AB & B & 0 & \cdots & 0 \\ A^2B & AB & B & \cdots & 0 \\ \vdots & \vdots & \vdots & \ddots & \vdots \\ A^{N-1}B & A^{N-2}B & A^{N-3}B & \cdots & 0 \end{bmatrix} \tag{3.7}$$

Combining (3.3) and (3.6), the optimization problem is written explicitly as a function of the decisions:

$$J(k; x, U) = (\mathcal{A}x(k) + \mathcal{B}U(k))^T \mathcal{Q} (\mathcal{A}x(k) + \mathcal{B}U(k)) + U(k)^T \mathcal{R} U(k) \tag{3.8}$$

Differentiating (3.8) w.r.t. the decisions $U(k)$ and setting the result equal to zero the optimal control sequence is obtained as seen below:

$$U(k) = -\left(\mathcal{B}^T \mathcal{Q} \mathcal{B} + \mathcal{R}\right)^{-1} \mathcal{B}^T \mathcal{Q} \mathcal{A} x(k) \tag{3.9}$$

As mentioned only the first element of the control sequence is hence

$$u(k) = \underline{1} \cdot U(k), \quad \underline{1} = [\underbrace{1\ 1\ \cdots\ 1}_{\text{m times}}\ \underbrace{0\ \cdots\ 0}_{\text{m·N times}}], \tag{3.10}$$

where m is the input dimension. It is seen that the receding horizon controller simply has the form of a linear feedback $u = Fx$ where

$$F = -\underline{1} \cdot \left(\mathcal{B}^T \mathcal{Q} \mathcal{B} + \mathcal{R}\right)^{-1} \mathcal{B}^T \mathcal{Q} \mathcal{A} \tag{3.11}$$

Hence stability can easily be established *a posteriori* by checking that the eigenvalues of the closed loop system matrix $A+BF$ are strictly inside the unit circle.

Letting the horizon go to infinity, one gets the celebrated infinity horizon linear quadratic (LQ) controller [32]. The solution to this problem can be found using dynamic programming or calculus of variation. This leads to a Riccati type equation which must be solved to find the optimal solution. The LQ optimal controller is given by the state feedback $u = F_\infty x$. The solution is usually said to be in closed-form since the properties of the Ricatti equation are well studied. The LQ controller stabilizes the system for which it is designed and also gives certain guarantees of robustness [83].

Remark 1. *It is important to emphasize that the structure of the problem, as described above, is a very basic formulation. For example, it is common to assign individual horizons for the control and the state predictions, respectively. Other formulations include a trajectory reference in the problem and explicitly penalize the control increments. However, all of these problem can be handled in the formulation above by straightforward manipulation of either the cost or the system.*

3.1.2 Including constraints

With no constraints there are no immediate justifications for solving the MPC problem online as the controller has the form of a constant feedback gain. However, the true advantage of receding horizon control lies in the ability to handle constraints on control u and states x

$$u \in \mathbb{U} \tag{3.12}$$
$$x \in \mathbb{X} \tag{3.13}$$

The basic type of constraints considered in MPC are polyhedral constraints, i.e., defined by linear inequalities:

$$\mathbb{U} = \{u \ : \ C_u u \leq b_u\} \tag{3.14}$$
$$\mathbb{X} = \{x \ : \ C_x x \leq b_x\} \tag{3.15}$$

With polyhedral constraints the N-step predictions X and U will be constrained by

$$U \in \mathbb{U}^N = \{U \ : \ \mathcal{E}_u U \leq \mathcal{F}_u\} \tag{3.16}$$
$$X \in \mathbb{X}^N = \{U \ : \ \mathcal{E}_x U \leq \mathcal{F}_x\} \tag{3.17}$$

where $\mathcal{E}_u$ and $\mathcal{F}_u$ take the following forms (equivalently for $\mathcal{E}_x$ and $\mathcal{F}_x$):

$$\mathcal{E}_u = I_{N\times N} \otimes E_u \tag{3.18}$$
$$\mathcal{F}_u = I_N \otimes f_u \tag{3.19}$$
$$\tag{3.20}$$

where $I_{N\times N}$ is the N-dimensional identity matrix and I_N is a N-dimensional column vector with ones in all entries. The linear operator $\otimes$ is the kronecker product. The relation between the input trajectory and state trajectory is naturally constrained by the dynamics. Using (3.6) the input and state constraint can hence be written as a constraint on the input sequence U alone.

$$U \in \mathcal{Z} = \left\{ U \ : \ \begin{bmatrix} \mathcal{E}_u \\ \mathcal{E}_x \mathcal{B} \end{bmatrix} U \leq \begin{bmatrix} \mathcal{F}_u \\ \mathcal{F}_x - \mathcal{E}_x \mathcal{A} x(k) \end{bmatrix} \right\} \tag{3.21}$$

Consequently, the MPC optimization problem can be written as the quadratic program

$$\min_U \quad J(k; x, U) = (\mathcal{A}x(k) + \mathcal{B}U(k))^T \, \mathcal{Q} \, (\mathcal{A}x(k) + \mathcal{B}U(k)) + U(k)^T \mathcal{R} U(k) \tag{3.22}$$

$$\text{subject to} \quad \begin{bmatrix} \mathcal{E}_u \\ \mathcal{E}_x \mathcal{B} \end{bmatrix} U(k) \leq \begin{bmatrix} \mathcal{F}_u \\ \mathcal{F}_x - \mathcal{E}_x \mathcal{A} x(k) \end{bmatrix} \tag{3.23}$$

Letting the horizon go to infinity, one gets the constrained version of the LQ controller. Contrary to the unconstrained problem, a closed form solution to this problem does not exist. However, it can be proved that the solution is a piecewise affine state feedback [4].

As for the unconstrained problem, the constrained MPC controller does not give any guarantees of stability. In the theoretical case of infinite horizon it will naturally be stabilizing [56]. However, there are ways of formulating the finite horizon problem so that the MPC controller is a stabilizing controller. The most common way of doing so is by defining suitable terminal constraints and/or terminal costs. The reader is referred to the survey paper [44] for an overview.

The basic theory of MPC has matured over the last decades and research has branched into various directions. By now, an overwhelming body of literature exists on advanced subjects. This includes MPC for uncertain systems, time-varying systems, nonlinear systems, stochastic systems, decentralized MPC etc. The main obstacle for the various advanced methods is eventually the on-line computational burden. Although it can be possible in theory to extend the standard MPC control problem directly to, e.g., nonlinear systems, it might not be applicable to practical problems due to computational complexity. Large parts of the literature focus on formulating the MPC problems, so that they are tractable for on-line implementation.

The focus in the thesis contributions has been on solutions to handle uncertain systems in linear MPC. The contributions mainly belong to the category of robust MPC. However, it should be noted that the contributions do not follow the general trend in the robust MPC literature. The contributions have a more integral relation to the Youla parameterizations for which 3.2 has been reserved. In the following, robust MPC will shortly be reviewed for completeness rather than strict relevance. Other relevant subjects for the contributions are output-feedback MPC and soft-constrained MPC.

3.1.3 Robust MPC

The area of robust MPC is one of the very large fields of study in the world of MPC. To exemplify robust MPC, consider the uncertain system:

$$x(k+1) = f(x(k), u(k), w(k)) \tag{3.24}$$

where x and u is the state and control signal respectively. w represents the uncertainty which at time k belongs to a set $w(k) \in \mathbb{W}(x(k), u(k))$. If $\mathbb{W}$ does not depend on states and input, w simply represent an external disturbance.

The canonical way of addressing an uncertain system description in connection to MPC (and optimal control in general), is to define the optimal control problem as a min-max problem. More specifically an optimal controller which minimizes the worst case cost. For the uncertain system (3.24) with constraints on states and input, the min-max receding horizon problem at time k will take the condensed form

$$\min_{u} \max_{w} J(k; x, u), \tag{3.25}$$

which should be solved subject to the dynamics and the time-domain constraints on state, input and disturbance. J is naturally a finite horizon cost. Along the same lines as the basic MPC problem, one can rewrite the optimization problem as a static problem in terms of the input trajectory and the uncertain disturbance trajectory.

With various assumptions on system, cost and constraints, the min-max solution exists and leads to a stabilizing robust control law. However, in general the min-max optimization problem is not computationally tractable. For this reason restrictions on the problem structure or approximations needs to be made. The interested reader is referred to the following papers for surveys on the subject [3, 44]

The vast majority of computational tractable approaches to robust MPC uses the concept of robust invariant sets and casts the optimization in form of linear matrix inequalities (LMI). LMIs can be solved in polynomial time and are hence considered applicable for on-line optimization. A landmark in this connection is the paper [29]. In this paper an upper bound on the min-max cost was minimized on-line, sacrificing optimality for computational simplicity. Furthermore, the optimization was done with respect to a state feedback policy rather than an open loop trajectory. This paper spurred a lot of interest on using LMIs as a tool in MPC. Improvements on the method are, e.g., reported in [31, 75]. Another formulation of robust MPC which exploits the notion of robust invariant sets but avoids the complexity of LMIs is tubed based MPC [33, 45, 53].

3.1.4 Soft constraints in MPC

Soft constraints are constraints that can be violated but with an associated cost. Soft constraints are generally not regarded as true constraints. Whereas hard constraints can be associated with physical limitations, such as saturation of actuators, soft constraints do not really pertain to any physical constraints on the dynamics. Rather they pertain to the controller design. Soft constraints can be implemented by associating a slack variable $s \geq 0$ with the constraint.

In the basic algorithm a soft constraint on u can implemented as

$$C_u u \leq f_u + s \tag{3.26}$$

$$s \geq 0 \tag{3.27}$$

and extending the cost function with a term quadratic in s. The optimization is performed with respect to both input and slack variable. Adjusting the weight associated with the slack variable will determine the cost associated with constraint violation. One of the major concerns with hard constraints is that situations can occur where the optimization problem does not have a solution i.e. it is not feasible. This problem is avoided with soft constraints. If in-feasibility occurs, a practical method is to "soften" hard constraints. For treatments on the subject see [55, 82].

3.1.5 Output-feedback MPC

In the treatment so far it has been assumed that full information about the states are available. In practice this will almost never be the case, either due to noise or the inability to measure all the states. A common approach is therefore to design an observer and use the estimated states in the prediction equations. Usually a Luenberger type observer is used, e.g., a Kalman filter [32] if uncertainties have a stochastic interpretation. A more canonical approach for MPC is to use a receding horizon estimation scheme in which constraints are taken into account [53].

For linear unconstrained systems, it is well known that a state estimator and a state feedback controller can be designed separately, yielding a stable output-feedback controller. In fact, the design of an optimal LQG/$\mathcal{H}_2$ can be done by designing a Kalman filter and an LQ controller separately (the Separation Theorem) [2]. The results of unconstrained control does, however, not extend directly to the constrained case.

A promising approach to output MPC is considered in [43, 53]. In this approach the uncertainty introduced by state estimation is handled using tubes. Surveys on output feedback MPC are given in [17, 44].

3.2 The Youla parameterizations

The Youla parameterizations are the parameterizations of all stabilizing controllers for a given plant (the primary) and all plants stabilized by a given

controller (the secondary). The primary parameterization has been used extensively for controller synthesis. Other uses have been reported such as controller reconfiguration/switching. The secondary is less commonly used and probably also less known. It has found its applications in connection to, e.g., system identification and fault detection.

The primary and secondary Youla parameterization are dual in the respect that one can be constructed from the other by simply reversing the roles of plant and controller. For this reason, the secondary parameterization is commonly denoted the dual Youla parameterization. The primary is referred to as the Youla parameterization.

In the following, the Youla parameterizations are derived. Similar derivations can be found e.g. [64, 83]. The original papers describing the Youla parameterization are [80, 81].

3.2.1 Constructing the Youla parameterizations

Consider plant G and controller K described by rational proper transfer matrices. The classical approach is to consider (left and right) coprime factorizations of G and K

$$G = M_l^{-1} N_l = N_r M_r^{-1} \tag{3.28}$$

$$K = V_l^{-1} U_l = U_r V_r^{-1} \tag{3.29}$$

where $M_l, N_l, V_l, U_l \in \mathcal{RH}_\infty$ are left coprime factors and $M_r, N_r, V_r, U_r \in \mathcal{RH}_\infty$ are right coprime factors. $\mathcal{RH}_\infty$ denotes rational transfer matrices with poles strictly inside the unit circle (we consider discrete time).

A pair M_l, N_l is termed left coprime in $\mathcal{RH}_\infty$ if they have the same number of rows and $\left[\begin{smallmatrix} M_l & N_l \end{smallmatrix}\right]$ has a right inverse in $\mathcal{RH}_\infty$. A pair M_r, N_r is termed right coprime in $\mathcal{RH}_\infty$ if they have the same number of columns and $\left[\begin{smallmatrix} M_r \\ N_r \end{smallmatrix}\right]$ has a left inverse in $\mathcal{RH}_\infty$

Now consider the feedback connection of G and K as shown in Fig. 3.2. The feedback connection in said to be internally stable if bounded inputs to the loop give rise to bounded signals everywhere in the loop. This is equivalent to saying that all loop transfer functions should belong to $\mathcal{RH}_\infty$:

$$\begin{bmatrix} I & -K \\ -G & I \end{bmatrix}^{-1} = \begin{bmatrix} (I-KG)^{-1} & K(I-GK)^{-1} \\ G(I-KG)^{-1} & (I-GK)^{-1} \end{bmatrix} \in \mathcal{RH}_\infty \tag{3.30}$$

Introducing the coprime factors of G and K, the condition can be reformulated

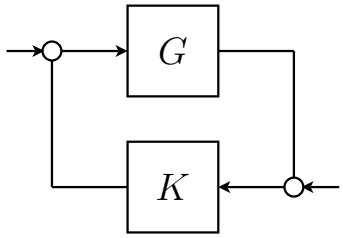

Figure 3.2: Feedback connection of plant G and controller K.

as:

$$\begin{bmatrix} I & -K \\ -G & I \end{bmatrix}^{-1} = \begin{bmatrix} M_r \\ N_r \end{bmatrix} (V_l M_r - U_r N_r)^{-1} \begin{bmatrix} V_l & U_l \end{bmatrix} + \begin{bmatrix} 0 & 0 \\ 0 & I \end{bmatrix} \tag{3.31}$$

Due to the definition of coprimeness it follows that the loop is stable if and only if coprime factors exist (in $\mathcal{RH}_\infty$) so that the following double Bezout identity holds

$$\begin{bmatrix} V_l & -U_l \\ -N_l & M_l \end{bmatrix} \begin{bmatrix} M_r & U_r \\ N_r & V_r \end{bmatrix} = \begin{bmatrix} M_r & U_r \\ N_r & V_r \end{bmatrix} \begin{bmatrix} V_l & -U_l \\ -N_l & M_l \end{bmatrix} = \begin{bmatrix} I & 0 \\ 0 & I \end{bmatrix} \tag{3.32}$$

Given coprime factors satisfying the double Bezout identity the parameterization of all stabilizing controllers is easily obtained and given by:

$$K(Q) = (U_r + M_r Q)(V_r + N_r Q)^{-1} = U_r(Q) V_r(Q)^{-1} \tag{3.33}$$

$$= (V_l + Q N_l)^{-1} (U_l + Q M_l) = V_l(Q)^{-1} U_l(Q) \tag{3.34}$$

where $Q \in \mathcal{RH}_\infty$ is the so-called Youla parameter. This follows from the fact that $U_r(Q), V_r(Q)$ and $V_l(Q), U_l(Q)$ themselves are coprime factors in $\mathcal{RH}_\infty$ and that they satisfy the double Bezout identity together with the coprime factors of G.

Based on the Youla parameterization the dual Youla parameterization is trivially obtained by reversing the roles of G and K in the derivations. Hence, the parameterization of all systems stabilized by a given controller is given as:

$$G(S) = (N_r + V_r S)(M_r + U_r S)^{-1} = N_r(S) M_r(S)^{-1} \tag{3.35}$$

$$= (M_l + S U_l)^{-1} (N_l + S V_l) = M_l(S)^{-1} N_l(S) \tag{3.36}$$

where $S \in \mathcal{RH}_\infty$ is the so-called dual Youla parameter. This follows from the fact that $N_r(S), M_r(S)$ and $M_l(S), N_l(S)$ themselves are coprime factors in $\mathcal{RH}_\infty$ and that they satisfy the double Bezout identity together with the coprime factors of K.

If the system is parameterized in terms of the dual Youla parameter S and the controller in terms of the Youla parameter Q, it can be shown that the loop is stable if and only if Q stabilizes S (see Fig. 3.3). An useful interpretation of S is that of an uncertainty. In fact various uncertainty descriptions can be parameterized in terms of the dual Youla parameter [47].

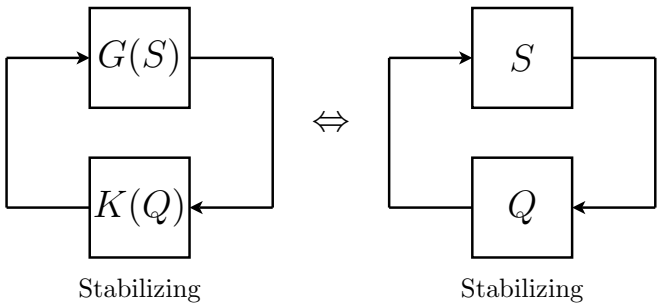

Figure 3.3: The feedback connection of $G(S)$ and $K(Q)$ is stabilizing iff the feedback connection of S and Q is stabilizing.

The Youla parameterizations have found various applications in the field of control theory. Arguably the most common application of the Youla parameterization is in connection to off-line controller synthesis e.g. LQG/$\mathcal{H}_2$, Loop Transfer Recovery (LTR) and $\mathcal{H}_\infty$. Treatments can be found in [10, 64, 74, 83].

Closed-loop system identification through the dual Youla parameter is treated in [15, 19, 19, 64]. The affine nature of the dual Youla parameterization makes the closed-loop identification problem equivalent to an open loop problem. Consequently, the challenges of closed-loop identification [39] are circumvented.

Besides off-line synthesis and identification, the Youla parameterizations have been utilized for on-line reconfiguring the controller and/or on-line identification of dynamics. Adaptive and iterative methods have been considered in [64, 65, 66, 67, 78, 79]. Controller switching/scheduling in [5, 50, 52]. Fault-detection has been considered in [49, 51, 63].

General treatments on clever architectures for control using the Youla parameterizations can be found in [48, 50, 51, 84].

A survey covering some of the mentioned subjects can be found in [1].

3.2.2 Applications of the Youla parameter to MPC

The Youla parameterization has found several uses in connection to MPC. The first documented application dates back to the days of Generalized Predictive Control (GPC) where the Youla parameter was introduced in [30] as part of a GPC algorithm with guaranteed stability. GPC is the predecessor of MPC and is usually characterized by its use of polynomial models (transfer functions) and not incorporating constraints.

The Youla parameter was introduced as the on-line optimization variable in [69, 70]. In the first paper [69] it was shown that nominal stability can be guaranteed in MPC by parameterizing the controller in terms of a time-varying Youla parameter. In [70] it was shown how model uncertainties with bounded 1-norm can be handled in their framework. Recursive feasibility is not proved and there is therefore no guarantee of stability of the overall algorithm.

More recent applications includes [61] and [13]. Both approaches apply the Youla parameter as a means of robustifying constrained MPC offline through the Youla parameterization. In reference [42] the Youla parameter is incorporated to set up a stable MPC scheme that can deal with computational delays.

None of the these methods take advantage of the dual Youla parameterization although an indication of possible advantages are given in [70].

3.3 Review of contributions

Two ways of utilizing the Youla parameterizations in connection to MPC have been considered. The aim has been to deal with an uncertain linear system description. The first method proposed (paper C) is a method for reconfiguring the MPC controller if the model is updated (identified) or the controller reconfigured. The second method (paper F and H) is a robust MPC method which provides sufficient conditions for stability, primarily for the case with soft constraints. The methods are reviewed separately in the following. Integral in both approaches is the fact that the uncertainty description can be parameterized in terms of the dual Youla parameter S.

3.3.1 Reconfiguring MPC through the Youla parameterization

In paper C the Youla parameterizations are used to setup a scheme for improving the MPC controller based on identification of the uncertainty and subsequent reconfiguration of the controller. The method can be seen as an application of the iterative method described in [64] to MPC.

Referring to Fig. 3.4 the setup consists of an uncertain system described by the feedback connection of an extended nominal system Σ and an uncertain system Δ. The systems Σ and Δ are both linear time and invariant. Δ is unknown but assumed norm-bounded

$$\|\Delta\|_\infty \leq 1 \tag{3.37}$$

The system is controlled by a robust controller K, i.e., a controller which ensures that the system is stable for all allowable Δ. The MPC controller is designed for this prestabilized system and acts as a perturbation v of the nominal control signal as illustrated in Fig. 3.4.

Just as the MPC control signal can be regarded as a perturbation of the nominal control loop, one can regard the Youla parameterization as a perturbation of the nominal controller K. This can be seen by considering the specific realization shown in Fig. 3.5a. For convenience, the uncertain system description has been parameterized in terms of the dual Youla parameter S assuming that S satisfies:

$$\Sigma(\Delta) = G(S) \tag{3.38}$$

where $\Sigma(\Delta)$ is the original uncertain system. The Youla parameterization is

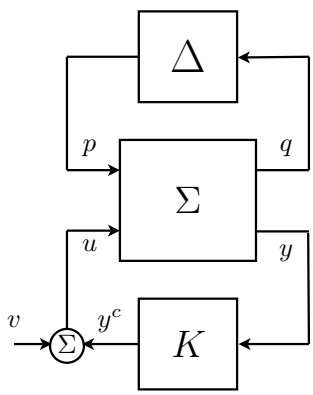

Figure 3.4: System setup: The system is controlled by the feedback controller K which stabilizes Σ subject to the uncertain system Δ.

constructed as an observer for the nominal system G and a dynamic feedback $Q \in \mathcal{RH}_\infty$ from ϵ (the output estimation error) to the input. Q is naturally the Youla parameter. With this realization it is seen that the MPC control signal v and the Youla parameter output η directly act as perturbations of the nominal control signal. Also of interest is the fact that the input-output system from v to ϵ is exactly the feedback of the Youla and the dual Youla parameter (see Fig. 3.5b). This makes it relatively easy to set up a scheme for identifying the uncertainty through the dual Youla parameter S.

Deriving the N-step predictions for the output y, one gets the following structure:

$$Y = Y^{(G,K)} + Y^{(S,Q)} \tag{3.39}$$

where $Y^{(G,K)}$ is the N-step prediction due to the nominal dynamics. $Y^{(S,Q)}$ is the contribution owing to the dual and primary Youla parameter. Due to this structure it is easy to reconfigure the MPC controller if knowledge is gained about the uncertainty S or the pre-stabilizing controller is reconfigured through Q. This could e.g. be done in a modular fashion. An example in paper C illustrates the idea.

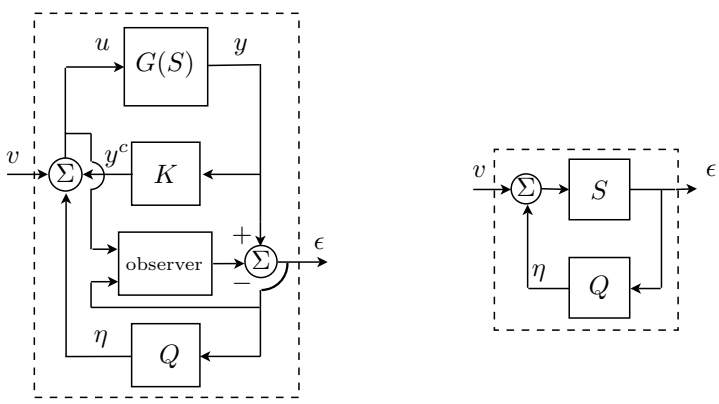

(a) Observer form of Youla parameterization

(b) Equivalent input-output representation

Figure 3.5: The Youla parameterization is realized in the observer form [23]. It follows from the theory that the dynamic system from v to ϵ is the closed loop connection of S and Q.

3.3.2 Parameterizing MPC through the Youla parameter

In paper F and H the Youla parameter is fully integrated in the MPC optimization problem as the on-line optimization variable itself. As a result, it is possible to establish a direct link between the optimization variable and stability. The method can be seen as an extension and generalization of the work in [69, 70]. The main extension is the application of the dual Youla parameter to deal with uncertain systems.

Fig. 3.6 shows the system and controller setup. The uncertain system setup is equivalent to that presented in Sec. 3.3.1, however, the external MPC signal has been removed. Instead a time-varying Youla parameter Q_k has been incorporated. The following structure is assumed for Q_k:

$$Q_k = \Theta_k \tilde{Q} \tag{3.40}$$

where Θ_k is a time-varying gain and $\tilde{Q} \in \mathcal{R}H_\infty$. Instead of deriving the predictions in terms of an open loop input sequence, they are derived in terms of the controller parameter Θ_k. Effectively, this is a closed loop parameterization of MPC. To distinguish the methodology from the standard open-loop formulation it is denoted YMPC (Youla Model Predictive Control). Due to the affine nature of the Youla parameter and the chosen structure (3.40), the predictions will be affine in the elements of Θ_k. Owing to this property the optimization problem

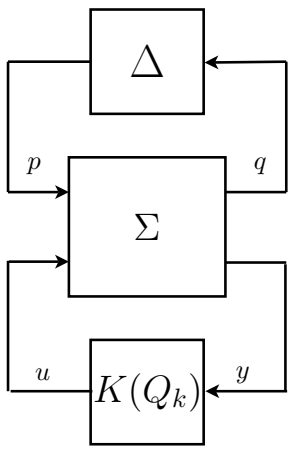

Figure 3.6: System setup: The system is controlled by the feedback controller K which stabilizes Σ subject to the unknown system Δ.

reduces to a quadratic optimization problem.

By parameterizing the uncertainty description in terms of the dual Youla parameter S, it is possible to guarantee stability if the loop in Fig. 3.7 is stable. However, as Δ is uncertain so is S. From the norm-bound on Δ it is possible to deduce a norm-bound on S as well. Applying the Small Gain Theorem [16] it is then possible to derive a bound on Θ_k. This bound should be respected at all times to guarantee robust stability. The bound on Θ_k can be included as a constraint in the on-line optimization problem. The constraint is convex and can be formulated as a linear matrix inequality if desired. The use of the Small Gain Theorem is a conservative choice as it gives a sufficient condition for stability, but not a necessary one. The theorem only accounts for the worst case gain along frequency. To reduce conservativeness it is recommended to filter Q_k such that the loop gain is flat along frequency.

Instead of solving the min-max problem (see Sec. 3.1.3), the nominal optimization problem is solved (i.e. $\Delta = S = 0$) with the additional stability constraint on Θ_k. Therefore, although robust stability can be guaranteed, no guarantees are given with respect to optimality or constraint satisfaction. Feasibility of the optimization problem can therefore in general not be guaranteed with hard constraints. One notable exception is when the uncertain system description is stable and only constraints on inputs are considered. Due to this fact the YMPC controller is mainly applicable when the constraints are soft (see Sec. 3.1.4) - in this case feasibility can be guaranteed at all times. The stability constraint has been derived without the assumption of full-state information and therefore applies to the more general output feedback problem.

The YMPC method is derived in a general framework. No assumptions are made on the actual realization of the Youla parameterization or on the structure of $\tilde{Q} \in \mathcal{RH}_\infty$.

A canonical choice of $\tilde{Q}$ in connection to MPC is arguably a shift-register struc-

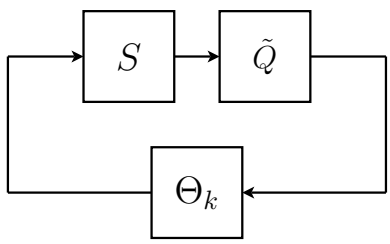

Figure 3.7: The YMPC controller stabilizes the uncertain system if the illustrated loop is a stable.

ture. In this case $\tilde{Q}$ does not do any intelligent processing of data but merely stores past information. The emphasis is hence on the on-line optimization variable Θ_k. Other approaches are described in the papers.

It should be noted that paper F is a reduced version of H. The setup considered in paper F is exactly that of Fig. 3.6. The setup considered in paper H is generalized to include a disturbance model. Numerical examples in the papers illustrate the advantages and and disadvantages of the method.

3.4 Discussion

From a theoretical point of view, the reconfiguration framework (paper C) has some unsolved open ends. The framework utilizes the Youla parameters to achieve a desirable modular structure. However, no theoretical guarantees of stability are given. Unfortunately, in the proposed framework it becomes quite difficult to fully utilize the integral relation between S and Q for guaranteeing stability. This is basically because the Youla parameters are being applied as an add-on rather than an integral part of the MPC optimization problem. Setting aside the theoretical shortcomings, the algorithm has practical appeal since it can be applied in a modular set up, i.e., without altering the pre-existing controller.

The potential of the Youla parameterizations is more easily exploited when incorporating them as an integral part of the MPC optimization itself. The approach considered in papers F and H is hence arguably the more natural approach. Parameterizing the online optimization problem directly in terms of the Youla parameter, the stability properties of the (Q, S) pair can be exploited to a larger extend. This effectively results in the robust stability result. Although the method has attractive properties with regards to stability, it still lacks guarantees of optimality. Hence, the question is whether there is a practical problem suited for the method.

3.5 Future developments

An obvious shortcoming of the YMPC method (paper F and H) is that no guarantee of optimality is given. Discrepancy between predictions and actual state evolution (prediction mis-match) could be reduces if the modular/iterative ideas presented in paper C are incorporated in the robust control method.

It is also of interest whether an optimal structure of the $\tilde{Q}$ parameter exists in the YMPC method. Perhaps the conservativeness of the method could be reduced in this way. The impact of the particular realization of the Youla parameterization is also an issue that would be interesting to clarify.

Bibliography

[1] Brian D. O. Anderson. From youla-kucera to identification, adaptive and nonlinear control. *Automatica*, 34(12):1485–1506, 1998.

[2] K.J. Åstrøm. *Introduction to stochastic control theory*. Academic Press New York, 1970.

[3] A. Bemporad and M. Morari. Robust model predictive control: a survey. *Robustness in Identification and Control (Lecture Notes in Control and Information Sciences Vol.245)*, pages 207–26, 1999.

[4] Alberto Bemporad, Manfred Morari, Vivek Dua, and Efstratios N. Pistikopoulos. The explicit linear quadratic regulator for constrained systems. *Automatica*, 38(1):3–20, 2002.

[5] J.D. Bendtsen, J. Stoustrup, and K. Trangbaek. Bumpless transfer between observer-based gain scheduled controllers. *International Journal of Control*, 78(7):491–504, 2005.

[6] E. A. Bossanyi. The design of closed loop controllers for wind turbines. *Wind Energy*, 3:149–163, 2001.

[7] E.A. Bossanyi. Individual Blade Pitch Control for Load Reduction. *Wind Energy*, 6(2):119–128, 2003. DOI: 10.1002/we.76.

[8] E.A. Bossanyi. Wind turbine control for load reduction. *Wind Energy*, 6(3):229–244, 2003. DOI:10.1002/we.95.

[9] E.A. Bossanyi. Further load reductions with individual pitch control. *Wind Energy*, 8(4):481–485, 2005. DOI:10.1002/we.166.

[10] Stephen Boyd and Barratt Craig. *Linear controller design: limits of performance*. Prentice Hall, 1991.

[11] Tony Burton, David Sharp, Nick Jenkins, and Ervin Bossanyi. *Wind Energy Handbook*. Wiley, 2001.

[12] H. Camblong, MR Vidal, and JR Puiggali. Principles of a Simulation Model for a Variable-speed Pitch-regulated Wind Turbine. *Wind Engineering*, 28(2):157–175, 2004.

[13] Qifeng Cheng, Basil Kouvaritakis, Mark Cannon, and J. Anthony Rossiter. A youla parameter approach to robust constrained linear model predictive control. In *Proceedings of the 48th IEEE Conference on Decision and Control*, 2009.

[14] R.P. Coleman and A.M. Feingold. Theory og self-excited mechanical oscillations of helicopter rotors with hinged blade. Technical report, NACA, 1958. naca-report-1351.

[15] F. De Bruyne, B. Anderson, and N. Linard. The hansen scheme revisited. *Decision and Control, 1998. Proceedings of the 37th IEEE Conference on*, 1:706–711, 1998.

[16] C. A. Desoer and M. Vidyasagar. *Feedback systems: Input-output properties*. Academic Press, 1975.

[17] Rolf Findeisen, Frank Allgöwer, Lars Imsland, and Bjarne A. Foss. State and output feedback nonlinear model predictive control: An overview. *European Journal of Control*, 9(2-3):190–206, 2003.

[18] M.J. Grimble. Horizontal axis wind turbine control: comparison of classical, LQG and $\mathcal{H}_\infty$ designs. *Dynamics and Control*, 6(2):143–161, 1996. DOI:10.1007/BF02169534.

[19] F. Hansen. *A fractional representation approach to closed-loop experiment design*. Phd thesis, Stanford University, 1989.

[20] M. Hansen. Aeroelastic stability analysis of wind turbines using an eigenvalue approach. *Wind Energy*, 7:133–143, 2004.

[21] M. O. L. Hansen. *Aerodynamics of Wind Turbines*. James & James, 2000.

[22] L. C. Henriksen. Model predictive control of a wind turbine. Master's thesis, Informatics and Mathematical Modelling, Technical University of Denmark, DTU, Richard Petersens Plads, Building 321, DK-2800 Kgs. Lyngby, 2007. Supervised by Assoc. Prof. Niels Kjølstad Poulsen, IMM, and co-supervisor Senior Scientist Morten Hartvig Hansen, Risø, DTU.

[23] J.Y. Ishihara and R.M.R.M. Sales. Doubly coprime factorizations related to any stabilizing controllers in state space. *Automatica*, 35(9):1573–1577, 1999.

[24] Alberto Isidori. *Nonlinear Control Systems*. Springer, third edition, 1995.

[25] W. Johnson. *Helicopter Theory*. Princeton University Press, 1980.

[26] Jason M. Jonkman and Marshall L. Buhl. Fast user's guide. Technical report, National Renewable Energy Laboratory, 2005.

[27] S. Kanev and T. G. van Engelen. Exploring the limits in individual pitch control. In *Proceedings of European Wind Energy Conference*, 2009.

[28] Hassan K. Khalil. *Nonlinear Systems*. Prentice Hall, third edition, 2002.

[29] M.V. Kothare, V. Balakrishnan, and M. Morari. Robust constrained model predictive control using linear matrix inequalities. *Automatica*, 32(10):1361–1379, 1996.

[30] B. Kouvaritakis, J. A. Rossiter, and A.O.T. Chang. Stable generalized predictive control: an algorithm with guaranteed stability. *IEE Proceedings-Control Theory and Applications*, 139:349–362, 1992.

[31] B. Kouvaritakis, J.A. Rossiter, and J. Schuurmans. Efficient robust predictive control. *IEEE Transactions on Automatic Control*, 45(8):1545–1549, 2000.

[32] Huibert Kwakernaak and Raphael Sivan. *Linear Optimal Control Systems*. Wiley-Interscience, 1972.

[33] W. Langson, I. Chryssochoos, S.V. Rakovic;, and D.Q. Mayne. Robust model predictive control using tubes. *Automatica*, 40(1):125–133, 2004.

[34] T.J. Larsen, H.A. Madsen, and K. Thomsen. Active load reduction using individual pitch, based on local blade flow measurements. *Wind Energy*, 8(1):67–80, 2005. DOI:10.1002/we.141.

[35] D.J. Leith and W.E. Leithead. Implementation of wind turbine controllers. *International Journal of Control*, 66(3):349–380, 1997.

[36] W.E. Leithead. Effective wind speed models for simple wind turbine simulations. *Wind Engineering*, pages 321–326, 1992.

[37] W.E. Leithead and B. Connor. Control of variable speed wind turbines: design task. *International Journal of Control*, 73(13):1189–1212, 2000.

[38] W.E. Leithead and B. Connor. Control of variable speed wind turbines: dynamic models. *International Journal of Control*, 73(13):1173–1188, 2000.

[39] L. Ljung. *System Identification: Theory for the User*. Prentice Hall, second edition edition, 1999.

[40] J.M. Maciejowski. *Predictive control with constraints*. Prentice Hall, 2002.

[41] Jakob Mann. Wind field simulation. *Probabilistic Engineering Mechanics*, 13(4):269–282, 1998.

[42] Karl Martensson and Andreas Wernrud. Dynamic model predictive control. In *Proceedings of the 17th IFAC World Congress*, volume 17. Elsevier, 2008.

[43] D.Q. Mayne, S.V. Rakovic, R. Findeisen, and F. Allgöwer. Robust output feedback model predictive control of constrained linear systems. *Automatica*, 42(7):1217–1222, 2006.

[44] D.Q. Mayne, J.B. Rawlings, C.V. Rao, and P.O.M. Scokaert. Constrained model predictive control: Stability and optimality. *Automatica*, 36(6):789–814, 2000.

[45] D.Q. Mayne, M.M. Seron, and S.V. Rakovic;. Robust model predictive control of constrained linear systems with bounded disturbances. *Automatica*, 41(2):219–224, 2005.

[46] Leonard Meirovitch. *Fundamentals of vibrations*. McGraw-Hill, 2001.

[47] H. Niemann. Dual youla parameterisation. *IEE Proceedings-Control Theory and Applications*, 150:493–497, 2003.

[48] H. Niemann. Parameterisation of extended systems. *Control Theory and Applications, IEE Proceedings-*, 153(2):221–227, 2006.

[49] H. Niemann. A setup for active fault diagnosis. *IEEE Transactions on Automatic Control*, 51(9):1572–1578, 2006.

[50] H. Niemann and N.K. Poulsen. Controller architectures for switching. *2009 American Control Conference*, pages 1098–1103, 2009.

[51] H. Niemann and J. Stoustrup. An architecture for fault tolerant controllers. *International Journal of Control*, 78(14):1091–1110, 2005.

[52] H. Niemann, J. Stoustrup, and R.B. Abrahamsen. Switching between multivariable controllers. *Optimal Control Applications & Methods*, 25(2):51–66, 2004.

[53] J.B. Rawlings and D.Q. Mayne. *Model Predictive Control: Theory and Design*. Nob Hill Publishing, 2009.

[54] J.A. Rossiter. *Model-based predictive control: A practical approach*. CRC Press, 2003.

[55] Pierre O. M. Scokaert, James B. Rawlings, and Pierre O. M. Scokaert. Feasibility issues in linear model predictive control. *AIChE Journal*, 45(8):1649–1659, 1999.

[56] P.O.M. Scokaert and J.B. Rawlings. Constrained linear quadratic regulation. *IEEE Transactions on Automatic Control*, 43(8):1163–1169, 1998.

[57] K. Selvam, S. Kanev, J.W. van Wingerden, T. van Engelen, and M. Verhaegen. Feedback-feedforward individual pitch control for wind turbine load reduction. *International Journal of Robust and Nonlinear Control*, 19(1):72–91, 2009. DOI:10.1002/rnc.1324.

[58] Ahmed A. Shabana. *Dynamics of multibody systems*. Cambridge University Press, 1998.

[59] Jean-Jacques E. Slotine and Weiping Li. *Applied Nonlinear Control*. Prentice Hall, 1991.

[60] P. Sørensen, A.D. Hansen, and P.A.C. Rosas. Wind models for simulation of power fluctuations from wind farms. *Journal of Wind Engineering & Industrial Aerodynamics*, 90(12-15):1381–1402, 2002.

[61] Cristina Stoica, Cristina Stoica, Pedro Rodriguez-Ayerbe, and Didier Dumur. Off-line improvement of multivariable model predictive control robustness. pages 2826–2831. Institute of Electrical and Electronics Engineers Inc., 2008. DOI:10.1109/CDC.2007.4434591.

[62] K.A. Stol, W. Zhao, and A. D. Wright. Individual blade pitch control for the controls advanced research turbine (cart). *Journal of Solar Energy Engineering*, 128:498–505, November 2006. DOI:10.1115/1.2349542.

[63] J. Stoustrup and H.H. Niemann. Fault estimation - a standard problem approach. *International Journal of Robust and Nonlinear Control*, 12(8):649–673, 2002.

[64] T-T. Tay, I. Mareels, and J.B. Moore. *High Performance Control*. Birkhäuser, 1998.

[65] T.T. Tay and J.B. Moore. Performance enhancement of two-degree-of-freedom controllers via adaptive techniques. *International Journal of Adaptive Control and Signal Processing*, 4(1):69–84, 1990.

[66] T.T. Tay and J.B. Moore. Enhancement of fixed controllers via adaptive-q disturbance estimate feedback. *Automatica*, 27:39–53, 1991.

[67] T.T. Tay, J.B. Moore, and R. Horowitz. Indirect adaptive techniques for fixed controller performance enhancement. *International Journal of Control*, 50(5):1941–1959, 1989.

[68] S. C. Thomsen. Nonlinear control of a wind turbine. Master's thesis, Informatics and Mathematical Modelling, Technical University of Denmark, DTU, Richard Petersens Plads, Building 321, DK-2800 Kgs. Lyngby, 2006. Supervised by Niels K. Poulsen, IMM.

[69] T.J.J. Van Den Boom and R.A.J. De Vries. Constrained predictive control using a time-varying youla parameter: a state space solution. *Proceedings of the Third European Control Conference. ECC 95*, (vol.4):3235–40 vol.4, 1995.

[70] T.J.J. Van Den Boom and R.A.J. De Vries. Robust predictive control using a time-varying youla parameter. *International Journal of Applied Mathematics and Computer Science*, 9:101–128, 1999.

[71] T. G. van Engelen. Design model and load reduction assessment for multi-rotational mode individual pitch control (higher harmonics control). In *Proceeding of European Wind Energy Conference*, 2006.

[72] T. G. van Engelen. Control design based on aero-hydro-servo-elastic linear model from turbu (ecn). In *Proceedings of European Wind Energy Conference*, 2007.

[73] Paul S. Veers. Three-dimensional wind simulation. Technical report, Sandia National Laboratories, 1988.

[74] M. Vidyasagar. *Control System Synthesis: a factorization approach.* The M.I.T. Press, 1985.

[75] Z. Wan and M.V. Kothare. An efficient off-line formulation of robust model predictive control using linear matrix inequalities. *Automatica*, 39:837–846, 2003.

[76] W. Weaver Jr., S. P. Timoshenko, and D. H. Young. *Vibration problems in engineering.* Wiley, 1990.

[77] M. Xin. *Adaptive Extremum Control and Wind Turbine Control.* PhD thesis, Informatics and Mathematical Modelling, Technical University of Denmark, 1997.

[78] Wei-Yong Yan and J.B. Moore. Stable linear fractional transformations with applications to stabilization and multistage h_∞ control design. *International Journal of Robust and Nonlinear Control*, 6(2):101–122, 1996.

[79] Weiyong Yan and John B. Moore. A multiple controller structure and design strategy with stability analysis. *Automatica*, 28(6):1239–1244, 1992.

[80] D. Youla, Jr. Bongiorno, J., and H. Jabr. Modern wiener–hopf design of optimal controllers part i: The single-input-output case. *IEEE Transactions on Automatic Control*, 21(1):3–13, 1976.

[81] D. Youla, H. Jabr, and Jr. Bongiorno, J. Modern wiener-hopf design of optimal controllers–part ii: The multivariable case. *IEEE Transactions on Automatic Control*, 21(3):319–338, 1976.

[82] Alex Zheng and Manfred Morari. Stability of model predictive control with soft constraints. *Proceedings of the IEEE Conference on Decision and Control*, 2:1018–1023, 1994.

[83] K. Zhou, J.C. Doyle, and Glover K. *Robust and optimal control*. Prentice Hall, 1996.

[84] Kemin Zhou and Zhang Ren. A new controller architecture for high performance, robust, and fault-tolerant control. *IEEE Transactions on Automatic Control*, 46(10):1613–1618, 2001.

[85] Kasper Zinck Østergaard. *Robust, Gain-Scheduled Control of Wind Turbines*. PhD thesis, Automation and Control, Department of Electronic Systems, Aalborg University, 2008.

Papers

Paper A

A disturbance decoupling nonlinear control law for variable speed wind turbines

abstract

This paper describes a nonlinear control law for controlling variable speed wind turbines using feedback linearization. The novel aspect of the control law is its ability to decouple the effect of wind fluctuations. Furthermore, the transformation to feedback linearizable coordinates is chosen intelligently so that the majority of the system structure is invariant under the transformation. Consequently the physical interpretation is preserved. The method assumes that the effective wind speed and acceleration are estimated from measurements on the wind turbine. The performance of the control is compared to that of a LQG controller using a specific wind turbine and wind model.

A.1 Introduction

As a result of increasing environmental concern, more and more electricity is being generated from renewable sources. In Denmark, wind turbines have experienced a broad popularity since the introduction in the early 1970s, now covering 20 percent of the Danish energy consumption. Ongoing research focuses on increasing the efficiency of the individual turbines and the parks of wind turbines as entities.

The basic operation of a wind turbine can be explained briefly: Wind turbines harness the power of the wind by using rotors, fitted with aerodynamic blades, to turn a drive shaft. The drive shaft rotates inside a generator which will then produce electricity. The type of wind turbine which is considered in this paper is horizontal axis pitch regulated wind turbines with variable speed asynchronous generators. 'Variable speed' simply means that it is possible to vary the relative speed of the generator, compared to the speed/frequency of the electrical grid. In effect, changing the relative speed changes the generator torque and thereby provides a useful control parameter.

Modern turbines rely on complex control systems to maximize efficiency and ensure safe operation. Control of wind turbines can be divided into three levels [7]. On the top level is the supervisory control, which monitors the turbine and wind resource in order to determine when to startup the turbine, shut down the turbine and shift between control strategies. On the middle level is the turbine controller which controls the blade pitch angle and generator torque. The turbine controller also controls the yaw of the nacelle, so that the nacelle points into the wind. However, this is a relatively slow motion compared to the dynamics of the turbine and hence is not of particular interest. The lowest level constitutes controllers for the power electronics, internal generator and pitch actuator.

In the present work the turbine controller has been considered. The primary objective of the turbine controller is to extract as much energy from the wind as possible. However, practical limitations of the generator and the turbine mechanics prevent such operation. Consequently the objective is changed according to the wind speed as illustrated in Fig. A.1. Region IV is considered in the present work. In this region, the power available in the wind exceeds the limit for which the generator and the turbine mechanics have been designed. Hence, to avoid failure, the rotational speed and output power should be kept constant at nominal values. A description of the other regions can be found in [11].

Much research has been focused at designing efficient turbine controllers. Clas-

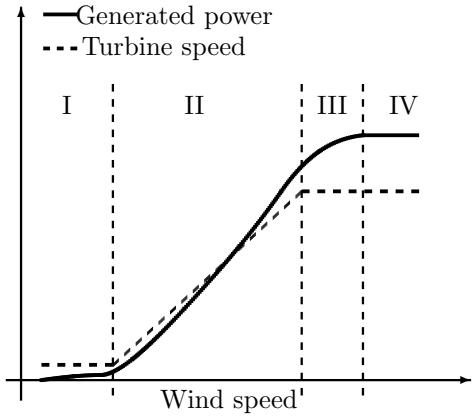

Figure A.1: Control regions for a turbine controller. The control law presented in this paper is designed for region IV.

sical methods (eg. PID control) have been widely applied in real life whereas advanced modern control has been applied to a lesser extend [2]. However, a huge body of literature concerning control of wind turbines with modern methods exist. Most prominent is the study on linear optimal and/or robust methods such as LQ, $\mathcal{H}_2$ and $\mathcal{H}_\infty$. Reference [5] gives a comparison between some of these advanced methods and classical control. Recently, nonlinear control of wind turbines has been the interest of several scientists. This ranges from well established methods such as sliding mode control and feedback linearization ([1], [3] and [8]) to methods such as neural networks and wavelets [9].

The main contribution of the present work is the derivation of a nonlinear control law which - ideally - cancels the nonlinearities of the system and decouples the fluctuations in the wind speed from the system states. Feedback linearization is utilized and it is shown that the nonlinearities can be targeted intelligently ie. only the subspace in which the nonlinearities occur is compensated. The design is based on a medium complexity turbine model, which includes dynamic characteristics commonly discarded when dealing with nonlinear wind turbine control.

A.2 Wind turbine model

This section presents the dynamic model of a pitch controlled variable speed wind turbine. The wind turbine characteristics which are incorporated in the model are aerodynamics, turbine mechanics, generator dynamics and pitch actu-

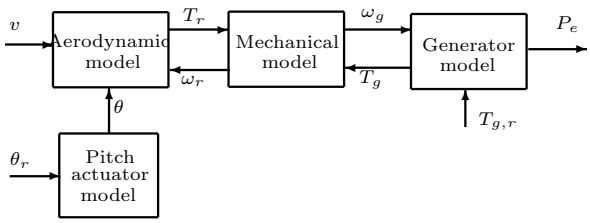

Figure A.2: Interconnection of sub-models describing the characteristics of the wind turbine

ator dynamics. Sub-models describing these characteristics will in the following be considered individually. The interconnections between these sub-models is illustrated in Fig. A.2. Detailed descriptions of the sub-blocks, and the associated mathematical models, are given in the following sections.

A.2.1 Mechanics

Fig. A.3 shows a schematic of the wind turbine mechanics. The turbine is split into two parts separated by the transmission: The rotor side and the generator side. The inertia on the rotor side J_r and generator side J_g are illustrated by the leftmost and the rightmost disk respectively. The shaft (drive train) connecting the rotor to the transmission is subject to immense torques that cause it to deflect. The shaft is appropriately modelled as a damped spring. This is illustrated by the damping D_s and the spring constant K_s. The gear ratio N_g is illustrated by the disks in the middle. On the left, the turbine is exited by the rotor torque T_r and on the right the generator torque T_g. The torques T_{sr} and T_{sg} are the torques on each side of the transmission, which are

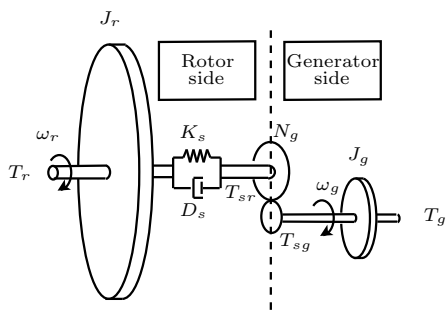

Figure A.3: Schematic of the wind turbine mechanics

related by the gear ratio:

$$T_{sg} = \frac{T_{sr}}{N_g} \tag{A.1}$$

The dynamics on the rotor side and generator side are described by (A.2) and (A.3).

$$\dot{\omega_r} J_r = T_r - T_{sr} \tag{A.2}$$

$$\dot{\omega_g} J_g = T_{sg} - T_g \tag{A.3}$$

where ω_r and ω_g are the rotational speeds on the rotor side and generator side respectively. Introducing a variable δ [rad] describing the deflection of the drive shaft, leads to the following equation describing the twist of the flexible shaft:

$$T_{sr} = D_s \dot{\delta} + K_s \delta \tag{A.4}$$

where

$$\dot{\delta} = \omega_r - \frac{\omega_g}{N_g} \tag{A.5}$$

A.2.2 Aerodynamics

The aerodynamic blades on the rotor converts the kinetic energy of the wind into mechanical energy, effectively providing the torque T_r on the rotor:

$$T_r = \frac{P_r}{\omega_r} \tag{A.6}$$

where the power P_r is given by the following relation [4]:

$$P_r = \frac{1}{2} \rho \pi R^2 v^3 c_p(\lambda, \theta) \tag{A.7}$$

ρ is the air density, R the wing radius and v the effective wind speed. c_p is the power coefficient which is a function of the blade pitch angle θ and the tip speed ratio λ defined below

$$\lambda = \frac{v}{v_{tip}} = \frac{v}{R\omega_r} \tag{A.8}$$

The power coefficients c_p for wind turbines are commonly attained utilizing blade element momentum (BEM) theory. A three dimensional plot of the power coefficient for a specific test turbine is shown in Fig. A.4.

Fig. A.5 shows iso-power curves given the power coefficient in Fig. A.4. The curves are calculated for the rotational speed fixed at the nominal value $\omega_{r,nom} =$

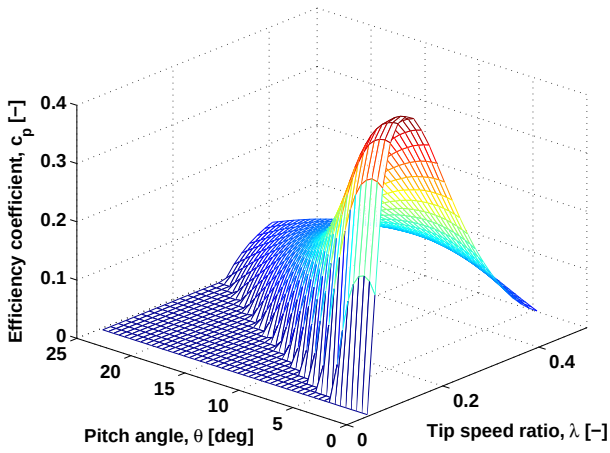

Figure A.4: The power coefficient c_p for the blades on the test turbine. Negative values have been truncated.

4.3 rad/s. Given the nominal power $P_{r,nom} = 225$ kW, Fig. A.5 shows that it is nessesary to decrease the efficiency of the blades when the effective wind speed exceeds approx. $v = 11$ m/s (ie. working in region IV). In the present work this is accomplished by increasing the pitch. Note that decreasing the pitch will also decrease the energy capture (socalled stall regulation [2]).

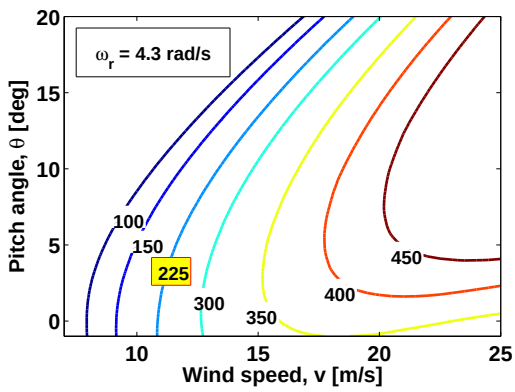

Figure A.5: Iso-power curves (kW) based on the power coefficient for the test turbine. The curves are generated at the nominal rotational speed.

A.2.3 Generator dynamics

The generator power is given by:

$$P_e = T_g \omega_g \tag{A.9}$$

As mentioned, the generator torque T_g can be controlled, however, it cannot be changed instantaneously. The dynamic response of the generator has therefore been modelled by a first order linear model with time constant τ_T:

$$\dot{T}_g = -\frac{1}{\tau_T} T_g + \frac{1}{\tau_T} T_{g,r} \tag{A.10}$$

$T_{g,r}$ is the reference and one of the control inputs for the wind turbine.

A.2.4 Pitch actuator

The pitch of the blades is changed by a hydraulic/mechanical actuator. A simplified model of the dynamics is presented by the following first order linear model:

$$\dot{\theta} = -\frac{1}{\tau_\theta} \theta + \frac{1}{\tau_\theta} \theta_r \tag{A.11}$$

θ_r is the reference and the other control input for the wind turbine.

A.2.5 Nonlinear state space description

Combining all the previous equations results in the following nonlinear state space model affine in the control variable.

$$\dot{x} = f(x, v) + Gu \tag{A.12}$$

$$= \begin{bmatrix} \frac{P_r(x_1, x_4, v)}{x_1 J_r} - \frac{x_1 D_s}{J_r} + \frac{x_2 D_s}{J_r N_g} - \frac{x_3 K_s}{J_r} \\ \frac{x_1 D_s}{J_g N_g} - \frac{x_2 D_s}{N_g^2 J_g} + \frac{x_3 K_s}{N_g J_g} - \frac{x_5}{J_g} \\ x_1 - \frac{x_2}{N_g} \\ -\frac{1}{\tau_\theta} x_4 \\ -\frac{1}{\tau_T} x_5 \end{bmatrix} + \begin{bmatrix} 0 & 0 \\ 0 & 0 \\ 0 & 0 \\ \frac{1}{\tau_\theta} & 0 \\ 0 & \frac{1}{\tau_T} \end{bmatrix} u \tag{A.13}$$

The state vector x and input vector u are defined as:

$$x = \begin{bmatrix}\omega_r & \omega_g & \delta & \theta & T_g\end{bmatrix}^T \tag{A.14}$$

$$u = \begin{bmatrix}\theta_r & T_{g,r}\end{bmatrix}^T \tag{A.15}$$

A.3 Wind model

Knowing the effective wind speed v and its time derivatives, makes it possible to compensate for wind speed fluctuations. However, the effective wind speed is an abstract quantity which describes the wind field experienced by the entire rotor disk. It is therefore not possible to obtain v directly from measurements.

In this work we therefore assume that the effective wind speed is described by a suitable stochastic model and that the states of this model can be estimated from measurements on the wind turbine. In the derivation of the control law in section A.4, only minor assumptions on this wind model will be made, however for the simulations in section A.5 a specific wind model will be used. Both the general model and the simulation model is introduced in this section.

A.3.1 General wind model

The control law presented in this paper allows for a general class of wind models. Therefore, to proceed in a general fashion it is assumed that the wind is described by the following finite dimensional nonlinear state space model:

$$\dot{w} = \alpha(w) + \beta(w)e \tag{A.16}$$

where e is a scalar stochastic process and the first element of w is equal to the effective wind speed ie.

$$w_1 = v \tag{A.17}$$

Additionally it is required that the relative degree between w_1 and e is larger than one (ie. e does not appear in $\dot{w}_1$). The reason for this requirement is justified in section A.4. The wind turbine model (A.12) is trivially augmented with the wind model (A.16), the resulting system is written in condenced form below:

$$\dot{w} = \alpha(w) + \beta(w)e \tag{A.18}$$

$$\dot{x} = f(x, w_1) + Gu \tag{A.19}$$

A.3.2 Simulation wind model

The simulations in section A.5 are based on a specific wind model which has been proposed in [11] and [12]. It is based on the observation that the effective wind speed can be described as a superposition of a slowly varying average wind speed v_m superimposed by a rapidly varying turbulent wind speed v_t ie. $v = v_m + v_t$. The mean wind speed is assumed measurable whereas the turbulent wind speed is described by a non-rational power spectrum which depends on v_m. For a fixed mean wind speed this spectrum can be reasonably approximated by a linear second order stochastic model driven by Gaussian distributed white noise [11]. Consequently, the effective wind speed can be described by the following state space model

$$\begin{bmatrix} \dot{w}_1 \\ \dot{w}_2 \end{bmatrix} = \begin{bmatrix} 0 & 1 \\ -a_1 & -a_2 \end{bmatrix} \begin{bmatrix} w_1 - v_m \\ w_2 \end{bmatrix} + \begin{bmatrix} 0 \\ k \end{bmatrix} e, \tag{A.20}$$

where $\begin{bmatrix} v & \dot{v} \end{bmatrix}^T = \begin{bmatrix} w_1 & w_2 \end{bmatrix}^T$ and $e \in N(0, 1^2)$. The parameters a_1, a_2 and k are scheduled according to v_m.

A.4 Nonlinear control law

This section will show that it is possible to compensate for the nonlinearities in the system and decouple the wind fluctuations. The tool with which the goal is accomplished is MIMO feedback linearization. Feedback linearization theory provides systematic methods with which nonlinear feedback compensators can be designed. This compensator is used in an inner loop which renders the system linear. Consequently, a linear controller can be designed for the compensated system. For a thorough review of the subject, readers are referred to [6] and [10]. Only input-state linearization will be considered in this paper.

A.4.1 Review of input-state linearization

This section provides the basics of input-state linearization. Consider a nonlinear system affine in the control variable

$$\dot{x} = f(x) + G(x)u = f(x) + \sum_{i=1}^{m} g_i(x) u_i, \tag{A.21}$$

where $x \in \mathbb{R}^n$, $u \in \mathbb{R}^m$ and $f(x), g_1(x), \ldots, g_m(x)$ are smooth vector fields defined on an open subset of $\mathbb{R}^n$. Assume that a diffeomorphic transformation

$$\begin{bmatrix} \eta \\ \xi \end{bmatrix} = T(x), \quad \eta \in \mathbb{R}^{n-r},\ \xi \in \mathbb{R}^r \tag{A.22}$$

exists, which brings the system to the following form:

$$\dot{\eta} = \phi(\eta, \xi) \tag{A.23}$$

$$\dot{\xi} = A\xi + B(f_\xi(x) + G_\xi(x)u) \tag{A.24}$$

The input state relation between u and ξ is input-state linearizable, since the following nonlinear feedback

$$u = G_\xi(x)^{-1}(-f_\xi(x) + \nu), \tag{A.25}$$

renders the relation between ν and ξ linear:

$$\dot{\xi} = A\xi + B\nu \tag{A.26}$$

The states η are readily decoupled from the input-state description (A.26) and are therefore denoted internal dynamics. If $r = n$ there are no internal dynamics and the system is said to be full-state linearizable.

A diffeomorphism which brings the system to feedback linearizable coordinates can be obtained through the solution to a set of partial differential equations [6]. Intuitively, this corresponds to finding m input-output relations with a total relative degree of $r = n$. This leads directly to a system description where the pair (A, B) is a canonical form. This is not necessarily the most intelligent choice since any useful structural properties are not considered. Essentially it takes all system with the same dimensions to the same canonical form. As shown in the next section we avoid such a transformation by exploiting that the nonlinearities only enter in a small part of the system description.

A.4.2 Input-state linearization applied to the wind turbine

It is interesting to note that when a diffeomorphic transformation confines the disturbances of the system to the internal dynamics, the input-state description (A.26) is effectively decoupled from these disturbances. In application to the augmented wind turbine model (A.18)-(A.19) we therefore seek a diffeomorphism which confines the stochastic process e to the internal dynamics such that the stochastic fluctuations can be decoupled from the feedback linearized system.

The nonlinearities of the turbine are confined to a subset of the system description. This structural property is easily exploited by choosing the following diffeomorphic transformation

$$\begin{bmatrix} w \\ T(w,x) \end{bmatrix} = \begin{bmatrix} w \\ x_1 - x_{1,0} \\ L_f x_1 \\ x_2 - x_{2,0} \\ x_3 - x_{3,0} \\ x_5 - x_{5,0} \end{bmatrix} = \begin{bmatrix} w \\ \xi \end{bmatrix}, \tag{A.27}$$

which essentially only touches the input-output channel between θ and ω_r. $x_{*,0}$ denotes stationary values. The transformed system takes the following form:

$$\dot{w} = \alpha(w) + \beta(w)e \tag{A.28}$$

$$\dot{\xi} = A\xi + B(f_\xi(x,w) + G_\xi(x,w)u+) \tag{A.29}$$

where

$$f_\xi(x,w) = \begin{bmatrix} \bar{L}^2_{\alpha,f} x_1 \\ 0 \end{bmatrix} \quad G_\xi(x,w) = \begin{bmatrix} \bar{L}_{\beta,g_1} \bar{L}_{\alpha,f} x_1 & 0 \\ 0 & 1 \end{bmatrix}$$

By the operator $\bar{L}$ we associate the following simple extension of the usual Lie derivative:

$$\bar{L}_{f,g} h(x,y) \equiv \begin{bmatrix} \frac{\partial h(x,y)}{\partial x} & \frac{\partial h(x,y)}{\partial y} \end{bmatrix} \begin{bmatrix} f(x,y) \\ g(x,y) \end{bmatrix}, \tag{A.30}$$

As indicated in the transformed system description (A.28)-(A.29), the stochastic process e is restricted to the internal dynamics. This is a consequence of the requirement that the relative degree between e and w_1 must be larger than 1.

By inspection it can be verified that f_ξ and G_ξ only depend on the wind model through the vector $w_s = \begin{bmatrix} w_1 & \frac{\partial w_1}{\partial w}\alpha(w) \end{bmatrix}^T = [v \ \dot{v}]^T$ ie.

$$f_\xi(x,w) \equiv f_\xi(x,w_s) \quad G_\xi(x,w) \equiv f_\xi(x,w_s) \tag{A.31}$$

Consequently, the effective wind speed and acceleration need to be known to compensate for the nonlinearities and the wind fluctuations.

The compensated wind turbine system is given by:

$$\dot{w} = \alpha(w) + \beta(w)e \tag{A.32}$$

$$\dot{\xi} = A\xi + B\nu \tag{A.33}$$

$$= \begin{bmatrix} 0 & 1 & 0 & 0 & 0 \\ 0 & 0 & 0 & 0 & 0 \\ \frac{D_s}{J_g N_g} & 0 & -\frac{D_s}{J_g N_g^2} & \frac{K_s}{J_g N_g} & -\frac{1}{J_g} \\ 1 & 0 & -\frac{1}{N_g} & 0 & 0 \\ 0 & 0 & 0 & 0 & -\frac{1}{\tau_T} \end{bmatrix} \xi + \begin{bmatrix} 0 & 0 \\ 1 & 0 \\ 0 & 0 \\ 0 & 0 \\ 0 & \frac{1}{\tau_T} \end{bmatrix} \nu \tag{A.34}$$

Hence, the variations in the wind speed have been completely decoupled from the closed loop wind turbine dynamics. Naturally, decoupling can only be attained perfectly given a perfect model and measurements. Although this requirement is not satisfied in real life, section A.5 shows that good performance can still be attained.

A.4.3 Linear controller for compensated system

The infinite horizon linear quadratic (LQ) controller has been chosen as the underlying linear control scheme in the nonlinear controller setup. Due to the inherent disturbances caused by non-perfect knowledge of the system, it is essential that integral control is utilized to robustify the system and minimize bias. The final design will be denoted LQI (linear quadratic integral). Since we are interested in stabilizing $P_e = x_2 x_5$ and $\omega_g = x_2$ the following first order approximation is introduced:

$$y = C\xi \tag{A.35}$$

$$= \begin{bmatrix} 0 & 0 & T_{g,nom} & 0 & \omega_{g,nom} \\ 0 & 0 & 1 & 0 & 0 \end{bmatrix} \bar{\xi} \tag{A.36}$$

This allows for the following trivial augmentation of the system

$$\begin{bmatrix} \dot{\xi} \\ \dot{z} \end{bmatrix} = \begin{bmatrix} A & 0 \\ C & 0 \end{bmatrix} \begin{bmatrix} \xi \\ z \end{bmatrix} + \begin{bmatrix} B \\ 0 \end{bmatrix} \nu \tag{A.37}$$

the first order approximation is reasonable since the closed loop system is designed so that the P_e and ω_g are close to their nominal values.

The LQI controller gain is obtained by minimizing cost (A.38) subject to (A.37).

$$J = \int_0^\infty \left(\begin{bmatrix} \xi \\ z \end{bmatrix}^T Q \begin{bmatrix} \xi \\ z \end{bmatrix} + \nu^T R \nu \right) dt \tag{A.38}$$

Figure A.6 shows a block diagram of the total setup for the nonlinear controller.

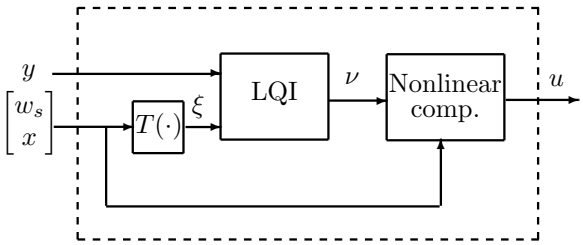

Figure A.6: Block diagram of the nonlinear controller

A.5 Simulations

This section presents simulations which test the performance of the nonlinear control algorithm. The nonlinear controller is compared to a LQG controller (also with integral action). The cost function used in the LQG design is almost equal to the one used in the nonlinear controller. The only difference is that θ is weighted instead of $\dot{\omega}_r$ due to the nonlinear state transformation. The wind model (A.20) has been used to provide the wind input to the turbine model.

Given ideal conditions (perfect model and full state information), the nonlinear control law is superior, since it effectively decouples the wind fluctuations. Perturbations have therefore been introduced to test the robustness of the controller.

A.5.1 Model perturbations

It is assumed that the physical output $y_1 = P_e$ and the turbine states x are measured. The measurements are perturbed with noise to reflect non-ideal knowledge of the system:

$$y_m = \begin{bmatrix} y_1 \\ x \end{bmatrix} + \zeta \tag{A.39}$$

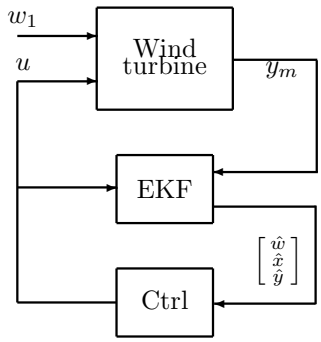

Figure A.7: Control setup with nonlinear controller and state estimator

Where y_m is the measurement vector and ζ is the measurement noise. The noise signals $\zeta_1, \zeta_2, \ldots, \zeta_6$ are modelled as uncorrelated Gaussian distributed white noise signals. The standard deviation is set to 1% of the stationary values. An extended Kalman filter has been designed to supply the estimates. The control setup is seen in figure A.7. To reflect a non-perfect knowledge of the power coefficient the 'true' c_p values are chosen to be 95% of the ones used in the controller.

A.5.2 Results

Figure A.8 shows the wind sequence used in the simulations. Fig. A.9 shows the response of P_e, ω_g and δ when controlled by the nonlinear controller and the LQG controller. Fig. A.10 shows the corresponding control signals.

The physical output P_e is compensated almost equally well by the two control strategies. However, the LQG controller does this at the cost of considerably larger control activity in the generator and larger stress on the turbine mechanics (ω_r, ω_g and δ). Hence, given the introduced perturbations, the nonlinear controller reduces the effect of the stochastic wind considerably better than the linear controller. As a final note it is worth mentioning that neither control strategy cause saturation of the actuators.

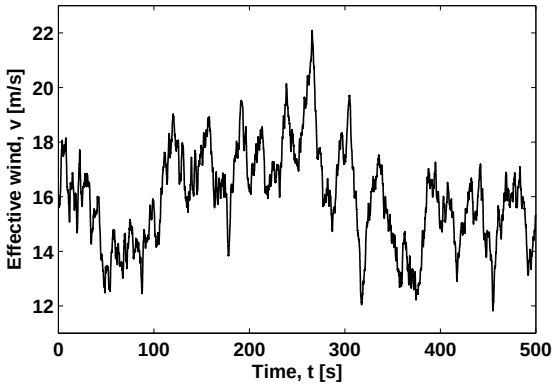

Figure A.8: Stochastic wind sequence used in simulations. The mean wind speed is v_m=16m/s.

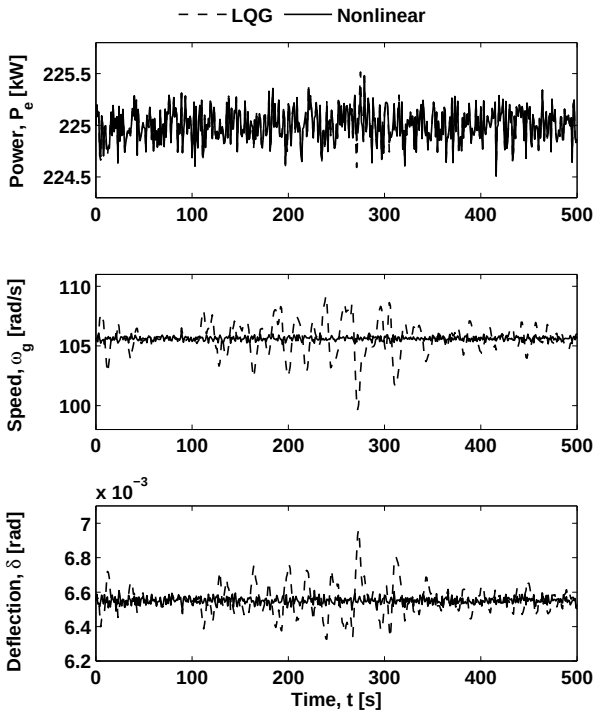

Figure A.9: Closed loop response associated with an LQG controller and the nonlinear controller

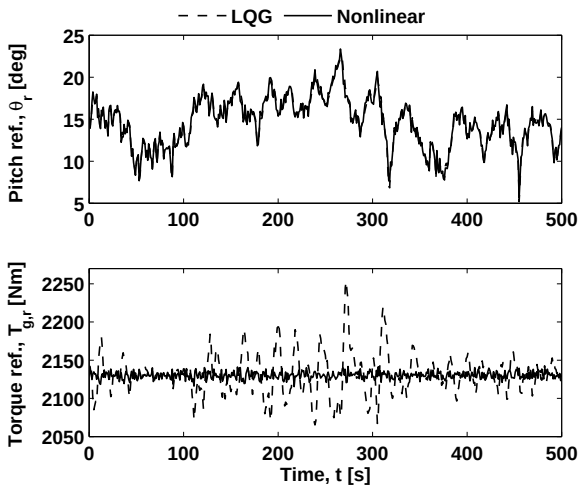

Figure A.10: Control signals from the LQG and nonlinear controller respectively.

A.6 Conclusion

A nonlinear control law based on feedback linearization has been designed for variable speed wind turbines in the present work. The main advantage of the control law is its ability to decouple the fluctuations in the wind from the dynamics of the turbine. Furthermore, the nonlinear compensation does not take the system to the usual canonical form but conserves large parts of the original dynamics. The control law assumes knowledge of the wind, but is valid for a fairly general class of wind models. Simulations with system perturbations show that the control law attenuates the effect of wind fluctuations effectively although the decoupling properties are essentially compromised. Comparison with a LQG controller shows the advantage gained using nonlinear control as compared to linear control.

Bibliography

[1] B. Boukhezzar and H. Siguerdidjane. Nonlinear control of variable speed wind turbines without wind speed measurement. *44th IEEE Conference on Decision and Control and European Control Conference 2005. CDC-ECC '05.*, pages 3456–3461, 2005.

[2] Tony Burton, David Sharp, Nick Jenkins, and Ervin Bossanyi. *Wind Energy Handbook*. Wiley, 2001.

[3] H. De Battista, R.J. Mantz, and C.F. Christiansen. Dynamical sliding mode power control of wind driven induction generators. *Energy Conversion, IEEE Transaction on*, 15(4):451 –457, 2000.

[4] DNV/Risø. *Guideline for design of wind turbines*. DNV/Risø, second edition, 2002.

[5] M.J. Grimble. Horizontal axis wind turbine control: comparison of classical, LQG and $\mathcal{H}_\infty$ designs. *Dynamics and Control*, 6(2):143–161, 1996. DOI:10.1007/BF02169534.

[6] Alberto Isidori. *Nonlinear Control Systems*. Springer, third edition, 1995.

[7] K.E. Johnson, L.Y. Pao, M.J. Balas, and L.J. Fingersh. Control of variable-speed wind turbines: standard and adaptive techniques for maximizing energy capture. *Control Systems Magazine, IEEE*, 26(3):70–81, 2006.

[8] D.J. Leith and W.E. Leithead. Implementation of wind turbine controllers. *International Journal of Control*, 66(3):349–380, 1997.

[9] M. Sedighizadeh, M. Kalantar, S. Esfandeh, and D. Arzaghi-Harris. Nonlinear model identification and control of wind turbine using wavenets. *Control*

Applications, 2005. CCA 2005. Proceedings of 2005 IEEE Conference on, pages 1057–1062, 2005.

[10] Jean-Jacques E. Slotine and Weiping Li. *Applied Nonlinear Control*. Prentice Hall, 1991.

[11] M. Xin. *Adaptive Extremum Control and Wind Turbine Control*. PhD thesis, Informatics and Mathematical Modelling, Technical University of Denmark, 1997.

[12] Ma Xin, Niels K. Poulsen, and Henrik Bindner. Estimation of wind speed in connection to wind turbine. In *Procededings for IASTED* International Conference on Control, Cancun, Mexico, pages 105–109, 1997.

Paper B

Individual pitch control of wind turbines using local inflow measurements

abstract

This paper describes a model based control approach for individually adjusting the pitch of wind turbine blades and thereby attenuating the effect of asymmetric wind loads. It is assumed that measurements of local inflow along each blade are available. This effectively provides an estimate of the load distribution along the blades. The load estimates are used in a predictive setup where inflow measured by one blade is used as basis for calculating future loads for the other blades. Simulations with a full stochastic wind field illustrate the effectiveness of the individual pitch controller as compared to controlling the pitch collectively.

B.1 Introduction

Wind turbines are subject to great attention due to their increasing importance in the energy production and their environmental properties. The demand for more and more power has set a trend for increasingly larger turbines. Increasing power efficiency and reducing mechanical and structural stress is therefore very important. One way to achieve this is through advanced model based control designs which explicitly take into account the challenging characteristics of wind turbines.

On the majority of modern wind turbines both the torque of the generator (variable speed control) and the pitch of the blades (pitch control) are used as control parameters for dealing with these challenges. In most documented research the pitch of the blades are controlled collectively applying a wide variety of methods. This ranges from linear methods such as LQ, LQG, and $\mathcal{H}_\infty$ ([2], [11], [3]) to adaptive techniques ([5]) and nonlinear methods such as feedback linearization ([7], [10]).

Collective pitch control has one major drawback: it is not possible to compensate for the asymmetric loads caused by the wind field. This can however be dealt with by using a strategy where the blades are pitched individually. Documented research on individual pitch control is more sparse. Most of the approaches assume that a collective pitch controller has been designed for the turbine and basically designs the individual pitch controllers as additional loops around the system (usually using classical control). This approach has eg. been taken in [1] and [6]. However it is more natural to formulate the turbine control problem as a MIMO problem taking into account the inherent cross-couplings in the system. A step in this direction was taken in [9] where the LQ method was used based on a periodic linear system description. The system description was obtained through numerical linearization of the aeroelastic code FAST. However, an analytical model suitable for model based individual pitch control has not been published.

The core contribution of this paper is the development of model elements for systematically designing individual pitch controllers. More specifically we derive a simplified model of the aerodynamics ie. a simplified description of the relation between the wind and the rotor loads which is suitable for individual pitch control. The wind is assumed to be measured through flow measurement devices along the blades. This knowledge can be used to gain information about future loads on the blades. It is shown how to use this as a model element suitable for controller design. Finally, it is illustrated how to combine these model elements (ie. model of aerodynamics and loads) together with a simple model of a wind turbine and formulate an optimal control problem. Simulations are used to

illustrate the advantages as compared to collective pitch control.

B.2 Method

Wind turbines extract power from the wind by converting the wind to lift forces using aerodynamic blades. This gives rise to a torque at the roots of the blades which causes a drive shaft to rotate inside a generator. This in effect produces energy. The presence of the wind turbine cause the wind field to slow down and rotate as indicated in Fig. B.1. This interaction between the blades and

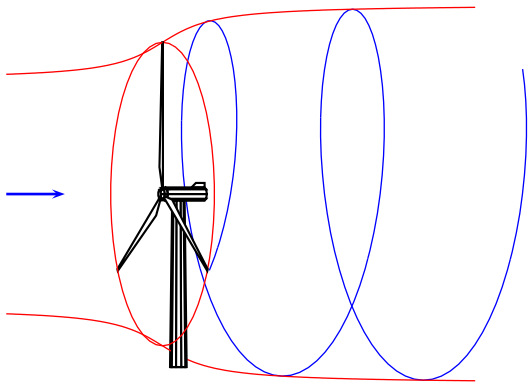

Figure B.1: Sketch of a horizontal axis wind turbine

the wind is very complex. Highly accurate models of the interaction are therefore unsuitable for model based controller designs. This section describes the approach we have taken in order to deal with this complexity. More specifically the following is described:

- Simplified model of aerodynamics and wind field
- Prediction of future loads based on local inflow measurements

B.2.1 Simplified model of aerodynamics and wind field

Simplified models of both the aerodynamics and the wind field are usually used when designing collective pitch controllers for wind turbines (See eg. [11], [10]). These models do not carry enough spatial information such that individual pitch controllers can be designed. However, the same general ideas used in collective

pitch control can be extended to individual pitch control. In the following we explain how.

With blade element momentum theory (BEM) it is possible to calculate how much torque that is delivered at the blade root owing to the wind field (See eg. [4]). This is in general an iterative procedure which cannot be used as a model element in a model based control design. Assuming a uniform wind field one can, however, calculate static relations from the wind speed v, rotational speed ω_r and pitch angles $\theta_1,\ \theta_2, \ldots,\ \theta_b$ (where b denotes the number of blades) to the root moments normal T_{N_i} and tangential T_{T_i} to the rotor disk ie.

$$T_{N_i} = g_N(v, \omega_r, \theta_i), \quad T_{T_i} = g_T(v, \omega_r, \theta_i) \tag{B.1}$$

where $i = 1, 2, \ldots, b$. It is important to note that induction is implicitly included in these relations. Hence v is the wind speed *without* induction. Induction is the phenomena that the presence of the rotor decreases the wind speed in the axial direction (axial induction) and cause the wind field to rotate (tangential induction). In Fig. B.2 this is illustrated for a cross-section element (airfoil) of a wind turbine blade rotating with angular velocity ω_r. The local radius is r. a and a' are called the axial and tangential induction factors respectively. v_r is the actual wind speed experienced by the blade element which has the angle of attack α. These two quantities, v_r and α, constitutes the so called local inflow measurements.

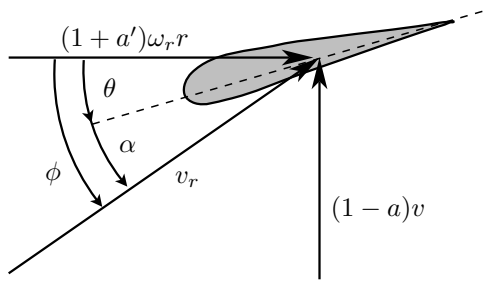

Figure B.2: Wind interaction with a cross-sectional element (airfoil) of a wind turbine blade.

The total tangential torque $T_T = \sum_{i=1}^{b} T_{T_i}$ with T_{T_i} given in (B.1) is widely used when designing collective pitch controllers. Since the wind field is nonuniform in real life the wind field is usually approximated with a single scalar that describes it as a whole. This is denoted the effective wind speed. Motivated by this approach we individually assign effective wind speeds for each blade to

obtain spatial resolution. We will denote these effective winds by $\bar{v}_1$, $\bar{v}_2$, ..., $\bar{v}_b$. The definition of effective wind speed which has been found suitable in this work is based on the definition in [8]. The definition is extended to comply with our specific needs.

To derive the effective wind speeds we linearize the blade root moment with respect to the wind along the span of the blade.

$$T_{N_i} = T_{N_i,0} + \int_{r_0}^{R} W_{N_i}(r)(v_i(r) - V_0)dr \tag{B.2}$$

$$T_{T_i} = T_{T_i,0} + \int_{r_0}^{R} W_{T_i}(r)(v_i(r) - V_0)dr, \tag{B.3}$$

where

$$W_{N_i}(r) = \frac{\partial T_{N_i}}{\partial v_i(r)} \quad W_{T_i}(r) = \frac{\partial T_{N_i}}{\partial v_i(r)}, \; i = 1, 2, \ldots, b \tag{B.4}$$

and $i = 1, 2, \ldots, b$. V_0 is the mean wind speed of the wind field. r_0 is the hub radius and R is the rotor radius. $W_{T_i}(\cdot)$ and $W_{N_i}(\cdot)$ can be regarded as influence or weight coefficient.

The effective wind speeds are now introduced as the constant quantities $\bar{v}_{N_i}$ and $\bar{v}_{T_i}$ that results in the same moments when substituting $v_i(r)$ in the equations (B.2)-(B.3):

$$T_{N_i} = T_{N_i,0} + \int_{r_0}^{R} W_{N_i}(r)(\bar{v}_{N_i} - V_0)dr \tag{B.5}$$

$$T_{T_i} = T_{T_i,0} + \int_{r_0}^{R} W_{T_i}(r)(\bar{v}_{T_i} - V_0)dr \tag{B.6}$$

where $i = 1, 2, \ldots, b$. Equating (B.2)-(B.3) with (B.5)-(B.6) leads to the following expression for the effective wind speed.

$$\bar{v}_{N_i} = \frac{\int_{r_0}^{R} W_{N_i}(r)v_i(r)dr}{\int_{r_0}^{R} W_{N_i}(r)} \tag{B.7}$$

$$\bar{v}_{T_i} = \frac{\int_{r_0}^{R} W_{T_i}(r)v_i(r)dr}{\int_{r_0}^{R} W_{T_i}(r)}, \; i = 1, 2, \ldots, b \tag{B.8}$$

What needs to be determined are the functions $W_{N_i}(\cdot)$ and $W_{T_i}(\cdot)$. Calculating these "exactly" (using BEM) involves total knowledge of the entire wind field swept by the blades. However, as stated in [8] a typical load distribution will be approximately proportional to r eg. $W_{N_i} = K \cdot r$ where K is some constant. It is easily verified that this results in $\bar{v}_{N_i} = \bar{v}_{T_i}$. Better weights may be attained

using knowledge of the blade elements, but either way we will be dealing with an approximation. In connection to real-time control this simple weight is also more suitable from a computational point of view. In the following we assume that:

$$\bar{v}_{N_i} = \bar{v}_{T_i} = \bar{v}_i \tag{B.9}$$

Using these effective wind speeds in the relations (B.1) we have directly a simplified model of the aerodynamics suitable for model based individual pitch control:

$$T_{N_i} = g_N(\bar{v}_i, \omega_r, \theta_i), \quad T_{T_i} = g_T(\bar{v}_i, \omega_r, \theta_i) \tag{B.10}$$

We have now established a simplified relation between the velocities (without induction) along the blades $v_i(r)$ and the root moments by relating $v_i(r)$ with $\bar{v}_i$. Knowing $v_i(r)$ we can therefore take this relation into consideration in a model based controller. However, we cannot measure $v_i(r)$ since this is the wind as it would look *without* axial induced speeds caused by the presence of the rotor. What we can measure is the local inflow along the blade ie. α and v_r as seen in Fig. B.2. Therefore, in order to attain $v_i(r)$ it is necessary to calculate the axial induction factor a. Using basic BEM theory (See [4]) we can approximate a by:

$$a = \frac{1}{\frac{4\sin(\phi)^2}{s \cdot c_N} + 1}, \quad s = \frac{c \cdot b}{2\pi r} \tag{B.11}$$

where c is the local cord length and c_N is a blade coefficient.

In summary, by measuring the angle of attack and the relative velocity it is possible to estimate the effective wind speed for each blade and use these in the controller design. The total algorithm for attaining estimates of the root moments based on inflow measurements is summarized in table B.1.

Table B.1: Algorithm for attaining root moments based on inflow measurements

	Action
1	Measure α and v_r along the blade
2	Use BEM theory to attain $v_i(r)$
3	Use a suitable weight to calculate the effective wind speeds
4	Calculate moments based the simplified aerodynamics

Remark 2. *It is possible to measure the inflow using flow measurement devices such as pitot tubes (See [6] and references therein). These measurements will in practice be of varying reliability, however this issue is beyond the scope of this work.*

Remark 3. *The inflow can be measured at discrete points along the blades. Therefore, when applying the method all the integrals will be substituted by finite sums.*

B.2.2 Model for future disturbances

The setup presented so far illustrates that it is possible to take into account the presence of an asymmetric wind field in a model with a complexity suitable for model based control. However, if our model does not describe the future evolution of the loads this puts heavy restrictions on the controller design.

The effective wind speeds $\bar{v}_i$ are independent of the induction caused by the presence of the rotor. Consequently it can be seen as a measure of the power in the wind which is independent of the presence of the rotor. It is therefore natural to setup a model of the evolution of $\bar{v}_i$.

In model based collective pitch control a common approach is to setup a stochastic model of the effective wind (See eg. [11]) and incorporate this model in the controller design. We will apply a more simple approach which is made possible through the local inflow measurements. When a blade passes through an area on the rotor disk we estimate the effective wind speed for this blade as described earlier. The slowly varying trends in the wind (such as wind shear) are likely to be present from the time that one blade passes an area to the next blade does. This estimate can therefore be used as an assessment of the future wind speed experienced by the next blade to pass through the area. Fig. B.3 illustrates the idea

This just needs to be formulated systematically such that it can be included in a controller design. The following discrete time model can be used to tell our control design that we know the wind evolution H_d time steps into the future.

$$w_i(k+1) = \underbrace{\begin{bmatrix} 0 & 1 & 0 & \cdots & 0 \\ 0 & 0 & 1 & \cdots & 0 \\ \vdots & \vdots & \vdots & \ddots & \vdots \\ 0 & 0 & 0 & \cdots & 1 \\ 0 & 0 & 0 & \cdots & 0 \end{bmatrix}}_{F_i} w_i(k) \tag{B.12}$$

$$d_i(k) = \underbrace{\begin{bmatrix} 1 & 0 & \cdots & 0 \end{bmatrix}}_{M_i} w_i(k), \; i = 1, 2, \ldots, b \tag{B.13}$$

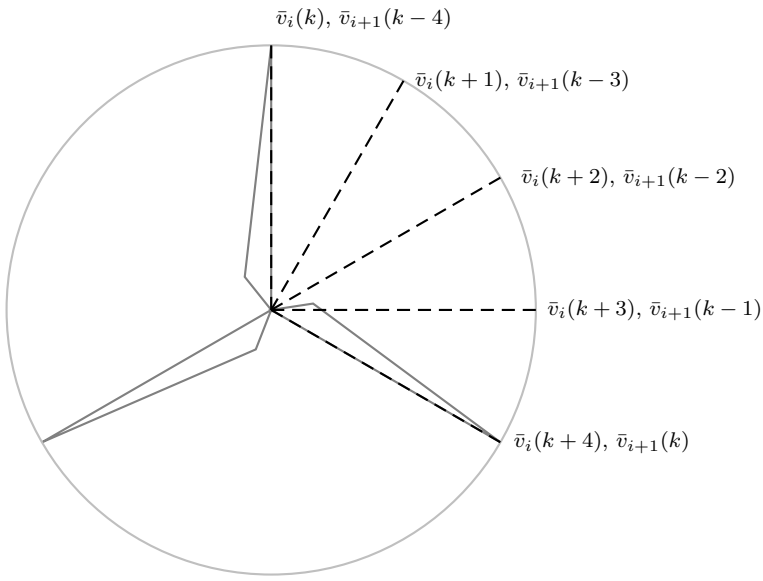

Figure B.3: The blades enter the same spatial regions. Winds experienced by one blade are therefore correlated with winds experienced by the next blade.

where the state vector is

$$w_i(k) = \begin{bmatrix} \Delta\bar{v}_i(k) & \Delta\bar{v}_i(k+1) & \cdots & \Delta\bar{v}_i(k+H_d) \end{bmatrix}^T \tag{B.14}$$

ie. it contains our knowledge of the wind H_d time steps into the future. The total effective wind speed is

$$\bar{v}_i(k) = d_i(k) + V_0 \tag{B.15}$$

where V_0 is the mean wind speed. The total wind model for all blades becomes:

$$w(k+1) = Fw(k) \tag{B.16}$$

$$d(k) = Mw(k) \tag{B.17}$$

where $w(k) = \begin{bmatrix} w_1^T(k) & w_2^T(k) & \cdots & w_b^T(k) \end{bmatrix}^T$. F and M are block diagonal matrices eg. $F = \mathrm{diag}(F_1,\ F_2, \ldots, F_b)$.

B.3 Control design

In this section we combine the simplified aerodynamic model derived in the previous section with a dynamic model of the wind turbine. The model is

linearized, discretized and augmented with the predictive wind model (B.12)-(B.13). We then design a controller using the linear quadratic method. The controller is designed for operation at high wind speeds where the rotational speed and the produced power should to be stabilized at nominal values.

B.3.1 Nonlinear design model

The wind turbine model used in this work models the following dominant characteristics: Aerodynamics, mechanics, actuators and a variable speed generator. The interconnection of the model parts is shown in Fig. B.4.

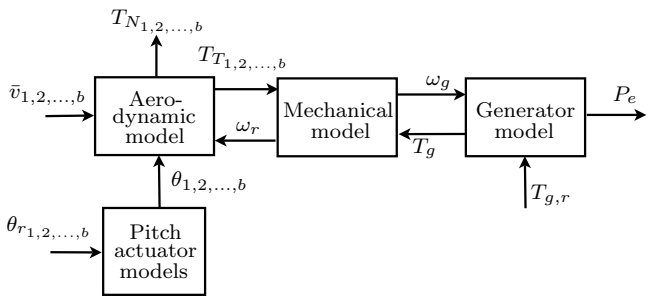

Figure B.4: Diagram showing the interconnection between the model parts

The aerodynamics is simply described by the relations (B.10) and the pitch actuator systems are approximated by first order systems ie.:

$$\dot{\theta}_i = -\frac{1}{\tau_\theta}\theta_i + \frac{1}{\tau_\theta}\theta_{r,i}, \; i = 1, 2, \ldots, b \tag{B.18}$$

A schematic of the mechanics is shown in Fig. B.5. The leftmost and rightmost disks represent the inertia on the rotor side J_r and the generator side J_g of the transmission respectively. The small disks in the middle represents the gear ratio N_g in the transmission. The flexibility of the shaft connected to the blades is represented by an equivalent spring constant and damping. The dynamic equations for the mechanics are:

$$\dot{\omega}_r = \frac{\sum_{i=1}^{b} T_{T_i}}{J_r} - \frac{\omega_r D_s}{J_r} + \frac{\omega_g D_s}{J_r N_g} - \frac{\delta K_s}{J_r} \tag{B.19}$$

$$\dot{\omega}_g = \frac{\omega_r D_s}{J_g N_g} - \frac{\omega_g D_s}{N_g^2 J_g} + \frac{\delta K_s}{N_g J_g} - \frac{T_g}{J_g} \tag{B.20}$$

$$\dot{\delta} = \omega_r - \frac{\omega_g}{N_g} \tag{B.21}$$

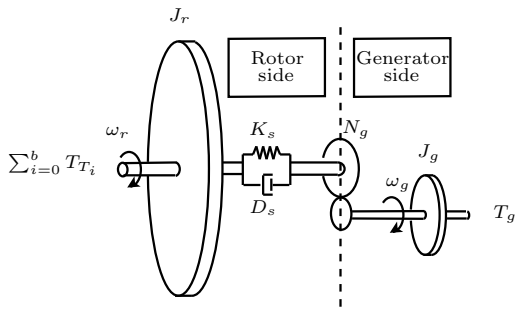

Figure B.5: Schematic of mechanics

where δ is the torsional deflection of the flexible drive shaft.

The power produced by the generator is given as (assuming a lossless generator):

$$P_e = \omega_g T_g \tag{B.22}$$

where the generator torque T_g can be varied. The torque demand $T_{g,r}$ versus the actual torque T_g is related through a first order response:

$$\dot{T}_g = -\frac{1}{\tau_T} T_g + \frac{1}{\tau_T} T_{g,r} \tag{B.23}$$

Combining all differential equations the result is a (4+b)th order nonlinear state space system

$$\dot{x} = f(x, u, d) \tag{B.24}$$

where the state x, input u and disturbance vector d are

$$x = \begin{bmatrix} \omega_r & \omega_g & \delta & \theta_1 & \theta_2 & \cdots & \theta_b & T_g \end{bmatrix}^T \tag{B.25}$$

$$u = \begin{bmatrix} \theta_{r,1} & \theta_{r,2} & \cdots & \theta_{r,b} & T_{g,r} \end{bmatrix}^T \tag{B.26}$$

$$d = \begin{bmatrix} \bar{v}_1 & \bar{v}_2 & \cdots & \bar{v}_b \end{bmatrix}^T \tag{B.27}$$

The physical output of the wind turbine is naturally P_e. However with control in mind it is natural to specify an output vector with the variables which we want to control. As mentioned earlier these are first and foremost the rotational speed and the generator power. Additionally we also want to attenuate the asymmetric loads. This leads to the following output vector:

$$y = h(x, d) \tag{B.28}$$

$$= \begin{bmatrix} \Delta\omega_g & \Delta P_e & \Delta T_{N_{1,2}} & \Delta T_{N_{2,3}} & \cdots & \Delta T_{N_{b-1,b}} \end{bmatrix}^T \tag{B.29}$$

Where Δ denotes deviations away from nominal values and $\Delta T_{N_{i,j}} = T_{N_i} - T_{N_j}$ ie. the difference between the root moments normal to the rotor disk for blade i and j. If we stabilize these differences at zero the loads will be perfectly symmetric.

B.3.2 Linear design model including wind model

The system equation (B.25) and the output equation (B.28) are linearized at conditions corresponding to a given mean wind speed. Furthermore, the model is discretized. The resulting model is:

$$x(k+1) = Ax(k) + Bu(k) + D_1 d(k) \tag{B.30}$$

$$y(k) = Cx(k) + D_2 d(k) \tag{B.31}$$

where x, u, y and d here denotes deviations from the point of linearization rather than absolute values. To include the predictive model of the wind in the design we augment the model with the wind model. Furthermore, to attain zero steady state error we add integral states corresponding to the vector y. The integral state vector is denoted y_I. The total augmented system becomes.

$$\begin{bmatrix} x(k+1) \\ y_I(k+1) \\ w(k+1) \end{bmatrix} = \begin{bmatrix} A & 0 & D_1 M \\ C & I & D_2 M \\ 0 & 0 & F \end{bmatrix} \begin{bmatrix} x(k) \\ y_I(k) \\ w(k) \end{bmatrix} + \begin{bmatrix} B \\ 0 \\ 0 \end{bmatrix} u(k) \tag{B.32}$$

$$y(k) = \begin{bmatrix} C & 0 & D_2 M \end{bmatrix} \begin{bmatrix} x(k) \\ y_I(k) \\ w(k) \end{bmatrix} \tag{B.33}$$

B.3.3 Linear controller

Having set up the linear design model the controller is designed using the standard LQ algorithm that gives a feedback law which minimizes the infinite horizon cost:

$$V = \sum_{k=0}^{\infty} \left\| \begin{matrix} y(k) \\ y_I(k) \end{matrix} \right\|_Q^2 + ||u(k)||_R^2 \tag{B.34}$$

where $||q||_W^2 = q^T W q$. The result is the linear feedback law

$$u(k) = -K \begin{bmatrix} x(k) \\ y_I(k) \\ w(k) \end{bmatrix} \tag{B.35}$$

In this design procedure we indirectly tell the design algorithm that we know the evolution H_d time steps into the future.

Remark 4. *Solving for the feedback gain K will naturally be computationally extensive when H_d is large. However, this is an offline calculation and will have no influence when doing real time control.*

B.4 Simulations

In this section results from simulations with the described controller design is presented. The parameters for the model (except the aerodynamics) are seen in table B.2.

Table B.2: Parameters for simulation model

Parameter	Value
b	3
N_g	87.97
K_s	$5.6 \cdot 10^9$ N/rad
D_s	$1 \cdot 10^7$ N/rad·s
J_g	53 kg·m^2
J_r	$2.956 \cdot 10^6$ kg·m^2
R	36.75 m
τ_θ	0.15 s
τ_T	0.1 s

The nominal speed of the turbine is $\omega_g = 185$ rad/s and the nominal power is $P_e = 1.5$ MW. The parameter values are adopted from a wind turbine model (WindPACT 1.5 MW) included in the distribution of the aeroelastic code `FAST`. `FAST` is developed by the National Renewable Energy Laboratory (NREL) in USA. To simulate realistic wind turbine aerodynamics a BEM algorithm is used to calculate the loads on the blades. The code `TurbSim` developed by NREL is used for generating a stochastic wind field. The wind time-series which is generated by `TurbSim` is a 10×10 grid of correlated point winds evolving in time. The mean wind speed for the times series is $V_0 = 16$m/s and an exponential shear is superimposed on the wind field. As basis for comparison the individual controller is compared to a collective pitch controller designed using the LQ method. The collective and individual controller designs are equivalent where possible. A sample time of $T_s = 0.01$s is used for the controllers and a prediction horizon of $H_d = 40$ is used in the individual pitch controller design.

Fig. B.6 shows the moments normal to the rotor disk for each blade when the turbine is controlled by both controllers. It is seen that the blade moments for the collective controller exhibit the same periodic trend (due to shear) but with different phase. It is readily seen that this periodic trend is heavily attenuated in the simulation with the individual pitch controller. Fig. B.7 shows the associated control signals for both controllers. The periodic trend seen in the loads associated with the collective pitch controller is naturally reflected in the control signals for the individual pitch controller.

Transforming the local moments to the yaw and tilt axis of the wind turbine, the effect of the individual controller becomes very apparent. This is seen in Fig. B.8 and B.9 respectively. The effect of the asymmetric wind field is attenuated to a high degree with the individual pitch controller.

Fig. B.10 shows the rotational speed w_g and the power P_e which were both objectives in the controller designs. Although the individual pitch controller has the additional objective to minimize asymmetric loads it gives approximately the same response for ω_g and P_e as the collective pitch controller.

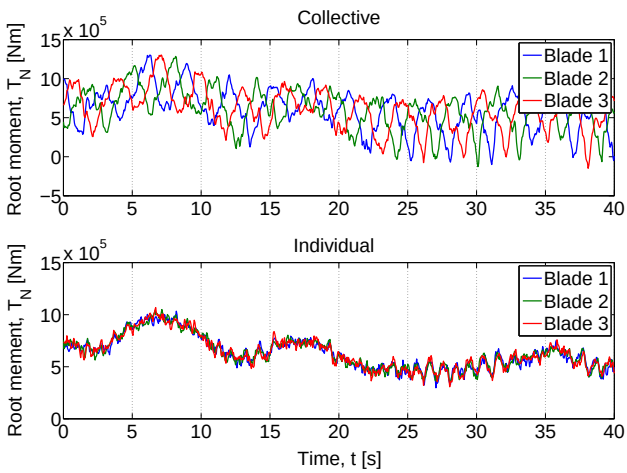

Figure B.6: Blade root moments normal to the rotor plane. Top: wind turbine controlled by collective controller. Bottom: wind turbine controlled by individual controller

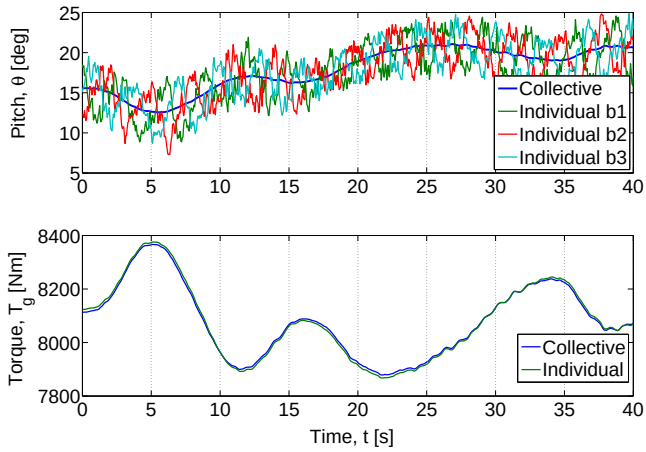

Figure B.7: Control signals for collective and individual pitch controller

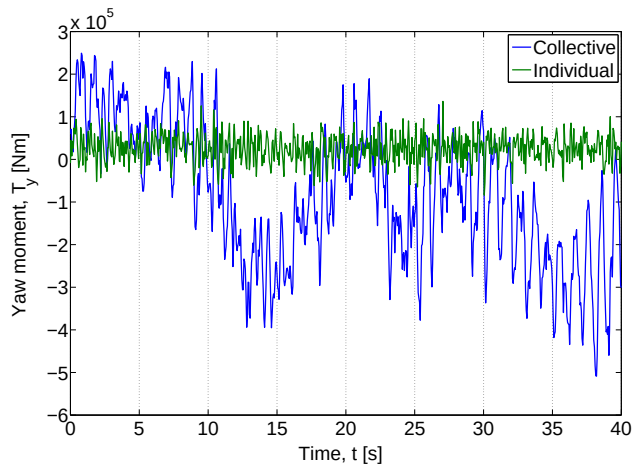

Figure B.8: Yaw moment when controlled by collective and individual pitch controller

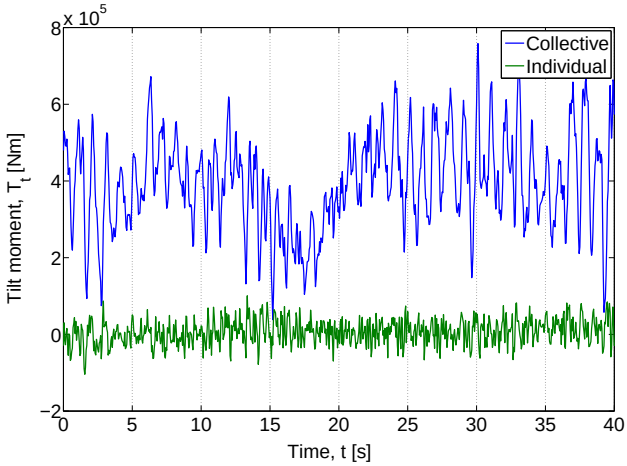

Figure B.9: Tilt moment when controlled by collective and individual pitch controller

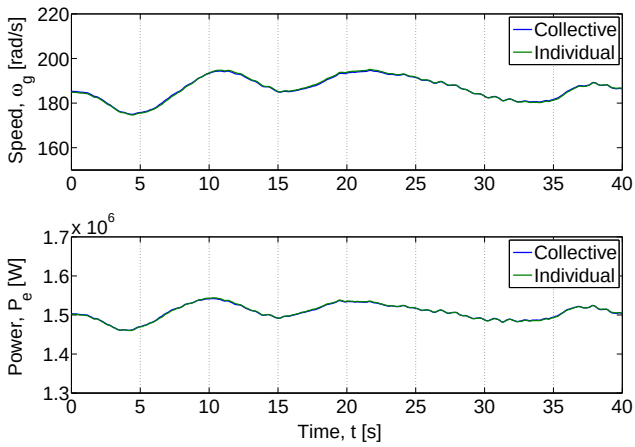

Figure B.10: Rotational speed ω_g and power P_e when controlled by collective and individual pitch controller

B.5 Conclusion

A framework for individual pitch control has been described in this paper. The framework relies on the notion of effective wind speed for each wind turbine blade. Knowing these effective wind speeds it is possible to attain estimates of the future blade root moments. It has been demonstrated how to derive the effective wind speeds based on local blade flow measurements along the blade. Furthermore, we have suggested to use the wind speeds experienced by advancing blades as future measurements for the other blades. The combined framework allows for systematically designing model based individual pitch controller in combination with variable speed control. Finally, it has been illustrated how to design a model based controller based on the framework and it is shown that a significant reduction of the asymmetric loads can be achieved.

Bibliography

[1] E.A. Bossanyi. Individual Blade Pitch Control for Load Reduction. *Wind Energy*, 6(2):119–128, 2003. DOI: 10.1002/we.76.

[2] E.A. Bossanyi. Wind turbine control for load reduction. *Wind Energy*, 6(3):229–244, 2003. DOI:10.1002/we.95.

[3] M.J. Grimble. Horizontal axis wind turbine control: comparison of classical, LQG and $\mathcal{H}_\infty$ designs. *Dynamics and Control*, 6(2):143–161, 1996. DOI:10.1007/BF02169534.

[4] M. O. L. Hansen. *Aerodynamics of Wind Turbines*. James & James, 2000.

[5] K.E. Johnson, L.Y. Pao, M.J. Balas, and L.J. Fingersh. Control of variable-speed wind turbines: standard and adaptive techniques for maximizing energy capture. *Control Systems Magazine, IEEE*, 26(3):70–81, 2006.

[6] T.J. Larsen, H.A. Madsen, and K. Thomsen. Active load reduction using individual pitch, based on local blade flow measurements. *Wind Energy*, 8(1):67–80, 2005. DOI:10.1002/we.141.

[7] D.J. Leith and W.E. Leithead. Implementation of wind turbine controllers. *International Journal of Control*, 66(3):349–380, 1997.

[8] P. Sørensen, A.D. Hansen, and P.A.C. Rosas. Wind models for simulation of power fluctuations from wind farms. *Journal of Wind Engineering & Industrial Aerodynamics*, 90(12-15):1381–1402, 2002.

[9] K.A. Stol, W. Zhao, and A. D. Wright. Individual blade pitch control for the controls advanced research turbine (cart). *Journal of Solar Energy Engineering*, 128:498–505, November 2006. DOI:10.1115/1.2349542.

[10] S.C. Thomsen and N.K. Poulsen. A disturbance decoupling nonlinear control law for variable speed wind turbines. In *Proceedings of the 15th Mediterranean Conference on Control and Automation*, pages 1268–1273, 2007.

[11] M. Xin. *Adaptive Extremum Control and Wind Turbine Control*. PhD thesis, Informatics and Mathematical Modelling, Technical University of Denmark, 1997.

Paper C

MPC for uncertain systems using the Youla parameterizations

abstract

Several approaches have been taken in the past to deal with uncertainty in constrained predictive control. The major drawbacks of these efforts are usually either conservativeness and/or on-line computational complexity. In this work we examine the possibility of dealing with uncertainty through the use of the primary and the dual Youla parameterizations. The dual Youla parameter can be seen as a frequency weighted measure of the uncertainty and the primary Youla parameter can be seen as a controller for this uncertainty. The work is an application of the methodology in [12] to constraint control.

C.1 Introduction

Model predictive control (MPC) - also commonly denoted constrained predictive control - is a model based control method which has attracted a lot of attention partly due to its popularity in the process industry. The feature which makes it truly innovative is its ability to handle constraints on control action and states/output. This is done through on-line optimization of the future trajectory based on a cost function. The theoretical foundation of nominal linear MPC has matured over the last decades and well established theorems for ensuring stability and feasibility have been established (See eg. [6], [7]).

There has also been established theories for dealing with model uncertainty and disturbances in MPC. These methods are commonly denoted robust MPC (RMPC). Invariant sets have proved effective to deal explicitly with these challenges and still leading to computational tractable problems. This usually leads to optimization problems involving constraints on the form of linear matrix inequalities [3][4][14]. Using this framework it is possible to guarantee (under certain conditions) that the constraints on control actions and states will never be violated. However, there are drawbacks with these methods: The optimization problem, although tractable, can be very complicated compared to basic MPC and therefore typically more computationally expensive. Furthermore, they have a tendency to be overly conservative. Due to the conservative nature of these methods, the trajectory of the system will generally not get very close to the constraints. However, MPC is usually employed in applications where it is attractive to work near the constraints.

We want to avoid the conservative nature of RMPC and still be able to deal with the uncertainties in some sense. In this work we therefore consider a framework with which to handle uncertainty through identification of the unmodeled dynamics. More specifically we identify the dual Youla parameter which can be considered a frequency weighted measure of the uncertainty. We then use the inherent relationship between the dual Youla parameter and primary Youla parameter to design an MPC controller with the objectives of both reducing sensitivity towards the uncertainty and obeying constraints. The idea of using the relationship between the primary and the dual Youla parameter in controller design has been used to design performance enhancing controllers for uncertain plants in [12]. The contribution of the work in this paper is an extension so that it can be incorporated in a natural way in constrained predictive control.

The Youla parameter has previously been used to design MPC controllers with reduced sensitivity towards disturbances in [9][10]. Since sensitivity toward disturbances is reduced the predictions are believed to be more reliable during constraint control. Although some of the same principles are used, it is stressed

that the framework in [9][10] has little resemblance to the framework derived in this paper.

C.2 Notation

We make use of the following matrix notation: $I_{N\times N}$ denotes the N-dimensional identity matrix. I_N denotes an N-dimensional column vector with ones. $\otimes$ denotes the Kronecker product. We will use the following short notation for the extended observability matrix and Toeplitz matrix:

$$\mathcal{O}^N(A,C) = \begin{bmatrix} C^T & (CA)^T & (CA^2)^T & \cdots & (CA^N)^T \end{bmatrix}^T \tag{C.1}$$

$$\mathcal{T}^N(A,B,C,D) = \begin{bmatrix} D & 0 & \cdots & 0 & 0 \\ CB & D & \cdots & 0 & 0 \\ CAB & CB & \cdots & 0 & 0 \\ \vdots & \vdots & \ddots & \vdots & \vdots \\ CA^{N-1}B & CA^{N-2}B & \cdots & CB & D \end{bmatrix} \tag{C.2}$$

The notation $\|x\|_W^2$ is used to denote the weighted 2-norm of a vector x ie.

$$\|x\|_W^2 = x^T W x \tag{C.3}$$

C.3 Setup and preliminaries

C.3.1 System setup

We consider the following linear discrete time-invariant system:

$$\Sigma = \begin{pmatrix} G_{qp} & G_{qu} \\ G_{yp} & G_{yu} \end{pmatrix} \tag{C.4}$$

$u_k \in \mathbb{R}^{n_u}$ is the control input. $p_k \in \mathbb{R}^{n_p}$ is the disturbance input. $q_k \in \mathbb{R}^{n_q}$ is an auxiliary output. $y_k \in \mathbb{R}^{n_y}$ is a measurable output. The uncertainty enters the system through the relation

$$p_k = \Delta q_k \tag{C.5}$$

where Δ is an unknown LTI perturbation. The system is assumed controlled by the controller K

$$u_k = K y_k \tag{C.6}$$

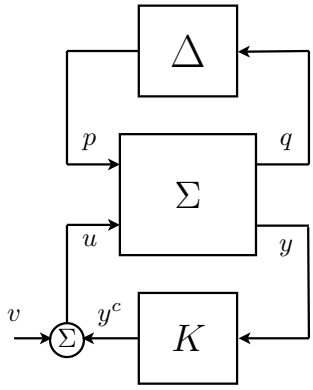

Figure C.1: System setup: The system is controlled by the feedback controller K which stabilizes Σ subject to the unknown LTI system Δ.

It is assumed that K has been designed such that the system is robustly stable for

$$\|\Delta\|_\infty = \sup_{|z|=1} \sigma_{max}(\Delta(z)) \leq 1 \tag{C.7}$$

where σ_{max} is the maximum singular value. The setup is illustrated in Fig. C.1. The auxiliary signal $v_k \in \mathbb{R}^{n_u}$ shown in the figure will be used to avoid constraint violation.

C.3.2 Model predictive control

Model predictive control (MPC) [6] or constrained predictive control is a receding horizon methodology where an optimization problem is solved at every sample time k. We introduce MPC in the context of the prestabilized system in Fig. C.1. The basic idea is to find the control sequence $V_k = \{v_k,\ v_{k+1},\ \ldots,\ v_{k+N}\}$ which minimizes a finite horizon cost. One then uses the first element of V_k as the control action. In the nominal case $\Delta = 0$ the cost is commonly a quadratic cost on output y_k and input v_k

$$J_k = \sum_{i=k}^{N+k} \|y_i\|^2_{W_y} + \|v_i\|^2_{W_v} \tag{C.8}$$

where $W_y \geq$ and $W_v > 0$ are suitable weighting matrices. Linear constraints on output and input are usually included and can be written on the form

$$P_y y_{i+1} \leq I_{n_{cy}} \quad k \leq i \leq N-1 \tag{C.9}$$

$$P_u u_i \leq I_{n_{cu}} \tag{C.10}$$

over the finite control horizon. The n_{cy} and n_{cu} denotes the number of output and input constraints respectively. The basic optimization problem is easily written explicitly as a problem in the control sequence V_k ie. as a static optimization problem. The problem with constraints can then be solved using a quadratic programming (QP) solver.

C.3.3 The Youla parameterizations

The Youla parameterization of all stabilizing controllers is well known and has been used to large extend in controller synthesis (See eg. [13]). With reference to Fig. C.1 we consider the system $G \equiv G_{yu}$ and stabilizing controller K (both transfer matrices). System and controller can be written as left or right co-prime factorizations:

$$G = N_r M_r^{-1} = M_l^{-1} N_l \tag{C.11}$$

$$K = U_r V_r^{-1} = V_l^{-1} U_l \tag{C.12}$$

where $N_r, M_r, U_r, V_r, N_l, M_l, U_l, V_l \in RH_\infty$ and satisfy the double Bezout identity

$$\begin{pmatrix} I & 0 \\ 0 & I \end{pmatrix} = \begin{pmatrix} V_l & -U_l \\ -N_l & M_l \end{pmatrix} \begin{pmatrix} M_r & U_r \\ N_r & V_r \end{pmatrix} \tag{C.13}$$

$$= \begin{pmatrix} M_r & U_r \\ N_r & V_r \end{pmatrix} \begin{pmatrix} V_l & -U_l \\ -N_l & M_l \end{pmatrix} \tag{C.14}$$

Then all controllers which stabilizes G are given as:

$$K(Q) = (U_r + M_r Q)(V_r + N_r Q)^{-1} \tag{C.15}$$

$$K(Q) = (V_l + Q N_l)^{-1}(U_l + Q M_l) \tag{C.16}$$

where $Q \in RH_\infty$ is called the Youla parameter.

The dual of the Youla parameterization is all systems stabilized by a given controller [8][12]. This is commonly denoted the dual Youla parameterization. The parameterization can be written as follows:

$$G(S) = (N_r + V_r S)(M_r + U_r S)^{-1} \tag{C.17}$$

$$G(S) = (M_l + S U_l)^{-1}(N_l + S V_l) \tag{C.18}$$

where $S \in RH_\infty$ is the dual Youla parameter. The nominal system G is naturally attained for $S = 0$. A useful interpretation of S is that of a frequency shaped version of the uncertainty [12]. Provided that K robustly stabilizes G there exist a map between Δ and $S \in RH_\infty$ [8]:

$$S(\Delta) = T_3 \Delta (I - T_1 \Delta)^{-1} T_2 \tag{C.19}$$

where

$$T_1 = G_{qp} + G_{qu} U_r M_l G_{yp} \tag{C.20}$$

$$T_2 = G_{qu} M_r, \; T_3 = M_l G_{yp} \tag{C.21}$$

An interesting property of the parameterization is that the Youla parameter Q looks directly into the dual Youla parameter S [8][12]:

$$\epsilon_k = S\eta_k \tag{C.22}$$

where ϵ_k and η_k are the input and output of Q respectively. One can therefore think of Q as a controller for the dual Youla parameter S. This also has the interpretation of Q controlling the model uncertainty. Actually, it turns out that the pair $(G(S), K(Q))$ is stabilizing if and only if the pair (S, Q) is stabilizing. The work in [12] is devoted to exploiting this principle.

C.4 Method

The main observation which we will take advantage of in MPC is the fact that the dual Youla parameter S can be regarded as the uncertainty of the system. Hence, if the performance of the system is unsatisfactory (eg. if constraints are violated), we can use an identification scheme to gain information about S and make actions accordingly ie. reconfigure the controller. Since standard identification procedures exist for solving this problem, we will only briefly cover this problem in the paper.

In constraint predictive control an optimization problem is setup by deriving explicitly how the trajectory of the system evolves over a finite horizon. Hence, in this section we establish how the trajectory of the system depends on the dual Youla parameter S. Furthermore, we show how to include the Youla parameter Q in the predictions.

Since the Youla parameterization is non-unique we need to introduce a specific realization. In this work we use an observer form of the Youla parameterization. The realization is shown in Fig. C.2 where the observer is based on the nominal system $G \equiv G_{yu}$ (For details see [2]). The realization is only valid for $K \in RH_\infty$. All stabilizing controllers for the nominal systems is hence parameterized by $Q \in RH_\infty$ with input ϵ_k and output η_k. We have included the auxiliary signal v_k which was used as the MPC control signal in section C.3. Looking at the input-output connection v_k-ϵ_k we look directly into the controlled dual Youla

parameter $\check{S}$:

$$\epsilon_k = \check{S} v_k = (I - SQ)^{-1} S v_k \tag{C.23}$$

This follows immediately from the theory presented in section C.3.3. We will show how this can be used when deriving the predictions for the MPC optimization problem.

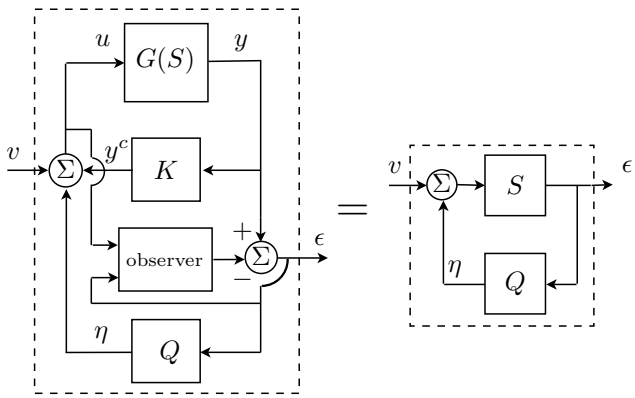

(a) Observer form of Youla parameterization (b) Equivalent representation

Figure C.2: The Youla parameterization is realized in the observer form [2]. It follows from the theory that the dynamic system from v_k to ϵ_k is the closed loop connection of S and Q.

C.4.1 Predictions in presence of the dual Youla parameter S

We will now derive the prediction equations in the presence of the assumed knowledge about $S = S(\Delta)$. We will for simplicity assume that $Q = 0$ for which relation (C.23) reduces to $\epsilon_k = S v_k$ Later we show how the result immediately generalizes to the case with non-zero Q.

The dynamics of the nominal system $G \equiv G_{yu}$, controller K and observer G_o

are:

$$G = \begin{cases} x_{k+1} = Ax_k + Bu_k \\ y_k \;\; = \quad\;\; Cx_k \end{cases} \tag{C.24}$$

$$K = \begin{cases} x^c_{k+1} = A_c x^c_k + B_c y_k \\ y^c_k \;\; = C_c x^c_k + D_c y_k \end{cases} \tag{C.25}$$

$$G_o = \begin{cases} \hat{x}_{k+1} = A\hat{x}_k + Bu_k + L\epsilon_k \\ \hat{y}_k \;\; = \quad\;\; C\hat{x}_k \end{cases} \tag{C.26}$$

$$u_k = v_k + y^c_k \;, \quad \epsilon_k = y_k - C\hat{x}_k \tag{C.27}$$

where $x_k \in \mathbb{R}^{n_x}$ is the state vector of the nominal system, $x^c_k \in \mathbb{R}^{n_k}$ is the state vector of the controller and $\hat{x}_k \in \mathbb{R}^{n_x}$ is the state vector of the observer. The output injection gain L is naturally chosen such that (A, CL) is a stabilizing pair.

The equations (C.24)-(C.26) represents the nominal dynamics $\Delta = 0$ ($S(\Delta) = 0$). Disregarding transients caused by disturbances and initial conditions the observer estimation error will be $\epsilon_k = 0$ no matter what the input sequence v_k is. In the presence of uncertainty $\Delta \neq 0$ ($S(\Delta) \neq 0$) the deterministic dynamic response of ϵ_k given the input v_k is determined by the dual Youla parameter S. We assume that S has the following state space representation:

$$S \equiv S(\Delta) = \begin{cases} x^s_{k+1} = A_s x^s_k + B_s v_k \\ \epsilon_k \;\; = \quad\;\; C_s x^s_k \end{cases} \tag{C.28}$$

where $x^s_k \in \mathbb{R}^{n_s}$ is the state vector of S. For the sake of simplicity we have assumed that there is no direct term in S. Combining equations (C.25)-(C.26) we get the following expression governing the evolution of y_k and u_k:

$$\begin{bmatrix} x^c_{k+1} \\ \hat{x}_{k+1} \end{bmatrix} = \underbrace{\begin{bmatrix} A_c & B_c C \\ BC_c & A + BD_c C \end{bmatrix}}_{\bar{A}} \begin{bmatrix} x^c_k \\ \hat{x}_k \end{bmatrix} + \underbrace{\begin{bmatrix} 0 \\ B \end{bmatrix}}_{\bar{B}} v_k + \underbrace{\begin{bmatrix} B_c \\ BD_c + L \end{bmatrix}}_{H} \epsilon_k \tag{C.29}$$

$$y_k = \underbrace{\begin{bmatrix} 0 & C \end{bmatrix}}_{\bar{C}_y} \begin{bmatrix} x^c_k \\ \hat{x}_k \end{bmatrix} + \epsilon_k \tag{C.30}$$

$$u_k = \underbrace{\begin{bmatrix} C_c & D_c C \end{bmatrix}}_{\bar{C}_u} \begin{bmatrix} x^c_k \\ \hat{x}_k \end{bmatrix} + v_k + D_c \epsilon_k \tag{C.31}$$

The residual ϵ_k has a natural interpretation as a correction term due to the perturbation S. Disregarding transients caused by disturbances and initial con-

ditions the deterministic evolution of y_k and u_k is therefore completely described by equations (C.29)-(C.31) and the dual Youla parameter (C.28).

Remark 5. *It is evident from equation (C.30) that ϵ_k only can be used to correct the predictions of y_k and not general linear combinations of x_k. Therefore, we can only handle constraint on the measurable output y_k and not general constraints on the states.*

Remark 6. *The states x_k^s of S are naturally not accessible in general. Therefore, we have to rely on estimated states $\hat{x}_k^s$ obtained through an observer:*

$$\hat{x}_{k+1}^s = A_s\hat{x}_k^s + B_s v_k + L_s(\epsilon_k - C_s\hat{x}_k^s) \tag{C.32}$$

$$\hat{\epsilon}_k = C_s\hat{x}_k^s \tag{C.33}$$

where $\hat{x}_k^s \in \mathbb{R}^{n_s}$ is the state vector of the dual Youla parameter. Hence, when referring to the state x_k^s in the following it is implicitly implied that it could be an estimate.

Based on the state x_k^s of the dual Youla parameter, the observer state $\hat{x}_k$ and the state of the controller x_k^c we can find (through iterations) the future trajectory of y_k, u_k and ϵ_k given the trajectory of v_k. Let Y_k, U_k, E_k, V_k denote the corresponding stacked vectors of N step trajectories eg.:

$$Y_k = \begin{bmatrix} y_k^T & y_{k+1}^T & y_{k+2}^T & \cdots & y_{k+N}^T \end{bmatrix}^T \tag{C.34}$$

We can write the future N predictions of y_k, u_k and ϵ_k as

$$Y_k = \mathcal{A}_y z_k + \mathcal{B}_y V_k + \mathcal{H}_y E_k \tag{C.35}$$

$$U_k = \mathcal{A}_u z_k + \mathcal{B}_u V_k + \mathcal{H}_u E_k \tag{C.36}$$

$$E_k = \mathcal{A}_s x_k^s + \mathcal{B}_s V_k \tag{C.37}$$

$$z_k = \begin{bmatrix} x_k^{c\,T} & \hat{x}_k^T \end{bmatrix}^T \tag{C.38}$$

where $\mathcal{A}_y$, $\mathcal{B}_y$, $\mathcal{H}_y$, $\mathcal{A}_u$, $\mathcal{B}_u$, $\mathcal{H}_u$, $\mathcal{A}_s$, $\mathcal{B}_s$ are defined as the following extended observability and Toeplitz matrices (See definition of $\mathcal{O}^N$ and $\mathcal{T}^N$ in section C.2).

$$\mathcal{A}_y = \mathcal{O}^N(\bar{A}, \bar{C}_y)\ ,\ \mathcal{B}_y = \mathcal{T}^N(\bar{A}, \bar{B}, \bar{C}_y, 0) \tag{C.39}$$

$$\mathcal{A}_u = \mathcal{O}^N(\bar{A}, \bar{C}_u)\ ,\ \mathcal{B}_y = \mathcal{T}^N(\bar{A}, \bar{B}, \bar{C}_u, 0) \tag{C.40}$$

$$\mathcal{A}_s = \mathcal{O}^N(A_s, C_s)\ ,\ \mathcal{B}_s = \mathcal{T}^N(A_s, B_s, C_s, 0) \tag{C.41}$$

$$\mathcal{H}_y = \mathcal{T}^N(\bar{A}, H, \bar{B}, I)\ ,\ \mathcal{H}_u = \mathcal{T}^N(\bar{A}, H, \bar{B}, D_c) \tag{C.42}$$

The closed form prediction of Y_k hence becomes

$$Y_k = \underbrace{\mathcal{A}_y z_k + \mathcal{B}_y V_k}_{\text{Nominal}} + \underbrace{\mathcal{H}_y\left(\mathcal{A}_s x_k^s + \mathcal{B}_s V_k\right)}_{\text{Perturbation}} \tag{C.43}$$

$$= Y_k^{(G,K)} + Y_k^S \tag{C.44}$$

where $Y_k^{(G,K)}$ is the contribution owing to the nominal dynamics and Y_k^S is the contribution owing to the dual Youla parameter. Likewise the closed loop predictions of u_k becomes:

$$U_k = \underbrace{\mathcal{A}_u z_k + \mathcal{B}_u V_k}_{\text{Nominal}} + \underbrace{\mathcal{H}_u \left(\mathcal{A}_s x_k^s + \mathcal{B}_s V_k\right)}_{\text{Perturbation}} \tag{C.45}$$

$$= U_k^{(G,K)} + U_k^S \tag{C.46}$$

where $U_k^{(G,K)}$ is the contribution owing to the nominal dynamics and U_k^S is the contribution owing to the dual Youla parameter.

Remark 7. *A nice property of the derived predictions is the separability into the nominal contribution ($S(\Delta) = 0$) and the contribution due to $S(\Delta) \neq 0$. Hence, there is no need for total reconfiguration of the MPC controller to take S into account, it should simply be able to take the corrections into account through a plug-in mechanism.*

Remark 8. *The future knowledge of a reference or set-point is easily incorporated in the predictions. The important thing to remember is that the reference should be input to the dual Youla parameter.*

C.4.2 Adding a Youla parameter Q for controlling S

Knowing the perturbation $S \equiv S(\Delta)$ the closed-loop performance can be enhanced by including a Youla parameter Q for controlling S. We assume that the Youla parameter has the following state space realization:

$$Q = \begin{cases} x_{k+1}^q = A_Q x_k^q + B_Q \epsilon_k \\ \eta_k \;\; = C_Q x_k^q + D_Q \epsilon_k \end{cases} \tag{C.47}$$

where $x_k^q \in \mathbb{R}^{n_q}$ is the state vector of the Youla parameter. Since Q looks directly into S the corrected predictions will now be made on the basis of the controlled dual Youla parameter:

$$\check{S} = (I - SQ)^{-1} S \tag{C.48}$$

It is straightforward to derive the predictions with the controlled dual Youla parameter. The predictions are simple made using $\check{S}$ with state vector $x_k^{\check{s}} = \begin{bmatrix} x_k^{s\,T} & x_k^{q\,T} \end{bmatrix}^T$ instead of S. The prediction of y_k and u_k can now be written on the following form over the prediction horizon:

$$Y_k = Y_k^{(G,K)} + Y_k^{(S,Q)} \tag{C.49}$$

$$U_k = U_k^{(G,K)} + U_k^{(S,Q)} \tag{C.50}$$

where the notation (S, Q) has been used to indicate the contribution owing to the controlled dual Youla parameter.

C.4.3 Identification of S

Using well established system identification methods it is possible to identify S using the auxiliary signal v_k as excitation signal. So far we have not considered noise, however, in the general noisy case the signal ϵ_k is related to the signal v_k through the following equation:

$$\epsilon_k = \check{S} v_k + e_k \tag{C.51}$$

where e_k is the noise contribution. With v_k persistently exiting and uncorrelated with e_k it is possible to get an unbiased estimate of $\check{S}$ using eg. an output-error method [5]. Since Q is user defined S is then easily established from $\check{S}$:

$$S = (I + \check{S}Q)^{-1}\check{S} \tag{C.52}$$

For a more rigorous treatment the reader is referred to [1][12].

Remark 9. *Identification of S should be done only when the constrained control action is inactive. When the constrained control is active we effectively have an extra nonlinear loop around the system. As will be shown shortly, we setup an MPC strategy where the constrained control action is active only when strictly necessary.*

C.4.4 MPC strategy

The predictions derived so far can be used to implement a MPC scheme which ensures satisfaction of constraints given the assumed knowledge of $S \equiv S(\Delta)$.

The cost for the MPC controller could in general be given by the cost in equation (C.8). If $W_y > 0$ this will give a control signal v_k which is active even though no constraints are violated over the prediction horizon. This is unattractive since we already assume that the controller K and the Youla parameter Q have been designed to deliver desired performance. It will basically interfere with the criteria on which the controllers K and Q were designed.

To make sure that the MPC controller only interferes when necessary we set $W_y = 0$ and the cost reduces to:

$$J_k = \sum_{i=k}^{N} \|v_i\|^2_{W_v} \tag{C.53}$$

We minimize this objective subject to the constraints (C.9)-(C.10) and the dynamics of the closed loop system consisting of the pair $(G(S), K(Q))$. The deterministic evolution of the trajectory is naturally described by the prediction equations given in the previous sections. Therefore, the constrained optimization problem can in the usual way be written as a constrained static optimization problem in the decision vector V_k and solved using a QP solver.

Under certain assumptions the suggested receding horizon control will guarantee stability: There exists a finite horizon $N \in \mathbb{N}$ for which cost (C.53) is equal to the infinite horizon cost. The infinite horizon problem is guaranteed stable if we know the system perfectly (ie. we have identified S) and the state estimation errors are sufficiently small. This is a special case of the results in [11] for prestabilized systems. In [11] an algorithm is given for choosing N online.

In practice these assumptions are unlikely to hold, and as is common practice in real applications, we might simply accept that situations could theoretically occur which leads to instability or infeasibility of the optimization problem.

C.4.5 Extensions

The true potential of the setup introduced so far lies in the extensions. The framework provides the basis for using the powerful ideas described in [12] together with constrained control action. We will confine ourself to a short description of one immediate extension possibility: The so-called iterative (S, Q) design. The framework derived so far is actually the first step of the iterative design.

C.4.5.1 Iterative design

After the first $Q = Q_1$ has been designed for the identified S the iterative method proceeds as follows: If performance is unacceptable we re-identify the uncertainty. However, this time it is the controlled dual Youla parameter we are looking into:

$$\check{S} = (I - SQ)^{-1} S \tag{C.54}$$

we then simply design an extra controller Q_2 for dealing with $\check{S}$. The total controller is hence $Q = Q_1 + Q_2$. These steps are repeated until acceptable performance is attained. The design is illustrated in Fig. C.3.

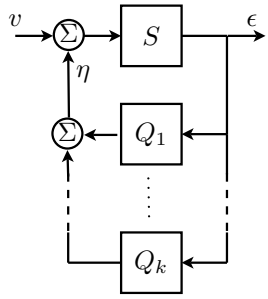

Figure C.3: Visualization of iterative design

After the kth iteration we have the Youla parameter

$$Q = Q_1 + Q_2 + \cdots + Q_k, \tag{C.55}$$

which is the sum of Youla parameters identified at each iteration. S can be derived from the controlled dual Youla parameter $\check{S}$ identified at the kth iteration using equation (C.52).

The algorithm is easily used together with the setup in section C.4 due to the modularity of the setup. The predictions of Y_k and U_k for the kth iteration are simply corrected based on the kth identified (closed-loop) dual Youla parameter and kth Youla parameter.

C.5 Illustrative example

In this section we illustrate the potential performance enhancement when using the presented framework. We consider a two cart system shown in Fig. C.4. The left cart (cart 1) represents the nominal dynamics and the cart to the right (cart 2) represents the perturbation. The objective is to regulate the position x of the left cart by applying a force u to the cart. We introduce the regulation constraint:

$$|x| \leq 1 \tag{C.56}$$

Introducing the following state vectors

$$z = \begin{bmatrix} x & \dot{x} \end{bmatrix}^T, \quad z_\Delta = \begin{bmatrix} x_\Delta & \dot{x}_\Delta \end{bmatrix}^T \tag{C.57}$$

and putting the system description in the form in Fig. C.1 we get the following continuous time description of the nominal dynamics:

$$\Sigma = \begin{cases} \dot{z} = \begin{bmatrix} 0 & 1 \\ -\frac{k}{m} & -\frac{d}{m} \end{bmatrix} z + \begin{bmatrix} 0 \\ 1 \end{bmatrix} p + \begin{bmatrix} 0 \\ \frac{1}{m} \end{bmatrix} u \\ q = z \\ y = z \end{cases} \tag{C.58}$$

and the following description of the perturbation:

$$\Delta = \begin{cases} \dot{z}_\Delta = \begin{bmatrix} 0 & 1 \\ -\frac{k_\Delta}{m_\Delta} & -\frac{d_\Delta}{m_\Delta} \end{bmatrix} z_\Delta + \begin{bmatrix} 0 & 0 \\ \frac{k_\Delta}{m_\Delta} & \frac{d_\Delta}{m_\Delta} \end{bmatrix} q \\ p = \begin{bmatrix} \frac{k_\Delta}{m} & \frac{d_\Delta}{m} \end{bmatrix} z_\Delta + \begin{bmatrix} -\frac{k_\Delta}{m} & -\frac{d_\Delta}{m} \end{bmatrix} q \end{cases} \tag{C.59}$$

The chosen parameter values are as follows: $m = 1$ kg. $k = 1$ N/m. $d = 1$ N/m·s. $m_\Delta = 0.5$ kg. $k_\Delta = 1$ N/m. $d_\Delta = 0.01$ N/m·s. For simulation purposes we consider the discretized dynamics of (C.58)-(C.59) where the sample time $T_s = 1.2s$ has been chosen. In the example we will assume perfect knowledge about S which can be found through the relation (C.19). In practice we would naturally be confined to identify S through an identification scheme as stated in section C.4.3. However, this is not the focus of this example. The minimal representation of $S \equiv S(\Delta)$ is a sixth order system.

To illustrate the potential improvements with the presented framework, we increase the complexity of the controller step by step. The following four control configurations are tested: Nominal (robust) feedback controller K (Labeled K1). Additional nominal constraint handling (K2). Additional correction of predictions based on the dual Youla parameter S (K3). Additional Youla parameter Q to control the dual Youla parameter (K4).

The nominal feedback controller is an LQ controller designed for the nominal dynamics ie. the dynamics of cart 1 which provides robust stability in the presence of the perturbation Δ. The state cost is $W_z = I_{2\times 2}$ and the control cost is $W_u = 10$. The dual Youla parameter Q is designed as an LQG controller based on the dynamics of S. The LQ state cost is $W_{x^s} = I_{6\times 6}$ and the LQ control

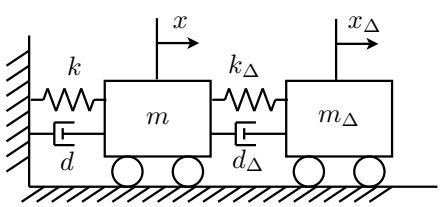

Figure C.4: Sketch of the two cart system

cost is $W_\eta = 0.1$. The state noise covariance matrix is chosen as $R_{x^s} = I_{6\times 6}$ and the output noise covariance matrix is chosen as $R_\epsilon = I_{2\times 2}$.

The MPC controller is designed for the system as described in section C.4.4. The control horizon is chosen to $N = 10$ and the control cost is $W_v = 1$.

In the simulations we step the reference from 0 to 1. This means that we want the position of cart 1 to end at $x = 1$ but without violating the constraint $|x| \leq 1$. The simulations are shown in Fig. C.5. The controller K1 does not satisfy the constraint, which is expected since constraint handling is not included in its design criteria. Constraints are still not met with nominal constraint handling due to erroneous predictions (K2). Correcting the predictions (K3) based on the dual Youla parameter constraints are respected. Performance is increased by the addition of the Youla parameter for controlling the dual Youla parameter (K4).

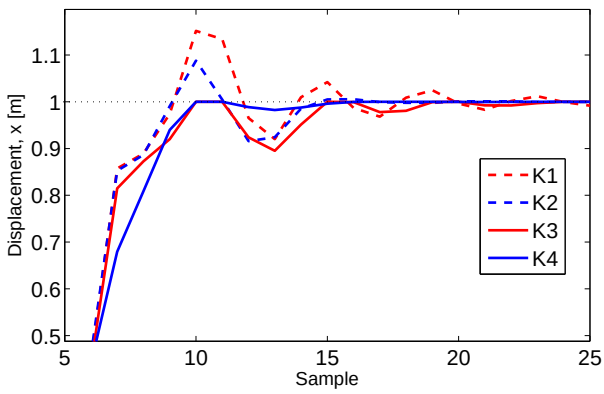

Figure C.5: Simulation with stepped reference

C.6 Conclusion

We have presented a framework for taking advantage of the primary and the dual Youla parameter in constrained predictive control. Based on a specific realization of the Youla parameterization we derive explicitly the predictions on which the MPC optimization should be made. It is shown that the predictions consist of a nominal contribution owing to the nominal dynamics and a contribution owing to the Youla parameterizations. The MPC problem is formulated such that the MPC controller is active only when there is danger of constraint

violation. An example illustrated the potential performance enhancement in using the framework.

Bibliography

[1] F. De Bruyne, B. Anderson, and N. Linard. The hansen scheme revisited. *Decision and Control, 1998. Proceedings of the 37th IEEE Conference on*, 1:706–711, 1998.

[2] J.Y. Ishihara and R.M.R.M. Sales. Doubly coprime factorizations related to any stabilizing controllers in state space. *Automatica*, 35(9):1573–1577, 1999.

[3] M.V. Kothare, V. Balakrishnan, and M. Morari. Robust constrained model predictive control using linear matrix inequalities. *Automatica*, 32(10):1361–1379, 1996.

[4] B. Kouvaritakis, J.A. Rossiter, and J. Schuurmans. Efficient robust predictive control. *IEEE Transactions on Automatic Control*, 45(8):1545–1549, 2000.

[5] L. Ljung. *System Identification: Theory for the User*. Prentice Hall, second edition edition, 1999.

[6] J.M. Maciejowski. *Predictive control with constraints*. Prentice Hall, 2002.

[7] D.Q. Mayne, J.B. Rawlings, C.V. Rao, and P.O.M. Scokaert. Constrained model predictive control: Stability and optimality. *Automatica*, 36(6):789–814, 2000.

[8] H. Niemann. Dual youla parameterisation. *IEE Proceedings-Control Theory and Applications*, 150:493–497, 2003.

[9] J.A. Rossiter, L. Chisci, and B. Kouvaritakis. Optimal disturbance rejection via youla parameterisation in constrained lq control. *Proceedings of the*

6th IEEE Mediterranean Conference. Theory and Practice of Control and Systems, pages 271–6, 1998.

[10] J.A. Rossiter and B. Kouvaritakis. Targetted sensitivity with constrained linear predictive control. *Proceedings of the IASTED International Conference Applied Simulation and Modelling*, pages 455–60, 2002.

[11] P.O.M. Scokaert and J.B. Rawlings. Constrained linear quadratic regulation. *IEEE Transactions on Automatic Control*, 43(8):1163–1169, 1998.

[12] T-T. Tay, I. Mareels, and J.B. Moore. *High Performance Control*. Birkhäuser, 1998.

[13] M. Vidyasagar. *Control System Synthesis: a factorization approach*. The M.I.T. Press, 1985.

[14] Z. Wan and M.V. Kothare. An efficient off-line formulation of robust model predictive control using linear matrix inequalities. *Automatica*, 39:837–846, 2003.

Paper D

Stochastic wind turbine modeling for individual pitch control

abstract

By pitching the blades of a wind turbine individually it is possible to attenuate the asymmetric loads caused by a non-uniform wind field - this is denoted individual pitch control. In this work we investigate how to set up a simplified stochastic and deterministic description of the wind and a simplified description of the aerodynamics with sufficient detail to design model-based individual pitch controllers. Combined with a simplified model of the wind turbine, we exemplify how to use the model elements to systematically design an individual pitch controller. The design is investigated in simulations.

D.1 INTRODUCTION

Wind turbines are currently the subject of great attention due to their increasing importance in energy production and their environmental properties. The demand for more and more power has set a trend for increasingly larger turbines. Reducing mechanical and structural stress, while also ensuring efficient power production, is therefore very important. One way to achieve this is through advanced model-based control designs which explicitly take into account the challenging characteristics of wind turbines.

On the majority of modern wind turbines the pitch of the blades is used as control parameters for dealing with the variations in the wind. In most documented research the pitch of the blades is controlled collectively by applying a wide variety of methods. These range from linear methods such as LQG, and $\mathcal{H}_\infty$ ([4]) to non-linear methods such as feedback linearization ([7], [12]).

Collective pitch control has one major drawback: it is not possible to compensate for the asymmetric loads caused by a non-uniform wind field. This can however be dealt with by using strategies where the blades are pitched individually. Most approaches assume that a collective pitch controller has been designed. The individual pitch controller is then included as an additional loop around the system (usually using classical control). This approach has e.g. been taken in [2] and [6]. However it is more natural to formulate the turbine control problem as an MIMO problem taking into account the inherent cross-couplings in the system. A step in this direction was taken in [10] and [11].

The contribution of this paper is the development of model elements to systematically design individual pitch controllers. In this respect, special emphasis is on the model of the wind. The wind model should have a suitable structure to capture the spatial variations. In particular we consider the stochastic nature of the turbulent wind. A short description on how to include deterministic effects is also included. Together with a structural model of a wind turbine, we demonstrate a controller design which is based on the $\mathcal{H}_2$ methodology. Simulations are used to show the potential of the approach.

The wind model which we set up is based on the work in [9]. Here it was shown how to set up frequency domain models of wind turbines given spectral descriptions of the wind. The method relies on making a Fourier series expansion of the wind in the azimuth angle.

D.2 MODELING

D.2.1 Wind model

The wind model describes the wind as it is seen by each *rotating* blade individually. The model is based on the frequency domain wind turbine modeling introduced in [9], where the focus was on load calculations. The derivation here is slightly different. We focus in particular on the relation between the winds seen by different blades. Furthermore, we consider time domain realization of the frequency descriptions. Of upmost importance in the following is the so-called blade effective wind speed:

D.2.1.1 The blade effective wind speed

The blades of a wind turbine are subject to a spatially distributed wind field. From a control engineering point of view the overhead would become too large if one were to incorporate the entire wind field explicitly as a disturbance model. A dimensionality reduction is therefore made through the so-called blade effective wind speed. The blade effective wind speed v^e is the speed of the uniform wind which results in the same generalized force as a given wind distribution $v(r)$ along the span of the blade. This can be expressed mathematically as

$$v^e = \frac{\int_{r_0}^{R} X(r)v(r)dr}{\int_{r_0}^{R} X(r)dr}. \tag{D.1}$$

The inner and outer radii of the blade (measured from hub center) are denoted by r_0 and R respectively. X is a weight function which describes how much influence the wind has along the span of the blade. The wind distribution $v(r)$ is assumed to be in axial direction (orthogonal to the plane of rotation).

In this work, the simple linear choice $X(r) = r$ has been chosen for all blade forces under consideration. Simulations indicates that this is a reasonable approximation for control purposes.

D.2.1.2 Stochastic model of the effective wind

As starting point we consider the wind speed at a single point on the rotor disc (the circular plane in which the blades rotate). We will denote the (auto) spectral density of a point wind $S(\omega)$. Given two point winds v_1 and v_2 separated

by the distance D, we denote the cross spectral density by $S(\omega, D)$. We assume that the cross spectral density can be separated into a product of the auto spectral density and the coherence $C(D, \omega)$.

$$S(\omega, D) = C(D, \omega)S(\omega) \tag{D.2}$$

For common auto spectral densities and coherence functions the reader is referred to [3].

Now, consider two point wind speeds at azimuth angles ψ_1, ψ_2 and radii r_1, r_2. We will denote these $v(t, r_1, \psi_1)$ and $v(t, r_2, \psi_2)$ as shown in Fig. D.1. At any given time t the point wind speeds will be periodic in the azimuth angle. We can therefore make a Fourier expansion in the azimuth angle for fixed t.

$$v(t, r, \psi) = \sum_{n=-\infty}^{\infty} \tilde{v}_n(t, r)e^{in\psi} \tag{D.3}$$

where $\tilde{v}_n(t, r)$ are the (time-varying) Fourier coefficients.

Based on the expansion above we can likewise make an expansion of the covariance between the point winds. The covariance $R(\tau, D)$ is assumed to depend uniquely on the euclidean distance $D = \sqrt{r_1^2 + r_2^2 - 2r_1r_2\cos(\Delta\psi)}$ between two point wind speeds (where $\Delta\psi = \psi_2 - \psi_1$). Accordingly we get:

$$R(\tau, D) = E\{\overline{v(t, r_1, \psi_1)}v(t + \tau, r_2, \psi_2)\} \tag{D.4}$$

$$= \sum_{n,m=-\infty}^{\infty} E\{\overline{\tilde{v}_n(t, r_1)}\tilde{v}_m(t + \tau, r_2)\}e^{i(m\psi_2 - n\psi_1)} \tag{D.5}$$

$$= \sum_{n=-\infty}^{\infty} \tilde{R}_{n,n}(\tau, r_1, r_2)e^{in\Delta\psi} \tag{D.6}$$

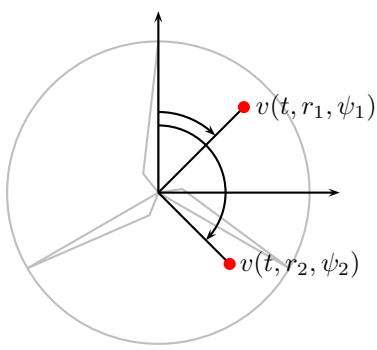

Figure D.1: Point winds on the rotor disc

where $\tilde{R}_{n,m}(\tau, r_1, r_2)$ is the covariance between the expansion coefficients:

$$\tilde{R}_{n,m} = E\{\overline{\tilde{v}(t, r_1)}\tilde{v}(t+\tau, r_2)\} \tag{D.7}$$

$$= \frac{1}{(2\pi)^2}\int_0^{2\pi}\int_0^{2\pi} E\{v(t, r_1, \psi_1)v(t, r_2, \psi_2)\}$$

$$\cdot\, e^{-i(m\psi_2 - n\psi_1)} d\psi_1 d\psi_2 \tag{D.8}$$

$$= \begin{cases} \frac{1}{2\pi}\int_0^{2\pi} R(\tau, D)e^{-im\Delta\psi}d\Delta\psi & m = n \\ 0 & \text{otherwise} \end{cases} \tag{D.9}$$

Eventually we want to describe the wind as seen by the rotating blade which we assume rotates with constant angular velocity $\dot{\psi} = \omega_r$. This gives a constant time evolution of the azimuth angles $\psi_1(t) = \omega_r t + \psi_1$, $\psi_2(t) = \omega_r t + \psi_2$. The covariance $R^r(\tau, D)$ of the rotating point winds becomes:

$$R^r(\tau, D) = E\{\overline{v(t, r_1, \psi_1(t))}v(t+\tau, r_2, \psi_2(t))\} \tag{D.10}$$

$$= \sum_{n,m=-\infty}^{\infty} E\{\overline{\tilde{v}_n(t, r_1)}\tilde{v}_m(t+\tau, r_2)\}$$

$$\cdot\, e^{im\omega_r\tau}e^{i(m\psi_2 - n\psi_1)}e^{i\omega_r(m-n)t} \tag{D.11}$$

$$= \sum_{n=-\infty}^{\infty} \tilde{R}_{nn}(\tau, r_1, r_2)e^{in\omega_r\tau}e^{in(\Delta\psi)} \tag{D.12}$$

It is seen that the only difference between the covariance of the non-rotating wind speeds and the rotating wind speeds is the exponential $e^{in\omega_r\tau}$. The effect of this will become clear when introducing the cross-spectral density of the rotating wind.

The cross spectral density of the rotating wind is derived by taking the Fourier transform (denoted by $\mathcal{F}$) of the covariance:

$$S^r(\omega, D) = \mathcal{F}\{R^r(\tau, D)\} \tag{D.13}$$

$$= \sum_{n=-\infty}^{\infty} \tilde{S}_{nn}(\omega - n\omega_r, r_1, r_2)e^{in\Delta\psi} \tag{D.14}$$

The derivation of the harmonic cross spectral densities $\tilde{S}_{nn}$ is written in detail below:

$$\tilde{S}_{nn}(\omega, r_1, r_2) = \frac{1}{2\pi}\int_0^{2\pi} \mathcal{F}\{R(\tau, D)\}e^{-in\Delta\psi}d\Delta\psi \tag{D.15}$$

$$= \frac{1}{2\pi}\int_0^{2\pi} C(\omega, D)e^{-in\Delta\psi}d\Delta\psi S(\omega) \tag{D.16}$$

$$= F_n(\omega, r_1, r_2)S(\omega) \tag{D.17}$$

The frequency shift of the harmonic cross spectral density $\tilde{S}_{nn}$ in (D.14) is due to the exponential originating from the time-dependent azimuth. This effectively causes the phenomena known as rotational sampling where the wind experienced by the blade has frequency contents which are centered around the frequencies $n \cdot \omega_r$.

To remove the dependency on the radial coordinates, we introduce the definition of the effective wind speed. Going through the previous calculations we trivially end with the following harmonic spectrum of the blade effective wind speed:

$$\begin{aligned}\tilde{S}^e_{nn}(\omega) &= \int_{r_0}^{R} X(r_2) \int_{r_0}^{R} X(r_1) F_n(\omega, r_1, r_2) dr_1 dr_2 S(\omega) \\ &\quad \cdot \left(\int_{r_0}^{R} \int_{r_0}^{R} X(r_2) X(r_1) dr_1 dr_2 \right)^{-1} && \text{(D.18)} \\ &= F^e_n(\omega) S(\omega) && \text{(D.19)}\end{aligned}$$

and the cross spectral density of the rotating effective wind likewise becomes:

$$S^e(\omega, \Delta\psi) = \sum_{n=-\infty}^{\infty} \tilde{S}^e_{nn}(\omega - n\omega_r) e^{in\Delta\psi} \tag{D.20}$$

We now relate the derived spectral description of the rotating effective wind speed to a three-bladed turbine. The blades are assumed evenly spaced giving an azimuth difference between two neighbors of $\Delta\psi = \frac{2\pi}{3}$. The effective wind vector is:

$$\begin{aligned}\boldsymbol{v}^e &= \begin{bmatrix} v^e_1(t) & v^e_2(t) & v^e_3(t) \end{bmatrix}^T && \text{(D.21)} \\ &= \begin{bmatrix} v^e(t, 0) & v^e(t, \frac{2\pi}{3}) & v^e(t, \frac{4\pi}{3}) \end{bmatrix}^T && \text{(D.22)}\end{aligned}$$

The corresponding spectral density matrix becomes

$$\boldsymbol{S}^e(\omega) = \sum_{n=-\infty}^{\infty} \tilde{S}^e_{nn} \boldsymbol{E} \tag{D.23}$$

where

$$\boldsymbol{E} = \begin{bmatrix} 1 & e^{in\frac{2\pi}{3}} & e^{in\frac{4\pi}{3}} \\ e^{in\frac{-2\pi}{3}} & 1 & e^{in\frac{2\pi}{3}} \\ e^{in\frac{-4\pi}{3}} & e^{in\frac{-2\pi}{3}} & 1 \end{bmatrix} \tag{D.24}$$

The description above clearly does not relate to a finite dimensional linear description. This is evident from the constant phase-shift in the cross-spectrum

for $n \geq 1$ and the infinite number of harmonics. For control purposes we will approximate this power spectrum with an LTI system driven by white noise. To this end we truncate the infinite series and disregard the covariance between the components of $\boldsymbol{v}^e$ for harmonics $n \geq 1$. The proposed wind model for blade j has the following structure:

$$v_j^e(t) = G_0 e_0(t) + \sum_{k=1}^{N} G_k e_{jk}(t) \tag{D.25}$$

where $e_x(t) \sim \mathcal{N}(0,1)$ (Gaussian distributed white noise process with mean 0 and intensity 1). G_n is the transfer function representing the n-th harmonic. More specifically $\overline{G_n(\omega)}G_n(\omega) = |G_n(\omega)|^2$ should approximately be equal to $2\pi\tilde{S}_{nn}^e(\omega)$ (See e.g. [1]). This can be done by minimizing the difference pointwise in frequency, e.g. by minimizing the following cost:

$$J = \min_{\theta} \| |G_n(\omega;\boldsymbol{\theta})|^2 - 2\pi |S_{nn}^e(\omega)| \|_2 \tag{D.26}$$

for a suitable parameterization of the transfer function $G_n(\omega) = G_n(\omega;\boldsymbol{\theta})$.

D.2.1.3 Deterministic model of the effective wind

Having introduced the stochastic wind model, it is straightforward to describe how the deterministic wind profile can be included in the model. Going through the previous calculations in a deterministic setup based on a mathematical description of the deterministic wind $v(r,\psi)$ we get the following result for the deterministic blade effective wind speed.

$$v^e(t) = \sum_{n=-\infty}^{\infty} \tilde{v}_n^e e^{i\psi_0} e^{in\omega_r t} \tag{D.27}$$

where

$$\tilde{v}_n^e = \frac{1}{2\pi} \frac{\int_{r_0}^{R} X(r) \int_{r_0}^{2\pi} v(r,\theta) e^{-in\theta} d\theta dr}{\int_{r_0}^{R} X(r) dr} \tag{D.28}$$

ψ_0 is the azimuth of the blade at $t = 0$.

Equation (D.27) represents a sum of sinusoids. The n-th harmonic of v^e can hence be modeled as the impulse response of

$$G_n(s) = |\tilde{v}_n^e| \frac{n \cdot \omega_r}{s^2 + (n \cdot \omega_r)^2} \tag{D.29}$$

As for the stochastic wind model, we propose to take a finite number of harmonics into account in the design model.

D.2.2 Aerodynamics

For a given blade (denoted with index j) we can calculate the lift/drag forces per unit length using the blade element momentum (BEM) method (See e.g. [5]). Assuming that this relation is static (e.g. by neglecting wake dynamics) it can be written as:

$$\frac{d\boldsymbol{F}_j(r)}{dl} = \boldsymbol{f}(v_j(r), \boldsymbol{p}_j(r)) \tag{D.30}$$

where $d\boldsymbol{F}_j/dl$ represents the lift and drag force per unit length, $v_j(r)$ represents the wind along the span of the blade and $\boldsymbol{p}_j$ represents relevant speed and position properties of the blade relative to the wind.

We simplify the aerodynamic description by adopting the definition of the blade effective wind speed (D.1). Furthermore, we are interested in the projection of $d\boldsymbol{F}_j/dl$ onto relevant generalized forces $\boldsymbol{Q}_j$. Consequently, the simplified aerodynamic model becomes:

$$\boldsymbol{Q}_j = \int_{r_0}^{R} \boldsymbol{\Gamma}(r)\boldsymbol{f}(v_j^e, \boldsymbol{p}_j(r))dr \tag{D.31}$$

where $\boldsymbol{\Gamma}$ is the projection function. For linear controller design, (D.31) is naturally linearized.

The relevant generalized forces in this work are: root force normal to rotor disc $Q_{t,j}$ (associated with tower displacement); root moment tangential to rotor disc $Q_{r,j}$ (associated with rotor rotation); and root moment normal to rotor disc $Q_{m,j}$. The vector $\boldsymbol{p}_j$ consists of: For-aft tower vibration speed $\dot{q}_t$, rotational speed of blades ω_r and the pitch of the blade β_j.

D.2.3 Model of wind turbine

In this paper we only consider the pitch control loop. For this reason we leave out dynamics which usually pertain to the power control loop (such as generator dynamics and drive train dynamics).

D.2.3.1 Structural model

A schematic of the structural model is shown in Fig. D.2. The model has two degrees of freedom: one degree associated with the for-aft bending moment of the tower (q_t) and one degree of freedom associated with the azimuth angle of

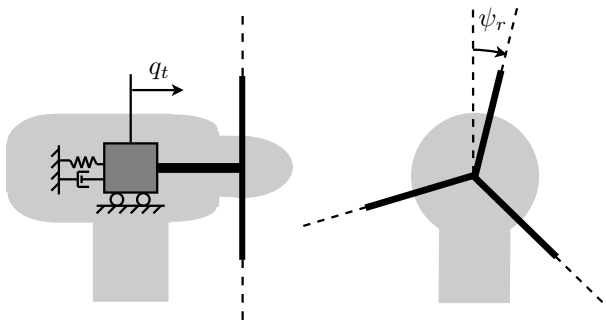

(a) Side view (b) Front view

Figure D.2: Schematic of wind turbine with degrees of freedom

the rotor (ψ_r). The orientation of the degrees of freedom are as indicated in Fig. D.2.

The model of the turbine is given by the following differential equations which are coupled through the aerodynamics:

$$m_t\ddot{q}_t + c_t\dot{q}_t + k_t q_t = \sum_{k=1}^{3} Q_{t,k} \tag{D.32}$$

$$J_r\ddot{\psi}_r + T_g = \sum_{k=1}^{3} Q_{r,k} \tag{D.33}$$

m_t, c_t, k_t are the generalized mass, damping and stiffness of tower respectively. J_r is the combined inertia of all rotating parts. T_g is the counter torque from the generator, which is assumed constant in this model. The forces $\boldsymbol{Q}_t = \begin{bmatrix} Q_{t,1} & Q_{t,2} & Q_{t,3} \end{bmatrix}^T$ and $\boldsymbol{Q}_r = \begin{bmatrix} Q_{r,1} & Q_{r,2} & Q_{r,3} \end{bmatrix}^T$ have been introduced in the previous section.

D.2.3.2 Actuator dynamics

The pitch of the blades β_j are changed by actuators. Local inner loops make a first order approximation reasonable:

$$\dot{\beta}_j = -1/\tau\beta_j + 1/\tau\beta_{j,r} \tag{D.34}$$

where $\beta_{j,r}$ is the pitch demand for the j-th blade.

D.3 CONTROLLER DESIGN

In this section we illustrate a controller design for a 1.5 MW wind turbine model. Only the stochastic part of the wind is considered and a mean wind speed of 16 m/s is assumed. This corresponds to *above rated* wind speed conditions (see e.g. [3] for a description of the operation modes of a wind turbine). In these conditions the primary purpose of the pitch loop is to keep the rotational speed constant. Table D.1 shows selected key parameters of the model.

D.3.1 Objectives

In the conditions under consideration the primary objective is to keep the rotational speed $\dot{\psi}_r = \omega_r$ constant. Since the tower is lightly damped, it is also of importance to ensure that the controller provides some damping to the tower. This will be done by targeting the tower deflection speed in the design. For load attenuation we want to attenuate the yaw and tilt moments in the support of the blades. The yaw and tilt moments are the projections of the blade root moments normal to the rotor disc

$$\boldsymbol{Q}_m = \begin{bmatrix} Q_{m,1} & Q_{m,2} & Q_{m,3} \end{bmatrix}^T \tag{D.35}$$

onto the fixed frame of reference. We will indirectly target the yaw and tilt moments by minimizing the difference between the root moments of the blades

$$\bar{\boldsymbol{Q}}_m = \begin{bmatrix} (Q_{m,1} - Q_{m,2}) & (Q_{m,2} - Q_{m,3}) \end{bmatrix}^T \tag{D.36}$$

This is a linear function of the state variables and can therefore be incorporated in a linear design.

Table D.1: Selected key parameters for 1.5 MW wind turbine model

Parameter	value	
m_t	$9.35 \cdot 10^4$	kg
k_t	$6.51 \cdot 10^5$	N/m
c_t	$3.25 \cdot 10^4$	s^{-1}
τ	0.1	s
J_r	$3.04 \cdot 10^6$	kg·m^2
ω_r rated	2.1	rad/s

D.3.2 Control model

In the control model we include a model of the stochastic effective wind. The stochastic model is based on the following auto power spectral density (Kaimal spectrum) and coherence:

$$S(\omega) = 170/(1 + 800\omega)^{5/3} \tag{D.37}$$

$$C(\omega, D) = e^{-12\sqrt{(\omega D/0.4)^2 + (35\cdot 10^{-5} D^2)}} \tag{D.38}$$

We include the harmonics 0 to 3. The harmonics are approximated as described in Sec. D.2.1 and the resulting transfer functions given in Table D.2. The model for the blade effective wind speeds becomes:

$$v_j^e = G_0 e_0 + G_1 e_{j,1} + G_2 e_{j,2} + G_3 e_{j,3}, \qquad j = 1, 2, 3 \tag{D.39}$$

where $e_x \sim \mathcal{N}(0, 1)$.

Since $\boldsymbol{v}^e$ by definition is associated with a given generalized force, we propose to use a separate wind model (D.39) for each of the generalized force vectors $\boldsymbol{Q}_t$, $\boldsymbol{Q}_r$, $\boldsymbol{Q}_m$. If this is not done, bias will be introduced in the controller when mapping the observations to the internal model. To this end we will associate the blade effective wind speeds $\boldsymbol{v}_t^e$, $\boldsymbol{v}_r^e$ and $\boldsymbol{v}_m^e$ with the generalized forces $\boldsymbol{Q}_t$, $\boldsymbol{Q}_r$ and $\boldsymbol{Q}_m$ respectively.

The dynamics of the wind turbine structure and the pitch actuators dynamics are linear and therefore used directly in the controller design. The aerodynamic relation (D.31) is non-linear and takes the following form when linearized and using separate wind signals for each generalized force:

$$\begin{bmatrix} \boldsymbol{Q}_t \\ \boldsymbol{Q}_r \\ \boldsymbol{Q}_m \end{bmatrix} = \begin{bmatrix} \boldsymbol{d}_{tv}\boldsymbol{v}_t^e \\ \boldsymbol{d}_{rv}\boldsymbol{v}_r^e \\ \boldsymbol{d}_{mv}\boldsymbol{v}_m^e \end{bmatrix} + \boldsymbol{d}_q \dot{q}_t + \boldsymbol{d}_\omega \omega_r + \boldsymbol{d}_\beta \boldsymbol{\beta} \tag{D.40}$$

The parameters $\boldsymbol{d}_x$ are constants of appropriate dimensions.

Table D.2: LTI approximation to wind

n	G_n
0	$\frac{0.017004(s+68.99)}{(s+2.873)(s+0.03357)}$
1	$\frac{-0.2807(s+2.617)(s+0.2683)}{(s+0.4707)(s^2+0.1992s+4.399)}$
2	$\frac{-1.4387(s^2+0.06123s+0.1993)}{(s+1.148)(s+0.5589)(s^2+0.3449s+17.61)}$
3	$\frac{-1.6613(s^2+1.059s+1.241)}{(s^2+3.143s+2.939)(s^2+0.4393s+39.58)}$

In the controller design we consider the combined linear model of the wind, aerodynamics, structural dynamics and actuators. We denote this model $\boldsymbol{P}$. The inputs and outputs of the model are defined in the following. The control inputs to the model are the pitch references:

$$\boldsymbol{u} = \begin{bmatrix} \beta_{1,r} & \beta_{2,r} & \beta_{3,r} \end{bmatrix}^T \tag{D.41}$$

The following measurements are assumed to be available as input to the controller:

$$\boldsymbol{y} = \begin{bmatrix} \dot{q}_t & \omega_r & \boldsymbol{Q}_m^T \end{bmatrix}^T \tag{D.42}$$

To evaluate performance we consider the following signal

$$\boldsymbol{z} = \begin{bmatrix} \dot{q}_t & \omega_r & \bar{\boldsymbol{Q}}_m^T & \boldsymbol{\beta}^T & \boldsymbol{u}^T \end{bmatrix}^T \tag{D.43}$$

where $\boldsymbol{\beta}$ is the vector of pitch angles. $\boldsymbol{z}$ reflects the control objectives as specified in Sec. D.3.1. The disturbances influencing the model are taken to be:

$$\boldsymbol{\xi} = \begin{bmatrix} \boldsymbol{e}^T & \boldsymbol{w}^T \end{bmatrix}^T \tag{D.44}$$

where $\boldsymbol{e}$ represents the inputs to the wind model and $\boldsymbol{w}$ represents measurement noise.

D.3.3 Controller synthesis

For the controller design we consider the generalized controller setup in Fig. D.3 where we have added input and output weights. $\boldsymbol{K}$ naturally denotes the feedback controller. The input weight has the following structure

$$\boldsymbol{W}_\xi = \begin{bmatrix} \boldsymbol{W}_e & \\ & \boldsymbol{W}_w \end{bmatrix} \tag{D.45}$$

$\boldsymbol{W}_e$ is the weight on the input to the wind model. Since the wind has been designed to reflect the shape of the actual disturbance, it will simply be the identity matrix $\boldsymbol{W}_e = \boldsymbol{I}$. $\boldsymbol{W}_w$ is the weight associated with the measurement noise and is chosen as a small fraction of measurement signal amplitudes.

The output weight $\boldsymbol{W}_z$ also serves as a tuning parameter and is roughly chosen to reflect the accepted signal amplitudes. The weight on the pitch angles $\boldsymbol{\beta}$ is more specifically chosen to be frequency-dependent. A high-pass filter of the form

$$W_\beta(s) = 23\frac{(s+7)^3}{(s+20)^3} \tag{D.46}$$

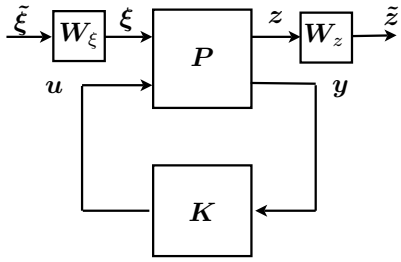

Figure D.3: General control setup

is associated with each of the pitch angle signals. It is included to limit high frequency pitch activity.

White noise disturbances have a nice interpretation performance-wise in connection to the $\mathcal{H}_2$ control methodology [8]. This motivates a controller design $\boldsymbol{K}$ which minimizes the $\mathcal{H}_2$ norm of the closed loop system

$$\tilde{\boldsymbol{z}} = \boldsymbol{F}_l(\tilde{\boldsymbol{P}}, \boldsymbol{K})\tilde{\boldsymbol{\xi}} \tag{D.47}$$

where $\boldsymbol{F}_l$ is the lower linear fractional transformation and $\tilde{\boldsymbol{P}}$ is the weighted plant. The $\mathcal{H}_2$ design is equivalent to an LQG controller for the weighted plant $\tilde{\boldsymbol{P}}$ (See [8]). The LQG synthesis has been done using the Control Systems Toolbox in MATLAB.

D.4 SIMULATIONS

The control setup in the previous section is illustrated with simulations. The individual pitch controller is compared to a collective pitch controller. The collective pitch controller is based on an equivalent setup, apart for the weights associated with $\bar{\boldsymbol{Q}}_m$. These are set to zero, which effectively causes collective pitch behavior.

The simulation model consists of the (non-simplified and non-linearized) model of the aerodynamics and the wind turbine model as described in Sec. D.2.2 and D.2.3. The time-varying wind field is generated using the Veers method based on the spectral description in equation (D.37) and (D.38) (See [3]). Fig. D.4 shows the wind realization at the hub center.

Fig. D.5 shows the closed loop trajectories for rotor rotation ω_r and tower deflection speed $\dot{q}_t$. Both the collective pitch controller and the individual pitch

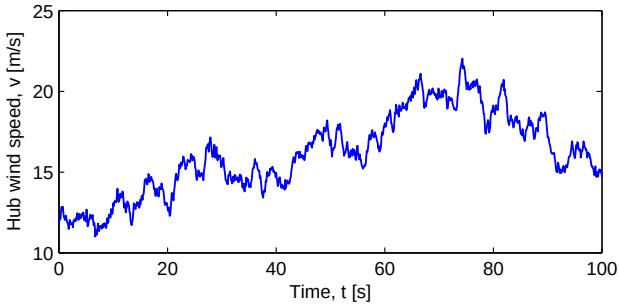

Figure D.4: Wind speed at hub center

controller manage to keep the rotational speed relatively constant while at the same time attenuating the vibrations in the tower.

Fig. D.6 shows the yaw and tilt moment of the wind turbine. It is seen that the individual pitch controller manages to attenuate the yaw and tilt moment significantly as compared to the collectively controlled system. Due to the frequency-dependent weight on the pitch signal, the high frequency variations are still very pronounced in the signals.

Fig. D.7 shows the pitch angle β_1 and pitch angle rate $\dot{\beta}_1$ for the individual pitch

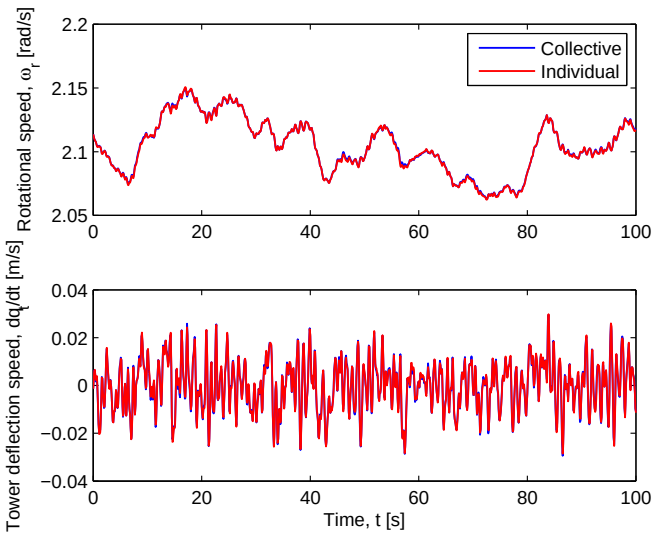

Figure D.5: Rotational speed ω_r and tower deflection speed $\dot{q}_t$

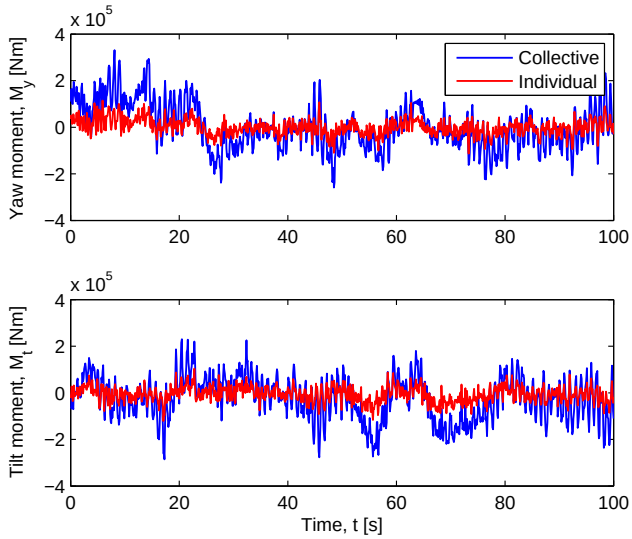

Figure D.6: Yaw moment M_y and tilt moment M_t

controlled system and the collective pitch controlled system. The plots clearly show that attenuating the asymmetric loads comes at a cost. The pitch activity is significantly higher with the individual pitch controller than the collective

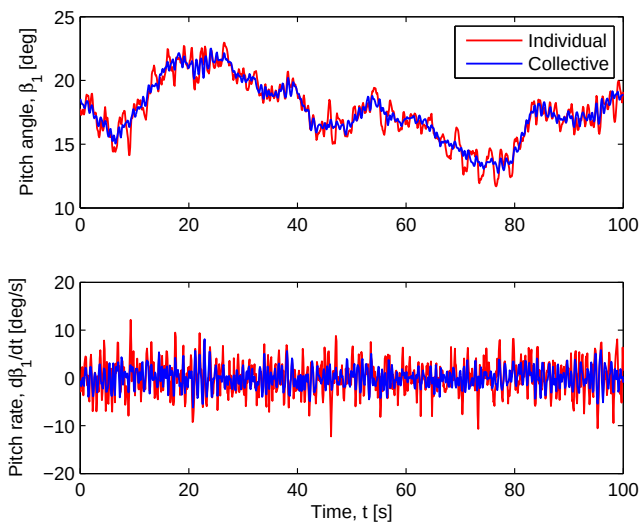

Figure D.7: Pitch angle β_1 and pitch angle speed $\dot{\beta}_1$

pitch controller. It is expected that the peak pitch rates are at the limits of what is acceptable. If further detuning is necessary, it is easily done by adjusting the frequency-dependent weight on the pitch.

It is stressed that a full wind turbine controller should be designed to handle varying operating conditions. However, the simulations indicate that a linear design can be justified when working around a given operating point.

D.5 CONCLUSION

In this paper we have shown how to set up simplified models of the wind which can be incorporated in individual pitch controller designs. The proposed model was applied together with a simplified model of the aerodynamics and a wind turbine in a $\mathcal{H}_2$ controller design. Simulations show that the resulting controller succeeds in attenuating the effect of the stochastic wind field.

Bibliography

[1] K.J. Åstrøm. *Introduction to stochastic control theory*. Academic Press New York, 1970.

[2] E.A. Bossanyi. Individual Blade Pitch Control for Load Reduction. *Wind Energy*, 6(2):119–128, 2003. DOI: 10.1002/we.76.

[3] Tony Burton, David Sharp, Nick Jenkins, and Ervin Bossanyi. *Wind Energy Handbook*. Wiley, 2001.

[4] M.J. Grimble. Horizontal axis wind turbine control: comparison of classical, LQG and $\mathcal{H}_\infty$ designs. *Dynamics and Control*, 6(2):143–161, 1996. DOI:10.1007/BF02169534.

[5] M. O. L. Hansen. *Aerodynamics of Wind Turbines*. James & James, 2000.

[6] T.J. Larsen, H.A. Madsen, and K. Thomsen. Active load reduction using individual pitch, based on local blade flow measurements. *Wind Energy*, 8(1):67–80, 2005. DOI:10.1002/we.141.

[7] D.J. Leith and W.E. Leithead. Implementation of wind turbine controllers. *International Journal of Control*, 66(3):349–380, 1997.

[8] Sigurd Skogestad and Ian Postlethwaite. *Multivariable Feedback Control: Analysis and design*. John Wiley & Sons, 1996.

[9] P. Sørensen. Frequency domain modelling of wind turbine structures. Technical report, Risø National Laboratory, Roskilde, Denmark, 1994.

[10] K.A. Stol, W. Zhao, and A. D. Wright. Individual blade pitch control for the controls advanced research turbine (cart). *Journal of Solar Energy Engineering*, 128:498–505, November 2006. DOI:10.1115/1.2349542.

[11] S.C. Thomsen, H. Niemann, and N.K. Poulsen. Individual pitch control of wind turbines using local inflow measurements. *Proceedings of the 17th IFAC World Congress, IFAC'08*, pages 5587–5592, 2008.

[12] S.C. Thomsen and N.K. Poulsen. A disturbance decoupling nonlinear control law for variable speed wind turbines. In *Proceedings of the 15th Mediterranean Conference on Control and Automation*, pages 1268–1273, 2007.

Paper E

Attenuating wind turbine loads through model based individual pitch control

abstract

In this paper we consider wind turbine load attenuation through model based control. Asymmetric loads caused by the wind field can be reduced by pitching the blades individually. To this end we investigate the use of stochastic models of the wind which can be included in a model based individual pitch controller design. In this way the variability of the wind can be estimated and compensated for by the controller. The wind turbine model is in general time-variant due to its rotational nature. For this reason the modeling and control is carried out in so-called multiblade coordinates. The individual pitch controller design in investigated in simulations.

E.1 INTRODUCTION

Reducing stress on the wind turbine structure while ensuring efficient power production is becoming increasingly important as the size of the wind turbines continuous to increase. One way to achieve this is through advanced model based control designs which explicitly take into account the dynamics of the wind turbine as well as the stochastic nature of the wind.

On the majority of modern wind turbines both the torque of the generator (variable speed control) and the pitch of the blades (pitch control) are used as control parameters for dealing with these challenges. In most documented research the pitch of the blades are controlled collectively applying a wide variety of methods. This ranges from linear methods such as LQ, LQG/$\mathcal{H}_2$, and $\mathcal{H}_\infty$ ([3], [4]) to nonlinear methods such as feedback linearization ([7], [12]).

Collective pitch control has one major drawback: it is not possible to compensate for the asymmetric loads caused by a nonuniform wind field. This can however be dealt with using strategies where the blades are pitched individually. Most of the approaches assume that a collective pitch controller has been designed for the turbine and basically designs the individual pitch controllers as additional loops around the system (usually using classical control). This approach has e.g. been taken in [2] and [6]. However it is more natural to formulate the turbine control problem as a MIMO problem taking into account the inherent cross-couplings in the system. A step in this direction was taken in [9], [10] and [11].

In this paper we investigate the use of stochastic wind models in connection to model based individual pitch control. Including an internal model of the wind will enable the controller to estimate the variability of the wind and consequently provide more effective compensation. Wind model as well as wind turbine model are derived in so-called multiblade coordinates. In multiblade coordinates the linearized dynamics of the wind turbine will not exhibit time-dependency caused by rotor rotation. Modeling the deterministic trends in the wind is not considered in this paper but is easily handled in the same framework. We apply LQG controller synthesis for designing the individual pitch controller. This paper extends the work in [11] where a stochastic wind model for model based control was setup in local blade coordinates.

The wind model which we setup is based on the work in [8]. Here it was shown how to setup frequency domain models of wind turbines given spectral descriptions of the wind. The method relies on making a Fourier series expansion of the wind in the azimuth angle.

The structure of this paper is as follows: In Sec. E.2 the multiblade transformation is introduced and the advantage of the transformation in connection to control is explained. In Sec. E.3 the stochastic wind model is derived. In Sec. E.4 the wind turbine model is derived - this includes the one used in simulation as well as the one used in connection to controller synthesis. In Sec. E.5 the LQG controller synthesis is described. The controller design in illustrated with simulations in Sec. E.6

E.2 Wind turbine control in multiblade coordinates

Due to the rotor rotation the linear dynamic description of a wind turbine will in general be time-dependent. Assuming that the rotor system is isotropic and rotating at a constant angular velocity it is however possible to transform the system equations into time-independent coordinates. This is done by transforming the local blade coordinates to the so-called multiblade coordinates. The multiblade coordinates describes the combined effect of the local blade dynamics in the support frame of reference i.e. the global coordinate system.

E.2.1 The multibody transformation

In the following we assume that the wind turbine under consideration has an isotropic rotor with three blades rotating with constant angular velocity ω_r. Assume that we have a vector $\boldsymbol{q}$ with 3 variables, pertaining to different blades and described in local blade coordinates.

$$\boldsymbol{q} = \begin{bmatrix} q_1 & q_2 & q_3 \end{bmatrix}^T \tag{E.1}$$

The elements of $\boldsymbol{q}$ are assumed to represent equivalent properties of each blade e.g. edgewise blade deflection. The transformation of blade variable triplets to multiblade coordinates is given by:

$$\bar{\boldsymbol{q}} = \boldsymbol{M}(t)\boldsymbol{q} \tag{E.2}$$

where $\bar{\boldsymbol{q}}$ denotes the multiblade coordinates and

$$\boldsymbol{M}(t) = \begin{bmatrix} \frac{1}{3} & \frac{1}{3} & \frac{1}{3} \\ \frac{2}{3}\cos(\omega_r t) & \frac{2}{3}\cos(\omega_r t + \frac{2\pi}{3}) & \frac{2}{3}\cos(\omega_r t + \frac{4\pi}{3}) \\ \frac{2}{3}\sin(\omega_r t) & \frac{2}{3}\sin(\omega_r t + \frac{2\pi}{3}) & \frac{2}{3}\sin(\omega_r t + \frac{4\pi}{3}) \end{bmatrix} \tag{E.3}$$

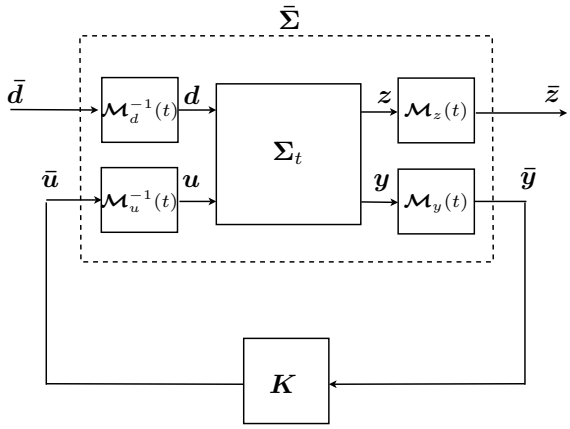

Figure E.1: From the point of view of the controller, the wind turbine and wind is described in the multiblade coordinates

A wind turbine model will in general contain several variable triplets describing the dynamics of the blades. Furthermore there will be a number of variables describing the non-rotating dynamics. Let $\boldsymbol{p}$ denote the augmented vector of the blade triplets and the variables describing the non-rotating dynamics. In the following $\boldsymbol{\mathcal{M}}_{\boldsymbol{p}}(t)$ will then denote the transform which takes the blade triplets to multiblade coordinates and leaves the variables in non-rotating coordinates untouched.

Now, assume that a linear wind turbine model is given which is time-variant due to the interaction between the rotating blade systems and the non-rotating system. We denote this model $\boldsymbol{\Sigma}_t$. The inputs are disturbances $\boldsymbol{d}$ and control signal $\boldsymbol{u}$. The outputs are the measurements $\boldsymbol{y}$ and a performance signal $\boldsymbol{z}$. Referring to Fig. E.1 we include a controller $\boldsymbol{K}$ which works in the multiblade coordinates. From the point of view of the controller it is controlling a time-invariant system $\bar{\boldsymbol{\Sigma}}$ which is affected by a disturbance $\bar{\boldsymbol{d}}$ described in the multiblade coordinates. From a control engineering point of view the most dominant disturbance which affects the wind turbine is the wind. Therefore, in order to make a high performing control design in multiblade coordinates a great advantage is gained by setting up a model of the wind in multiblade coordinates and using this knowledge in the controller design.

E.3 Wind model

The wind model describes the wind as it is seen by each *rotating* blade individually. The model is based on the frequency domain wind turbine modeling introduced in [8], where the focus was on load calculations. We focus in particular on the relation between the winds seen by different blades, furthermore, we take the description to multiblade coordinates and consider time domain realization of the frequency descriptions. Of up-most importance in the following is the so-called blade effective wind speed:

E.3.0.1 The blade effective wind speed

The blade effective wind speed v^e is the speed of the uniform wind which results in the same generalized force as a given wind distribution $v(r)$ along the span of the blade. This can be expressed mathematically as

$$v^e = \frac{\int_{r_0}^{R} X(r)v(r)dr}{\int_{r_0}^{R} X(r)dr}. \tag{E.4}$$

The inner and outer radii of the blade (measured from hub center) are denoted by r_0 and R respectively. X is a weight function which describes how much influence the wind has along the span of the blade. The wind distribution $v(r)$ is assumed to be in axial direction (orthogonal to the plane of rotation).

In this work, the simple linear choice $X(r) = r$ has been chosen for all blade forces under consideration. Simulations indicates that this is a reasonable approximation for control purposes.

E.3.0.2 Stochastic model of the effective wind

As starting point we consider the wind speed at a single point on the rotor disc (the circular plane in which the blades rotate). The point wind is expressed in polar coordinates as illustrated in Fig. E.2, the coordinates being the radii r and the azimuth angle ψ. At any given time t the point wind speed will be periodic in the azimuth angle. The main idea is now to make a Fourier expansion of the point wind in the azimuth angle. This results in the following expression where the Fourier coefficients $\tilde{v}_n(t,r)$ are time-dependent.

$$v(t,r,\psi) = \sum_{n=-\infty}^{\infty} \tilde{v}_n(t,r)e^{in\psi} \tag{E.5}$$

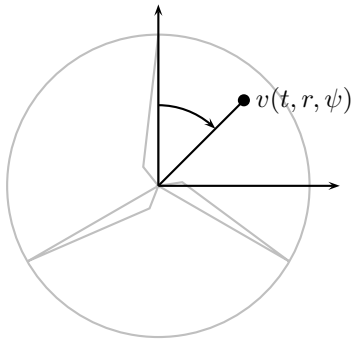

Figure E.2: Point wind on the rotor disc described in polar coordinates

we can now go from this expansion to a spectral description of the effective wind speed. Since the effective wind speed follows the rotating blade we enforce a constant angular velocity $\dot{\psi}(t) = \omega_r$ of the point winds as well as the definition of the effective wind speed. The spectral description is then obtained by first calculating the covariance between the two effective wind speeds and taking the Fourier transform. For two effective wind speed with an angular separation of $\Delta\psi$ we get the following cross-spectral density.

$$S^e(\omega, \Delta\psi) = \sum_{n=-\infty}^{\infty} \tilde{S}^e_{nn}(\omega - n\omega_r)e^{in\Delta\psi} \tag{E.6}$$

The derivation as well as an expression for $\tilde{S}^e_{nn}$ can be found in [11]. Equation (E.6) shows a very interesting property of the effective wind speed. Considering the auto-spectral density $S^e(\omega) \equiv S^e(\omega, 0)$ we see that in consist of a sum of spectra shifted in frequency as illustrated in Fig. E.3.

We now relate the derived spectral description of the effective wind speed to a three-bladed turbine. The blades are assumed evenly spaced giving an azimuth difference between two neighbors of $\Delta\psi = \frac{2\pi}{3}$. The effective wind vector is:

$$\boldsymbol{v}^e = \begin{bmatrix} v^e_1(t) & v^e_2(t) & v^e_3(t) \end{bmatrix}^T \tag{E.7}$$

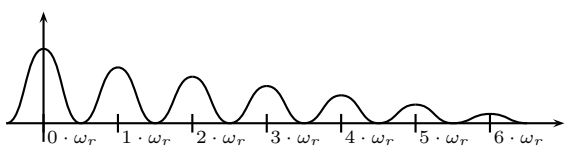

Figure E.3: Auto spectral density of effective wind speed

The corresponding spectral density matrix becomes

$$\boldsymbol{S}^e(\omega) = \sum_{n=-\infty}^{\infty} \tilde{S}^e_{nn}(\omega - n\omega_r)\boldsymbol{E} \tag{E.8}$$

where

$$\boldsymbol{E} = \begin{bmatrix} 1 & e^{in\frac{2\pi}{3}} & e^{in\frac{4\pi}{3}} \\ e^{in\frac{-2\pi}{3}} & 1 & e^{in\frac{2\pi}{3}} \\ e^{in\frac{-4\pi}{3}} & e^{in\frac{-2\pi}{3}} & 1 \end{bmatrix} \tag{E.9}$$

E.3.1 Spectral representation of wind in multiblade coordinates

For doing control we want the spectral description in multiblade coordinates. Applying the multiblade transformation $\boldsymbol{M}(t)$ to the the wind vector $\boldsymbol{v}^e$ we obtain the multiblade effective wind:

$$\bar{\boldsymbol{v}}^e = \boldsymbol{M}(t)\boldsymbol{v}^e \tag{E.10}$$

doing the math we get the spectral density matrix for the multiblade effective wind speed vector:

$$\bar{\boldsymbol{S}}(\omega) = \sum_{n=-\infty}^{\infty} \begin{bmatrix} \bar{\tilde{S}}^1_{nn}(\omega) & 0 & 0 \\ 0 & \bar{\tilde{S}}^{2,3}_{nn}(\omega) & \bar{\tilde{S}}^{2,3}_{n\underline{n}}(\omega)e^{\theta(n)} \\ 0 & \bar{\tilde{S}}^{2,3}_{nn}(\omega)e^{-\theta(n)} & \bar{\tilde{S}}^{2,3}_{nn}(\omega) \end{bmatrix} \tag{E.11}$$

where

$$\theta(n) = \begin{cases} -i\frac{\pi}{2} & \text{for } n \in \mathbb{U}^+ \\ i\frac{\pi}{2} & \text{for } n \in \mathbb{U}^- \end{cases} \tag{E.12}$$

$$\bar{\tilde{S}}^1_{nn}(\omega) = \begin{cases} \bar{\tilde{S}}^e_{nn}(\omega + n\omega_r) & \text{for } n \in \mathbb{U}_0 \\ 0 & \text{otherwise} \end{cases} \tag{E.13}$$

$$\bar{\tilde{S}}^{2,3}_{nn}(\omega) = \begin{cases} \bar{\tilde{S}}^e_{nn}(\omega + (n+1)\omega_r) & \text{for } n \in \mathbb{U}_+ \\ \bar{\tilde{S}}^e_{nn}(\omega + (n-1)\omega_r) & \text{for } n \in \mathbb{U}_- \\ 0 & \text{otherwise} \end{cases} \tag{E.14}$$

The sets $\mathbb{U}_0$, $\mathbb{U}_+$ and $\mathbb{U}_-$ are defined as follows:

$$\mathbb{U}_0 = \{\ldots, -6, -3, 0, 3, 6, \ldots\} \tag{E.15}$$

$$\mathbb{U}_+ = \{\ldots, -10, -7, -4, -1, 2, 5, 8, 11, \ldots\} \tag{E.16}$$

$$\mathbb{U}_- = \{\ldots, -11, -8, -5, -2, 1, 4, 7, 10, \ldots\} \tag{E.17}$$

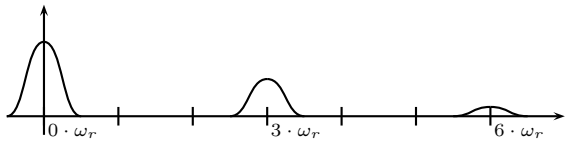

(a) 1. multiblade wind component

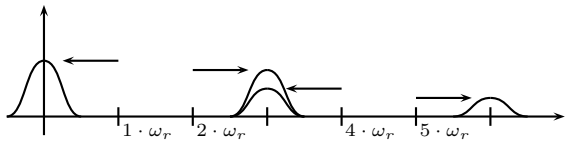

(b) 2. & 3. multiblade wind component

Figure E.4: The spectral description of the wind in multiblade coordinates

It is seen that the first component is uncorrelated with the second and third component whereas the second and third element are correlated by a constant phase-shift.

Fig. E.4a shows the structure of the auto spectral density of the first component. It is seen that the spectra $\tilde{S}^e_{nn}$ which are an integer multiple of 3 are retained from the original spectral description. Fig. E.4b shows the structure for the second and third component. Here is seen that the spectra $\tilde{S}^e_{nn}$ which are *not* an integer multiple of 3 are retained from the original description. However these spectra are shifted in frequency.

E.3.2 Control model of effective wind in multiblade coordinates

In this section we derive a linear model of the effective wind in multiblade coordinates suitable for use with linear controller synthesis. In essence we will describe the stochastic process with a LTI stochastic system. In the following it is useful to consider the following representation of such a system:

$$\boldsymbol{y}(t) = \int_{-\infty}^{t} \boldsymbol{g}(t-s)\boldsymbol{e}(s)dt \tag{E.18}$$

$\boldsymbol{g}(t)$ is the convolution kernel and $\boldsymbol{e}(t)$ is Gaussian distributed white noise with mean $\mathbf{0}$ and intensity $\boldsymbol{I}$ ($\boldsymbol{e}(t) \sim \mathcal{N}(\mathbf{0}, \boldsymbol{I})$).

The spectral density of $\boldsymbol{y}$ is given by (see e.g. [1])

$$\boldsymbol{S}_{yy} = \frac{1}{2\pi}\boldsymbol{G}(-i\omega)\boldsymbol{G}(i\omega) \tag{E.19}$$

where $\boldsymbol{G}(s)$ is the Laplace transform of the convolution kernel $\boldsymbol{g}(t)$, i.e. $\boldsymbol{G}(s) = \mathcal{L}(\boldsymbol{g}(t))$.

The spectral description of the wind $\bar{\boldsymbol{v}}$ does not pertain to a finite dimensional linear description in the time domain. This is evident from the constant phase-shift in the cross-spectrum and the infinite number of harmonics. Some information will therefore be lost in the approximation. To this end we propose to truncate the infinite series and disregard the covariance between the components. Recalling the structure of the auto-spectral densities it is natural to propose the following structure:

$$\bar{v}_1^e(t) = \sum_{n=0}^{N_1} G_{1,n} e_{1,n}(t) \tag{E.20}$$

$$\bar{v}_2^e(t) = \sum_{n=0}^{N_2} G_{2,n} e_{2,n}(t) \tag{E.21}$$

$$\bar{v}_3^e(t) = \sum_{n=0}^{N_3} G_{3,n} e_{3,n}(t) \tag{E.22}$$

where $G_{x,x}$ are the multiplicative operators associated with scalar stochastic linear systems. We will then obtain a good approximation to the auto-spectral densities when

$$\frac{1}{2\pi}|G_{1,n}(\omega)|^2 \approx \bar{\tilde{S}}_{nn}^1(\omega) \tag{E.23}$$

$$\frac{1}{2\pi}|G_{2,n}(\omega)|^2 \approx \bar{\tilde{S}}_{nn}^{2,3}(\omega) \tag{E.24}$$

$$\frac{1}{2\pi}|G_{3,n}(\omega)|^2 \approx \bar{\tilde{S}}_{nn}^{2,3}(\omega) \tag{E.25}$$

over the frequencies ω of interest.

Let $G_{x,n}(\omega) \equiv G(\omega;\boldsymbol{\theta})_{x,n}$ denote appropriate parameterization of the transfer functions. The approximation can then be done by solving the following optimization problem numerically.

$$J = \min_{\boldsymbol{\theta}} \sum_{\omega \in \mathcal{I}} \left(\frac{1}{2\pi}|G_n^s(\omega;\boldsymbol{\theta})|^2 - |S_{nn}^e(\omega)| \right)^2 \tag{E.26}$$

where $\mathcal{I}$ is the frequency range of interest.

E.4 Wind turbine model

E.4.1 Simulation model

The model which we use for simulation incorporates tower dynamics, rotational dynamics, aerodynamics, pitch actuators and a stochastic wind model.

The model of the tower includes the primary modal displacement in for-aft and side-to-side motion. The dynamics can be written in the following second order matrix equation:

$$\begin{bmatrix} m_T & 0 \\ 0 & m_T \end{bmatrix} \begin{bmatrix} \ddot{q}_T^Y \\ \ddot{q}_T^X \end{bmatrix} + \begin{bmatrix} k_T & 0 \\ 0 & k_T \end{bmatrix} \begin{bmatrix} \dot{q}_T^Y \\ \dot{q}_X^Z \end{bmatrix} + \begin{bmatrix} c_T & 0 \\ 0 & c_T \end{bmatrix} \begin{bmatrix} q_T^Y \\ q_T^X \end{bmatrix} = \begin{bmatrix} Q_T^Y \\ Q_T^X \end{bmatrix} \quad \text{(E.27)}$$

The generalized fores Q_F^X and Q_F^Y are the total forces in the X and Y directions respectively.

The model of the rotor is simply given by the inertia of all rotating parts (blades, drive shaft, generator, etc). The dynamics is given by the equation:

$$J_r \dot{\omega}_r + T_g = Q_M^Y \quad \text{(E.28)}$$

where J_r is the inertia and T_g is the generator torque which we assume is constant an chosen to balance out the torque from to rotor in equilibrium. Q_M^Y is the total moment about the Y-axis.

The aerodynamic are calculated using a simple BEM calculations as described

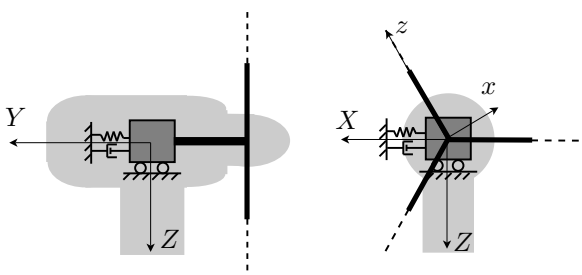

(a) Side view (b) Front view

Figure E.5: Structural model of wind turbine. Note that the local y-axis of the blades co-insides with the global Y-axis

in [5]. We assume that the relation is purely algebraic i.e. we do not consider e.g. dynamic inflow. With the chosen degrees of freedom in the model we can express the conversion of kinetic energy in the wind field $\boldsymbol{V}$ to the generalized forces of interest by the following functional.

$$\begin{bmatrix}\boldsymbol{Q}_F^y & \boldsymbol{Q}_F^x & \boldsymbol{Q}_M^y & \boldsymbol{Q}_M^x\end{bmatrix} = \boldsymbol{f}(\boldsymbol{V}, \dot{q}_T^Y, \dot{q}_T^X, \boldsymbol{\beta}, t) \tag{E.29}$$

The generalized forces on the left hand side are: The blade root force in y- and x-direction $\boldsymbol{Q}_F^y$, $\boldsymbol{Q}_F^x$. The blade root moments about the y- and x-axis $\boldsymbol{Q}_M^y$,$\boldsymbol{Q}_M^x$. We can relate these local generalized forces to the global generalized forces appearing in equation (E.27) and (E.28) through the multiblade transformation:

$$Q_F^Y = \begin{bmatrix}3 & 0 & 0\end{bmatrix} \boldsymbol{M}(t)\boldsymbol{Q}_F^y \tag{E.30}$$

$$Q_F^X = \begin{bmatrix}0 & 0 & \frac{3}{2}\end{bmatrix} \boldsymbol{M}(t)\boldsymbol{Q}_F^x \tag{E.31}$$

$$Q_M^Y = \begin{bmatrix}3 & 0 & 0\end{bmatrix} \boldsymbol{M}(t)\boldsymbol{Q}_M^y \tag{E.32}$$

The yaw and tilt moments which we want to minimize using a controller are given as follows:

$$\begin{bmatrix}Q_{yaw} \\ Q_{tilt}\end{bmatrix} = \begin{bmatrix}0 & 0 & \frac{3}{2} \\ 0 & \frac{3}{2} & 0\end{bmatrix} \boldsymbol{M}(t)\boldsymbol{Q}_M^x \tag{E.33}$$

We use the Veers method [13] for simulating the point winds affecting the blades. This results in a rectangular grid of point wind speeds. A resolution of 10×10 wind speeds is chosen and the point wind at a specific location is found by cubic spline interpolation. The vector point wind speeds at a given time is denoted by $\boldsymbol{V}(t)$

The actuator dynamics is given by the following set of uncoupled differential equations

$$\begin{bmatrix}\tau_\beta & 0 & 0 \\ 0 & \tau_\beta & 0 \\ 0 & 0 & \tau_\beta\end{bmatrix} \dot{\boldsymbol{\beta}} + \boldsymbol{\beta} = \boldsymbol{\beta}_r \tag{E.34}$$

where τ_β is the time constant of the actuator dynamics and $\boldsymbol{\beta}_r$ is the pitch reference for the blades.

E.4.2 Linear design model

The tower and rotor dynamics described in the previous section is already linear and given in non-rotating coordinates. The dynamics in equations (E.27) and (E.28)) will therefore be used directly.

When linearizing the aerodynamics we introduce the definition of the effective wind speed. Since the effective wind speed pertains to a specific generalized blade force, we introduce independent effective wind speeds for each generalized blade force in the model. The effective wind speed vectors $\boldsymbol{v}_F^y$, $\boldsymbol{v}_F^x$, $\boldsymbol{v}_M^y$, $\boldsymbol{v}_M^x$ are therefore associated with $\boldsymbol{Q}_F^y$, $\boldsymbol{Q}_F^x$, $\boldsymbol{Q}_M^y$, $\boldsymbol{Q}_M^x$ respectively. The linearized aerodynamics takes the following form:

$$Q_F^Y = \begin{bmatrix} d_{F,\beta}^Y & 0 & 0 \end{bmatrix} \boldsymbol{M}(t)\boldsymbol{\beta} + \begin{bmatrix} d_{F,v}^Y & 0 & 0 \end{bmatrix} \boldsymbol{M}(t)\boldsymbol{v}_F^y \tag{E.35}$$

$$Q_F^X = \begin{bmatrix} 0 & 0 & d_{F,\beta}^X \end{bmatrix} \boldsymbol{M}(t)\boldsymbol{\beta} + \begin{bmatrix} 0 & 0 & d_{F,v}^X \end{bmatrix} \boldsymbol{M}(t)\boldsymbol{v}_F^x \tag{E.36}$$

$$Q_M^Y = \begin{bmatrix} d_{M,\beta}^Y & 0 & 0 \end{bmatrix} \boldsymbol{M}(t)\boldsymbol{\beta} + \begin{bmatrix} d_{M,v}^Y & 0 & 0 \end{bmatrix} \boldsymbol{M}(t)\boldsymbol{v}_M^y \tag{E.37}$$

$$Q_{yaw} = \begin{bmatrix} 0 & 0 & d_{M,\beta}^{yaw} \end{bmatrix} \boldsymbol{M}(t)\boldsymbol{\beta} + \begin{bmatrix} 0 & 0 & d_{M,v}^{yaw} \end{bmatrix} \boldsymbol{M}(t)\boldsymbol{v}_M^x \tag{E.38}$$

$$Q_{tilt} = \begin{bmatrix} 0 & d_{M,\beta}^{tilt} & 0 \end{bmatrix} \boldsymbol{M}(t)\boldsymbol{\beta} + \begin{bmatrix} 0 & d_{M,v}^{tilt} & 0 \end{bmatrix} \boldsymbol{M}(t)\boldsymbol{v}_M^x \tag{E.39}$$

The relations above are rendered time-invariant by transforming the inputs to the following multiblade equivalents:

$$\bar{\boldsymbol{\beta}} = \boldsymbol{M}(t)\boldsymbol{\beta} \tag{E.40}$$

$$\bar{\boldsymbol{v}}_F^y = \boldsymbol{M}(t)\boldsymbol{v}_F^y \ , \quad \bar{\boldsymbol{v}}_F^x = \boldsymbol{M}(t)\boldsymbol{v}_F^x \tag{E.41}$$

$$\bar{\boldsymbol{v}}_M^y = \boldsymbol{M}(t)\boldsymbol{v}_M^y \ , \quad \bar{\boldsymbol{v}}_M^x = \boldsymbol{M}(t)\boldsymbol{v}_M^x \tag{E.42}$$

For each effective wind speed vector we associate a linear stochastic model as described in Sec. E.3.2. Denoting the multiplicative operator associated with the system $\boldsymbol{G}_v$ the total model of the wind becomes:

$$\begin{bmatrix} \bar{\boldsymbol{v}}_F^y \\ \bar{\boldsymbol{v}}_F^x \\ \bar{\boldsymbol{v}}_M^y \\ \bar{\boldsymbol{v}}_M^x \end{bmatrix} = \begin{bmatrix} \boldsymbol{G}_v & & & \\ & \boldsymbol{G}_v & & \\ & & \boldsymbol{G}_v & \\ & & & \boldsymbol{G}_v \end{bmatrix} \begin{bmatrix} \boldsymbol{e}_1 \\ \boldsymbol{e}_2 \\ \boldsymbol{e}_3 \\ \boldsymbol{e}_4 \end{bmatrix} \tag{E.43}$$

where $\boldsymbol{e}_1, \ldots, \boldsymbol{e}_4$ are mutually uncorrelated. The LTI wind model which we use in this paper approximates the harmonic spectra for $n = 0, 1, 2, 3, 4$.

Transforming the pitch dynamics to multiblade coordinates we get

$$\begin{bmatrix} \tau_\beta & 0 & 0 \\ 0 & \tau_\beta & 0 \\ 0 & 0 & \tau_\beta \end{bmatrix} \dot{\bar{\boldsymbol{\beta}}} + \begin{bmatrix} 1 & 0 & 0 \\ 0 & 1 & \omega_r \tau_\beta \\ 0 & -\omega_r \tau_\beta & 1 \end{bmatrix} \bar{\boldsymbol{\beta}} = \bar{\boldsymbol{\beta}}_r \tag{E.44}$$

E.4.3 Parameters and operating conditions

The parameters used in the simulation model and design model has been adapted from a 1.5 MW wind turbine. A selection of key-parameters for the model is

Table E.1: Selected key parameters for 1.5 MW wind turbine model

Parameter	value	
m_t	$9.35 \cdot 10^4$	kg
k_t	$6.51 \cdot 10^5$	N/m
c_t	$3.25 \cdot 10^4$	s^{-1}
τ	0.1	s
J_r	$3.04 \cdot 10^6$	kg·m^2
ω_r rated	2.1	rad/s

shown in Table E.1. In the simulations we operate the wind turbine at a mean wind speed of $v_m = 16$ m/s. The stochastic properties of the wind are chosen realistically. The auto-spectral density of the point wind is e.g. chosen as a Kaimal spectrum. Further details are omitted in this paper.

The wind speed conditions are *above rated*, which means that the energy in the wind exceeds the limits of the generator. The primary objective is therefore to keep the rotational speed $\dot{\psi}_r = \omega_r$ constant. Since the tower is lightly damped, it is also of importance to ensure that the controller provides some damping to the tower. This will be done by targeting the tower deflection speed in the design. For load attenuation we want to attenuate the yaw and tilt moments in the support of the blades.

E.5 Controller synthesis

For the controller synthesis we will assume that the linear design model in multiblade coordinates is given in the following state space form:

$$\bar{\boldsymbol{\Sigma}} \; : \; \begin{cases} \dot{\bar{\boldsymbol{x}}} &= \boldsymbol{A}\bar{\boldsymbol{x}} + \boldsymbol{B}_u\bar{\boldsymbol{u}} + \boldsymbol{B}_e\bar{\boldsymbol{e}} \\ \bar{\boldsymbol{y}} &= \boldsymbol{C}\bar{\boldsymbol{x}} + \boldsymbol{D}\bar{\boldsymbol{u}} + \bar{\boldsymbol{w}} \\ \bar{\boldsymbol{z}} &= \begin{bmatrix} \boldsymbol{C}_z & 0 \\ 0 & \boldsymbol{I} \end{bmatrix} \begin{bmatrix} \bar{\boldsymbol{x}} \\ \bar{\boldsymbol{u}} \end{bmatrix} \end{cases} \tag{E.45}$$

where $\bar{\boldsymbol{x}}$ is the state vector, $\bar{\boldsymbol{u}}$ is the control signal, $\bar{\boldsymbol{e}}$ is the state noise, $\bar{\boldsymbol{w}}$ is the measurement noise, $\bar{\boldsymbol{y}}$ is the measurable output and $\bar{\boldsymbol{z}}$ is the signal which we seek to minimize in some sense using a controller. We use the $(\cdot)$ notation to emphasize that the dynamics is given in multiblade coordinates. To obtain a realistic controller design we embed a high-pass filtration of the multiblade pitch signal $\bar{\boldsymbol{\beta}}$ in the state space model. The high pass filter is used in the controller design to punish high frequency activity more heavily than low frequency

activity. The high pass filter has been chosen as the following transfer function:

$$\bar{\beta}_{W,k} = \frac{(s+0.8)^3}{(s+3)^3}\bar{\beta}_k \ , \quad k = 1,2,3 \tag{E.46}$$

where $\bar{\beta}_{W,k}$ is the filtered pitch signal.

The signals $\boldsymbol{u}$, $\boldsymbol{x}$, $\boldsymbol{y}$, $\boldsymbol{z}$, $\boldsymbol{e}$, $\boldsymbol{w}$ are specified in the following. $\bar{\boldsymbol{u}}$ is the vector of multiblade pitch references.

$$\bar{\boldsymbol{u}} = \bar{\boldsymbol{\beta}}_r \tag{E.47}$$

$\bar{\boldsymbol{e}}$ is the white noise input to the wind model

$$\bar{\boldsymbol{e}} = \begin{bmatrix}(\boldsymbol{e}_1)^T & (\boldsymbol{e}_2)^T & (\boldsymbol{e}_3)^T & (\boldsymbol{e}_4)^T\end{bmatrix}^T \tag{E.48}$$

$\bar{\boldsymbol{y}}$ is the measurable output. We assume that we have measurements of the following quantities: tower deflection speed, tilt and yaw moment, rotational speed and the pitch angles. The measurements are assumed to be corrupted by measurement noise $\bar{\boldsymbol{w}}$.

$$\bar{\boldsymbol{y}} = \begin{bmatrix}\dot{q}_T^X & \dot{q}_T^Z & Q_{yaw} & Q_{tilt} & \omega_r & \bar{\boldsymbol{\beta}}^T\end{bmatrix}^T + \bar{\boldsymbol{w}} \tag{E.49}$$

The level of the measurement noise $\bar{\boldsymbol{w}}$ is used as an artificial parameter in the controller design for tuning the controller. We do not actually include measurement noise in the simulations. $\bar{\boldsymbol{z}}$ is the signal which we seek to optimize in the controller design. To achieve the desired objectives $\boldsymbol{z}$ consists of the side-side and for-aft deflection speeds, the yaw and tilt moment, the rotational speed, the filtered pitch angles and the pitch angle references:

$$\bar{\boldsymbol{z}} = \begin{bmatrix}\dot{q}_T^X & \dot{q}_T^Z & Q_{yaw} & Q_{tilt} & \omega_r & \bar{\boldsymbol{\beta}}_W & \bar{\boldsymbol{\beta}}_r\end{bmatrix}^T \tag{E.50}$$

Although the input-output map of the system is unique the internal model is non-unique. The state vector $\bar{\boldsymbol{x}}$ is therefore not unique and the details of the actual choice is omitted.

The controller design used in this work minimizes the following quadratic cost on the performance signal $\boldsymbol{z}$:

$$J = \lim_{t\to\infty} \mathbb{E}\left\{\int_0^t \left(\boldsymbol{z}^T \begin{bmatrix}\boldsymbol{W}_1 & 0 \\ 0 & \boldsymbol{W}_2\end{bmatrix} \boldsymbol{z}\right) dt\right\} \tag{E.51}$$

$$= \lim_{t\to\infty} \mathbb{E}\left\{\int_0^t \left(\boldsymbol{x}^T \boldsymbol{C}_z^T \boldsymbol{W}_1 \boldsymbol{C}_z \boldsymbol{x} + \boldsymbol{u}^T \boldsymbol{W}_2 \boldsymbol{u}\right) dt\right\} \tag{E.52}$$

The solution to this problem is the celebrated LQG controller which can be expressed as follows:

$$\bar{\boldsymbol{K}} \ : \ \begin{cases} \dot{\hat{\bar{\boldsymbol{x}}}} &= \boldsymbol{A}\hat{\bar{\boldsymbol{x}}} + \boldsymbol{B}\bar{\boldsymbol{u}} + \boldsymbol{L}(\bar{\boldsymbol{y}} - (\boldsymbol{C}\hat{\bar{\boldsymbol{x}}} + \boldsymbol{D}\bar{\boldsymbol{u}})) \\ \bar{\boldsymbol{u}} &= \boldsymbol{F}\hat{\bar{\boldsymbol{x}}} \end{cases} \tag{E.53}$$

The matrix $\boldsymbol{L}$ is the so-called Kalman filter gain and the matrix $\boldsymbol{F}$ is the LQ state feedback gain. See e.g. [1] for details on the LQG controller.

E.6 SIMULATIONS

The control setup in the previous section is illustrated with simulations. The individual pitch controller is compared to a collective pitch controller. The collective pitch controller is based on an equivalent setup apart for the weights associated with Q_{yaw} and Q_{tilt}. These are set to zero, which effectively causes collective pitch behavior.

The model of the wind turbine and wind used in the simulation are as described in Sec. E.4.1. The realization of the wind at hub center is shown in Fig. E.6.

Fig. E.7 shows the closed loop trajectories for rotor rotation ω_r and tower deflection speeds $\dot{q}_T^Y$ and $\dot{q}_T^X$. Both the collective pitch controller and the individual pitch controller manage to keep the rotational speed relatively constant while at the same time attenuating the vibrations in the tower. Although the individual pitch controller hos more objectives than the collective pitch controller, they perform equally well w.r.t. attenuating deviations in rotational speed and tower vibrations.

Fig. E.8 shows the yaw and tilt moment of the wind turbine. It is seen that the individual pitch controller manages to attenuate the yaw and tilt moment significantly as compared to the collectively controlled system. If the blades were allowed to pitch at high frequencies (if we removed the high-pass filter in the design) further attenuation can be obtained. However, this would cause a very aggressive pitch activity.

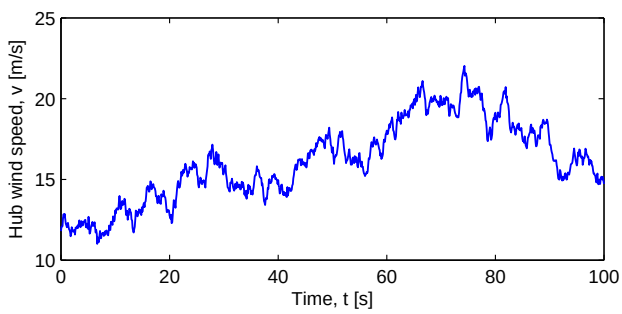

Figure E.6: Wind speed at hub center

Fig. E.9 shows the pitch angle β_1 and pitch angle rate $\dot{\beta}_1$ for the individual pitch controlled system and the collective pitch controlled system. The plots clearly show that attenuating the asymmetric loads comes at a cost. The pitch activity is significantly higher with the individual pitch controller than the collective pitch controller. It is expected that the peak pitch rates are at the limits of what is acceptable. If further detuning is necessary, it is easily done by adjusting the frequency-dependent weight on the pitch.

It is stressed that a full wind turbine controller should be designed to handle varying operating conditions. However, the simulations indicate that a linear design can be justified when working around a given operating point.

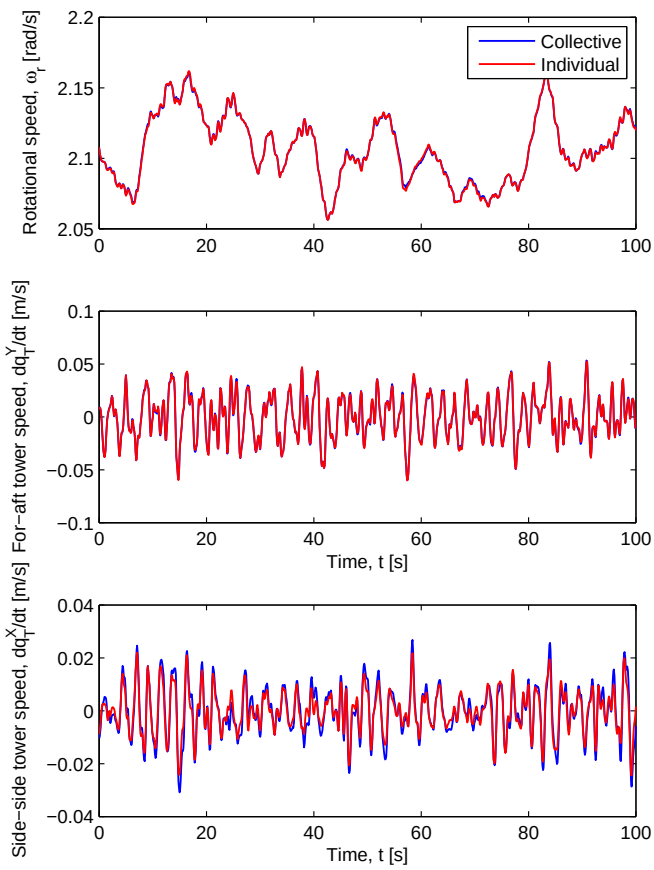

Figure E.7: Rotational speed ω_r and tower deflection speed $\dot{q}_t$

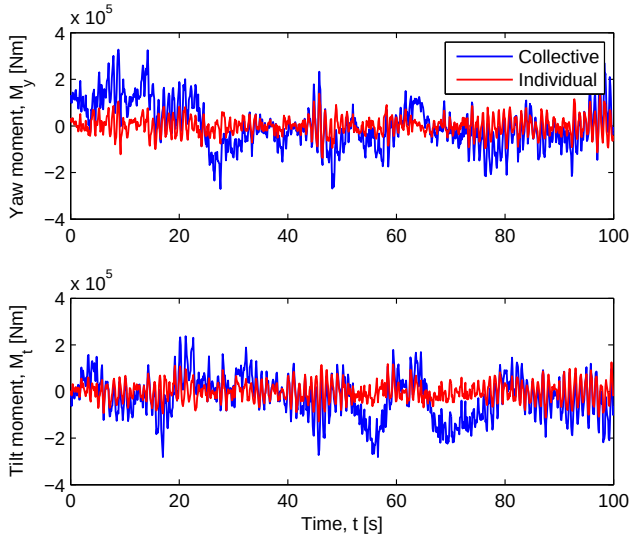

Figure E.8: Yaw moment M_y and tilt moment M_t

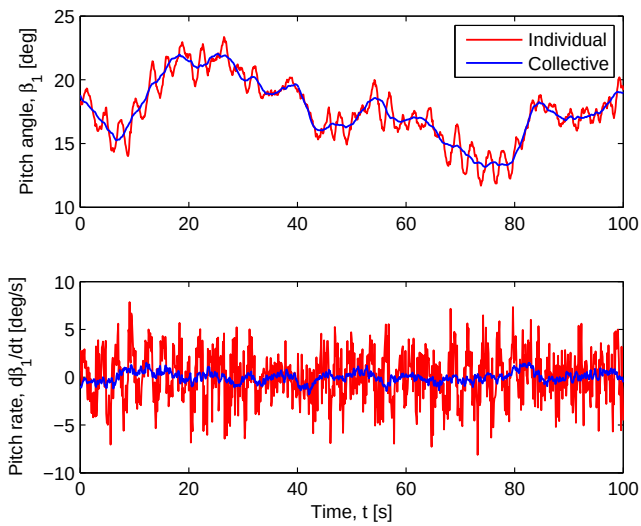

Figure E.9: Pitch angle β_1 and pitch angle speed $\dot{\beta}_1$

E.7 CONCLUSION

In this paper we have shown how to set up simplified models of the wind which can be incorporated in individual pitch controller designs. Since it is advantageous to do control in multiblade coordinates the wind model was derived in these coordinates. The proposed model was applied together with a simplified model of the aerodynamics and a wind turbine in a LQG controller design. Simulations show that the resulting controller succeeds in attenuating the effect of the stochastic wind field.

Bibliography

[1] K.J. Åstrøm. *Introduction to stochastic control theory.* Academic Press New York, 1970.

[2] E.A. Bossanyi. Individual Blade Pitch Control for Load Reduction. *Wind Energy*, 6(2):119–128, 2003. DOI: 10.1002/we.76.

[3] E.A. Bossanyi. Wind turbine control for load reduction. *Wind Energy*, 6(3):229–244, 2003. DOI:10.1002/we.95.

[4] M.J. Grimble. Horizontal axis wind turbine control: comparison of classical, LQG and $\mathcal{H}_\infty$ designs. *Dynamics and Control*, 6(2):143–161, 1996. DOI:10.1007/BF02169534.

[5] M. O. L. Hansen. *Aerodynamics of Wind Turbines.* James & James, 2000.

[6] T.J. Larsen, H.A. Madsen, and K. Thomsen. Active load reduction using individual pitch, based on local blade flow measurements. *Wind Energy*, 8(1):67–80, 2005. DOI:10.1002/we.141.

[7] D.J. Leith and W.E. Leithead. Implementation of wind turbine controllers. *International Journal of Control*, 66(3):349–380, 1997.

[8] P. Sørensen. Frequency domain modelling of wind turbine structures. Technical report, Risø National Laboratory, Roskilde, Denmark, 1994.

[9] K.A. Stol, W. Zhao, and A. D. Wright. Individual blade pitch control for the controls advanced research turbine (cart). *Journal of Solar Energy Engineering*, 128:498–505, November 2006. DOI:10.1115/1.2349542.

[10] S.C. Thomsen, H. Niemann, and N.K. Poulsen. Individual pitch control of wind turbines using local inflow measurements. *Proceedings of the 17th IFAC World Congress, IFAC'08*, pages 5587–5592, 2008.

[11] S.C. Thomsen, H. Niemann, and N.K. Poulsen. Stochastic wind turbine modeling for individual pitch control. In *Proceedings of the European Control Conference*, 2009.

[12] S.C. Thomsen and N.K. Poulsen. A disturbance decoupling nonlinear control law for variable speed wind turbines. In *Proceedings of the 15th Mediterranean Conference on Control and Automation*, pages 1268–1273, 2007.

[13] Paul S. Veers. Three-dimensional wind simulation. Technical report, Sandia National Laboratories, 1988.

Paper F

Robust stability in predictive control with soft constraints

abstract

In this paper we take advantage of the primary and dual Youla parameterizations for setting up a soft constrained model predictive control (MPC) scheme for which stability is guaranteed in face of norm-bounded uncertainties. Under special conditions guarantees are also given for hard input constraints. In more detail, we parameterize the MPC predictions in terms of the primary Youla parameter and use this parameter as the online optimization variable. The uncertainty is parameterized in terms of the dual Youla parameter. Stability can then be guaranteed through small gain arguments on the loop consisting of the primary and dual Youla parameter. This is included in the MPC optimization as a constraint on the induced gain of the optimization variable. We illustrate the method with a numerical simulation example.

F.1 Introduction

Model predictive control (MPC) - also commonly denoted constrained predictive control - is a model based control method which has attracted a lot of attention partly due to its popularity in the process industry. The feature which makes it truly innovative is its ability to handle constraints on control action and states/output. This is done through on-line optimization of the future trajectory. More specifically, at each sampling time, starting at the current state, an open-loop optimal control problem is solved over a finite horizon. The theoretical foundation of nominal linear MPC has matured over the last decades and a well established theoretical basis for ensuring stability and feasibility has been established (See eg. [5], [7]).

In this work we propose a method for guaranteeing robust stability in the model predictive control framework. In the setup we consider general disturbances belonging to the l_2 function class and therefore primarily consider soft constraints. The method can be seen as a closed loop re-parameterization of nominal soft-constrained MPC such that robust stability has a simple interpretation in terms of the on-line optimization variable. The aim of the method is to guarantee stability with minimal addtional complexity to the nominal optimization problem. To this end we emphasise that no guarantees are given with respect to robust constraint handling nor robust performance.

We take advantage of the classical system theoretical approach of the Youla parameterizations. For this reason the method will be denoted Youla-MPC (YMPC) in the paper. The primary Youla parameterization is the parameterization of all stabilizing controllers, whereas the dual Youla parameterization is the parameterization of all systems stabilized by a given controller. The nominal closed-loop system has an affine dependency on the primary Youla parameter, which makes it attractive as an optimization variable. We parameterize the MPC optimization problem in terms of the primary Youla parameter. This results in a (nominal) optimization problem with complexity similar to standard MPC, ie. given a quadratic cost and linear inequality constraints, the problem reduces to a quadratic programming problem. Uncertainty is handled by expressing the uncertainty in terms of the dual Youla parameter. Stability of the closed loop can then be reduced to a problem involving the primary and dual Youla parameter alone. This leads to a norm constraint on the primary Youla parameter which can be included in the online optimization problem.

The work in this paper can be seen partly as a generalization and partly as an extension of the work in [13, 14]. In the first paper [13] it was shown that nominal stability can be guaranteed in MPC by parameterizing the controller in terms of a time-varying Youla parameter. In [14] it was shown how model

uncertainties with bounded 1-norm can be handled in their framework. All investigations in [13, 14] were made with a state estimate feedback realization of all stabilizing controllers.

The Youla parameterization has been considered in connection with MPC in other works as well. Back in the days of GPC it was introduced in [4] as part of a GPC algorithm (no constraints) with guaranteed stability. Recently several authors have considered various Youla approaches: [10] and [2] have considered algorithms for robustifying MPC offline through the Youla parameterization. [6] used the Youla parameter to set up a stable MPC scheme that can deal with computational delays. [12] investigated the use of both the primary and dual Youla parameterizations in gaining information about the uncertainty and reconfiguring the controller in a modular setup.

F.2 Setup and preliminaries

F.2.1 System setup

We consider the following discrete linear time-invariant system:

$$\Sigma \ : \ \begin{cases} q(k) & = & G_{qp}p(k) + G_{qu}u(k) \\ y(k) & = & G_{yp}p(k) + G_{yu}u(k) \end{cases} \tag{F.1}$$

where u is the control input. p is the disturbance input. q is an auxiliary output. $y(k)$ is a measurable output. An uncertainty enters the system through the relation

$$p(k) = \Delta q(k) \tag{F.2}$$

where Δ is an unknown LTI perturbation. The system is assumed controlled by the controller K_0

$$u(k) = K_0 y(k) \tag{F.3}$$

which has been designed such that the system is robustly stable for

$$\|\Delta\|_\infty = \sup_{|z|=1} \bar{\sigma}(\Delta(z)) \leq 1 \tag{F.4}$$

where $\bar{\sigma}$ is the maximum singular value.

We assume that input and output disturbances (e_1 and e_2 respectively) are perturbing the closed loop system as seen in Fig. F.1.

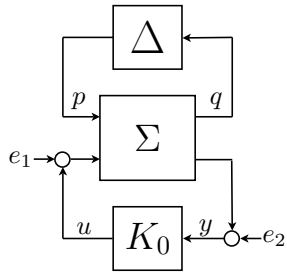

Figure F.1: System setup: The system is controlled by the feedback controller K_0 which stabilizes Σ subject to the unknown LTI system Δ.

F.2.2 The Youla parameterizations

The Youla parameterization of all stabilizing controllers is well known and has been used to large extent in controller synthesis (See e.g. [15]). With reference to equation (F.1) we consider the system $G_0 \equiv G_{yu}$ and stabilizing controller K_0 (both transfer matrices). System and controller can be written as left or right co-prime factorizations:

$$G_0 = N_r M_r^{-1} = M_l^{-1} N_l \tag{F.5}$$

$$K_0 = U_r V_r^{-1} = V_l^{-1} U_l \tag{F.6}$$

where $N_r, M_r, U_r, V_r, N_l, M_l, U_l, V_l \in \mathcal{RH}_\infty$ and satisfy the double Bezout identity

$$\begin{pmatrix} I & 0 \\ 0 & I \end{pmatrix} = \begin{pmatrix} V_l & -U_l \\ -N_l & M_l \end{pmatrix} \begin{pmatrix} M_r & U_r \\ N_r & V_r \end{pmatrix} \tag{F.7}$$

$$= \begin{pmatrix} M_r & U_r \\ N_r & V_r \end{pmatrix} \begin{pmatrix} V_l & -U_l \\ -N_l & M_l \end{pmatrix} \tag{F.8}$$

Then all controllers which stabilize G_0 are given as:

$$K(Q) = (U_r + M_r Q)(V_r + N_r Q)^{-1} \tag{F.9}$$

$$K(Q) = (V_l + Q N_l)^{-1}(U_l + Q M_l) \tag{F.10}$$

where $Q \in \mathcal{RH}_\infty$ is called the Youla parameter. K_0 is naturally attained when $Q = 0$.

The dual of the Youla parameterization is all systems stabilized by a given controller [8][11]. This is commonly denoted the dual Youla parameterization. The parameterization can be written as follows:

$$G(S) = (N_r + V_r S)(M_r + U_r S)^{-1} \tag{F.11}$$

$$G(S) = (M_l + S U_l)^{-1}(N_l + S V_l) \tag{F.12}$$

where $S \in \mathcal{RH}_\infty$ is the dual Youla parameter. The nominal system G_0 is naturally attained for $S = 0$. A useful interpretation of S is that of a frequency-shaped version of the uncertainty. The relation between Δ and S is given by [8]:

$$S(\Delta) = M_3\Delta(I - M_1\Delta)^{-1}M_2 \tag{F.13}$$

where

$$M_1 = G_{qp} + G_{qu}U_rM_lG_{yp} \tag{F.14}$$

$$M_2 = G_{qu}M_r, \quad M_3 = M_lG_{yp} \tag{F.15}$$

An important observation for the method in this paper is that $S \equiv S(\Delta)$ is stable if and only if the system is robustly stabilized by K_0[11].

Having the controller parameterized in terms of Q and the uncertainty in terms of S the transfer function from the disturbances $r = \begin{bmatrix} e_1^T & e_2^T \end{bmatrix}^T$ to the outputs $z = \begin{bmatrix} y^T & u^T \end{bmatrix}^T$ can be written in the following convenient form:

$$F(S,Q) = T_{zr}(S) + T_{z\eta}(S)S(I - SQ)^{-1}T_{\epsilon r}(S) \tag{F.16}$$

where

$$T(S) = \begin{pmatrix} T_{zr}(S) & T_{z\eta}(S) \\ T_{\epsilon r}(S) & S \end{pmatrix} \tag{F.17}$$

$$= \begin{pmatrix} \begin{pmatrix} I & -K \\ -G(S) & I \end{pmatrix}^{-1} & \begin{pmatrix} N_r(S) \\ M_r(S) \end{pmatrix} \\ \begin{pmatrix} N_l(S) & M_l(S) \end{pmatrix} & S \end{pmatrix} \tag{F.18}$$

F.3 Method

The fundamental idea of YMPC is to parameterize the predictions in terms of the primary Youla parameter Q. Likewise the uncertainty description is parameterized in terms of a dual Youla parameter S. Consequently, a direct link can be established between the properties of Q and stability.

F.3.1 Predictions for YMPC

In the following we assume that the structure of the Youla parameter is given as follows:

$$Q_k = \Theta(k)\tilde{Q} \tag{F.19}$$

where $\tilde{Q} \in \mathcal{RH}_\infty$ and $\Theta(k)$ is a time-varying gain of appropriate dimensions. $\Theta(k)$ is the free parameter with which the cost is to be optimized in the YMPC controller at every sample k. The structure is chosen such that the predictions will have an affine dependency on the free parameters.

In deriving the prediction equations we use the following matrix notation: $I_{N\times N}$ denotes the N-dimensional identity matrix. I_N denotes an N-dimensional column vector with ones. $\otimes$ denotes the Kronecker product and $vec(\cdot)$ denotes the vectorization operator. The extended observability matrix and Toeplitz matrix are denoted by:

$$\mathcal{O}^N(A,C) = \begin{bmatrix} C^T & (CA)^T & (CA^2)^T & \cdots & (CA^N)^T \end{bmatrix}^T \tag{F.20}$$

$$\mathcal{T}^N(A,B,C,D) = \begin{bmatrix} D & 0 & \cdots & 0 & 0 \\ CB & D & \cdots & 0 & 0 \\ CAB & CB & \cdots & 0 & 0 \\ \vdots & \vdots & \ddots & \vdots & \vdots \\ CA^{N-1}B & CA^{N-2}B & \cdots & CB & D \end{bmatrix} \tag{F.21}$$

The N step predictions of a signal v from knowledge up until time k will be denoted $\vec{v}_N(k)$:

$$\vec{v}_N(k) = \begin{bmatrix} v(k|k)^T & v(k+1|k)^T & \dots & v(k+N|k)^T \end{bmatrix}^T \tag{F.22}$$

Since Δ is unknown we base the predictions on the nominal dynamics ($\Delta = 0 \Rightarrow S = 0$). For $S = 0$ we can write the closed loop system from r to z (using equation (F.16))

$$z(k) = F(0, Q_k)r(k) \tag{F.23}$$
$$= T_{zr}(0)r(k) + T_{z\eta}(0)Q_k T_{\epsilon r}(0)r(k) \tag{F.24}$$
$$= T_{zr}r(k) + T_{z\eta}\Theta(k)\tilde{Q}T_{\epsilon r}r(k) \tag{F.25}$$

In deriving the prediction equations the internal form (state space) of T and $\tilde{Q}$ are assumed to be as follows (using standard compact notation [16])

$$T \overset{s}{=} \left[\begin{array}{c|cc} A_T & B_{T,r} & B_{T,\eta} \\ \hline C_{T,z} & D_{T,zr} & D_{T,z\eta} \\ C_{T,\epsilon} & D_{T,\epsilon\eta} & D_{T,\epsilon\eta} \end{array}\right] \quad \tilde{Q} \overset{s}{=} \left[\begin{array}{c|c} A_Q & B_Q \\ \hline C_Q & D_Q \end{array}\right] \tag{F.26}$$

The state vector of T and $\tilde{Q}$ will be denoted x_T and x_Q respectively. To simplify the prediction equations, we divide the signal z into the nominal part ($Q = 0$) and the contribution due to $Q \neq 0$.

$$z(k) = z_0(k) + z_Q(k) \tag{F.27}$$

Defining the following extended observability matrices and Toeplitz matrices we can write the N-step prediction explicitly:

$$\mathcal{A}_z = \mathcal{O}^N(A, C_z) \quad \mathcal{A}_Q = \mathcal{O}^N(A_Q, C_Q) \tag{F.28}$$
$$\mathcal{A}_\epsilon = \mathcal{O}^N(A, C_\epsilon) \tag{F.29}$$
$$\mathcal{B}_{zr} = \mathcal{T}^N(A, B_r, C_r, D_{zr}) \tag{F.30}$$
$$\mathcal{B}_{z\eta} = \mathcal{T}^N(A, B_\eta, C_z, D_{z\eta}) \tag{F.31}$$
$$\mathcal{B}_{\epsilon r} = \mathcal{T}^N(A, B_r, C_\epsilon, D_{\epsilon r}) \tag{F.32}$$
$$\mathcal{B}_Q = \mathcal{T}^N(A_Q, B_Q, C_Q, D_Q) \tag{F.33}$$

The N-step prediction of z_0 due to the N-step trajectory of r is trivially

$$\vec{z}_{0,N}(k) = \mathcal{A}_z x_T(k) + \mathcal{B}_{zr}\vec{r}(k) \tag{F.34}$$

The N-step prediction of z_Q is given by

$$\vec{z}_{Q,N}(k) = \mathcal{B}_{z\eta}(I \otimes \Theta(k))(\mathcal{A}_Q x_Q(k) + \mathcal{B}_Q\vec{\epsilon}(k)) \tag{F.35}$$
$$= \mathcal{B}_{z\eta}((\mathcal{A}_Q x_Q(k) + \mathcal{B}_Q\vec{\epsilon}(k))^T \otimes I)vec(\Theta(k)) \tag{F.36}$$

where

$$\vec{\epsilon}(k) = A_\epsilon x_T(k) + B_{\epsilon r}\vec{r}(k) \tag{F.37}$$

The Kronecker product is a bilinear operator and therefore we see that the predictions have an affine dependency on the elements of $\Theta(k)$. This means that the resulting MPC optimization problem has complexity similar to standard MPC where the predictions are affine in the open loop trajectory.

Remark 10. *The predictions depend on the state of x_T which in general consists of the states of the system G, the controller K_0, and the co-prime factors M_r, N_r, M_l, N_l. In the output feedback case, we do not know the actual state of the system, but must in this case resort to a state estimate.*

Remark 11. *The parameterization and thereby T is especially simple when K is a state estimate feedback controller i.e. a controller consisting of an observer and a feedback gain. The input ϵ to Q_k is in this case the output estimation error $y - \hat{y}$ and the output η of Q_k is added to the control signal i.e. $u = F\hat{x} + \eta$ where F is the feedback gain and $\hat{x}$ is the state estimate. The state x_T of T is the state of the system x and the state estimate $\hat{x}$.*

F.3.2 Guaranteeing stability through the Youla parameterizations

In this section we derive the condition that the free parameter $\Theta(k)$ needs to fulfill at all sample times such that stability is guaranteed.

The primary Youla parameter Q_k chosen as in equation (F.19) will by construction be a BIBO stable operator if

$$\bar{\sigma}\Theta(k) \leq b \ , \forall k \tag{F.38}$$

where b is a positive real number. This implies that the induced l_2-gain of $\Theta(k)$ is bounded by b. Based on this observation we can give the following Theorem

Theorem 1. *With Q_k parameterized as in (F.19), stability of the closed loop system (F.16) is guaranteed if*

$$\bar{\sigma}\Theta(k) < \gamma^{-1} \ , \forall k \tag{F.39}$$

where

$$\gamma = \sup_{\|\Delta\|_\infty \leq 1} \left\{ \|\tilde{Q}S\|_\infty \right\} \tag{F.40}$$

Proof. From equations (F.16)-(F.18) it is readily seen that the closed loop system will be stable if the loop of S and Q_k is stable. Since $\Theta(k)$ bounded implies Q_k is a BIBO-stable system and S by construction is BIBO stable for all $\|\Delta\|_\infty \leq 1$ we can apply the small gain theorem [3]. The theorem states that the loop is stable if the loop gain is less than 1. The loop can be seen as a series connection of the stable system $\tilde{Q}S$ with induced worst case l_2 gain γ and the time-varying gain $\Theta(k)$. Therefore, if we restrict $\bar{\sigma}\Theta(k) < \gamma^{-1}$ for all k then the loop gain will be less than 1. □

The constraint (F.39) will allow us to guarantee stability of the MPC formulation. The constraint can be reformulated as the following linear matrix inequality, which we will incorporate in the optimization problem (See e.g. [1]).

$$\begin{bmatrix} \gamma^{-1}I & \Theta \\ \Theta^T & \gamma^{-1}I \end{bmatrix} < 0 \tag{F.41}$$

The equivalent formulation follows from the definition of the singular value and the use of the Schur complement.

So far we have implicitly assumed that we can estimate an upper bound on $\|\tilde{Q}S\|_\infty$. Since S depends on the uncertain system Δ it complicates matters. However, algorithms exist for solving this problem. The reader is referred to

[9] for an algorithm [1]. It is stressed that finding the upper bound is not part of the on-line MPC optimization. Speed of convergence is therefore of little importance.

F.3.3 The Youla-MPC controller

In the optimization problem we introduce the following vector

$$\bar{z} = \begin{bmatrix} z_0^T & z_Q^T \end{bmatrix}^T \tag{F.42}$$

for which we naturally have that $z = \begin{bmatrix} I & I \end{bmatrix} \bar{z}$. The reason is that we potentially want to weight the nominal contribution z_0 and the forced contribution z_Q separately. We might e.g. be in the situation that the unconstrained controller achieves desired performance when constraints are inactive. In this situation it might be preferable to force $\Theta(k) = 0$ when constraints are inactive. This can be done by only targeting z_Q in the cost function.

In this work we suggest using the following optimization problem, which is similar to the one usually used in (standard) linear MPC:

$$\min_{\Theta,s} \left\{ \|\bar{z}(k+N+1|k)\|_{R_1}^2 + \sum_{i=0}^{N} \|\bar{z}(k+i|k)\|_{R_2}^2 + \|s\|_{R_3}^2 \right\} \tag{F.43}$$

subject to

$$\begin{cases} \text{nominal dynamics (F.25) \& (F.26)} \\ C_h \bar{z}(k+i|k) \leq 1 \quad \text{for} \quad i = 0, 1, \ldots, N \\ C_s \bar{z}(k+i|k) \leq 1 + s \quad \text{for} \quad i = 0, 1, \ldots, N \\ s \geq 0 \\ \begin{bmatrix} \gamma^{-1} I & \Theta \\ \Theta^T & \gamma^{-1} I \end{bmatrix} > 0 \end{cases} \tag{F.44}$$

This problem is solved at every sample time and the solution $\Theta(k) = \Theta$ actuated in the controller.

As is usual practice we use a finite horizon quadratic cost on input and output (i.e. $\bar{z}$) which includes a terminal cost. Both hard and soft constraints on $\bar{z}$ are included. Soft constraints are implemented by allowing constraint violation through the slack variable s. Finally we have the stability constraint on $\Theta(k)$ which is represented in its LMI form.

[1] This is also the algorithm which is implemented in the Matlab function `wcgain`

Generally we cannot guarantee that the optimization problem is feasible when including hard constraints ($C_h \neq 0$). For soft constraints we supply the following theorem:

Theorem 2. *If only soft constraints are included in the optimization problem (i.e. $C_h = 0$), then the optimization problem is feasible at all times and leads to a stable closed loop system.*

Proof. It follows directly from the stability conditions of the system. Due to the soft constraints $\Theta(k) = 0$ will always be a feasible solution with $s(k)$ chosen sufficiently high. Since $\Theta(k) = 0$ will lead to stability, $s(k)$ will not grow unbounded. □

For systems which are perturbed stable and the trivial controller $K_0 = 0$ is chosen, the Youla parameter can be chosen such that hard constraints on control signal u are satisfied.

Theorem 3. *Consider systems Σ which are stable for all $\|\Delta\|_\infty \leq 1$ with the trivial pre-stabilization $K_0 = 0$. Choosing $M_r = M_l = I$, $N_r = N_l = G$ and $V_r = V_l = I$ and $U_r = U_l = 0$ the YMPC optimization will remain feasible at all times with hard constraints on input u.*

Proof. The Youla parameterized controller will be given by

$$\mathcal{K}(Q_k) = \Theta(k)\tilde{Q}(I + G_0\Theta(k)\tilde{Q})^{-1} \tag{F.45}$$

$$= (I + \Theta(k)\tilde{Q}G_0)^{-1}\Theta(k)\tilde{Q} \tag{F.46}$$

It is seen that the feasible solution $\Theta(k) = 0$ will give the control signal $u(k) = 0$, irrespective of the internal state of the Youla parameterized controller. □

F.3.4 Reducing conservativeness

To reduce conservativeness we suggest using knowledge about the dual Youla parameter S to operate at frequencies which are less affected by the uncertainty Δ. We can estimate (point-wise in frequency) the worst case gain of $\tilde{Q}S$

$$H(\omega) = \bar{\sigma}\left\{\tilde{Q}(\omega)S(\omega)\right\} \tag{F.47}$$

given that $\|\Delta\|_\infty \leq 1$ (E.g. by using the algorithm in [9]). Since S represents our uncertainty it will be advantageous not to excite S where it is large. If we introduce pre-filtration of the input to Q_k or post-filtration of the output from

Q_k which is the "inverse" of $H(\omega)$ we effectively avoid that the system operates at frequencies where the gain of S is large. All equations containing $\tilde{Q}$ in the previous sections should naturally incorporate the filters as well.

F.3.5 On choosing the structure of $\tilde{Q}$

There is a design flexibility in choosing $\tilde{Q}$. We will briefly describe two approaches with distinct advantages:

An approach which leads to significant reduction of on-line computation is to choose $\tilde{Q}$ as a collection of a few carefully designed controllers and simply use Θ to provide the optimal blend.

An approach which lends itself to standard MPC is to have the main emphasis on the on-line part. Hence $\tilde{Q}$ should merely store information rather than actually compute the control. The obvious choice is to choose $\tilde{Q}$ as a (multi dimensional) FIR filter with a suitable large dimension. In this way we simply store information about the past over a finite horizon. The role of Θ is to choose the optimal linear combination of past information.

F.4 Example

In this section we investigate the suggested method with a simple example. We compare the method with a standard soft constrained MPC scheme.

We consider the dynamics of a cart connected to a wall by a spring (see Fig. F.2). The spring constant is negative $k < 0$ making the system unstable. The actual value of the spring constant is uncertain. The nominal value is $k_0 = -5$ and the uncertainty is known to lie in the interval $\Delta k \in [-0.5 \;\; 0.5]$. The mass of the cart is $m = 1$.

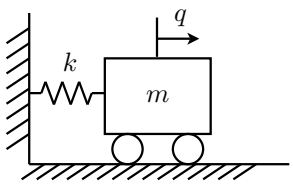

Figure F.2: Cart system used in simulation

In the design and simulations we consider the discretized system with sample

time $T_s = 0.45$. The uncertain system is described as the interconnection of the extended system Σ

$$\Sigma \stackrel{s}{=} \left[\begin{array}{cc|cc} 1.543 & 0.5256 & \begin{bmatrix}0.1086\\0.5256\end{bmatrix} & \begin{bmatrix}0.1086\\0.5256\end{bmatrix} \\ 2.628 & 1.543 & & \\ \hline \multicolumn{2}{c|}{\begin{bmatrix}2 & 0\end{bmatrix}} & \multicolumn{2}{c}{0} \\ \multicolumn{2}{c|}{\begin{bmatrix}1 & 0\\0 & 1\end{bmatrix}} & & \end{array}\right] \tag{F.48}$$

and the uncertainty Δ satisfying $\|\Delta\|_\infty \leq 1$. The states of the system are the position of the cart $x_1 = q$ and the cart speed $x_2 = \dot{q}$. The speed of the cart can - but should not - exceed $\dot{q} = \pm 2$, and therefore we would like to put a soft constraint on the speed in the design.

To stabilize the uncertain system a state-estimation feedback controller has been designed. The state feedback gain is an LQ controller for which the cost function is specified by the state weight $R_x = \text{diag}([1 \quad 1])$ and input weight $R_u = 100$. The state estimator is designed as a Kalman filter assuming state noise with covariance $Q_x = \text{diag}([1 \quad 1])$ and measurement noise with covariance $Q_y = \text{diag}([10 \quad 10])$. The controlled system is stable for all perturbations Δ.

As described in remark 11 the Youla parameterization can be chosen especially simple when a state estimate feedback controller has been used for prestabilization. It is simply a matter of connecting the Youla parameter Q_k at the right places on the controller. The realization of the augmented model T (see equation (F.26)) follows accordingly.

In this example we parameterize Q_k as an FIR filter as explained in section F.3.5. The order of the FIR filter is chosen as $N = 10$, which will also be chosen as the length of our prediction horizon.

To reduce conservativeness we implement the method suggested in section F.3.4. We design a post-filter W_2 for $Q(k)$ which is approximately inverse to $H(\omega) = \bar{\sigma}\{\tilde{Q}(\omega)S(\omega)\}$. With a fourth order filter a reasonable approximation is achieved.

If we assume that the nominal controller has been designed for desired unconstrained performance it is reasonable to define the cost such that YMPC controller is inactive when constraint violation is not predicted. Refering to the cost in equation (F.43) we choose only to punish the u_Q element of the vector $\bar{u}$. A slack variable vector is naturally associated with the constraints. The chosen cost is:

$$J = \left\{ \sum_{i=0}^{10} u_Q(k+i|k)^2 + 1000\|s\|^2 \right\} \tag{F.49}$$

The constraints follow immediately from the problem description.

For comparison, a standard MPC controller with soft constraints is also designed. It is likewise designed for the pre-stabilized system and is designed with the same cost and constraints; the only difference being that the standard controller lacks the stability constraint. The standard MPC control signal is denoted u_{mpc}.

F.4.1 Simulations

We will first illustrate the performance of the YMPC controller when controlling the nominal system. Fig. F.3 shows the speed of the cart and the MPC control signal i.e. the perturbation of the control signal of the unconstrained controller. The initial condition in the simulation is $x = [1 \;\; 0]^T$ which means that the cart is placed at position 1 with speed 0. The figure shows that the YMPC controller manages to reduce the violation of the constraint significantly. However, due to the robust stability constraint the performance is slightly more conservative than the standard MPC controller.

The conservativeness of the controller becomes very pronounced when initiating the system at a more extreme position. Fig. F.4 shows the simulation when

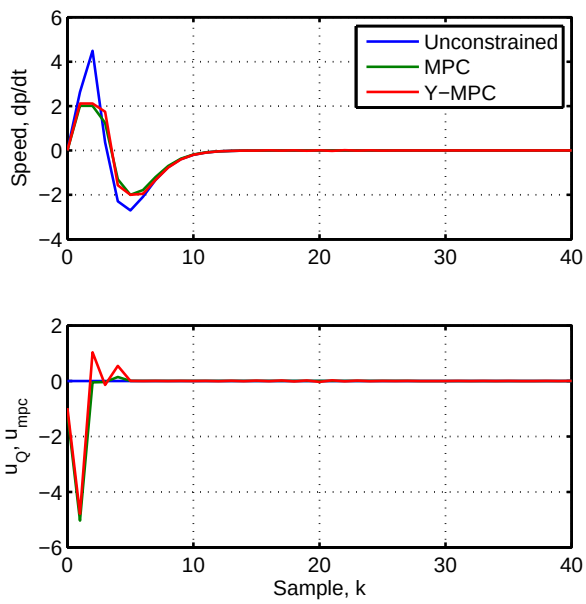

Figure F.3: Simulations with nominal model and initial condition $x = [1 \;\; 0]^T$.

initiating the cart at $x = [10 \;\; 0]^T$ i.e. position 10 and speed 0. Since there is a limit on the gain in the YMPC controller it cannot do much in order to minimize the constraint violation. The standard MPC controller naturally ensures that the constraint violation is very small.

The advantage of the YMPC controller becomes obvious when the system is no longer the nominal one. Fig. F.5 shows the simulation when the perturbation is $\Delta = 1$ and the initial condition is $x = [10 \;\; 0]$. As could be expected, the YMPC controller still cannot minimize the constraint violation. However, the situation is much worse for the standard MPC controller. In its endeavor to keep within the limits of the constraint, it causes unstable closed loop behavior.

F.5 Conclusion

In this paper we have described an approach to dealing with dynamical uncertainties bounded by the ∞-norm in a soft/hard constrained MPC setup. Conditions for robust stability have been derived when parameterizing the receding horizon problem in terms of a primary Youla parameter and the uncertainty

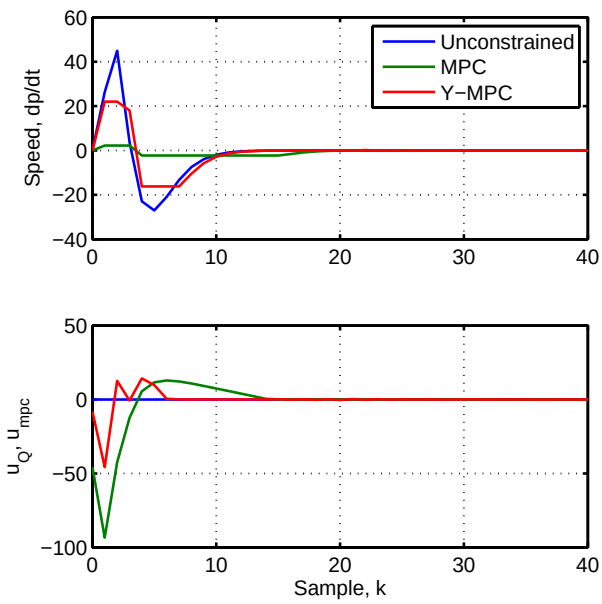

Figure F.4: Simulations with nominal model and initial condition $x = [10 \;\; 0]^T$.

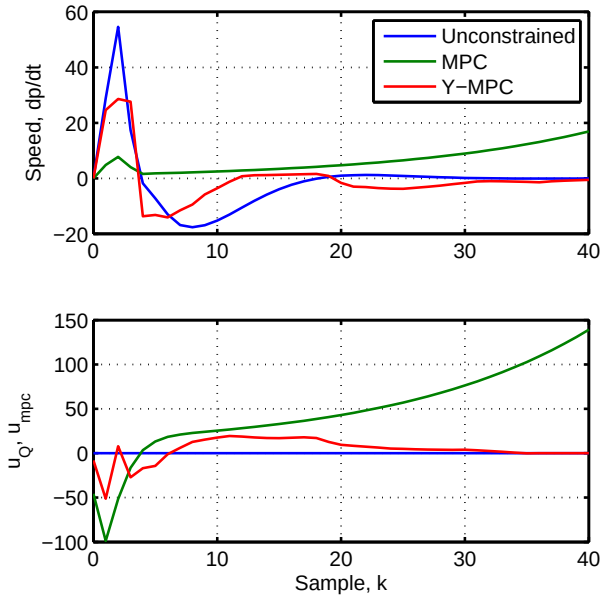

Figure F.5: Simulations with perturbed model and initial condition $x = [10 \;\; 0]^T$.

in terms of a dual Youla parameter. This condition has been incorporated in the receding horizon problem as an LMI. For soft constraints it is proved that the optimization problem is feasible at all times and leads to a stable closed loop system. For perturbed stable systems it is proved that hard constraints on inputs can be handled as well. A method for reducing conservativeness of the robust controller has been described. Simulations have illustrated the potential advantages of the described algorithm.

Bibliography

[1] Stephen Boyd, Laurent El Ghaoui, Eric Feron, and Venkataramenan Balakrishnan. *Linear Matrix Inequalities in System and Control Theory*. SIAM, 1994.

[2] Qifeng Cheng, Basil Kouvaritakis, Mark Cannon, and J. Anthony Rossiter. A youla parameter approach to robust constrained linear model predictive control. In *Proceedings of the 48th IEEE Conference on Decision and Control*, 2009.

[3] C. A. Desoer and M. Vidyasagar. *Feedback systems: Input-output properties*. Academic Press, 1975.

[4] B. Kouvaritakis, J. A. Rossiter, and A.O.T. Chang. Stable generalized predictive control: an algorithm with guaranteed stability. *IEE Proceedings-Control Theory and Applications*, 139:349–362, 1992.

[5] J.M. Maciejowski. *Predictive control with constraints*. Prentice Hall, 2002.

[6] Karl Martensson and Andreas Wernrud. Dynamic model predictive control. In *Proceedings of the 17th IFAC World Congress*, volume 17. Elsevier, 2008.

[7] D.Q. Mayne, J.B. Rawlings, C.V. Rao, and P.O.M. Scokaert. Constrained model predictive control: Stability and optimality. *Automatica*, 36(6):789–814, 2000.

[8] H. Niemann. Dual youla parameterisation. *IEE Proceedings-Control Theory and Applications*, 150:493–497, 2003.

[9] Andy Packard, Gary Balas, Richard Liu, and Jong-Yeob Shin. Results on worst-case performance assessment. In *Proceedings of the American Control Conference*, 2000.

[10] Cristina Stoica, Cristina Stoica, Pedro Rodriguez-Ayerbe, and Didier Dumur. Off-line improvement of multivariable model predictive control robustness. pages 2826–2831. Institute of Electrical and Electronics Engineers Inc., 2008. DOI:10.1109/CDC.2007.4434591.

[11] T-T. Tay, I. Mareels, and J.B. Moore. *High Performance Control*. Birkhäuser, 1998.

[12] S. C. Thomsen, H. Niemann, and N.K. Poulsen. Mpc for uncertain systems using the youla parameterizations. In *Proceedings of 47th IEEE Conference on Decision and Control*, 2008.

[13] T.J.J. Van Den Boom and R.A.J. De Vries. Constrained predictive control using a time-varying youla parameter: a state space solution. *Proceedings of the Third European Control Conference. ECC 95*, (vol.4):3235–40 vol.4, 1995.

[14] T.J.J. Van Den Boom and R.A.J. De Vries. Robust predictive control using a time-varying youla parameter. *International Journal of Applied Mathematics and Computer Science*, 9:101–128, 1999.

[15] M. Vidyasagar. *Control System Synthesis: a factorization approach*. The M.I.T. Press, 1985.

[16] K. Zhou, J.C. Doyle, and Glover K. *Robust and optimal control*. Prentice Hall, 1996.

Paper G

Stochastic wind turbine control in multiblade coordinates

abstract

In this paper we consider wind turbine load attenuation through model based control. Asymmetric loads caused by the wind field can be reduced by pitching the blades individually. To this end we investigate the use of stochastic models of the wind which can be included in a model based individual pitch controller design. In this way the variability of the wind can be estimated and compensated for by the controller. The wind turbine model is in general time-variant due to its rotational nature. For this reason the modeling and control is carried out in so-called multiblade coordinates. A controller based on the $\mathcal{H}_2$ methodology is designed and tested in simulations.

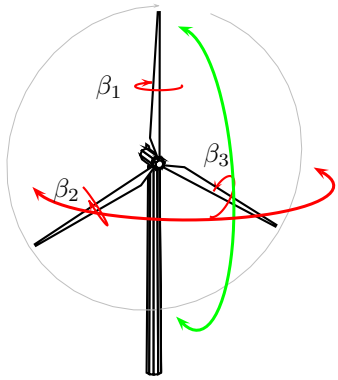

Figure G.1: Sketch of wind turbine with individually adjustable pitch angles. The big arcs represents the asymmetric loads - yaw and tilt moments

G.1 Introduction

Reducing stress on the wind turbine structure while ensuring efficient power production is becoming increasingly important as the size of the wind turbines continues to increase. One way to achieve this is through advanced model based control designs which explicitly take into account the dynamics of the wind turbine as well as the stochastic nature of the wind.

On the majority of modern wind turbines both the torque of the generator (variable speed control) and the pitch of the blades (pitch control) are used as control parameters for dealing with these challenges. In most documented research the pitch of the blades are controlled collectively applying a wide variety of methods. This ranges from linear methods such as LQ, LQG/$\mathcal{H}_2$, and $\mathcal{H}_\infty$ ([3], [4]) to nonlinear methods such as feedback linearization ([9], [14]).

Collective pitch control has one major drawback: it is not possible to compensate for the asymmetric loads caused by a nonuniform wind field. This can however be dealt with using strategies where the blades are pitched individually. Fig. G.1 shows a sketch of a wind turbine where the pitch angles are β_1, β_2 and β_3. The asymmetric loads are typically quantified by the yaw and tilt moments Q_{yaw} and Q_{tilt} which are visualized by the horizontal and vertical arc respectively in the figure. Most of the approaches taken so far incorporate classical control theory (PID) control for the individual pitch control loop. Examples of this are [2] and [8]. Multi-variable control theory has also been applied, see e.g. [11], [12] and [13].

In this paper we investigate the use of stochastic wind models in connection to

model based individual pitch control. Including an internal model of the wind will enable the controller to estimate the variability of the wind and consequently provide more effective compensation. Wind model as well as wind turbine model are derived in so-called multiblade coordinates. In multiblade coordinates the linearized dynamics of the wind turbine will not exhibit time-dependency caused by rotor rotation. Furthermore the dynamics related to collective pitch control and individual pitch control are decoupled in the multiblade coordinates. This facilitates a decentralized controller design instead of a monolithic design. Modeling the deterministic trends in the wind is not considered in this paper but is easily handled in the same framework. We apply $\mathcal{H}_2$ controller synthesis for designing the individual pitch controller. This paper extends the work in [13] where modeling and control was carried out in local blade coordinates.

The wind model which we setup is based on the work in [10]. Here it was shown how to setup frequency domain models of wind turbines given spectral descriptions of the wind. The method relies on making a Fourier series expansion of the wind in the azimuth angle.

G.2 Wind turbine control in multiblade coordinates

Due to the rotor rotation the linear dynamic description of a wind turbine will in general have a non-linear dependency on the azimuth angle. Assuming that the rotor system is isotropic and rotating at a constant angular velocity it is however possible to transform the system equations into time-independent coordinates. This is done by transforming the local blade coordinates to the so-called multiblade coordinates (See [7],[5]). The multiblade coordinates describes the combined effect of the local blade dynamics in the support frame of reference i.e. the global coordinate system.

In the following we assume that the wind turbine under consideration has an isotropic rotor with three blades rotating with constant angular velocity ω_r. Assume that we have a vector $\boldsymbol{q}$ with 3 variables, pertaining to different blades and described in local blade coordinates.

$$\boldsymbol{q} = \begin{bmatrix} q_1 & q_2 & q_3 \end{bmatrix}^T \tag{G.1}$$

The elements of $\boldsymbol{q}$ are assumed to represent equivalent properties of each blade e.g. edgewise blade deflection. The transformation of blade variable triplets to multiblade coordinates is given by:

$$\bar{\boldsymbol{q}} = \boldsymbol{M}(t)\boldsymbol{q} \tag{G.2}$$

where $\bar{\boldsymbol{q}}$ denotes the multiblade coordinates and

$$\boldsymbol{M}(t) = \begin{bmatrix} \frac{1}{3} & \frac{1}{3} & \frac{1}{3} \\ \frac{2}{3}\cos(\psi(t)) & \frac{2}{3}\cos(\psi(t)+\frac{2\pi}{3}) & \frac{2}{3}\cos(\psi(t)+\frac{4\pi}{3}) \\ \frac{2}{3}\sin(\psi(t)) & \frac{2}{3}\sin(\psi(t)+\frac{2\pi}{3}) & \frac{2}{3}\sin(\psi(t)+\frac{4\pi}{3}) \end{bmatrix} \tag{G.3}$$

where $\psi(t)$ is the rotor azimuth angle at a given time. For a constant rotational speed we will have $\dot{\psi}(t) = \omega_r$.

A wind turbine model will in general contain several variable triplets describing the dynamics of the blades. Furthermore there will be a number of variables describing the non-rotating dynamics. Let $\boldsymbol{p}$ denote the augmented vector of the blade triplets and the variables describing the non-rotating dynamics. In the following $\boldsymbol{\mathcal{M}}_{\boldsymbol{p}}(t)$ will then denote the transform which takes the blade triplets to multiblade coordinates and leaves the variables in non-rotating coordinates untouched.

Now, assume that a linear wind turbine model is given which is time-variant due to the interaction between the rotating blade systems and the non-rotating system. We denote this model $\boldsymbol{P}_t$. The inputs are disturbances $\boldsymbol{d}$ and control signal $\boldsymbol{u}$. The outputs are the measurements $\boldsymbol{y}$ and a performance signal $\boldsymbol{z}$. We can then transforms the time-varying system $\boldsymbol{P}_t$ to a time-invariant description in multiblade coordinates:

$$\begin{bmatrix} \bar{\boldsymbol{z}} \\ \bar{\boldsymbol{y}} \end{bmatrix} = \begin{bmatrix} \boldsymbol{\mathcal{M}}_z(t) & \\ & \boldsymbol{\mathcal{M}}_y(t) \end{bmatrix} \boldsymbol{P}_t \begin{bmatrix} \boldsymbol{\mathcal{M}}_d^{-1}(t) & \\ & \boldsymbol{\mathcal{M}}_u^{-1}(t) \end{bmatrix} \begin{bmatrix} \bar{\boldsymbol{d}} \\ \bar{\boldsymbol{u}} \end{bmatrix} \tag{G.4}$$

$$= \bar{\boldsymbol{P}} \begin{bmatrix} \bar{\boldsymbol{d}} \\ \bar{\boldsymbol{u}} \end{bmatrix} \tag{G.5}$$

adding a controller $\bar{\boldsymbol{K}}$ by a lower linear fractional transformation to the multiblade system, we get the closed loop system:

$$\bar{\boldsymbol{z}} = \mathcal{F}_l\left(\bar{\boldsymbol{P}}, \bar{\boldsymbol{K}}\right)\bar{\boldsymbol{d}} \tag{G.6}$$

The controller for the multiblade system should hence be designed such that it achieves the desired response from the multiblade disturbance $\bar{\boldsymbol{d}}$ to the multiblade output $\bar{\boldsymbol{z}}$. The controller for the original system $\boldsymbol{P}_t$ will naturally be the time-varying controller:

$$\boldsymbol{K}_t = \boldsymbol{\mathcal{M}}_u^{-1}(t)\bar{\boldsymbol{K}}\boldsymbol{\mathcal{M}}_y(t) \tag{G.7}$$

The setup is visualized in Fig. G.2.

From a control engineering point of view the most dominant disturbance which affects the wind turbine is the wind. Therefore, it is desirable to set up a model of the wind in multiblade coordinates and incorporating it in the controller design.

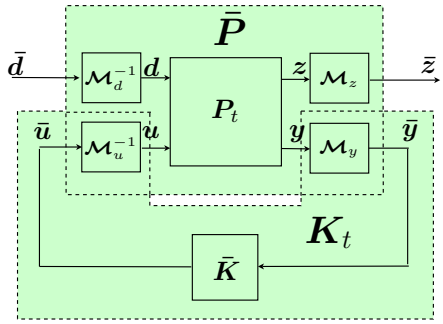

Figure G.2: From the point of view of the controller, the wind turbine and wind is described in the multiblade coordinates

In practice the rotational speed will not be constant and the transformed system will therefore not be perfectly time-independent. When working at high wind speed conditions the rotational speed will be close to constant due to the controller. The perturbation introduced by the small variations in the rotational speed will therefore only have little effect. All transformations in the model derivation will therefore be carried out assuming a constant rotational speed $\dot{\psi}(t) = \omega_r$.

G.3 Wind model

The wind model describes the wind as it is seen by the *rotating* blades. In [13] we showed how to setup the model in local blade coordinates based on the work in [10]. In this paper we transform this model to multiblade coordinates. We shortly describe the model in [13] and show how it looks when transformed to multiblade coordinates.

Of up-most importance in the model is the so-called blade effective wind speed: The blade effective wind speed v^e is the speed of the uniform wind which results in the same generalized force as a given wind distribution $v(r)$ along the span of the blade. This can be expressed mathematically as

$$v^e = \frac{\int_{r_0}^{R} X(r)v(r)dr}{\int_{r_0}^{R} X(r)dr}. \tag{G.8}$$

The inner and outer radii of the blade (measured from hub center) are denoted by r_0 and R respectively. X is a weight function which describes how much

influence the wind has along the span of the blade. The wind distribution $v(r)$ is assumed to be in axial direction (orthogonal to the plane of rotation).

For a three bladed wind turbine we will have three effective wind speeds offset to each other with an azimuth angle of $\frac{2\pi}{3}$ radians. It can be shown that the cross-spectral density between to effective wind speeds with azimuth offset $\Delta\psi$ can be written as an expansion of harmonic spectral densities:

$$S^e(\omega, \Delta\psi) = \sum_{n=-\infty}^{\infty} \tilde{S}^e_{nn}(\omega - n\omega_r)e^{in\Delta\psi} \tag{G.9}$$

The harmonic spectral densities $\tilde{S}^e_{nn}$ depends on statistical characteristics of the wind field. The details of the expression will not be given in this paper but can be found in [13]. The expression reveals an interesting property of the effective wind speed: it consist of a sum of spectra shifted in frequency where the shifts depend on the rotational speed ω_r.

Relating (G.9) to a three bladed wind turbine we have the effective wind speed vector

$$\boldsymbol{v}^e = \begin{bmatrix} v^e_1(t) & v^e_2(t) & v^e_3(t) \end{bmatrix}^T \tag{G.10}$$

with the corresponding spectral density matrix

$$\boldsymbol{S}^e(\omega) = \sum_{n=-\infty}^{\infty} \tilde{S}^e_{nn}(\omega - n\omega_r)\boldsymbol{E}(n) \tag{G.11}$$

where

$$\boldsymbol{E} = \begin{bmatrix} 1 & e^{in\frac{2\pi}{3}} & e^{in\frac{4\pi}{3}} \\ e^{in\frac{-2\pi}{3}} & 1 & e^{in\frac{2\pi}{3}} \\ e^{in\frac{-4\pi}{3}} & e^{in\frac{-2\pi}{3}} & 1 \end{bmatrix} \tag{G.12}$$

For doing control we want the spectral description in multiblade coordinates. Applying the multiblade transformation $\boldsymbol{M}(t)$ to the the wind vector $\boldsymbol{v}^e$ we obtain the multiblade effective wind:

$$\bar{\boldsymbol{v}}^e = \boldsymbol{M}(t)\boldsymbol{v}^e \tag{G.13}$$

doing the math we get the spectral density matrix for the multiblade effective wind speed vector:

$$\bar{\boldsymbol{S}}(\omega) = \sum_{n=-\infty}^{\infty} \begin{bmatrix} \bar{\tilde{S}}^1_{nn}(\omega) & 0 & 0 \\ 0 & \bar{\tilde{S}}^{2,3}_{nn}(\omega) & \bar{\tilde{S}}^{2,3}_{nn}(\omega)e^{\theta(n)} \\ 0 & \bar{\tilde{S}}^{2,3}_{nn}(\omega)e^{-\theta(n)} & \bar{\tilde{S}}^{2,3}_{nn}(\omega) \end{bmatrix} \tag{G.14}$$

where

$$\theta(n) = \begin{cases} -i\frac{\pi}{2} & \text{for } n \in \mathbb{U}^+ \\ i\frac{\pi}{2} & \text{for } n \in \mathbb{U}^- \end{cases} \tag{G.15}$$

$$\bar{\tilde{S}}^1_{nn}(\omega) = \begin{cases} \bar{\tilde{S}}^e_{nn}(\omega + n\omega_r) & \text{for } n \in \mathbb{U}_0 \\ 0 & \text{otherwise} \end{cases} \tag{G.16}$$

$$\bar{\tilde{S}}^{2,3}_{nn}(\omega) = \begin{cases} \bar{\tilde{S}}^e_{nn}(\omega + (n+1)\omega_r) & \text{for } n \in \mathbb{U}_+ \\ \bar{\tilde{S}}^e_{nn}(\omega + (n-1)\omega_r) & \text{for } n \in \mathbb{U}_- \\ 0 & \text{otherwise} \end{cases} \tag{G.17}$$

The sets $\mathbb{U}_0$, $\mathbb{U}_+$ and $\mathbb{U}_-$ are defined as follows:

$$\mathbb{U}_0 = \{\ldots, -6, -3, 0, 3, 6, \ldots\} \tag{G.18}$$

$$\mathbb{U}_+ = \{\ldots, -10, -7, -4, -1, 2, 5, 8, 11, \ldots\} \tag{G.19}$$

$$\mathbb{U}_- = \{\ldots, -11, -8, -5, -2, 1, 4, 7, 10, \ldots\} \tag{G.20}$$

It is seen that the first component is uncorrelated with the second and third component whereas the second and third components are correlated by a constant phase-shift. As will be seen later the first wind component relates to the collective pitch control loop whereas the second and third component relates to the individual pitch control loop.

For control purposes the spectral description of the blade effective wind in multi-blade coordinates is approximated with a linear time-invariant model. In essence we will describe the stochastic process with an LTI stochastic system. In the following it is useful to consider the following representation of such a system:

$$\boldsymbol{y}(t) = \int_{-\infty}^{t} \boldsymbol{g}(t-s)\boldsymbol{e}(s)ds \tag{G.21}$$

$\boldsymbol{g}(t)$ is the convolution kernel and $\boldsymbol{e}(t)$ is Gaussian distributed white noise with mean $\mathbf{0}$ and intensity $\boldsymbol{I}$ ($\boldsymbol{e}(t) \sim \mathcal{N}(\mathbf{0}, \boldsymbol{I})$).

The spectral density of $\boldsymbol{y}$ is given by (see e.g. [1])

$$\boldsymbol{S}_{yy} = \frac{1}{2\pi}\boldsymbol{G}(-i\omega)\boldsymbol{G}(i\omega) \tag{G.22}$$

where $\boldsymbol{G}(s)$ is the Laplace transform of the convolution kernel $\boldsymbol{g}(t)$, i.e. $\boldsymbol{G}(s) = \mathcal{L}(\boldsymbol{g}(t))$.

The spectral description of the wind $\bar{\boldsymbol{v}}$ does not pertain to a finite dimensional linear description in the time domain. This is evident from the constant phase-shift in the cross-spectrum and the infinite number of harmonics. Some information will therefore be lost in the approximation. To this end we propose

to truncate the infinite series and disregard the covariance between the components. Recalling the structure of the auto-spectral densities it is natural to propose the following structure for the multiblade effective wind speeds:

$$\bar{v}_i^e(t) = \sum_{n=0}^{N_i} G_{i,n} e_{i,n}(t) \ , \quad i = 1, 2, 3 \tag{G.23}$$

where $G_{i,n}$ are the multiplicative operators associated with scalar stochastic linear systems. We will then obtain a good approximation to the auto-spectral densities when

$$\frac{1}{2\pi}|G_{1,n}(\omega)|^2 \approx \bar{\tilde{S}}_{nn}^1(\omega) \tag{G.24}$$

$$\frac{1}{2\pi}|G_{2,n}(\omega)|^2 = \frac{1}{2\pi}|G_{3,n}(\omega)|^2 \approx \bar{\tilde{S}}_{nn}^{2,3}(\omega) \tag{G.25}$$

over the frequencies ω of interest. This can be done by numerically fitting transfer functions to the spectra.

G.4 Wind turbine model

G.4.1 Simulation model

The model which we use for simulation incorporates tower dynamics, rotational dynamics, aerodynamics, pitch actuators and a stochastic wind model. The structural model is sketched in Fig. G.3 where the axis of the global coordinate system is denoted with X, Y and Z and the local blade coordinate systems with x, y and z. Note that Y and y co-inside.

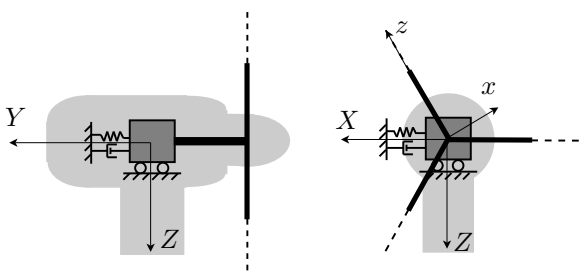

(a) Side view (b) Front view

Figure G.3: Structural model of wind turbine. Note that the local y-axis of the blades co-insides with the global Y-axis

The model of the tower includes the primary modal displacement in for-aft and side-to-side motion (q_T^Y and q_T^X respectively). The dynamics can be written in the following second order matrix equation:

$$\begin{bmatrix} m_T & 0 \\ 0 & m_T \end{bmatrix} \begin{bmatrix} \ddot{q}_T^Y \\ \ddot{q}_T^X \end{bmatrix} + \begin{bmatrix} k_T & 0 \\ 0 & k_T \end{bmatrix} \begin{bmatrix} \dot{q}_T^Y \\ \dot{q}_X^Z \end{bmatrix} + \begin{bmatrix} c_T & 0 \\ 0 & c_T \end{bmatrix} \begin{bmatrix} q_T^Y \\ q_T^X \end{bmatrix} = \begin{bmatrix} Q_F^Y \\ Q_F^X \end{bmatrix} \tag{G.26}$$

The generalized fores Q_F^X and Q_F^Y are the total forces in the X and Y directions respectively.

The model of the rotor is simply given by the inertia of all rotating parts (blades, drive shaft, generator, etc). The dynamics is given by the equation:

$$J_r \dot{\omega}_r + T_g = Q_M^Y \tag{G.27}$$

where J_r is the inertia and T_g is the generator torque. We assume that T_g is constant an chosen such that $\dot{\omega}_g = 0$ for the chosen operating conditions. Q_M^Y is the total moment about the Y-axis.

The aerodynamics are calculated using simple BEM calculations as described in [6]. We assume that the relation is purely algebraic i.e. we do not consider e.g. dynamic inflow. With the chosen degrees of freedom in the model we can express the conversion of kinetic energy in the wind field $\boldsymbol{V}$ to the generalized forces of interest by the following functional.

$$\begin{bmatrix} \boldsymbol{Q}_F^y & \boldsymbol{Q}_F^x & \boldsymbol{Q}_M^y & \boldsymbol{Q}_M^x \end{bmatrix} = \boldsymbol{f}(\boldsymbol{V}, \dot{q}_T^Y, \dot{q}_T^X, \boldsymbol{\beta}, t) \tag{G.28}$$

The generalized forces on the left hand side are: The blade root force in y- and x-direction $\boldsymbol{Q}_F^y$, $\boldsymbol{Q}_F^x$. The blade root moments about the y- and x-axis $\boldsymbol{Q}_M^y$,$\boldsymbol{Q}_M^x$. We can relate these local generalized forces to the global generalized forces appearing in equation (G.26) and (G.27) through the multiblade transformation:

$$Q_F^Y = \begin{bmatrix} 3 & 0 & 0 \end{bmatrix} \boldsymbol{M}(t) \boldsymbol{Q}_F^y \tag{G.29}$$

$$Q_F^X = \begin{bmatrix} 0 & 0 & \frac{3}{2} \end{bmatrix} \boldsymbol{M}(t) \boldsymbol{Q}_F^x \tag{G.30}$$

$$Q_M^Y = \begin{bmatrix} 3 & 0 & 0 \end{bmatrix} \boldsymbol{M}(t) \boldsymbol{Q}_M^y \tag{G.31}$$

The yaw and tilt moments which represents the asymmetric forces acting on the wind turbine are given as follows:

$$\begin{bmatrix} Q_{yaw} \\ Q_{tilt} \end{bmatrix} = \begin{bmatrix} 0 & 0 & \frac{3}{2} \\ 0 & \frac{3}{2} & 0 \end{bmatrix} \boldsymbol{M}(t) \boldsymbol{Q}_M^x \tag{G.32}$$

We use the Veers method [15] for simulating the wind field. This results in a rectangular grid of point wind speeds. A resolution of 10×10 wind speeds is chosen and the point wind at a specific location is found by interpolation.

The actuator dynamics is given by the following set of uncoupled differential equations

$$\boldsymbol{\tau}\dot{\boldsymbol{\beta}} + \boldsymbol{\beta} = \boldsymbol{\beta}_r \tag{G.33}$$

where $\boldsymbol{\tau} = \text{diag}([\tau\ \tau\ \tau])$ is a diagonal matrix containing the time constants of the actuator dynamics and $\boldsymbol{\beta}_r$ is the pitch reference for the blades.

G.4.2 Linear model in multiblade coordinates

We start by deriving the linear model of the aerodynamics. When linearizing the aerodynamics we introduce the definition of the effective wind speed. Since the effective wind speed pertains to a specific generalized blade force, we introduce independent effective wind speeds for each generalized blade force in the model. The effective wind speed vectors $\boldsymbol{v}_F^y$, $\boldsymbol{v}_F^x$, $\boldsymbol{v}_M^y$, $\boldsymbol{v}_M^x$ are therefore associated with $\boldsymbol{Q}_F^y$, $\boldsymbol{Q}_F^x$, $\boldsymbol{Q}_M^y$, $\boldsymbol{Q}_M^x$ respectively. Denoting a specific generalized force by Q and a specific effective wind speed vector by $\boldsymbol{v}^e$ the linearized relation will in general be:

$$Q = \boldsymbol{d}_\beta \boldsymbol{M}(t)\boldsymbol{\beta} + \boldsymbol{d}_v \boldsymbol{M}(t)\boldsymbol{v}^e \tag{G.34}$$

where $\boldsymbol{d}_\beta$ and $\boldsymbol{d}_v$ are row vectors with linearization coefficients. The time-periodic relations are rendered time-invariant by transforming the inputs to the following multiblade equivalents:

$$\bar{\boldsymbol{\beta}} = \boldsymbol{M}(t)\boldsymbol{\beta} \tag{G.35}$$

$$\bar{\boldsymbol{v}}_F^y = \boldsymbol{M}(t)\boldsymbol{v}_F^y\ , \quad \bar{\boldsymbol{v}}_F^x = \boldsymbol{M}(t)\boldsymbol{v}_F^x \tag{G.36}$$

$$\bar{\boldsymbol{v}}_M^y = \boldsymbol{M}(t)\boldsymbol{v}_M^y\ , \quad \bar{\boldsymbol{v}}_M^x = \boldsymbol{M}(t)\boldsymbol{v}_M^x \tag{G.37}$$

The tower and rotor dynamics described in the previous section are already linear and given in non-rotating coordinates. The dynamics in equations (G.26) and (G.27) will therefore be used directly. For each effective wind speed vector we associate a linear stochastic model as described in Sec. G.3. Referring to equations (G.23)-(G.42) we choose $N_1 = 0$, $N_2 = N_3 = 4$ based on the known structure of the wind. The spectral model of the effective wind is based on the same statistical properties as the simulation wind model.

Transforming the pitch dynamics to multiblade coordinates we get

$$\boldsymbol{\tau}\dot{\bar{\boldsymbol{\beta}}} + (\boldsymbol{I} + \boldsymbol{\tau}\boldsymbol{M}(t)\dot{\boldsymbol{M}}^{-1}(t))\bar{\boldsymbol{\beta}} = \bar{\boldsymbol{\beta}}_r \tag{G.38}$$

It is easily verified that $\boldsymbol{M}(t)\dot{\boldsymbol{M}}^{-1}(t)$ is a constant matrix.

Inspecting the combined dynamic equations for the wind turbine, wind and actuators in multiblade coordinates we see that the dynamics affected by the first element of multiblade pitch reference and the first elements of the wind signals is decoupled from the dynamics affected by the second and third elements of the multiblade pitch reference and the second and third elements of the wind signals. It is easily verified that the first multiblade pitch element is responsible for the collective pitch variation whereas the second and third multiblade pitch elements are responsible for individual pitch variations. The wind model itself is also characterized by this separability as shown in Sec. G.3. As a consequence, when designing the pitch controller we can design the collective pitch controller and the individual pitch controller independently.

G.4.3 Parameters and operating conditions

The parameters used in the simulation model and design model has been adapted from a 1.5 MW wind turbine. A selection of key-parameters for the model is shown in Table G.1. In the simulations we operate the wind turbine at a mean wind speed of $v_m = 16$ m/s. The stochastic properties of the wind are chosen realistically. The auto-spectral density of the point wind is e.g. chosen as a Kaimal spectrum. Further details are omitted in this paper.

The wind speed conditions are *above rated*, which means that the energy in the wind exceeds the limits of the generator. The primary objective is therefore to keep the rotational speed $\dot{\psi}_r = \omega_r$ constant. Since the tower is lightly damped, it is also of importance to ensure that the controller provides some damping to the tower. This will be done by targeting the tower deflection speed in the design. For load attenuation we want to attenuate the yaw and tilt moments in the support of the blades.

Table G.1: Selected key parameters for 1.5 MW wind turbine model

Parameter	value	
m_t	$9.35 \cdot 10^4$	kg
k_t	$6.51 \cdot 10^5$	N/m
c_t	$3.25 \cdot 10^4$	s^{-1}
τ	0.1	s
J_r	$3.04 \cdot 10^6$	kg·m^2
ω_r rated	2.1	rad/s

G.5 Controller synthesis

As described in Sec. G.5 the dynamics of the system in multiblade coordinates is decoupled into two independent systems - one system pertaining to collective pitch control and one system pertaining to individual pitch control. We will take advantage of this separability in the controller design.

The design models used for synthesizing the collective pitch controller and the individual pitch controller will be denoted by $\bar{\boldsymbol{P}}_c$ and $\bar{\boldsymbol{P}}_i$ respectively. The models include both the dynamics of the wind turbine and the wind. Both models have input and output ports such that they fit in a general control setup as shown in Fig. G.2. The performance objectives are built into the models by suitable (frequency dependent) scaling of the disturbance input and performance output.

The performance signals for the collective and individual model respectively are shown below:

$$\bar{\boldsymbol{z}}_c = \boldsymbol{W}_{z,c} \begin{bmatrix} \dot{q}_T^Y & \omega_r & \bar{\beta}_1 & \bar{\beta}_{r,1} \end{bmatrix}^T \tag{G.39}$$

$$\bar{\boldsymbol{z}}_i = \boldsymbol{W}_{z,i} \begin{bmatrix} \dot{q}_T^X & Q_{yaw} & Q_{tilt} & \bar{\beta}_2 & \bar{\beta}_3 & \bar{\beta}_{r,2} & \bar{\beta}_{r,3} \end{bmatrix}^T \tag{G.40}$$

Where $\boldsymbol{W}_{z,c}$ and $\boldsymbol{W}_{z,i}$ are weight matrices. The disturbance signals $\bar{\boldsymbol{d}}_c$ and $\bar{\boldsymbol{d}}_i$ includes the white noise processes input to the wind model and white noise associated with measurement noise. The measurement signals represents a realistic subset of signals measured on a wind turbine:

$$\bar{\boldsymbol{y}}_c = \begin{bmatrix} \dot{q}_T^Y & \omega_r \end{bmatrix}^T + \begin{bmatrix} \boldsymbol{0} & \boldsymbol{W}_{m,c} \end{bmatrix} \bar{\boldsymbol{d}}_c \tag{G.41}$$

$$\bar{\boldsymbol{y}}_i = \begin{bmatrix} \dot{q}_T^X & Q_{yaw} & Q_{tilt} \end{bmatrix}^T + \begin{bmatrix} \boldsymbol{0} & \boldsymbol{W}_{m,i} \end{bmatrix} \bar{\boldsymbol{d}}_i \tag{G.42}$$

The second terms on the right hand side of (G.41) and (G.42) represent measurement noise. Essentially the terms are filtered white noise. The control signals are:

$$\bar{\boldsymbol{u}}_c = \bar{\boldsymbol{\beta}}_{r,1} \tag{G.43}$$

$$\bar{\boldsymbol{u}}_i = \begin{bmatrix} \bar{\boldsymbol{\beta}}_{r,2} & \bar{\boldsymbol{\beta}}_{r,3} \end{bmatrix}^T \tag{G.44}$$

The weights $\boldsymbol{W}_{z,c}$,$\boldsymbol{W}_{z,i}$ and $\boldsymbol{W}_{m,c}$,$\boldsymbol{W}_{m,i}$ are simply used as tuning parameters and are chosen to suitably reflect the control objectives. The elements are generally algebraic apart from the weights associated with the pitch signals. These weights are chosen as a high pass filters to minimize high frequency pitch activity. The filters have the following form for each pitch signal:

$$W_\beta = \frac{(s+0.8)^3}{(s+3)^3} \tag{G.45}$$

Since $\bar{\boldsymbol{P}}_c$ and $\bar{\boldsymbol{P}}_i$ are decoupled we can design the controllers separately. Let the collective pitch controller be denoted by $\bar{\boldsymbol{K}}_c$ and the individual pitch controller by $\bar{\boldsymbol{K}}_i$. We choose to design the controllers such that we minimize the $\mathcal{H}_2$-norm of the closed loop systems

$$\bar{\boldsymbol{z}}_c = \mathcal{F}_l(\bar{\boldsymbol{P}}_c, \bar{\boldsymbol{K}}_c)\bar{\boldsymbol{d}}_c \tag{G.46}$$

$$\bar{\boldsymbol{z}}_i = \mathcal{F}_l(\bar{\boldsymbol{P}}_i, \bar{\boldsymbol{K}}_i)\bar{\boldsymbol{d}}_i \tag{G.47}$$

The $\mathcal{H}_2$-norm is chosen due to its interpretations in connection to white noise disturbances [16]. The $\mathcal{H}_2$ controller is designed using the Control Toolbox in Matlab and taking advantage of the fact that it can be realized as the combination of a Kalman filter and an LQ state feedback controller [16]. The controller for the original system is naturally attained by transforming the designs as indicated in equation (G.7).

G.6 Simulations

The control setup in the previous section is illustrated with simulations. Simulations with and without individual pitch control action are made.

Fig. G.4 shows the closed loop trajectories for rotor rotation ω_r and tower deflection speed $\dot{q}_T^Y$. As mentioned the dynamics associated with these signals

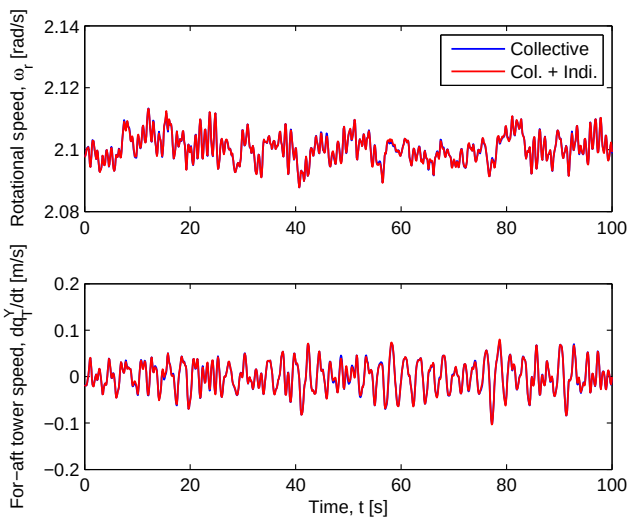

Figure G.4: Rotational speed ω_r and for-aft tower deflection speed $\dot{q}_T^Y$

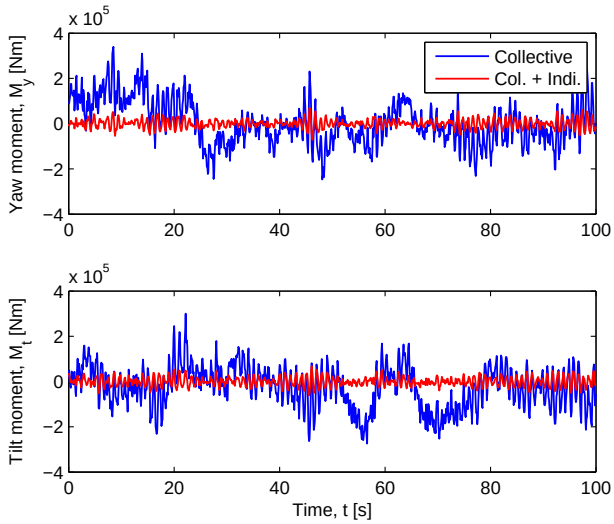

Figure G.5: Yaw moment Q_{yaw} and tilt moment Q_{tilt}

pertain to the collective pitch dynamics. The simulation shows that these signals are unaffected by the individual pitch controller. This clearly shows the decoupling property of the multiblade transformation. The plot shows that the rotational speed is kept close to constant. As mentioned earlier this is important

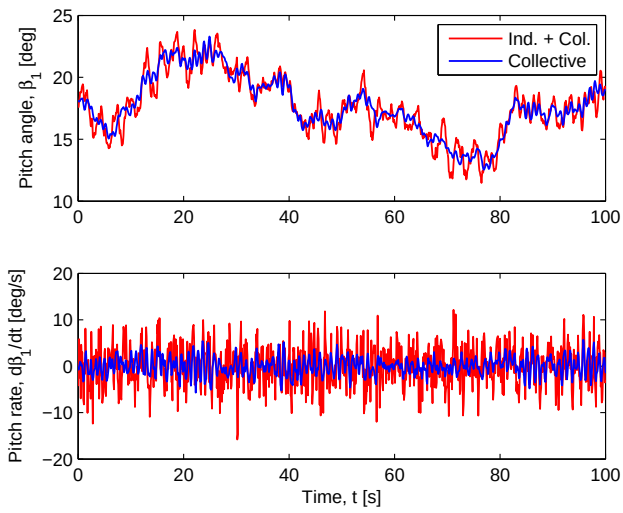

Figure G.6: Pitch angle β_1 and pitch angle speed $\dot{\beta}_1$

since the transformed linear model was derived assuming a constant rotational speed.

Fig. G.5 shows the yaw and tilt moment of the wind turbine. It is seen that the individual pitch controller manages to attenuate the yaw and tilt moment significantly. If the blades were allowed to pitch at high frequencies (if we removed the high-pass filter in the design) further attenuation can be obtained. However, this would cause extremely aggressive pitch activity.

Fig. G.6 shows the pitch angle β_1 and pitch angle rate $\dot{\beta}_1$ for the individual pitch controlled system and the collective pitch controlled system. The plots clearly show that attenuating the asymmetric loads comes at a cost. The pitch activity is significantly higher with the individual pitch controller than only the collective pitch controller. It is expected that the peak pitch rates are at the limits of what is acceptable. If further detuning is necessary, it is easily done by adjusting the frequency-dependent weight on the pitch.

The simulations indicate that a linear design can be justified when working around a given operating point.

G.7 Conclusion

In this paper we have shown how to set up simplified models of the wind which can be incorporated in individual pitch controller designs. Since it is advantageous to do control in multiblade coordinates the wind model was derived in these coordinates. The proposed model was applied together with a simplified model of the aerodynamics and a wind turbine in a $\mathcal{H}_2$ controller design. Simulations show that the resulting controller succeeds in attenuating the effect of the stochastic wind field.

Bibliography

[1] K.J. Åstrøm. *Introduction to stochastic control theory.* Academic Press New York, 1970.

[2] E.A. Bossanyi. Individual Blade Pitch Control for Load Reduction. *Wind Energy*, 6(2):119–128, 2003. DOI: 10.1002/we.76.

[3] E.A. Bossanyi. Wind turbine control for load reduction. *Wind Energy*, 6(3):229–244, 2003. DOI:10.1002/we.95.

[4] M.J. Grimble. Horizontal axis wind turbine control: comparison of classical, LQG and $\mathcal{H}_\infty$ designs. *Dynamics and Control*, 6(2):143–161, 1996. DOI:10.1007/BF02169534.

[5] M. Hansen. Aeroelastic stability analysis of wind turbines using an eigenvalue approach. *Wind Energy*, 7:133–143, 2004.

[6] M. O. L. Hansen. *Aerodynamics of Wind Turbines.* James & James, 2000.

[7] W. Johnson. *Helicopter Theory.* Princeton University Press, 1980.

[8] T.J. Larsen, H.A. Madsen, and K. Thomsen. Active load reduction using individual pitch, based on local blade flow measurements. *Wind Energy*, 8(1):67–80, 2005. DOI:10.1002/we.141.

[9] D.J. Leith and W.E. Leithead. Implementation of wind turbine controllers. *International Journal of Control*, 66(3):349–380, 1997.

[10] P. Sørensen. Frequency domain modelling of wind turbine structures. Technical report, Risø National Laboratory, Roskilde, Denmark, 1994.

[11] K.A. Stol, W. Zhao, and A. D. Wright. Individual blade pitch control for the controls advanced research turbine (cart). *Journal of Solar Energy Engineering*, 128:498–505, November 2006. DOI:10.1115/1.2349542.

[12] S.C. Thomsen, H. Niemann, and N.K. Poulsen. Individual pitch control of wind turbines using local inflow measurements. *Proceedings of the 17th IFAC World Congress, IFAC'08*, pages 5587–5592, 2008.

[13] S.C. Thomsen, H. Niemann, and N.K. Poulsen. Stochastic wind turbine modeling for individual pitch control. In *Proceedings of the European Control Conference*, 2009.

[14] S.C. Thomsen and N.K. Poulsen. A disturbance decoupling nonlinear control law for variable speed wind turbines. In *Proceedings of the 15th Mediterranean Conference on Control and Automation*, pages 1268–1273, 2007.

[15] Paul S. Veers. Three-dimensional wind simulation. Technical report, Sandia National Laboratories, 1988.

[16] K. Zhou, J.C. Doyle, and Glover K. *Robust and optimal control*. Prentice Hall, 1996.

Paper H

Robust stability in constrained predictive control through the Youla parameterizations

abstract

In this paper we take advantage of the primary and dual Youla parameterizations to set up a soft constrained model predictive control (MPC) scheme. In this framework it is possible to guarantee stability in face of norm-bounded uncertainties. Under special conditions guarantees are also given for hard input constraints. In more detail, we parameterize the MPC predictions in terms of the primary Youla parameter and use this parameter as the on-line optimization variable. The uncertainty is parameterized in terms of the dual Youla parameter. Stability can then be guaranteed through small gain arguments on the loop consisting of the primary and dual Youla parameter. This is included in the MPC optimization as a constraint on the induced gain of the optimization variable. We illustrate the method with a numerical simulation example.

H.1 Introduction

Model predictive control (MPC) - also commonly denoted constrained predictive control - is a model-based control method which has attracted a lot of attention, partly due to its popularity in the process industry. The feature which makes it truly innovative is its ability to handle constraints on control actions and states/output. This is done through on-line optimization of the future trajectory. More specifically, at each sampling time, starting at the current state, an open-loop optimal control problem is solved over a finite horizon. The theoretical foundation of nominal linear MPC has matured over recent decades and well established theorems for ensuring stability and feasibility have been established (See e.g. [10, 12]).

Theories have also been established for dealing with model uncertainty and disturbances in MPC. These methods are commonly denoted 'robust MPC'. Invariant sets have proved effective in dealing explicitly with these challenges and lead to computationally tractable optimization problems. This usually leads to optimization problems involving constraints in the form of linear matrix inequalities (See e.g. [6, 9, 24]). However, there are drawbacks with these methods. The optimization problem, although tractable, can be very complicated compared to basic MPC and therefore typically more computationally expensive. Furthermore, they have a tendency to be overly conservative.

In this paper a method is proposed for guaranteeing robust stability in the model predictive control framework. In the setup we consider general disturbances belonging to the l_2 function class and therefore primarily consider soft constraints. The method can be seen as a closed loop re-parameterization of nominal soft-constrained MPC such that robust stability has a simple interpretation in terms of the on-line optimization variable. The aim of the method is to guarantee stability with minimal additional complexity to the nominal optimization problem. To this end it is emphasized that no guarantees are given with respect to robust constraint handling or robust performance.

The classical system theoretical approach of the Youla parameterizations is utilized. For this reason the method will be denoted Youla-MPC (YMPC) in this paper. The primary Youla parameterization is the parameterization of all stabilizing controllers, whereas the dual Youla parameterization is the parameterization of all systems stabilized by a given controller. The nominal closed-loop system has an affine dependency on the primary Youla parameter, which makes it attractive as an optimization variable. The MPC optimization problem is parameterized in terms of the primary Youla parameter. This results in a (nominal) optimization problem with complexity similar to standard MPC, i.e. given a quadratic cost and linear inequality constraints, the problem reduces to

a quadratic programming problem. Uncertainty is handled by expressing the uncertainty in terms of the dual Youla parameter. Stability of the closed loop can then be reduced to a problem involving the primary and dual Youla parameter alone. This leads to a norm constraint on the primary Youla parameter which can be included in the on-line optimization problem.

It is shown that the MPC optimization problem is always feasible when including soft constraints on inputs and outputs. For perturbed stable open-loop systems we furthermore show that hard input constraints can be satisfied under certain conditions. The type of uncertainty considered is a general LTI uncertainty with bounded $\mathcal{H}_\infty$-norm.

The work in this paper can be seen partly as a generalization and partly as an extension of the work in [21, 22]. In the first paper [21] it was shown that nominal stability can be guaranteed in MPC by parameterizing the controller in terms of a time-varying Youla parameter. In [22] it was shown how model uncertainties with bounded 1-norm can be handled in their framework. All investigations in [21, 22] were made with a state estimate feedback realization of all stabilizing controllers.

The Youla parameterization has been considered in connection with MPC in other works as well. Back in the days of GPC it was introduced in [8] as part of a GPC algorithm (no constraints) with guaranteed stability. This algorithm was later extended to account for constraints and disturbances (see [5]). The conceptual paper [15] introduced the idea of robustifying constraint handling by desensitising the loop through the use of a Youla parameter.

Recently several authors have considered various Youla approaches: [17] and [2] have considered algorithms for robustifying MPC offline through the Youla parameterization. [11] used the Youla parameter to set up a stable MPC scheme that can deal with computational delays. [20] investigated the use of both the primary and dual Youla parameterizations in gaining information about the uncertainty and reconfiguring the controller in a modular setup.

As mentioned soft constraint are considered in this paper due to the class of exogeneous disturbances under consideration. It should however be noted that for other classes of disturbances it is indeed possible to handle hard constraints - at least without the model uncertainty - by means of constraint tightening such as described in e.g. [5] for GPC and later [3] for MPC. More recently stochastic MPC has gained popularity as a framework for dealing with stochastic disturbances which otherwise make it impossible to guarantee constraint satisfaction. In stochastic MPC the constraints are probabilistic and therefore allow constraint violation up to a certain probability. A review on stochastic MPC and applications can be found in [7].

H.2 Notation

The following matrix notation is used: $I_{N\times N}$ denotes the N-dimensional identity matrix. I_N denotes an N-dimensional column vector with ones. $\otimes$ denotes the Kronecker product and $vec(\cdot)$ denotes the vectorization operator. We will use the following short notation for the extended observability matrix and Toeplitz matrix:

$$\mathcal{O}^N(A,C) = \begin{bmatrix} C^T & (CA)^T & (CA^2)^T & \cdots & (CA^N)^T \end{bmatrix}^T \tag{H.1}$$

$$\mathcal{T}^N(A,B,C,D) = \begin{bmatrix} D & 0 & \cdots & 0 & 0 \\ CB & D & \cdots & 0 & 0 \\ CAB & CB & \cdots & 0 & 0 \\ \vdots & \vdots & \ddots & \vdots & \vdots \\ CA^{N-1}B & CA^{N-2}B & \cdots & CB & D \end{bmatrix} \tag{H.2}$$

The notation $\|x\|_W^2$ is used to denote the weighted 2-norm of a vector x i.e.

$$\|x\|_W^2 = x^T W x \tag{H.3}$$

The following standard notation

$$G \stackrel{s}{=} \left[\begin{array}{c|c} A & B \\ \hline C & D \end{array}\right] \tag{H.4}$$

is used to indicate the state-space realization of a linear system G. Notation will be abused slightly by letting G denote both the multiplicative operator in the time domain as well as the corresponding transfer function. The actual domain of the operator should be clear from the context. The operators $\mathcal{F}_u$ and $\mathcal{F}_l$ will be used to denote the upper and lower fractional transformations.

The N step predictions of a signal v from knowledge up until time k will be denoted $\vec{v}_N(k)$:

$$\vec{v}_N(k) = \begin{bmatrix} v(k|k)^T & v(k+1|k)^T & \ldots & v(k+N|k)^T \end{bmatrix}^T \tag{H.5}$$

Whenever referring to BIBO (bounded input - bounded output) stability in this paper we mean in the l_2 sense. $\bar{\sigma}$ denotes the maximum singular value.

H.3 Setup and preliminary results

H.3.1 System setup

The following discrete linear time-invariant system is considered:

$$\Sigma \ : \ \begin{cases} q(k) &= G_{qp}p(k) + G_{qr}r(k) + G_{qu}u(k) \\ z(k) &= G_{zp}p(k) + G_{zr}r(k) + G_{zu}u(k) \\ y(k) &= G_{yp}p(k) + G_{yr}r(k) + G_{yu}u(k) \end{cases} \tag{H.6}$$

where u is the control input, r is a reference/disturbance input and p is an input from an uncertainty. y is the measurable output, z is a performance signal and q is a signal which excites an uncertainty.

The uncertainty enters the system through the relation

$$p(k) = \Delta q(k) \tag{H.7}$$

where $\Delta \in \mathcal{RH}_\infty$ is an unknown LTI perturbation. The system is assumed controlled by the controller K

$$u(k) = Ky(k) \tag{H.8}$$

which has been designed such that the system is robustly stable for

$$\|\Delta\|_\infty = \sup_{|z|=1} \bar{\sigma}(\Delta(z)) \leq 1 \tag{H.9}$$

where $\bar{\sigma}$ is the maximum singular value. The setup is illustrated in Fig. H.1.

In the following Σ^Δ will denote the open loop system where the uncertainty Δ has been absorbed into the model

$$\Sigma^\Delta = \mathcal{F}_u(\Sigma, \Delta) = \begin{bmatrix} G_{zr}^\Delta & G_{zu}^\Delta \\ G_{yr}^\Delta & G_{yu}^\Delta \end{bmatrix} \tag{H.10}$$

H.3.2 The Youla parameterizations

The Youla parameterization of all stabilizing controllers is well known and has been used extensively in controller synthesis (See e.g. [23]). With reference to Fig. H.1 we consider the system $G \equiv G_{yu}$ and stabilizing controller K_0 (both transfer matrices). System and controller can be written as left or right co-prime factorizations:

$$G = N_r M_r^{-1} = M_l^{-1} N_l \tag{H.11}$$

$$K = U_r V_r^{-1} = V_l^{-1} U_l \tag{H.12}$$

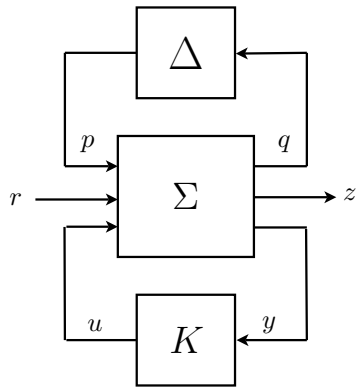

Figure H.1: System setup: The system is controlled by the feedback controller K which stabilizes Σ subject to the unknown LTI system Δ.

where $N_r, M_r, U_r, V_r, N_l, M_l, U_l, V_l \in \mathcal{RH}_\infty$ and satisfy the double Bezout identity

$$\begin{pmatrix} I & 0 \\ 0 & I \end{pmatrix} = \begin{pmatrix} V_l & -U_l \\ -N_l & M_l \end{pmatrix} \begin{pmatrix} M_r & U_r \\ N_r & V_r \end{pmatrix} = \begin{pmatrix} M_r & U_r \\ N_r & V_r \end{pmatrix} \begin{pmatrix} V_l & -U_l \\ -N_l & M_l \end{pmatrix} \tag{H.13}$$

In fact K stabilizes G if and only if coprime factors exist such that the double Bezout identity is satisfied.

All controllers which stabilize G can be expressed as:

$$\mathcal{K}(Q) = (U_r + M_r Q)(V_r + N_r Q)^{-1} = \mathcal{U}_r(Q)\mathcal{V}_r^{-1}(Q) \tag{H.14}$$

$$\mathcal{K}(Q) = (V_l + Q N_l)^{-1}(U_l + Q M_l) = \mathcal{V}_l^{-1}(Q)\mathcal{U}_l(Q) \tag{H.15}$$

where $Q \in \mathcal{RH}_\infty$ is called the Youla parameter. This follows from the fact that $\mathcal{U}_r(Q), \mathcal{V}_r(Q)$ and $\mathcal{V}_l(Q), \mathcal{U}_l(Q)$ are coprime factors of $\mathcal{K}(Q)$ and satisfy the double Bezout identity together with the coprime factors of G. K is naturally attained when $Q = 0$.

The dual of the Youla parameterization is all systems stabilized by a given controller ([13, 18]). This is commonly denoted the 'dual Youla parameterization'. The parameterization can be written as follows:

$$\mathcal{G}(S) = (N_r + V_r S)(M_r + U_r S)^{-1} = \mathcal{N}_r(S)\mathcal{M}_r^{-1}(S) \tag{H.16}$$

$$\mathcal{G}(S) = (M_l + S U_l)^{-1}(N_l + S V_l) = \mathcal{M}_l^{-1}(S)\mathcal{N}_l(S) \tag{H.17}$$

where $S \in \mathcal{RH}_\infty$ is the dual Youla parameter. This follows from the fact that $\mathcal{N}_r(S), \mathcal{M}_r(S)$ and $\mathcal{M}_l(S), \mathcal{N}_l(S)$ are coprime factors of $\mathcal{G}(S)$ and satisfy the

double Bezout identity together with the coprime factors of K. The nominal system G is naturally attained for $S = 0$.

Now, considering the system $G^\Delta = G^\Delta_{yu}$, which is robustly stabilized by K. Since all system stabilized by K is spanned by $\mathcal{G}(S)$, $S \in \mathcal{RH}_\infty$, there exists a S^Δ such that $G^\Delta = \mathcal{G}(S^\Delta)$. Hence, the uncertainty can be expressed in terms of an uncertain $S^\Delta \in \mathcal{RH}_\infty$ rather than $\Delta \in \mathcal{RH}_\infty$. The relation between the uncertainty Δ and the uncertain dual Youla parameter S^Δ can be given explicitly ([13]):

$$S^\Delta = M_l G_{yp} \Delta (I - (G_{qp} + G_{qu} U_r M_l G_{yp})\Delta)^{-1} G_{qu} M_r \tag{H.18}$$

Since $G^\Delta = \mathcal{G}(S^\Delta)$ the coprime factorization of G^Δ can directly be chosen as:

$$G^\Delta = N_r^\Delta {M_r^\Delta}^{-1} = (N_r + V_r S^\Delta)(M_r + U_r S^\Delta)^{-1} \tag{H.19}$$

$$= {M_l^\Delta}^{-1} N_l^\Delta = (M_l + S^\Delta U_l)^{-1}(N_l + S^\Delta V_l) \tag{H.20}$$

Parameterizing the controller K in terms of the Youla parameter Q (based on nominal G), the transfer function from disturbances r to the output z will, in the uncertain case, be:

$$F_Q^\Delta = T_{zr}^\Delta + T_{z\eta}^\Delta S^\Delta (I - QS^\Delta)^{-1} T_{\epsilon r}^\Delta \tag{H.21}$$

where

$$T^\Delta = \begin{pmatrix} T_{zr}^\Delta & T_{z\eta}^\Delta \\ T_{\epsilon r}^\Delta & S^\Delta \end{pmatrix} \tag{H.22}$$

$$= \begin{pmatrix} G_{zr}^\Delta + G_{zu}^\Delta U_r M_l^\Delta G_{yr}^\Delta & G_{zu}^\Delta M_r^\Delta \\ M_l^\Delta G_{yr}^\Delta & S^\Delta \end{pmatrix} \tag{H.23}$$

The derivation of T^Δ is given in Appendix H.8. The following theorem establishes stability of T^Δ.

Theorem 4. *$T^\Delta \in \mathcal{RH}_\infty$ if and only if K robustly stabilizes Σ^Δ*

Proof. The proof is given in Appendix H.9 and is an extension of the result for nominal systems ($\Delta = 0$) in [19] Lemma 2, p. 43. □

When $T^\Delta \in \mathcal{RH}_\infty$ it is readily seen that F_Q^Δ is stable if the loop of Q and S^Δ (Fig. H.2) is a stable loop. In general we can close the loop with a time-varying, nonlinear Q. In the following sections the nominal systems F_Q^0 and T^0 (i.e. $\Delta = 0$) will simply be denoted by F_Q and T.

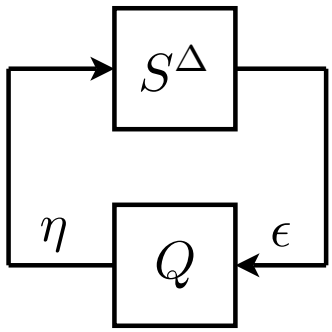

Figure H.2: When K robustly stabilizes G^Δ then the closed loop is stable if Q stabilizes S^Δ

.

Remark 12. *The setup simplifies significantly when* $r = \begin{bmatrix} e_1^T & e_2^T \end{bmatrix}^T$ *represents input noise* e_1 *and output noise* e_2 *and* $z = \begin{bmatrix} y^T & u^T \end{bmatrix}^T$ *is the vector of measurable outputs and inputs.*

$$T^\Delta = \begin{pmatrix} \begin{pmatrix} I & -K \\ -G^\Delta & I \end{pmatrix}^{-1} & \begin{pmatrix} N_r^\Delta \\ M_r^\Delta \end{pmatrix} \\ \begin{pmatrix} N_l^\Delta & M_l^\Delta \end{pmatrix} & S^\Delta \end{pmatrix} \tag{H.24}$$

H.4 Youla model predictive control

The basis of the method is to parameterize the predictions in terms of a time-varying primary Youla parameter. This is shown in Sec. H.4.1. Robust stability is enforced by taking advantage of the relation between the time-varying primary Youla and dual Youla parameter, which essentially leads to a norm constraint on the primary Youla parameter. The conditions are derived in Sec. H.4.2. In Sec. H.4.3 the pieces are put together to obtain the Youla MPC optimization problem.

H.4.1 Predictions based on Youla parameterization

In this section the prediction equations which will be used in the YMPC optimization are derived. In the following it is assumed that the structure of the

Youla parameter is given as follows:

$$Q_k = \Theta(k)\tilde{Q} \tag{H.25}$$

where $\tilde{Q} \in \mathcal{RH}_\infty$ and $\Theta(k)$ is a time-varying gain of appropriate dimensions. $\Theta(k)$ is the free parameter with which the cost is to be optimized in the YMPC controller at every sample k. The structure is chosen such that the predictions will have an affine dependency on the free parameters.

Since Δ is unknown we base the predictions on the nominal dynamics ($\Delta = 0 \Rightarrow S^\Delta = 0$). For $S^\Delta = 0$ we can write the closed loop system from r to z (using equation (H.21))

$$\begin{aligned} z(k) &= F_{Q_k} r(k) && \text{(H.26)} \\ &= T_{zr} r(k) + T_{z\eta} Q_k T_{\epsilon r} r(k) && \text{(H.27)} \\ &= T_{zr} r(k) + T_{z\eta} \Theta(k) \tilde{Q} T_{\epsilon r} r(k) && \text{(H.28)} \end{aligned}$$

In deriving the prediction equations the internal form (state space) of T and $\tilde{Q}$ is assumed to be as follows:

$$T \stackrel{s}{=} \left[\begin{array}{c|cc} A_T & B_{T,r} & B_{T,\eta} \\ \hline C_{T,z} & D_{T,zr} & D_{T,z\eta} \\ C_{T,\epsilon} & D_{T,\epsilon\eta} & D_{T,\epsilon\eta} \end{array}\right] \quad \tilde{Q} \stackrel{s}{=} \left[\begin{array}{c|c} A_Q & B_Q \\ \hline C_Q & D_Q \end{array}\right] \tag{H.29}$$

The state vector of T and $\tilde{Q}$ will be denoted x_T and x_Q respectively. To simplify the prediction equations, the signal z is divided into the nominal part ($Q = 0$) and the contribution due to $Q \neq 0$.

$$z(k) = z_0(k) + z_Q(k) \tag{H.30}$$

To reduce notation we introduce the following extended observability matrices and Toeplitz matrices we can write the N-step prediction explicitly:

$$\begin{aligned} \mathcal{A}_z &= \mathcal{O}^N(A, C_z) \quad \mathcal{A}_Q = \mathcal{O}^N(A_Q, C_Q) && \text{(H.31)} \\ \mathcal{A}_\epsilon &= \mathcal{O}^N(A, C_\epsilon) && \text{(H.32)} \\ \mathcal{B}_{zr} &= \mathcal{T}^N(A, B_r, C_r, D_{zr}) && \text{(H.33)} \\ \mathcal{B}_{z\eta} &= \mathcal{T}^N(A, B_\eta, C_z, D_{z\eta}) && \text{(H.34)} \\ \mathcal{B}_{\epsilon r} &= \mathcal{T}^N(A, B_r, C_\epsilon, D_{\epsilon r}) && \text{(H.35)} \\ \mathcal{B}_Q &= \mathcal{T}^N(A_Q, B_Q, C_Q, D_Q) && \text{(H.36)} \end{aligned}$$

The N-step prediction of z_0 due to the N-step trajectory of r is trivially

$$\vec{z}_{0,N}(k) = \mathcal{A}_z x_T(k) + \mathcal{B}_{zr} \vec{r}(k) \tag{H.37}$$

The N-step prediction of z_Q is given by

$$\vec{z}_{Q,N}(k) = \mathcal{B}_{z\eta}(I \otimes \Theta(k))(\mathcal{A}_Q x_Q(k) + \mathcal{B}_Q \vec{\epsilon}(k)) \tag{H.38}$$

$$= \mathcal{B}_{z\eta}((\mathcal{A}_Q x_Q(k) + \mathcal{B}_Q \vec{\epsilon}(k))^T \otimes I) vec(\Theta(k)) \tag{H.39}$$

where

$$\vec{\epsilon}(k) = A_\epsilon x_T(k) + B_{\epsilon r} \vec{r}(k) \tag{H.40}$$

This results from straight forward manipulations. The Kronecker product is a bilinear operator and therefore we see that the predictions have an affine dependency on the elements of $\Theta(k)$. This means that the resulting MPC optimization problem has complexity similar to standard MPC where the predictions are affine in the open loop trajectory.

The choice of $\tilde{Q} \in \mathcal{RH}_\infty$ is free, however, some choices are more intuitive than others. Following the approach in [21, 22] the simplest choice is to let $\tilde{Q}$ store information rather than do any complicated processing of the input ϵ. In essence we choose $\tilde{Q}$ as the multi-dimensional shift-register (FIR-filter)

$$\tilde{Q} \stackrel{s}{=} \left[\begin{array}{c|c} I_{n_u \times n_u} \otimes A_{fir} & I_{n_u \times n_u} \otimes B_{fir} \\ \hline I_{n_u \times n_u} \otimes C_{fir} & I_{n_u \times n_u} \otimes D_{fir} \end{array}\right] \tag{H.41}$$

where

$$A_{fir} = \begin{bmatrix} 0 & 1 & 0 & \cdots & 0 \\ 0 & 0 & 1 & \cdots & 0 \\ \vdots & \vdots & \vdots & \ddots & \vdots \\ 0 & 0 & 0 & \cdots & 1 \\ 0 & 0 & 0 & \cdots & 0 \end{bmatrix} \quad B_{fir} = \begin{bmatrix} 0 \\ 0 \\ \vdots \\ 0 \\ 1 \end{bmatrix} \tag{H.42}$$

$$C_{fir} = I \quad D_{fir} = \begin{bmatrix} 1 & 0 & \dots & 0 \end{bmatrix} \tag{H.43}$$

With this choice, past information is simply stored in $\tilde{Q}$ without any complex processing being made. All emphasis is hence put on the on-line optimization parameter Θ to construct the optimal trajectory of z based on the stored information in $\tilde{Q}$. Other choices of $\tilde{Q}$ are discussed and motivated in Sec. H.5.2.

How the Youla parameterization is realized i.e. the choice of coprime factors, is likewise a freedom in the design. If the unconstrained robust controller K is a state estimate feedback controller, the realization becomes especially simple ([25]). Let the state space representation of the generalized system Σ be given as:

$$\Sigma \stackrel{s}{=} \left[\begin{array}{c|ccc} A & B_p & B_r & B_u \\ \hline C_q & D_{qp} & D_{qr} & D_{qu} \\ C_z & D_{zp} & D_{zr} & D_{zu} \\ C_y & D_{yp} & D_{yr} & D_{yu} \end{array}\right] \tag{H.44}$$

A state estimate feedback controller K then has the form K

$$K \overset{s}{=} \left[\begin{array}{c|c} A + B_u F + LC_y + LD_{yu}F & -L \\ \hline F & 0 \end{array}\right] \tag{H.45}$$

where the state feedback F and the output injection L have been chosen such that K robustly stabilizes the uncertain system (for $\|\Delta\|_\infty \leq 1$). Referring to Fig. H.3 the input ϵ to Q_k is in this case simply the output estimation error $y - \hat{y}$. The output η of Q_k is simply added to the control signal i.e. $u = F\hat{x} + \eta$ where F is the feedback gain and $\hat{x}$ is the state estimate. With this realization

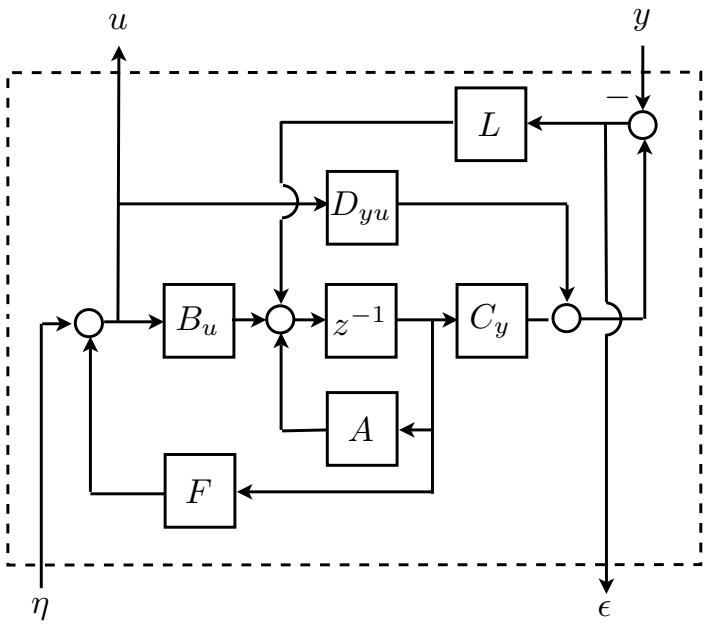

Figure H.3: State estimate feedback controller realization of the Youla parameterization

the matrices in (H.29) become

$$A_T = \begin{bmatrix} A & B_u F \\ -LC_u - LD_{yu}F & A + B_u F + LC_y + LD_{yu}F \end{bmatrix} \tag{H.46}$$

$$B_{T,r} = \begin{bmatrix} B_u \\ -LD_{yr} \end{bmatrix}, \quad B_{T,\eta} = \begin{bmatrix} B_u \\ B_u \end{bmatrix}, \quad C_{T,z} = \begin{bmatrix} C_z & D_{zu}F \end{bmatrix}, \quad C_{T,\epsilon} = \begin{bmatrix} C_y & -C_y \end{bmatrix} \tag{H.47}$$

$$D_{T,zr} = D_{zr}, \quad D_{T,zu} = D_{zu}, \quad D_{T,\epsilon r} = D_{yr}, \quad D_{T,\epsilon\eta} = 0 \tag{H.48}$$

The state vector of T is the augmentation of the system states x and the con-

troller states x_K

$$x_T = \begin{bmatrix} x^T & x_K^T \end{bmatrix}^T \tag{H.49}$$

Remark 13. *If the state x of the system is unknown it is necessary to use a state estimate $\hat{x}$ instead. Since this is an integral part of the state estimate feedback controller K no additional calculations need to be made.*

H.4.2 Stability guarantee through the dual Youla parameter

In this section a stability condition is derived for the free parameter $\Theta(k)$. This essentially leads to a constraint on the norm of $\Theta(k)$ which must be respected at all sample times.

The stability condition is derived by applying the small gain theorem ([4]) to the loop of S^Δ and Q_k. Before stating the condition it is convenient to introduce the following transfer function consisting of the series connection of S^Δ and $\tilde{Q}$:

$$Z^\Delta = \tilde{Q} S^\Delta \tag{H.50}$$

The worst case gain point-wise-in-frequency of Z^Δ will be denoted by $Z_\infty(\omega)$

$$Z_\infty(\omega) = \sup\left(\bar{\sigma}\{Z^\Delta(\omega)\} \mid \bar{\sigma}\{\Delta(\omega)\} \leq 1\right) \ , \quad \forall \omega \tag{H.51}$$

Having introduced the above notation, the following Theorem is provided

Theorem 5. *With K robustly stabilizing Σ^Δ and Q_k parameterized as in (H.25), stability of the closed loop system (H.21) is guaranteed if*

$$\bar{\sigma}\{\Theta(k)\} < \frac{1}{\sup_\omega(Z_\infty(\omega))} = \frac{1}{\gamma_L} \ , \quad \forall k \tag{H.52}$$

Proof. As stated in Sec. H.3, F_Q^Δ is stable if Q_k stabilizes S^Δ. The loop can be seen as a series connection of the stable system $Z^\Delta = \tilde{Q} S^\Delta$ and $\Theta(k)$. The induced l_2 gain of Z^Δ is bounded by $\gamma = \sup_\omega(Z_\infty)$. According to the small gain theorem the closed loop is stable if the induced gain of $\Theta(k)$ is smaller than $\frac{1}{\gamma}$. This implies the inequality (H.52). □

The constraint (H.52) will allow us to guarantee stability of the MPC formulation. The constraint can be reformulated as the following linear matrix inequality, which we will incorporate in the optimization problem (See e.g. [1]).

$$\begin{bmatrix} \gamma_L^{-1} I & \Theta \\ \Theta^T & \gamma_L^{-1} I \end{bmatrix} < 0 \tag{H.53}$$

The equivalent formulation follows from the definition of the singular value and the use of the Schur complement.

It is not the scope the paper to describe how Z_∞ can be calculated. However, algorithms exist for solving this problem. The reader is referred to [14] for an algorithm[1]. It is stressed that finding the upper bound is not part of the on-line MPC optimization. Speed of convergence is therefore of minor importance.

H.4.3 The optimization problem

In this section the pieces are combined and the optimization problem for the Youla-MPC controller is introduced.

In the optimization problem the following vector is introduced

$$\bar{z} = \begin{bmatrix} z_0^T & z_Q^T \end{bmatrix}^T \tag{H.54}$$

for which the following relation naturally holds $z = \begin{bmatrix} I & I \end{bmatrix} \bar{z}$ (See e.q. (H.30)). The reason is that it might be beneficial to weight the nominal contribution z_0 and the forced contribution z_Q separately. This is e.g. the case when the unconstrained controller achieves desired performance when constraints are inactive. In this situation it is natural to force $\Theta(k) = 0$ when constraints are inactive. This can be done by only targeting z_Q in the cost function.

In this work the following optimization problem is used

$$\min_{\Theta, s} \left\{ \|\bar{z}(k+N+1|k)\|_{R_1}^2 + \sum_{i=0}^{N} \|\bar{z}(k+i|k)\|_{R_2}^2 \; + \|s\|_{R_3}^2 \right\} \tag{H.55}$$

subject to

$$\begin{cases} \text{nominal dynamics (H.28) \& (H.29)} \\ C_h \bar{z}(k+i|k) \leq 1 \quad \text{for} \quad i = 0, 1, \ldots, N \\ C_s \bar{z}(k+i|k) \leq 1 + s \quad \text{for} \quad i = 0, 1, \ldots, N \\ s \geq 0 \\ \begin{bmatrix} \gamma_L^{-1} I & \Theta \\ \Theta^T & \gamma_L^{-1} I \end{bmatrix} > 0 \end{cases} \tag{H.56}$$

This problem is solved at every sample time and the solution $\Theta(k) = \Theta$ is actuated in the controller.

As is usual practice in MPC, a finite horizon cost is used which includes a terminal cost. Both hard and soft constraints on $\bar{z}$ are included. Soft constraints

[1] This is also the algorithm which is implemented in the Matlab function `wcgain`

are implemented by allowing constraint violation through the slack variable s. Finally the stability constraint on $\Theta(k)$ is included in its LMI form.

In the nominal case $\Delta = 0$ the LMI constraint can be removed from the optimization problem. An artificial bound should however still be placed on $\Theta(k)$ to ensure stability. A computational simple way is to require that the elements Θ_{ij} of $\Theta(k)$ are bounded by a (large) positive number ξ.

$$|\Theta_{ij}| \leq \xi \quad ,\forall\ i,j \tag{H.57}$$

The consequent optimization problem then simply reduces to a quadratic programming problem.

Generally, it cannot be guaranteed that the optimization problem is feasible at all times when including hard constraints ($C_h \neq 0$). For soft constraints we supply the following theorem:

Theorem 6. *If only soft constraints are included (i.e. $C_h = 0$), the optimization problem is feasible at all times and leads to a stable closed loop system.*

Proof. . This follows directly from the stability conditions of the system. Due to the soft constraints $\Theta(k) = 0$ will always be a feasible solution with $s(k)$ chosen sufficiently high. Since $\Theta(k) = 0$ will lead to stability, $s(k)$ will not grow unbounded. □

For systems Σ^{Δ} which are stable for $\|\Delta\|_\infty \leq 1$ and for which the trivial controller $K = 0$ is chosen, it is possible to guarantee satisfaction of hard constraints on control signal u at all times

Theorem 7. *Consider systems Σ^{Δ} which are stable for all $\Delta \in \mathcal{RH}_\infty$, $\|\Delta\|_\infty \leq 1$ with the trivial pre-stabilization $K = 0$. Choosing $M_r = M_l = I$, $N_r = N_l = G$ and $V_r = V_l = I$ and $U_r = U_l = 0$ the YMPC optimization will remain feasible at all times with hard constraints on input u.*

Proof. The Youla parameterized controller will be given by

$$\mathcal{K}(Q_k) = \Theta(k)\tilde{Q}(I + G\Theta(k)\tilde{Q})^{-1} = (I + \Theta(k)\tilde{Q}G)^{-1}\Theta(k)\tilde{Q} \tag{H.58}$$

It is seen that the feasible solution $\Theta(k) = 0$ will give the control signal $u(k) = 0$, irrespective of the internal state of the Youla parameterized controller. □

We conclude this section with a short outline of the design algorithm. The algorithm is divided into its offline part and on-line part.

Offline The first step is to design a robust (unconstrained) stabilizing controller K - this ensures $S^{\Delta} \in \mathcal{RH}_{\infty}$ which is necessary for the small gain theorem. A realization of the Youla parameterization now needs to be chosen (the canonical choice is the state estimate feedback realization). The Youla parameter should be parameterized on the form $\Theta(k)\tilde{Q}$ with the canonical choice of $\tilde{Q}$ being a FIR filter. To guarantee stability of YMPC an upper bound on the $\|\tilde{Q}S^{\Delta}\|_{\infty}$ has to be established.

On-line The on-line optimization problem simply consists of solving the optimization problem in section H.4.3 at every sample time and implementing the solution.

H.5 Reducing conservativeness and extensions

The gain constraint on Θ might be very conservative. This section describes how to reduce the conservativeness of the gain constraint. Moreover, two extensions are described. Firstly, it is described how to use the freedom in choosing $\tilde{Q}$ to reduce on-line computations. Secondly, how to take into account knowledge of a future trajectory of a reference/disturbance in the YMPC framework.

H.5.1 Reducing conservativeness

Implementing the norm-constraint directly will generally lead to a conservative controller. The ∞-norm is the supremum of the gain (maximum singular value) evaluated along the frequency axis. Therefore, the norm constraint does not take into account that the gain of Θ could be significantly higher when operating at frequencies which are less affected by the uncertainty without compromising stability.

To reduce conservativeness it is suggested to include pre- and/or post-filtration of Q_k. Referring to Fig. H.4 the filtered Youla parameter $Q_k^W \in \mathcal{RH}_{\infty}$ is given by

$$Q_k^W = W_2 Q_k W_1 \tag{H.59}$$

where $W_1 \in \mathcal{RH}_{\infty}$ and $W_2 \in \mathcal{RH}_{\infty}$ are the pre- and post-filters respectively. Excluding the time-varying gain $\Theta(k)$ the filtered loop transfer is given by:

$$Z_W^{\Delta} = \tilde{Q} W_1 S^{\Delta} W_2 \tag{H.60}$$

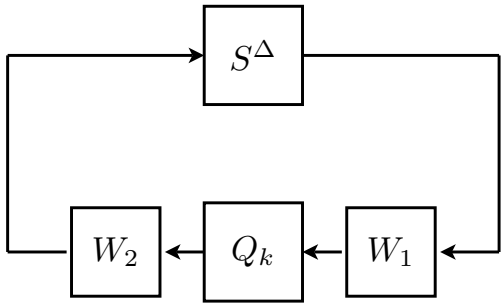

Figure H.4: Loop with pre- and post-filters

The filters should be designed such that the worst case loop gain is (approximately) constant over frequency. For simplicity and without loss of generality the constant is chosen to be 1 i.e.:

$$Z_{W,\infty}(\omega) = \sup\left(\bar{\sigma}\{Z_W^{\Delta}(\omega)\} \mid \bar{\sigma}\{\Delta(\omega)\} \leq 1\right) \approx 1, \ , \quad \forall\omega \tag{H.61}$$

This leads to the following extension of the robust stability result in Theorem 5:

Corrolary 1. *With pre- and post-filtration of the Youla parameter Q (denoted W_1 and W_2 respectively) the following is a sufficient condition for stability*

$$\bar{\sigma}\Theta(k) < \frac{1}{\sup_{\omega}(Z_{W,\infty}(\omega))} \ , \ \forall k \tag{H.62}$$

The prediction equations in Sec. H.4.1 need to include the effect of the pre- and -post filtering. This is trivially included by using the filtered Youla parameter $\tilde{Q}_W$ everywhere that $\tilde{Q}$ previously appeared. The LMI constraint (H.53) should naturally also incorporate these weights.

H.5.2 Reducing the on-line complexity

There is a design flexibility in choosing $\tilde{Q}$. In connection with MPC, where focus is on finding the optimal solution on-line, the natural choice is arguably the FIR filter as shown in Sec. H.4. However, any choice $\tilde{Q} \in \mathcal{RH}_\infty$ is a valid choice in YMPC. This can be exploited to reduce the on-line computational burden. An approach which leads to significant reduction of on-line computation is to

choose $\tilde{Q}$ as a collection of a few carefully designed controllers and simply use Θ to provide the optimal blend. Let the structure of $\tilde{Q}$ be given as:

$$\tilde{Q} = \begin{bmatrix} \tilde{Q}_1 \\ \tilde{Q}_2 \\ \vdots \\ \tilde{Q}_n \end{bmatrix} \tag{H.63}$$

where each $\tilde{Q}_k$ has been designed such that $\mathcal{K}(\tilde{Q}_k)$ meets some desired criteria. $\{\mathcal{K}(\tilde{Q}_k) \ : \ k = 1, \ldots, n\}$ could represent a family of sub-optimal controllers e.g. a collection of sluggish and aggressive control strategies.

Comparable approaches to reduce on-line complexity are described in [16] in which invariant sets are used to ensure recursive feasibility and stability.

H.5.3 Reference tracking

A common application of MPC is to track a reference, given knowledge of its future trajectory $\vec{r}$. In essence this allows the MPC controller to anticipate the changes and react. The MPC controller can therefore react before the reference actually changes and thereby control more smoothly than otherwise possible. The YMPC controller, however, adjusts its control action by changing the gain $\Theta(k)$. If the system has not been excited by some external source (e.g. a reference) adjusting $\Theta(k)$ has no effect. By constructing a suitable disturbance model it is possible react to future changes in the reference trajectory. The disturbance model should simply describe the future N-step evolution of the reference.

For simplicity, assume that the exogenous signal r only consists of references. The future N-step evolution of r can then be described with the system P_r:

$$P_r \stackrel{s}{=} \left[\begin{array}{c|c} I_{n_u \times n_u} \otimes A_{fir} & I_{n_u \times n_u} \otimes B_{fir} \\ \hline I_{n_u \times n_u} \otimes C_{fir} & I_{n_u \times n_u} \otimes D_{fir} \end{array}\right] \tag{H.64}$$

The output of P_r is:

$$r_p(k) = \begin{bmatrix} r(k)^T & r(k+1)^T & \cdots & r(k+N)^T \end{bmatrix}^T \tag{H.65}$$

and the input is

$$\tilde{r}(k) = r(k+N) \tag{H.66}$$

The original system Σ should be augmented with this model. The reference signal to this model is $\tilde{r}$ and the measurable output is:

$$\tilde{y} = \begin{bmatrix} y \\ r_p \end{bmatrix} \tag{H.67}$$

The disturbance model belongs to $\mathcal{RH}_\infty$, and therefore it does not affect stability. Designing the YMPC controller based on the augmented system will effectively cause it to take into account the future reference r_p.

H.6 Example

In this section a robust YMPC controller design is exemplified. The example is based on a simple mass-spring system as sketched in Fig. H.5. In the example

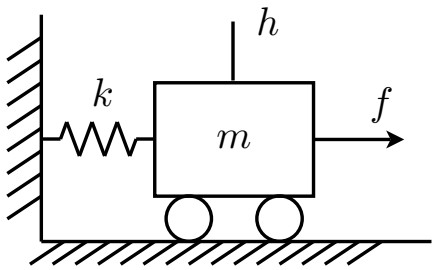

Figure H.5: Cart system used in simulation. m, k and c are the mass, stiffness and damping respectively. h is the position. F is a force acting on the cart.

a state estimate feedback realization of the Youla parameterization is used (See end of Sec. H.4.1).

The spring constant of the system in Fig. H.5 is chosen negative $k < 0$ making the system unstable. The actual value of the spring constant is uncertain. The nominal value is $k_0 = -5$ and the uncertainty is $\Delta k = \pm 0.5$. The mass of the cart is $m = 1$. The system description is sampled with $T_s = 0.45$.

The sampled dynamics of the cart are governed by the following state space equation

$$x(k+1) = \left(\begin{bmatrix} 1.543 & 0.5256 \\ 2.628 & 1.543 \end{bmatrix} + \begin{bmatrix} 0.1086 \\ 0.5256 \end{bmatrix} \Delta \begin{bmatrix} 2 & 0 \end{bmatrix} \right) x(k) + \begin{bmatrix} 0.1086 \\ 0.5256 \end{bmatrix} u(k) \tag{H.68}$$

where the state of the system $x = [h \;\; \dot{h}]^T$ consists of the position and speed. The control signal $u = f$ is the force acting on the cart. The uncertainty Δ is a real number in the interval $(-1,\ 1)$. It is assumed that the measurement y consists of the states. The performance signal z consists of the states and control signal. The disturbance r consists of state noise and measurement noise.

The state feedback gain F and the input injection gain L used in the pre-

stabilizing controller is

$$F = \begin{bmatrix} -6.8393 & -3.0588 \end{bmatrix}, \quad L = \begin{bmatrix} -0.5224 & -0.8453 \\ -1.0812 & -1.9194 \end{bmatrix} \tag{H.69}$$

F is the optimal LQ gain for the nominal system when the state weight is chosen as $R_x = \text{diag}([1 \;\; 1])$ and input weight $R_u = 100$. L is the Kalman gain for the nominal system with state noise covariance $Q_x = \text{diag}([1 \;\; 1])$ and measurement noise covariance $Q_y = \text{diag}([10 \;\; 10])$

To reduce conservativeness the method suggested in section H.5.1 is implemented. A post-filter W_2 is designed which is approximately inverse to $Z_\infty(\omega)$. The following stable filter provides a reasonable approximation:

$$W_2(z) = \frac{-10.14z^4 + 10.37z^3 - 4.425z^2 + 2.259z - 2.229}{z^4 - 0.2708z^3 + 0.4388z^2 - 0.4172z} \tag{H.70}$$

The fit is shown in figure H.6. With this filter the upper bound on the worst case gain is $Z_{w,\infty} = 1$.

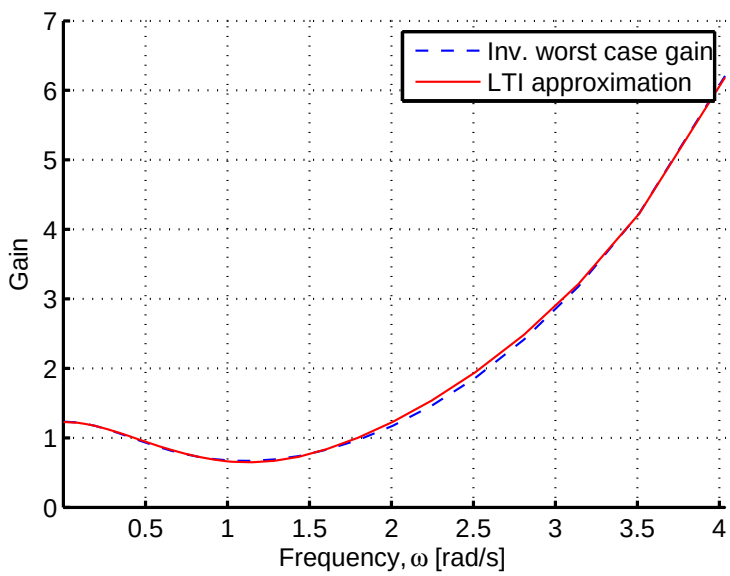

Figure H.6: Fit to worst case inverse

It is assumed that the nominal controller has been designed for desired unconstrained performance. The YMPC cost is therefore constructed such that the YMPC controller is inactive when constraint violation is not predicted. As

explained previously this can be done by penalizing the part of the control signal u_Q which arises from $\Theta \neq 0$. For the chosen realization this corresponds to $u_Q = \epsilon$ (see Fig. H.3). The design includes a soft constraint on the cart speed. A slack variable $s = [s_1 \;\; s_2]^T$ is associated with the soft constraints. The optimization problem at each sample time k is:

$$\min_{\Theta,s} \left\{ \sum_{i=0}^{10} \epsilon(k+i|k)^2 + 1000\|s\|^2 \right\} \tag{H.71}$$

subject to

$$\begin{cases} \text{Nominal dynamics} \\ \dot{h}(k+i|k) \leq 2 + s_1 \quad \text{for } i = 0, 1, \ldots, N \\ -\dot{h}(k+i|k) \leq 2 + s_2 \quad \text{for } i = 0, 1, \ldots, N \\ s \geq 0 \\ \begin{bmatrix} I & \Theta(k) \\ \Theta(k)^T & I \end{bmatrix} > 0 \end{cases} \tag{H.72}$$

For comparison, a standard MPC controller with soft constraints is also designed. It is likewise designed for the pre-stabilized system and is designed with the same cost and constraints. Referring to Fig. H.3, the control signal u_{mpc} is a perturbation of the unconstrained control law and hence coinsides with ϵ. The standard MPC algorithm naturally lacks the robustness constraint.

Fig. H.7 shows the speed and the perturbation of the unconstrained control law for both YMPC and the standard MPC algorithm. The initial condition in the simulation is $x = [1 \;\; 0]^T$ which means that the cart is placed at position 1 with speed 0. The figure shows that the YMPC controller manages to reduce the violation of the constraint significantly and that the performance is comparable to the standard MPC controller.

The conservativeness of the YMPC controller becomes apparent when initiating the system at a more extreme position. Fig. H.8 shows the simulation when initiating the cart at $x = [10 \;\; 0]^T$ i.e. position 10 and speed 0. Since there is a limit on the gain in the YMPC controller, it cannot do much in order to minimize the constraint violation. The standard MPC controller naturally ensures that the constraint violation is very small.

The advantage of the YMPC controller is however illustrated when the system is no longer the nominal one. Fig. H.9 shows the simulation when the perturbation is $\Delta = 1$ and the initial condition is $x = [10 \;\; 0]$. As could be expected, the YMPC controller still cannot minimize the constraint violation. However, the situation is much worse for the standard MPC controller. In its endeavor to keep within the limits of the constraint, it causes unstable closed loop behavior.

As a final illustration, it is shown that post-filtering the Youla parameter has

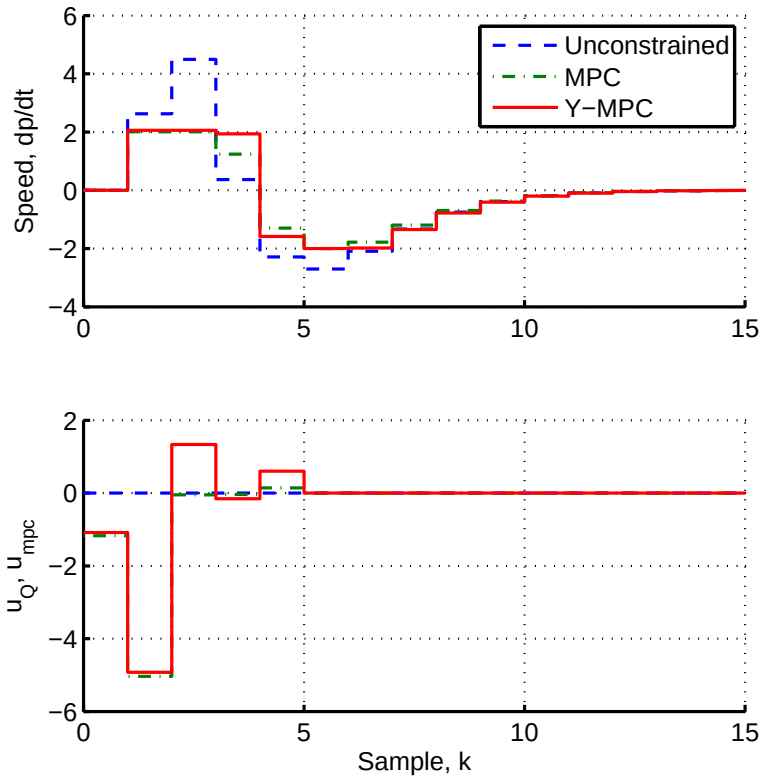

Figure H.7: Simulations with nominal model and initial condition $x = [1 \;\; 0]^T$.

a big impact on the conservativeness. Fig. H.10 shows the simulation with the nominal system initiated in $x = [1 \;\; 0]$ with and without including the post-filter W_2 in the design. It is seen that the Y-MPC controller without the filter is much more conservative.

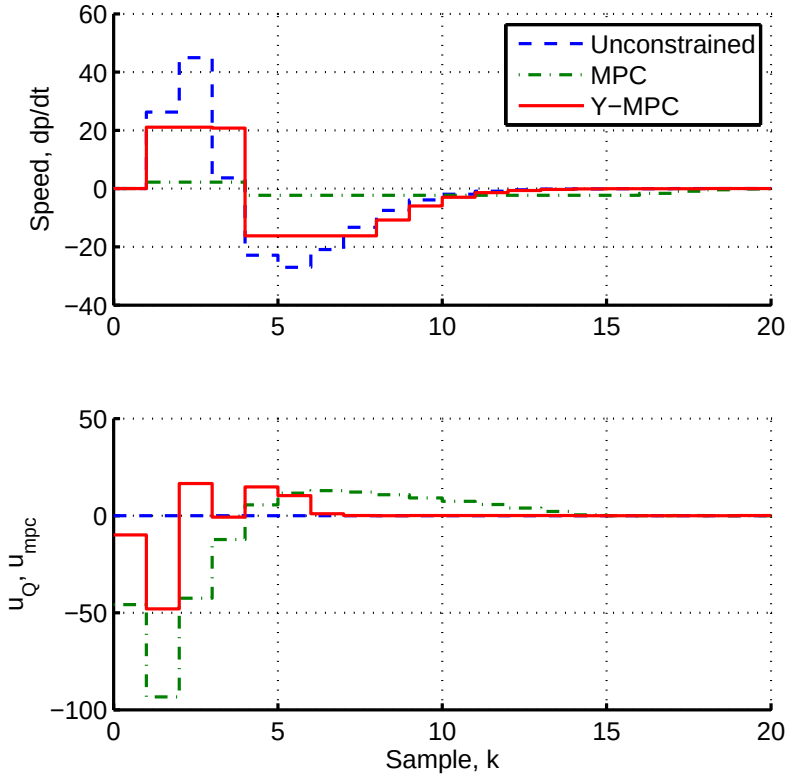

Figure H.8: Simulations with nominal model and initial condition $x = [10 \;\; 0]^T$.

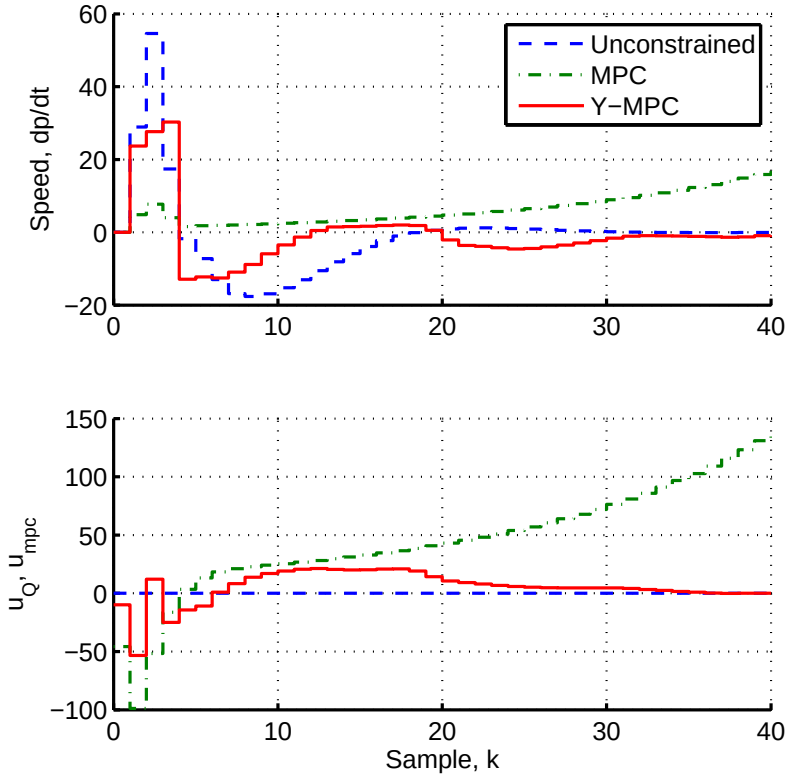

Figure H.9: Simulations with perturbed model and initial condition $x = [10 \;\; 0]^T$.

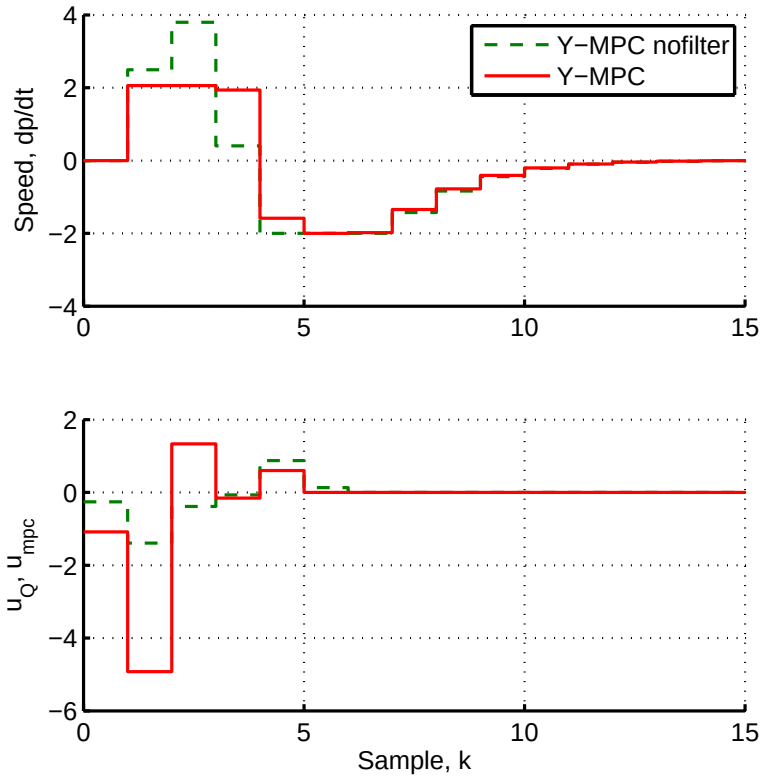

Figure H.10: Simulations with YMPC controller with and without post-filtered Youla parameter. Nominal model and initial condition $x = [1 \;\; 0]^T$.

H.7 Conclusion

In this paper we have described an approach to dealing with dynamic uncertainties bounded by the ∞-norm in a soft/hard constrained MPC setup. Conditions for robust stability have been derived when parameterizing the receding horizon problem in terms of a primary Youla parameter and the uncertainty in terms of a dual Youla parameter. This condition has been incorporated in the receding horizon problem as an LMI. For soft constraints it was proved that the optimization problem is feasible at all times and leads to a stable closed loop system. For perturbed stable systems it is proved that hard constraints on inputs can be handled as well. A method for reducing the conservativeness of the robust controller has been described. The stability property of the YMPC algorithm was illustrated in an example. It was seen that the method for reducing conservativeness had a large impact in the specific example.

H.8 Derivation of (H.23)

Let Σ^Δ denote the uncertain system

$$\Sigma^\Delta = \mathcal{F}_u(\Sigma, \Delta) \tag{H.73}$$

$$= \begin{bmatrix} G^\Delta_{zr} & G^\Delta_{zu} \\ G^\Delta_{yr} & G^\Delta \end{bmatrix} \tag{H.74}$$

Using the Bezout identity (H.13)-(H.13) the Youla parameterized controller can be rearranged as follows

$$K^Q = K + V_l^{-1} Q (1 - V_r^{-1} N_r Q)^{-1} V_r^{-1} \tag{H.75}$$

$$= \mathcal{F}_l(J, Q) \ , \ J = \begin{bmatrix} K & V_l^{-1} \\ V_r^{-1} & -V_r^{-1} N_r \end{bmatrix} \tag{H.76}$$

Using the Redheffer star product (See [25]) the uncertain transfer function T^Δ is given by:

$$T^\Delta = \mathcal{S}(\Sigma^\Delta, J) \tag{H.77}$$

$$= \begin{bmatrix} \Sigma^\Delta_{11} + \Sigma^\Delta_{12} J_{11} (I - \Sigma^\Delta_{22} J_{11})^{-1} \Sigma^\Delta_{21} & \Sigma^\Delta_{12} (I - J_{11} \Sigma^\Delta_{22})^{-1} J_{12} \\ J_{21} (I - \Sigma^\Delta_{22} J_{11})^{-1} \Sigma^\Delta_{21} & J_{22} + J_{21} \Sigma^\Delta_{22} (I - J_{11} \Sigma^\Delta_{22})^{-1} J_{12} \end{bmatrix} \tag{H.78}$$

$$= \begin{bmatrix} G^\Delta_{zr} + G^\Delta_{zu} K (I - G^\Delta K)^{-1} G^\Delta_{yr} & G^\Delta_{zu} (I - K G^\Delta)^{-1} V_l^{-1} \\ V_r^{-1} (I - G^\Delta K)^{-1} G^\Delta yr & -V_r^{-1} N_r + V_r^{-1} G^\Delta (I - K G^\Delta)^{-1} V_l^{-1} \end{bmatrix} \tag{H.79}$$

Manipulating the Bezout identity the following relations are given:

$$M_r^\Delta V_l = (I - K G^\Delta)^{-1} \tag{H.80}$$

$$V_r M_l^\Delta = (I - G^\Delta K)^{-1} \tag{H.81}$$

Together with the fact that $N_r^\Delta = N_r + V_r S^\Delta$ the following expression for T^Δ is given:

$$T^\Delta = \begin{bmatrix} G^\Delta_{zr} + G^\Delta_{zu} U_r M_l^\Delta G^\Delta_{yr} & G^\Delta_{zu} M_r^\Delta \\ M_l^\Delta G^\Delta_{yr} & S^\Delta \end{bmatrix} \tag{H.82}$$

H.9 Proof of Theorem 4

A necessary and sufficient condition for K stabilizing Σ^Δ is

$$\begin{bmatrix} I & -\begin{bmatrix} 0 & 0 \\ 0 & K \end{bmatrix} \\ -\Sigma^\Delta & I \end{bmatrix}^{-1} \in \mathcal{RH}_\infty \tag{H.83}$$

or equivalently

$$\begin{bmatrix} I & -K \\ -G^{\Delta} & I \end{bmatrix}^{-1} \in \mathcal{RH}_{\infty} \tag{H.84}$$

$$G_{zu}^{\Delta}(I - KG^{\Delta})^{-1} \begin{bmatrix} I & K \end{bmatrix} \in \mathcal{RH}_{\infty} \tag{H.85}$$

$$\begin{bmatrix} I \\ K \end{bmatrix} (I - G^{\Delta}K)^{-1} G_{yr}^{\Delta} \in \mathcal{RH}_{\infty} \tag{H.86}$$

$$G_{zr}^{\Delta} + G_{zu}^{\Delta}(I - KG^{\Delta})^{-1} K G_{yr}^{\Delta} \in \mathcal{RH}_{\infty} \tag{H.87}$$

It follows from the construction of the dual Youla parameterization that $S^{\Delta} \in \mathcal{RH}_{\infty}$ iff (H.84) is satisfied. T_{zr}^{Δ} is equivalent to the the left hand side of (H.87), hence $T_{zr}^{\Delta} \in \mathcal{RH}_{\infty}$ iff (H.87) is satisfied. Using (H.80) and (H.81) the conditions (H.85) and (H.86) can be reformulated

$$G_{zu}^{\Delta} M_r^{\Delta} \begin{bmatrix} V_l & U_l \end{bmatrix} \in \mathcal{RH}_{\infty} \tag{H.88}$$

$$\begin{bmatrix} U_r \\ V_r \end{bmatrix} M_l^{\Delta} G_{yr}^{\Delta} \in \mathcal{RH}_{\infty} \tag{H.89}$$

Utilizing coprimeness of V_l, U_l, V_r, U_r it follows that

$$G_{zu}^{\Delta} M_r^{\Delta} = T_{z\eta}^{\Delta} \in \mathcal{RH}_{\infty} \tag{H.90}$$

$$M_l^{\Delta} G_{yr}^{\Delta} = T_{\epsilon r}^{\Delta} \in \mathcal{RH}_{\infty} \tag{H.91}$$

Hence, $T_{z\eta}^{\Delta} \in \mathcal{RH}_{\infty}$ iff (H.85) is satisfied and $T_{\epsilon r}^{\Delta} \in \mathcal{RH}_{\infty}$ iff (H.86) is satisfied. This concludes the proof.

Bibliography

[1] Stephen Boyd, Laurent El Ghaoui, Eric Feron, and Venkataramenan Balakrishnan. *Linear Matrix Inequalities in System and Control Theory*. SIAM, 1994.

[2] Qifeng Cheng, Basil Kouvaritakis, Mark Cannon, and J. Anthony Rossiter. A youla parameter approach to robust constrained linear model predictive control. In *Proceedings of the 48th IEEE Conference on Decision and Control*, 2009.

[3] L. Chisci, J.A. Rossiter, and G. Zappa. Systems with persistent disturbances: predictive control with restricted constraints. *Automatica*, 37(7):1019–1028, 2001.

[4] C. A. Desoer and M. Vidyasagar. *Feedback systems: Input-output properties*. Academic Press, 1975.

[5] J. R. Gossner, B. Kouvaritakis, and J. A. Rossiter. Stable generalized predictive control with constraints and bounded disturbances. *Automatica*, 33(4):551–568, 1997.

[6] M.V. Kothare, V. Balakrishnan, and M. Morari. Robust constrained model predictive control using linear matrix inequalities. *Automatica*, 32(10):1361–1379, 1996.

[7] B. Kouvaritakis, M. Cannon, and V. Tsachouridis. Recent developments in stochastic mpc and sustainable development. *Annual Reviews in Control*, 28(Supplement 1):23–35, 2004.

[8] B. Kouvaritakis, J. A. Rossiter, and A.O.T. Chang. Stable generalized predictive control: an algorithm with guaranteed stability. *IEE Proceedings-Control Theory and Applications*, 139:349–362, 1992.

[9] B. Kouvaritakis, J.A. Rossiter, and J. Schuurmans. Efficient robust predictive control. *IEEE Transactions on Automatic Control*, 45(8):1545–1549, 2000.

[10] J.M. Maciejowski. *Predictive control with constraints*. Prentice Hall, 2002.

[11] Karl Martensson and Andreas Wernrud. Dynamic model predictive control. In *Proceedings of the 17th IFAC World Congress*, volume 17. Elsevier, 2008.

[12] D.Q. Mayne, J.B. Rawlings, C.V. Rao, and P.O.M. Scokaert. Constrained model predictive control: Stability and optimality. *Automatica*, 36(6):789–814, 2000.

[13] H. Niemann. Dual youla parameterisation. *IEE Proceedings-Control Theory and Applications*, 150:493–497, 2003.

[14] Andy Packard, Gary Balas, Richard Liu, and Jong-Yeob Shin. Results on worst-case performance assessment. In *Proceedings of the American Control Conference*, 2000.

[15] J. A. Rossiter and B. Kouvaritakis. Youla parameter and robust predictive control with constraint handling. In *Workshop on Non-linear Predictive control (NMPC), Ascona*, 1998.

[16] J.A. Rossiter, B. Kouvaritakis, and M. Cannon. Computationally efficient algorithms for constraint handling with guaranteed stability and near optimality. *International Journal of Control*, 74(17):1678–1689, 2001.

[17] Cristina Stoica, Cristina Stoica, Pedro Rodriguez-Ayerbe, and Didier Dumur. Off-line improvement of multivariable model predictive control robustness. pages 2826–2831. Institute of Electrical and Electronics Engineers Inc., 2008. DOI:10.1109/CDC.2007.4434591.

[18] T-T. Tay, I. Mareels, and J.B. Moore. *High Performance Control*. Birkhäuser, 1998.

[19] T.T. Tay and J.B. Moore. Enhancement of fixed controllers via adaptive-q disturbance estimate feedback. *Automatica*, 27:39–53, 1991.

[20] S. C. Thomsen, H. Niemann, and N.K. Poulsen. Mpc for uncertain systems using the youla parameterizations. In *Proceedings of 47th IEEE Conference on Decision and Control*, 2008.

[21] T.J.J. Van Den Boom and R.A.J. De Vries. Constrained predictive control using a time-varying youla parameter: a state space solution. *Proceedings of the Third European Control Conference. ECC 95*, (vol.4):3235–40 vol.4, 1995.

[22] T.J.J. Van Den Boom and R.A.J. De Vries. Robust predictive control using a time-varying youla parameter. *International Journal of Applied Mathematics and Computer Science*, 9:101–128, 1999.

[23] M. Vidyasagar. *Control System Synthesis: a factorization approach.* The M.I.T. Press, 1985.

[24] Z. Wan and M.V. Kothare. An efficient off-line formulation of robust model predictive control using linear matrix inequalities. *Automatica*, 39:837–846, 2003.

[25] K. Zhou, J.C. Doyle, and Glover K. *Robust and optimal control.* Prentice Hall, 1996.

Paper I

Pitch control in multiblade coordinates - a stochastic approach

abstract

In this article we consider collective and individual pitch control. Due to the stochastic nature of the wind field we take a stochastic approach to designing an optimal model-based control solution. To this end we set up a stochastic model of the wind suitable for wind turbine control. The model is based on the spectral characteristics of the wind and describes the wind as it is perceived by the rotating blades. The description is transformed to multiblade coordinates in which the wind turbine dynamics are (nearly) time-invariant. This is advantageous since it allows us to use powerful synthesis methods for linear time-invariant systems. The spectral description of the wind in multiblade coordinates is approximated with a linear stochastic system which can be incorporated as an internal model in a model-based controller design. Together with a simplified model of the wind turbine, we design a stochastic controller based on the $\mathcal{H}_2$ method. The performance of the method is shown in simulations together with a stochastic wind field with a deterministic wind shear.

I.1 INTRODUCTION

Reducing stress on the wind turbine structure while ensuring efficient power production is now more important than ever due to the enormous size of modern wind turbine structures. One way to achieve this is through advanced model-based control designs which explicitly take into account the dynamics of the wind turbine as well as the spatial and temporal variability of the wind.

On the majority of modern wind turbines, both the torque of the generator (torque control) and the collective pitch of the blades (pitch control) are used as control parameters for dealing with these challenges. The generator torque is primarily used to achieve the desired speed-torque relationship. Additionally, the torque is commonly used for damping the drive train oscillations. The blades are primarily pitched to obtain the desired rotational speed. Another potential use of pitch control is to dampen for-aft tower vibrations. In practice, classical control methods are used (PI/PID) and the objectives are handled by separate control loops. This is justified by suitably constraining their activity to non-overlapping frequencies. The advantage of the classical approach is its transparency, however, it is likely that more optimal solutions can be constructed using multi-variable (MIMO) control theory. Studies on MIMO control of wind turbines (linear and nonlinear) can e.g. be seen in ([8, 15, 22]). In recent years there has been increased focus on pitch strategies in which the blades are allowed to pitch individually ([2, 3, 4, 12, 14, 16, 19, 20, 21, 23]). By allowing the pitch of the blades to be controlled individually it is possible to alleviate asymmetric loads caused by the spatial and temporal variation in the wind. Whatever the underlying methodology we will denote such methods as 'individual pitch control'.

In this work we focus specifically on the pitch control loop. For transparency and simplicity we do not consider the torque control loop and simply assume that the loops do not interfere. Both collective pitch control and individual pitch control are considered. We take a stochastic approach, modeling the wind by a dynamic system driven by white noise. This model is used as an internal model in a model-based controller design. Including an internal model of the wind will enable the controller to estimate the variability of the wind and consequently provide optimal compensation. The wind model as well as the wind turbine model have been derived in so-called multiblade/Coleman coordinates ([6, 9, 11]). In multiblade coordinates the linearized dynamics of the wind turbine will not exhibit time-dependency caused by rotor rotation, if the wind turbine rotates at a constant speed. Furthermore, for simple structural turbine models, the dynamics related to collective pitch control and individual pitch control are decoupled in the multiblade coordinates. This facilitates a decentralized controller design instead of a monolithic design. In reality the rotational speed

will not be constant, however the time-independent linear model will still provide a good first- order approximation for controller design.

Besides the stochastic nature of the wind we also consider deterministic trends such as wind shear. The $\mathcal{H}_2$ controller synthesis method (See [17, 27] is applied to design the individual pitch controller. The $\mathcal{H}_2$ methodology provides an optimal controller in a stochastic sense.

Individual pitch control in multiblade coordinates has been considered in other works as well (See [2, 3, 4, 12, 16, 23]). Although e.g. [12, 16, 23] exploit the periodic structure of the wind, none of these papers explicitly account for the inherent stochastic description of the wind. It should be noted that control in multiblade coordinates is commonly referred to as cyclic pitch control. Approaches, which are truly individual (do not make use of the multiblade transformation) can be seen in [14, 19, 20, 21].

The wind model which we set up is based on the work in [18]. Here it was shown how to construct frequency domain models of wind turbines given spectral descriptions of the wind. The method relies on making a Fourier series expansion of the wind in the azimuth angle. It has come to the authors' attention that the same modeling principles are used by researchers at the Energy Research Center of the Netherlands (ECN). The ECN code TURBU [7] incorporates spectral models of the wind for load calculations. In a recent version of TURBU the wind model used internally is seemingly identical to the multiblade spectral model derived in this work. The TURBU wind model has not been published but we would like to acknowledge the work of the TURBU developers. Technical descriptions of earlier TURBU versions can be seen in [24, 25].

The structure of this paper is as follows: In Sec. I.2 the multiblade transformation is introduced and the advantage of the transformation in connection with control is explained. In Sec. I.3 the stochastic wind model is derived. In Sec. I.4 the stochastic controller design is described. This includes modeling the wind turbine and controller synthesis. The controller design is illustrated with simulations in Sec. I.5.

I.2 Wind turbine control in multiblade coordinates

Due to rotor rotation, the linear dynamic description of a wind turbine will in general depend on the azimuth angle. Assuming that the rotor system is isotropic and rotating at a constant angular velocity, the linear description will

be time-periodic. It is, however, possible to transform the periodic system equations into time-independent coordinates. This is done by transforming the local blade coordinates to the so-called multiblade coordinates (See [6, 9, 11]). The multiblade coordinates describe the combined effect of the local blade dynamics in the support frame of reference i.e. the global coordinate system.

I.2.1 The multibody transformation

Assume that we have a vector $\boldsymbol{q}$ with 3 parameters (one for each blade) in the local blade coordinates

$$\boldsymbol{q} = \begin{bmatrix} q_1 & q_2 & q_3 \end{bmatrix}^T \tag{I.1}$$

the three elements should represent equivalent parameters for each blade e.g. edgewise blade deflection as shown in Fig. I.1.

The transformation of blade parameter triplets to multiblade coordinates depends on the azimuth angle $\psi(t)$ and is given by:

$$\bar{\boldsymbol{q}} = \boldsymbol{M}(\psi(t))\boldsymbol{q} \tag{I.2}$$

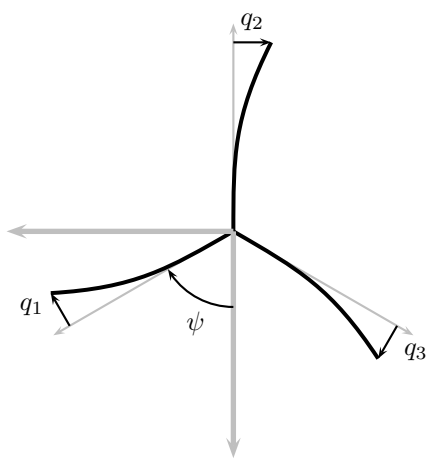

Figure I.1: Example of a parameter triplet in local blade coordinates: Edgewise blade deflection. Thin gray lines are local blade axis. Thick gray lines are global axis.

where $\bar{\boldsymbol{q}}$ denotes the multiblade coordinates and

$$\boldsymbol{M}(\psi(t)) = \begin{bmatrix} \frac{1}{3} & \frac{1}{3} & \frac{1}{3} \\ \frac{2}{3}\cos(\psi(t)) & \frac{2}{3}\cos(\psi(t)+\frac{2\pi}{3}) & \frac{2}{3}\cos(\psi(t)+\frac{4\pi}{3}) \\ \frac{2}{3}\sin(\psi(t)) & \frac{2}{3}\sin(\psi(t)+\frac{2\pi}{3}) & \frac{2}{3}\sin(\psi(t)+\frac{4\pi}{3}) \end{bmatrix} \tag{I.3}$$

The inverse transformation is given by

$$\boldsymbol{M}^{-1}(\psi(t)) = \begin{bmatrix} 1 & \cos(\psi(t)) & \sin(\psi(t)) \\ 1 & \cos(\psi(t)+\frac{2\pi}{3}) & \sin(\psi(t)+\frac{2\pi}{3}) \\ 1 & \cos(\psi(t)+\frac{4\pi}{3}) & \sin(\psi(t)+\frac{4\pi}{3}) \end{bmatrix} \tag{I.4}$$

The elements of the $\bar{\boldsymbol{q}}$ will be denoted as:

$$\bar{\boldsymbol{q}} = \begin{bmatrix} q_s & q_{a1} & q_{a2} \end{bmatrix}^T \tag{I.5}$$

Studying the transformation it is clear that the first multiblade q_s coordinate represents the symmetric/collective variation of the blade variables q_1, q_2 and q_3. The second and third multiblade coordinates q_{a1}, q_{a2} represent asymmetric variations of the blade variables. If the variables q_1, q_2 and q_3 represented pitch angles then q_s would be responsible for *collective* pitch actions and q_{a1}, q_{a2} would be responsible for *individual* pitch actions.

Only in the case that the azimuth angle has a linear evolution over time (constant rotational speed) will the multiblade transformed system be time-invariant. Hence, in the following treatment we assume that the rotational speed is constant $\dot{\psi}(t) = \omega_{r,0}$ ($\psi(t) = \omega_{r,0} \cdot t + \psi_0$) where $\omega_{r,0}$ is the constant angular velocity. In this case we will denote the multiblade transformation by $\boldsymbol{M}(t)$, i.e.:

$$\boldsymbol{M}(t) \equiv \boldsymbol{M}(\omega_{r,0} \cdot t) \tag{I.6}$$

The multiblade transformation represents a transformation from the local blade coordinates to the support frame of reference. An important observation is therefore that the time-invariant dynamics in rotating blade frames also have a time-invariant description in the support frame of reference given. Augmenting the multiblade blade dynamics with a time-invariant description of the support (tower, nacelle, etc.), the result is a time-invariant description of the entire wind turbine. The transformation has e.g. been carried out on a wind turbine model in [9]. The following section will explain the advantages of the multiblade transformation in connection with controller design.

I.2.2 Control of multiblade transformed wind turbine

A wind turbine model will in general contain several variable triplets describing the dynamics of the blades (e.g. triplets for pitch angles, blade deflection, wind speeds, etc.). Furthermore there will be a number of variables describing the non-rotating dynamics (e.g. tower deflection, yaw angle, drive-shaft torsional twist, etc.). Let $\boldsymbol{p}$ denote the augmented vector of the blade triplets and the variables describing the non-rotating dynamics. In the following $\boldsymbol{\mathcal{M}}_{\boldsymbol{p}}(t)$ will then denote the transformation which takes the blade triplets to multiblade coordinates and leaves the variables in non-rotating coordinates untouched.

Now, assume that a linear wind turbine model is given which is time-variant due to the interaction between the rotating blade systems and the non-rotating system. We denote this model $\boldsymbol{P}_t$. The inputs are disturbances $\boldsymbol{d}$ and control signals $\boldsymbol{u}$. The outputs are the measurements $\boldsymbol{y}$ and a performance signal $\boldsymbol{z}$. We can then transform the time-varying system $\boldsymbol{P}_t$ to a time-invariant description in multiblade coordinates:

$$\begin{bmatrix} \bar{\boldsymbol{z}} \\ \bar{\boldsymbol{y}} \end{bmatrix} = \begin{bmatrix} \boldsymbol{\mathcal{M}}_z^{-1}(t) & \\ & \boldsymbol{\mathcal{M}}_y^{-1}(t) \end{bmatrix} \boldsymbol{P}_t \begin{bmatrix} \boldsymbol{\mathcal{M}}_d(t) & \\ & \boldsymbol{\mathcal{M}}_u(t) \end{bmatrix} \begin{bmatrix} \bar{\boldsymbol{d}} \\ \bar{\boldsymbol{u}} \end{bmatrix} \tag{I.7}$$

$$= \bar{\boldsymbol{P}} \begin{bmatrix} \bar{\boldsymbol{d}} \\ \bar{\boldsymbol{u}} \end{bmatrix} \tag{I.8}$$

adding a controller $\bar{\boldsymbol{K}}$ to the multiblade system, we get the closed loop system

$$\bar{\boldsymbol{z}} = \mathcal{F}_l\left(\bar{\boldsymbol{P}}, \bar{\boldsymbol{K}}\right) \bar{\boldsymbol{d}} = \bar{\boldsymbol{P}}_{\bar{\boldsymbol{K}}} \bar{\boldsymbol{d}} \tag{I.9}$$

where the operator $\mathcal{F}_l$ is the lower linear fractional transformation (LFT)[17]. The controller for the multiblade system should therefore be designed such that it achieves the desired response from the multiblade disturbance $\bar{\boldsymbol{d}}$ to the multiblade output $\bar{\boldsymbol{z}}$. The controller for the original system $\boldsymbol{P}_t$ will naturally be the time-varying controller:

$$\boldsymbol{K}_t = \boldsymbol{\mathcal{M}}_u^{-1}(t) \bar{\boldsymbol{K}} \boldsymbol{\mathcal{M}}_y(t) \tag{I.10}$$

The setup is visualized in Fig. I.2.

From a control engineering point of view the most dominant disturbance affecting the wind turbine is the wind. Therefore, it is desirable to set up a model of the wind in multiblade coordinates and incorporate it in the controller design. This is the subject of Sec. I.3.

In practice the rotational speed will not be perfectly constant and the transformed system will therefore not be perfectly time-independent. When working in high wind speed conditions, the rotational speed will be close to constant

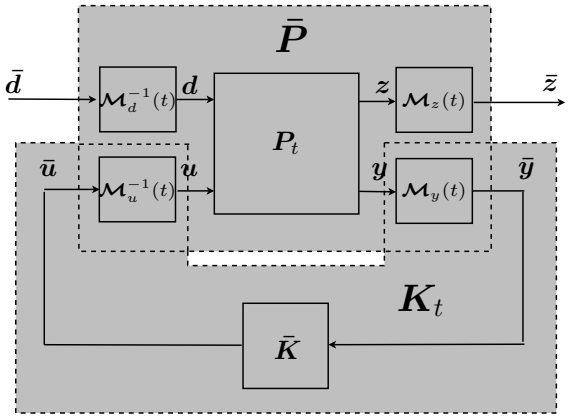

Figure I.2: From the point of view of the controller, the wind turbine and wind is described in the multiblade coordinates

due to the collective pitch control actions. The perturbation introduced by the small variations in the rotational speed will only have little effect. Setting up the multiblade model for controller synthesis we therefore assume that the rotational speed is constant. In the actual simulations the transformation will be based on the actual azimuth angle, resulting in the azimuth-dependent controller:

$$\boldsymbol{K}_{\psi(t)} = \boldsymbol{\mathcal{M}}_u^{-1}(\psi(t))\bar{\boldsymbol{K}}\boldsymbol{\mathcal{M}}_y(\psi(t)) \tag{I.11}$$

I.3 Wind modeling for control

In this section both the stochastic and deterministic wind model are derived. The wind model describes the wind as it is seen by each *rotating* blade individually. The model is based on the frequency domain wind turbine modeling introduced in [18], where the focus was on load calculations. The derivation here is slightly different. We focus in particular on the relation between the winds seen by different blades. Furthermore, we consider time domain realization of the frequency descriptions. Before going into the actual derivations we introduce the blade effective wind speed, which is an integral part of the model:

I.3.1 The blade effective wind speed

The blades of a wind turbine are subject to a spatially distributed wind field. From a control engineering point of view, the overhead would become too large if one were to incorporate the entire wind field explicitly as the disturbance model in the design. A much more elegant approach is to consider the distribution of the wind implicitly through a blade effective wind speed. We use the following definition:

Definition 1. *The* blade effective wind speed v^e *is the speed of the uniform wind which results in the same generalized force as a given wind distribution* $v(r)$ *along the span of the blade.*

This leads to the following expression for the blade effective wind speed.

$$v^e = \frac{\int_{r_0}^{R} X(r)v(r)dr}{\int_{r_0}^{R} X(r)dr} \tag{I.12}$$

where X is a weight/projection function which describes how much influence the wind at radius r has on the generalized force. It includes the projection of the wind onto local forces acting on the blade and the projection of these forces onto the generalized force under consideration.

Remark 14. *From the definition of effective wind speed it is clear that the effective wind speed is dependent on the associated generalized force. In the authors' experience, simply choosing the weight proportional to the radius, i.e.* $X(r) = r$*, is a reasonable approximation for control purposes. Little if any improvement is gained by making more precise descriptions.*

I.3.2 Spectral representation of the stochastic wind

As a starting point we consider the wind speed at a single point on the rotor disc (the circular plane in which the blades rotate). We will denote the (auto) spectral density of a point wind $S(\omega)$. Given two point winds v_1 and v_2 separated by the distance D we denote the cross spectral density by $S(\omega, D)$. We assume that the cross spectral density can be separated into a product of the auto spectral density $S(\omega) \equiv S(\omega, 0)$ and the coherence $C(D, \omega)$.

$$S(\omega, D) = C(D, \omega)S(\omega) \tag{I.13}$$

For common auto spectral densities and coherence functions the reader is referred to [5] . The separability of the cross spectral density into a coherence spectrum and a point spectrum is exploited in the derivation.

Now, consider two point wind speeds at azimuth angles ψ_1, ψ_2 and radii r_1, r_2. We will denote these $v(t, r_1, \psi_1)$ and $v(t, r_2, \psi_2)$ (See Fig. I.3). At any given time t the point wind speeds will be periodic in the azimuth angle. We can therefore make a Fourier expansion in the azimuth angle for fixed t.

$$v(t, r_1, \psi_1) = \sum_{n=-\infty}^{\infty} \tilde{v}_n(t, r_1) e^{in\psi_1} \tag{I.14}$$

$$v(t, r_2, \psi_2) = \sum_{n=-\infty}^{\infty} \tilde{v}_n(t, r_2) e^{in\psi_2} \tag{I.15}$$

where $\tilde{v}_n(t, r)$ are the (time-varying) Fourier coefficients.

Based on the expansion above we can likewise make an expansion of the covariance between the point winds. The covariance $R(\tau, D)$ is assumed to depend uniquely on the euclidean distance $D = \sqrt{r_1^2 + r_2^2 - 2r_1 r_2 \cos(\Delta\psi)}$ between two point wind speeds (where $\Delta\psi = \psi_2 - \psi_1$). Accordingly we get:

$$R(\tau, D) = E\{v(t, r_1, \psi_1)^* v(t + \tau, r_2, \psi_2)\} \tag{I.16}$$

$$= \sum_{n,m=-\infty}^{\infty} E\{\tilde{v}_n(t, r_1)^* \tilde{v}_m(t + \tau, r_2)\} e^{i(m\psi_2 - n\psi_1)} \tag{I.17}$$

$$= \sum_{n=-\infty}^{\infty} \tilde{R}_{n,n}(\tau, r_1, r_2) e^{in\Delta\psi} \tag{I.18}$$

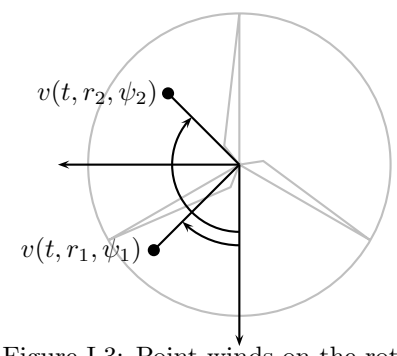

Figure I.3: Point winds on the rotor disc

where $\tilde{R}_{n,m}(\tau, r_1, r_2)$ is the covariance between the expansion coefficients:

$$\tilde{R}_{n,m} = E\{\tilde{v}(t, r_1)^* \tilde{v}(t+\tau, r_2)\} \tag{I.19}$$

$$= \frac{1}{(2\pi)^2} \int_0^{2\pi} \int_0^{2\pi} E\{v(t, r_1, \psi_1) v(t, r_2, \psi_2)\} \cdot e^{-i(m\psi_2 - n\psi_1)} d\psi_1 d\psi_2 \tag{I.20}$$

$$= \begin{cases} \frac{1}{2\pi} \int_0^{2\pi} R(\tau, D) e^{-im\Delta\psi} d\Delta\psi & m = n \\ 0 & \text{otherwise} \end{cases} \tag{I.21}$$

Eventually we want to describe the wind as seen by the rotating blade, which we assume rotates at constant angular velocity $\dot{\psi} = \omega_{r,0}$. This gives a constant time evolution of the azimuth angles $\psi_1(t) = \omega_{r,0} t + \psi_1$ and $\psi_2(t) = \omega_{r,0} t + \psi_2$. The covariance $R^r(\tau, D)$ of the rotating point winds becomes:

$$R^r(\tau, D) = E\{v(t, r_1, \psi_1(t))^* v(t+\tau, r_2, \psi_2(t))\} \tag{I.22}$$

$$= \sum_{n,m=-\infty}^{\infty} E\{\tilde{v}_n(t, r_1)^* \tilde{v}_m(t+\tau, r_2)\} \cdot e^{im\omega_{r,0}\tau} e^{i(m\psi_2 - n\psi_1)} e^{i\omega_{r,0}(m-n)t} \tag{I.23}$$

$$= \sum_{n=-\infty}^{\infty} \tilde{R}_{nn}(\tau, r_1, r_2) e^{in\omega_{r,0}\tau} e^{in(\Delta\psi)} \tag{I.24}$$

It is seen that the only difference between the covariance of the non-rotating wind speeds and the rotating wind speeds is the exponential $e^{in\omega_{r,0}\tau}$. The effect of this will become clear when introducing the cross-spectral density of the rotating wind.

The cross spectral density of the rotating wind is derived by taking the Fourier transform (denoted by $\mathcal{F}$) of the covariance:

$$S^r(\omega, D) = \mathcal{F}\{R^r(\tau, D)\} \tag{I.25}$$

$$= \sum_{n=-\infty}^{\infty} \tilde{S}_{nn}(\omega - n\omega_{r,0}, r_1, r_2) e^{in\Delta\psi} \tag{I.26}$$

The derivation of the harmonic cross spectral densities $\tilde{S}_{nn}$ is written in detail below:

$$\tilde{S}_{nn}(\omega, r_1, r_2) = \frac{1}{2\pi} \int_0^{2\pi} \mathcal{F}\{R(\tau, D)\} e^{-in\Delta\psi} d\Delta\psi \tag{I.27}$$

$$= \frac{1}{2\pi} \int_0^{2\pi} C(\omega, D) e^{-in\Delta\psi} d\Delta\psi S(\omega) \tag{I.28}$$

$$= F_n(\omega, r_1, r_2) S(\omega) \tag{I.29}$$

The frequency shift of the harmonic cross spectral density $\tilde{S}_{nn}$ in (I.26) is due to the exponential originating from the time-dependent azimuth. This effectively causes the phenomena known as rotational sampling, where the wind experienced by the blade has frequency contents which are centered around the frequencies $n \cdot \omega_{r,0}$.

Having set up the spectral description for the rotating point winds, we now consider the effective wind speed for azimuth $\psi_1(t)$ and $\psi_2(t)$. The covariance is given by:

$$R^e(\tau) = \mathbb{E}\left\{ \left(\frac{\int_{r_0}^{R} X(r) v(t, r, \psi_1(t)) dr}{\int_{r_0}^{R} X(r) dr} \right) \left(\frac{\int_{r_0}^{R} X(r) v(t+\tau, r, \psi_2(t)) dr}{\int_{r_0}^{R} X(r) dr} \right) \right\} \tag{I.30}$$

$$= \frac{\int_{r_0}^{R} \int_{r_0}^{R} X(r_1) X(r_2) R(\tau, D) dr_2 dr_1}{\int_{r_0}^{R} \int_{r_0}^{R} X(r_1) X(r_2) dr_2 dr_1} \tag{I.31}$$

where $R^r(\tau, D)$ is the covariance of the two rotating point winds (recall that D is the euclidean distance which is a function of r_1, r_2, $\Delta\psi$ as defined earlier). Fourier transforming R^e we get the cross-spectrum:

$$S^e(\omega) = \sum_{n=-\infty}^{\infty} \tilde{S}_{nn}(\omega - \omega_{r,0}) e^{in\Delta\psi} \tag{I.32}$$

where the harmonic spectra $\tilde{S}_{nn}$ of the blade effective wind speed is given by:

$$\tilde{S}^e_{nn}(\omega) = \int_{r_0}^{R} X(r_2) \int_{r_0}^{R} X(r_1) F_n(\omega, r_1, r_2) dr_1 dr_2 S(\omega) \tag{I.33}$$

$$\cdot \left(\int_{r_0}^{R} \int_{r_0}^{R} X(r_2) X(r_1) dr_1 dr_2 \right)^{-1} \tag{I.34}$$

$$= F^e_n(\omega) S(\omega) \tag{I.35}$$

The expression reveals an interesting property of the effective wind speed: it consists of a sum of spectra shifted in frequency where the shifts depend on the rotational speed $\omega_{r,0}$. This is illustrated in Fig. I.4.

We now relate the derived spectral description of the rotating effective wind speed to a three bladed turbine. The blades are assumed evenly spaced, giving an azimuth difference between two neighbors of $\Delta\psi = \frac{2\pi}{3}$. The effective wind vector is:

$$\boldsymbol{v}^e = \begin{bmatrix} v^e(t, 0) & v^e(t, \frac{2\pi}{3}) & v^e(t, \frac{4\pi}{3}) \end{bmatrix}^T \tag{I.36}$$

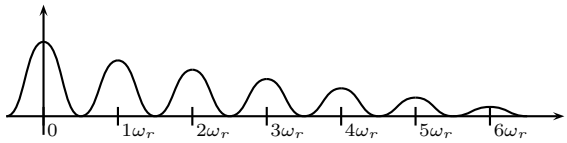

Figure I.4: Auto spectral density of effective wind speed

The corresponding spectral density matrix becomes

$$\boldsymbol{S}^e(\omega) = \sum_{n=-\infty}^{\infty} \tilde{S}^e_{nn} \boldsymbol{E} \tag{I.37}$$

where

$$\boldsymbol{E} = \begin{bmatrix} 1 & e^{in\frac{2\pi}{3}} & e^{in\frac{4\pi}{3}} \\ e^{in\frac{-2\pi}{3}} & 1 & e^{in\frac{2\pi}{3}} \\ e^{in\frac{-4\pi}{3}} & e^{in\frac{-2\pi}{3}} & 1 \end{bmatrix} \tag{I.38}$$

I.3.3 Spectral representation of wind in multiblade coordinates

We will now investigate what happens to the spectral description when we apply the multiblade transformation to the effective wind vector $\boldsymbol{v}^e$:

$$\bar{\boldsymbol{v}}^e = \begin{bmatrix} v^e_s(t) & v^e_{a1}(t) & v^e_{a2}(t) \end{bmatrix}^T \tag{I.39}$$

$$= \boldsymbol{M}(t)\boldsymbol{v}^e \tag{I.40}$$

After doing the harmonic expansion of the effective wind speed we get the following expression for the symmetric component of the wind

$$v^e_s = \frac{1}{3} \sum_{n=-\infty}^{\infty} \left(1 + e^{in\frac{2\pi}{3}} + e^{in\frac{4\pi}{3}}\right) \tilde{v}^e_n(t) e^{in\omega_{r,0}t} \tag{I.41}$$

$$= \sum_{n=-\infty}^{\infty} \mathbf{1}_{\mathbb{U}_0}(n) \tilde{v}^e_n(t) e^{in\omega_{r,0}t} \tag{I.42}$$

$$\tag{I.43}$$

where $\mathbf{1}_A(\cdot)$ is the indicator function and is defined as

$$\mathbf{1}_A(x) = \begin{cases} 1 & \text{if } x \in A \\ 0 & \text{if } x \notin A \end{cases} \tag{I.44}$$

The set $\mathbb{U}_0$ is given by

$$\mathbb{U}_0 = \{\ldots, -6, -3, 0, 3, 6, \ldots\} \tag{I.45}$$

The first asymmetric component of the wind becomes

$$v_{a1}^e = \frac{1}{3}\sum_{-\infty}^{\infty}\left(\left(1+e^{i(n+1)\frac{2\pi}{3}}+e^{i(n+1)\frac{4\pi}{3}}\right)\tilde{v}_n^e(t)e^{i(n+1)\omega_{r,0}t}\right. \tag{I.46}$$

$$\left.+\left(1+e^{i(n-1)\frac{2\pi}{3}}+e^{i(n-1)\frac{4\pi}{3}}\right)\tilde{v}_n^e(t)e^{i(n-1)\omega_{r,0}t}\right) \tag{I.47}$$

$$=\sum_{n=-\infty}^{\infty}\left(\mathbf{1}_{\mathbb{U}_+}(n)\tilde{v}_n^e(t)e^{i(n+1)\omega_{r,0}t}+\mathbf{1}_{\mathbb{U}_-}(n)\tilde{v}_n^e(t)e^{i(n-1)\omega_{r,0}t}\right) \tag{I.48}$$

where the sets $\mathbb{U}_+$ and $\mathbb{U}_-$ are given by

$$\mathbb{U}_+ = \{\ldots,-10,-7,-4,-1,2,5,8,11,\ldots\} \tag{I.49}$$

$$\mathbb{U}_- = \{\ldots,-11,-8,-5,-2,1,4,7,10,\ldots\} \tag{I.50}$$

The second asymmetric component of the wind becomes

$$v_{a2}^e = \frac{1}{3i}\sum_{n=-\infty}^{\infty}\left(\left(1+e^{i(n+1)\frac{2\pi}{3}}+e^{i(n+1)\frac{4\pi}{3}}\right)\tilde{v}_n^e(t)e^{i(n+1)\omega_{r,0}t}\right. \tag{I.51}$$

$$\left.-\left(1+e^{i(n-1)\frac{2\pi}{3}}+e^{i(n-1)\frac{4\pi}{3}}\right)\tilde{v}_n^e(t)e^{i(n-1)\omega_{r,0}t}\right) \tag{I.52}$$

$$=\sum_{n=-\infty}^{\infty}\left(\mathbf{1}_{\mathbb{U}_+}(n)\tilde{v}_n^e(t)ie^{i(n+1)\omega_{r,0}t}-\mathbf{1}_{\mathbb{U}_-}(n)\tilde{v}_n^e(t)ie^{i(n-1)\omega_{r,0}t}\right) \tag{I.53}$$

From these expressions it is straight forward to calculate the auto-spectral densities between the components. The auto-spectral density for the symmetric component is:

$$S_{nn}^s = \sum_{n=-\infty}^{\infty}\tilde{S}_{nn}^s(\omega+n\omega_{r,0}) \tag{I.54}$$

where

$$\tilde{S}_{nn}^s(\omega) = \begin{cases}\tilde{S}_{nn}^e(\omega) & \text{for } n\in\mathbb{U}_0\\ 0 & \text{otherwise}\end{cases} \tag{I.55}$$

The auto-spectral densities for the asymmetric components are equal and given by

$$S_{nn}^a = \sum_{n=-\infty}^{\infty}\tilde{S}_{nn}^a(\omega+n\omega_{r,0}) \tag{I.56}$$

where

$$\tilde{S}_{nn}^a = \begin{cases}\tilde{S}_{nn}^e(\omega+(n+1)\omega_{r,0}) & \text{for } n\in\mathbb{U}_+\\ \tilde{S}_{nn}^e(\omega+(n-1)\omega_{r,0}) & \text{for } n\in\mathbb{U}_-\\ 0 & \text{otherwise}\end{cases} \tag{I.57}$$

The cross-spectral density between the symmetric component and the asymmetric components is trivially zero since the harmonic content in v_s^e is not shared by either v_{a1}^e nor v_{a2}^e. The two asymmetric components are however perfectly correlated since all harmonics are shared. The cross spectral density between the two components is

$$S^{ax} = \sum_{n=-\infty}^{\infty} \tilde{S}_{nn}^{ax}(\omega + n\omega_{r,0}) \tag{I.58}$$

where

$$\tilde{S}_{nn}^{ax} = \begin{cases} \tilde{S}_{nn}^{e}(\omega + (n+1)\omega_{r,0})e^{-i\frac{\pi}{2}} & \text{for } n \in \mathbb{U}_+ \\ \tilde{S}_{nn}^{e}(\omega + (n-1)\omega_{r,0})e^{i\frac{\pi}{2}} & \text{for } n \in \mathbb{U}_- \\ 0 & \text{otherwise} \end{cases} \tag{I.59}$$

The spectral density matrix becomes:

$$\bar{\boldsymbol{S}} = \sum_{n=-\infty}^{\infty} \begin{bmatrix} \tilde{S}_{nn}^{s}(\omega) & 0 & 0 \\ 0 & \tilde{S}_{nn}^{a}(\omega) & \tilde{S}_{nn}^{ax}(\omega) \\ 0 & (\tilde{S}_{nn}^{ax}(\omega))^* & \tilde{S}_{nn}^{a}(\omega) \end{bmatrix} \tag{I.60}$$

Fig. I.5a shows the structure of the auto spectral density of the symmetric wind component. Fig. I.5b shows the structure of the auto-spectral density of the asymmetric components.

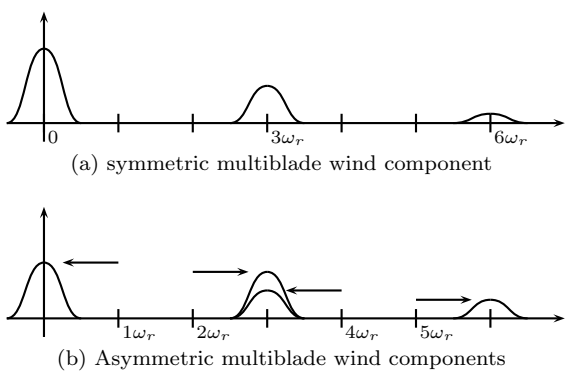

(a) symmetric multiblade wind component

(b) Asymmetric multiblade wind components

Figure I.5: The spectral description of the wind in multiblade coordinates

I.3.4 Control model of effective wind in multiblade coordinates

For control purposes the spectral description of the blade effective wind in multiblade coordinates is approximated with a linear time-invariant model. In essence we will describe the stochastic process with an asymptotically stable LTI stochastic system. In the following it is useful to consider the following representation of such a system:

$$\boldsymbol{y}(t) = \int_{-\infty}^{t} \boldsymbol{g}(t-s)\boldsymbol{e}(s)ds \tag{I.61}$$

$\boldsymbol{g}(t)$ is the convolution kernel (impulse response) and $\boldsymbol{e}(t)$ is Gaussian distributed white noise with mean $\mathbf{0}$ and intensity $\boldsymbol{I}$ ($\boldsymbol{e}(t) \sim \mathcal{N}(\mathbf{0}, \boldsymbol{I})$).

The spectral density of $\boldsymbol{y}$ is given by (see e.g. [1])

$$\boldsymbol{S}_{yy} = \frac{1}{2\pi}\boldsymbol{G}(-i\omega)\boldsymbol{G}(i\omega) \tag{I.62}$$

where $\boldsymbol{G}(s)$ is the Laplace transform of the convolution kernel $\boldsymbol{g}(t)$, i.e. $\boldsymbol{G}(s) = \mathcal{L}(\boldsymbol{g}(t))$.

The spectral description of the wind $\bar{\boldsymbol{v}}$ does not pertain to a finite dimensional linear description in the time domain. This is evident from the constant phase-shift in the cross-spectrum and the infinite number of harmonics. Some information will therefore be lost in the approximation. To this end we propose to truncate the infinite series and disregard the covariance between the components. Recalling the structure of the auto-spectral densities it is natural to propose the following structure:

$$\bar{v}_s^e(t) = \sum_{n=0}^{N_s} G_{s,n} e_{1,n}(t) \tag{I.63}$$

$$\bar{v}_{a1}^e(t) = \sum_{n=0}^{N_a} G_{a,n} e_{a1,n}(t) \tag{I.64}$$

$$\bar{v}_{a2}^e(t) = \sum_{n=0}^{N_a} G_{a,n} e_{a2,n}(t) \tag{I.65}$$

where $G_{x,n}$ are the multiplicative operators associated with scalar stochastic linear systems. We will then obtain a good approximation to the auto-spectral

densities when

$$\frac{1}{2\pi}|G_{s,n}(\omega)|^2 \approx \tilde{S}^s_{nn}(\omega) \tag{I.66}$$

$$\frac{1}{2\pi}|G_{a,n}(\omega)|^2 \approx \tilde{S}^a_{nn}(\omega) \tag{I.67}$$

over the frequencies ω of interest.

Let $G_{x,n}(\omega) \equiv G(\omega;\boldsymbol{\theta})_{x,n}$ denote appropriate parameterization of the transfer functions. The approximation can then be done by solving the following optimization problem numerically.

$$J = \min_{\boldsymbol{\theta}} \sum_{\omega\in\mathcal{I}} \left(\frac{1}{2\pi}|G_{x,n}(\omega;\boldsymbol{\theta})|^2 - |S^x_{nn}(\omega)| \right)^2 \tag{I.68}$$

where $\mathcal{I}$ is the frequency range of interest.

The blade effective wind speed is by definition related to a specific generalized blade force. In the controller design we propose to relate an effective wind speed vector to each generalized blade force of interest. To each of these wind vectors we will associate a wind model (I.63)-(I.65). This is illustrated in Sec. I.4.

I.3.5 Deterministic model of the effective wind

Having introduced the stochastic wind model, it is straightforward to describe how the deterministic wind profile can be included in the model. Going through the previous calculations in a deterministic setup based on a mathematical description of the deterministic wind $v(r,\psi)$, we get the following result for the deterministic blade effective wind speed.

$$v^e(t) = \sum_{n=-\infty}^{\infty} \tilde{v}^e_n e^{i\psi_0} e^{in\omega_{r,0}t} \tag{I.69}$$

where

$$\tilde{v}^e_n = \frac{1}{2\pi} \frac{\int_{r_0}^{R} X(r) \int_{r_0}^{2\pi} v(r,\theta) e^{-in\theta} d\theta dr}{\int_{r_0}^{R} X(r) dr} \tag{I.70}$$

ψ_0 is the azimuth of the blade at $t = 0$.

Transforming this description to multiblade coordinates we get

$$v_s^e = \sum_{n=-\infty}^{\infty} \mathbf{1}_{\mathbb{U}_0}(n)\tilde{v}_n^e(t)e^{in\omega_{r,0}t} \tag{I.71}$$

$$v_{a1}^e = \sum_{n=-\infty}^{\infty} \left(\mathbf{1}_{\mathbb{U}_+}(n)\tilde{v}_n^e(t)e^{i(n+1)\omega_{r,0}t} + \mathbf{1}_{\mathbb{U}_-}(n)\tilde{v}_n^e(t)e^{i(n-1)\omega_{r,0}t}\right) \tag{I.72}$$

$$v_{a2}^e = \sum_{n=-\infty}^{\infty} \left(\mathbf{1}_{\mathbb{U}_+}(n)\tilde{v}_n^e(t)ie^{i(n+1)\omega_{r,0}t} - \mathbf{1}_{\mathbb{U}_-}(n)\tilde{v}_n^e(t)ie^{i(n-1)\omega_{r,0}t}\right) \tag{I.73}$$

$\tilde{v}_n$ is a real and uneven function of n, hence (I.71)-(I.73) essentially represent a sum of sinusoids and an offset. The sinusoidal part of the deterministic wind can therefore be modeled as the impulse response of oscillatory systems. The offset is the impulse response of an integrator.

Incorporating the deterministic model directly as a disturbance model will introduce uncontrollable, marginally stable modes. The deterministic trends in the wind will therefore be handled by adding integrators and oscillatory systems at the output of the model (See e.g. [27]). Regulating the integrator and oscillator outputs to zero will effectively attenuate the deterministic offset and oscillations due to the deterministic wind profile.

I.3.6 Numeric realization of stochastic wind model

In this section a specific realization of the wind model is derived for later use in the controller design. The model will include harmonics up until $n = 4$.

The starting point is the spectral density of the point wind. In this realization we use the Kaimal spectral density [5]:

$$S(\omega) = \frac{4\sigma^2 \frac{L}{v_m}}{(1 + 6\frac{\omega}{2\pi}\frac{L}{v_m})^{5/3}} \tag{I.74}$$

where L, v_m are the turbulence length scale and mean wind speed respectively. σ is the standard deviation of the wind. The coherence function is chosen as:

$$C(D,\omega) = \exp\left(-12\sqrt{(\frac{\omega}{2\pi}f\frac{D}{v_m})^2 + (0.12\frac{D}{L})^2}\right) \tag{I.75}$$

The following parameter values are chosen:

$$v_m = 16 \text{ m/s} \quad L = 340.2 \text{ m} \quad \sigma = 2.112 \tag{I.76}$$

The weighting function X is chosen linear

$$X(r) = r \tag{I.77}$$

Numerical calculation of the harmonic spectra results in the spectra shown in Fig. I.6.

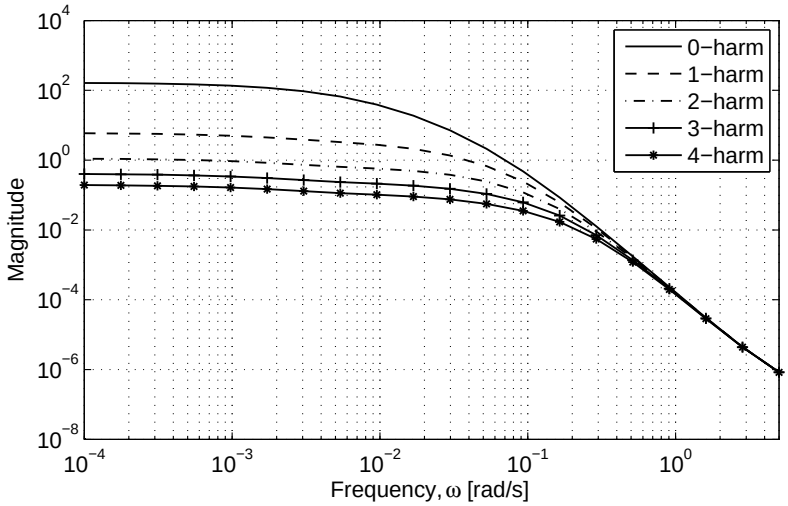

Figure I.6: Harmonic spectra $\tilde{S}_n^e$ for $n = 0, 1, 2, 3, 4$

Based on these harmonic spectra and an assumed rotational speed of $\omega_{r,0} = 2.09$ rad/s, we can set up the power spectrum in multiblade coordinates. Fig. I.7 shows the true power spectrum for the symmetric component of the wind and the power spectrum of an LTI approximation. The LTI approximation is given by

$$v_s = G_{s,0} e_{s,0} + G_{s,3} e_{s,3} \tag{I.78}$$

where $e_{s,0}, e_{s,3} \sim \mathcal{N}(\mathbf{0}, I)$ and

$$G_{s,0} = \frac{-0.0096903(s + 102.9)(s + 0.01297)}{(s + 2.002)(s + 0.05227)(s + 0.009776)} \tag{I.79}$$

$$G_{s,3} = \frac{-0.36909(s^2 + 0.2477s + 0.7216)(s^2 + 5.569s + 40.74)}{(s + 5.552)(s^2 + 2.155s + 1.785)(s^2 + 0.4217s + 39.54)} \tag{I.80}$$

Fig. I.8 shows the true power spectrum for the asymmetric components of the wind and the power spectrum of an LTI approximation. The LTI approximation is given by

$$v_{aj} = G_{a,1} e_{aj,1} + G_{a,2} e_{aj,2} + G_{a,4} e_{aj,4} \ , \quad j = 1, 2 \tag{I.81}$$

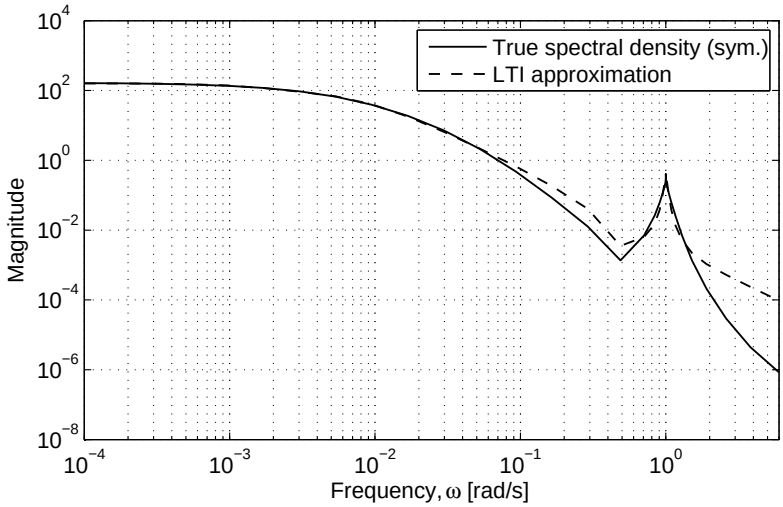

Figure I.7: Spectral density of the symmetric wind component v_s^e and spectral density of an LTI approximation

where $e_{aj1,0}, e_{aj,2}, e_{aj,4} \sim \mathcal{N}(\mathbf{0}, I)$ and

$$G_{a,1} = \frac{-0.019712(s+189.9)(s+0.01585)}{(s+12.97)(s+0.164)(s+0.01164)} \tag{I.82}$$

$$G_{a,2} = \frac{-0.039629(s+107.8)(s^2+7.135s+13.13)}{(s+16.14)(s+0.6972)(s^2+0.3438s+39.52)} \tag{I.83}$$

$$G_{a,4} = \frac{0.22795(s^2+0.2013s+0.3618)(s^2+5.323s+32.26)}{(s+1.346)(s+1.214)(s+0.4702)(s^2+0.4827s+39.53)} \tag{I.84}$$

I.4 Stochastic pitch control

In this section we design a pitch controller which incorporates the multiblade stochastic model of the wind. The design is based on a relatively simple model of the wind turbine which incorporates the main dynamics that should be considered when doing pitch control. Dynamics which usually pertain to the power control loop are therefore not considered (e.g. generator dynamics and drive train dynamics). A list of key parameters for the model is shown in Table I.1. The tower mass, stiffness and damping relates to a second order approximation of the dynamics.

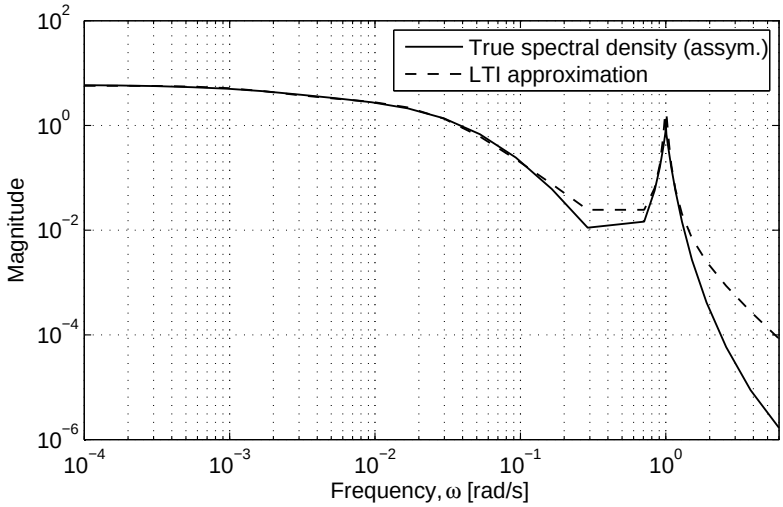

Figure I.8: Spectral density of the symmetric wind components $v^e_{a,1}$ and $v^e_{a,1}$ and spectral density of an LTI approximation

Pitch control is mainly employed in high wind speed conditions where the power in the wind exceeds the rated power for the generator. The stochastic pitch controller illustrated in this work is based on a linear model corresponding to a mean wind speed of 16 m/s. This is approximately 4 m/s above the rated wind speed.

The pitch controller design can be split into the design of a collective pitch controller and an individual pitch controller. The primary objective for the collective pitch controller is to keep the rotational speed ω_r constant. Since the tower is lightly damped, it is also important to ensure that the controller provides some damping to the tower. The collective pitch controller will target the for-aft tower vibrations. This will be done by targeting the tower deflection

Table I.1: Selected key parameters for 1.5 MW wind turbine model

Parameter	value	
Tower mass m_t	$9.35 \cdot 10^4$	kg
Tower stiffness k_t	$6.51 \cdot 10^5$	N/m
Tower damping c_t	$3.25 \cdot 10^4$	s^{-1}
Actuator time constant τ	0.1	s
Rotor inertia J_r	$3.04 \cdot 10^6$	kg·m^2
Rated speed $\omega_{r,0}$	2.1	rad/s

speed $\dot{q}_T^Y$ in the design. The primary individual pitch objective is to attenuate the asymmetric loads (the yaw and tilt moments) in the support of the blades. Furthermore, the side-side tower vibrations are targeted through the side-side tower speed $\dot{q}_T^X$.

We use the $\mathcal{H}_2$ design method for optimal controller synthesis. This method has a meaningful interpretation in connection to stochastic disturbances and provides a systematic procedure when model and objectives have been represented with suitable mathematical structures i.e. linear systems. Both single-input/single-output and multi-variable problems are handled with equal ease. It is not the scope of this work to make a comparison with a classical controller design (PID control). The comparison will be unfair unless a thorough effort is put into the design. Knowledge about the wind model structure could just as well be incorporated in suitable pre- and post-filters used together with a classical controller. Hence, a well tuned classical design which is cast in a similar framework is likely to achieve comparable performance.

I.4.1 Linear wind turbine model

The model we use for the controller design incorporates tower dynamics, rotational dynamics, aerodynamics, pitch actuators and a stochastic wind model. The structural model is sketched in Fig. I.9 where the axis of the global coordinate system is denoted with X, Y and Z, and the local blade coordinate systems with x, y and z. Note that Y and y co-inside.

The model of the tower includes the primary modal displacement in for-aft and side-to-side motion (q_T^Y and q_T^X respectively). The dynamics can be written in

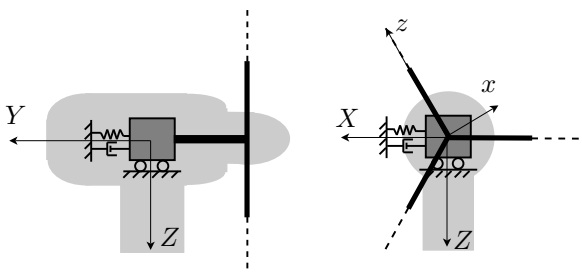

(a) Side view (b) Front view

Figure I.9: Structural model of wind turbine. Note that the local y-axis of the blades co-insides with the global Y-axis

the following second order matrix equation:

$$\begin{bmatrix} m_T & 0 \\ 0 & m_T \end{bmatrix} \begin{bmatrix} \ddot{q}_T^Y \\ \ddot{q}_T^X \end{bmatrix} + \begin{bmatrix} k_T & 0 \\ 0 & k_T \end{bmatrix} \begin{bmatrix} \dot{q}_T^Y \\ \dot{q}_X^Z \end{bmatrix} + \begin{bmatrix} c_T & 0 \\ 0 & c_T \end{bmatrix} \begin{bmatrix} q_T^Y \\ q_T^X \end{bmatrix} = \begin{bmatrix} Q_T^Y \\ Q_T^X \end{bmatrix} \tag{I.85}$$

The generalized forces Q_F^X and Q_F^Y are the total forces in the X and Y directions respectively.

The model of the rotor is simply given by the inertia of all rotating parts (blades, drive shaft, generator, etc). The dynamics are given by the equation:

$$J_r \dot{\omega}_r + T_{g,0} = Q_M^Y \tag{I.86}$$

where J_r is the inertia and $T_{g,0}$ is the generator torque, which we assume is constant and chosen to balance out the torque from the rotor under static considerations (equilibrium). Q_M^Y is the total moment about the Y-axis.

The aerodynamics are calculated using simple BEM calculations as described in [10]. For simplicity we assume that the relation is purely algebraic i.e. we do not consider e.g. dynamic inflow. With the chosen degrees of freedom we can express the conversion of kinetic energy in the wind field $\boldsymbol{V}$ to the generalized forces of interest by the following functional.

$$\begin{bmatrix} \boldsymbol{Q}_F^y & \boldsymbol{Q}_F^x & \boldsymbol{Q}_M^y & \boldsymbol{Q}_M^x \end{bmatrix} = \boldsymbol{f}(\boldsymbol{V}, \dot{q}_T^Y, \dot{q}_T^X, \boldsymbol{\beta}, t) \tag{I.87}$$

The generalized forces on the left hand side are: the blade root force in the y and x direction $\boldsymbol{Q}_F^y$, $\boldsymbol{Q}_F^x$, and the blade root moments about the y and x-axis $\boldsymbol{Q}_M^y$,$\boldsymbol{Q}_M^x$. These blade forces gives rise to the following global forces of interest: Q_F^Y, Q_F^X, Q_M^Y, Q_{yaw}, Q_{tilt}. The latter two are the yaw and tilt moment respectively. The relation between local generalized forces and the global generalized forces is as follows:

$$Q_F^Y = \begin{bmatrix} 3 & 0 & 0 \end{bmatrix} \boldsymbol{M}(t) \boldsymbol{Q}_F^y \tag{I.88}$$

$$Q_F^X = \begin{bmatrix} 0 & 0 & \frac{3}{2} \end{bmatrix} \boldsymbol{M}(t) \boldsymbol{Q}_F^x \tag{I.89}$$

$$Q_M^Y = \begin{bmatrix} 3 & 0 & 0 \end{bmatrix} \boldsymbol{M}(t) \boldsymbol{Q}_M^y \tag{I.90}$$

$$Q_{yaw} = \begin{bmatrix} 0 & 0 & \frac{3}{2} \end{bmatrix} \boldsymbol{M}(t) \boldsymbol{Q}_M^x \tag{I.91}$$

$$Q_{tilt} = \begin{bmatrix} 0 & \frac{3}{2} & 0 \end{bmatrix} \boldsymbol{M}(t) \boldsymbol{Q}_M^x \tag{I.92}$$

Since the effective wind speed pertains to a specific generalized blade force, we introduce independent effective wind speeds for each generalized blade force in the model. The effective wind speed vectors $\boldsymbol{v}_F^y$, $\boldsymbol{v}_F^x$, $\boldsymbol{v}_M^y$, $\boldsymbol{v}_M^x$ are therefore associated with $\boldsymbol{Q}_F^y$, $\boldsymbol{Q}_F^x$, $\boldsymbol{Q}_M^y$, $\boldsymbol{Q}_M^x$ respectively. The linearized aerodynamics

take the following form:

$$Q_F^Y = \begin{bmatrix} d_{F,\beta}^Y & 0 & 0 \end{bmatrix} \boldsymbol{M}(t)\boldsymbol{\beta} + \begin{bmatrix} d_{F,v}^Y & 0 & 0 \end{bmatrix} \boldsymbol{M}(t)\boldsymbol{v}_F^y \tag{I.93}$$

$$Q_F^X = \begin{bmatrix} 0 & 0 & d_{F,\beta}^X \end{bmatrix} \boldsymbol{M}(t)\boldsymbol{\beta} + \begin{bmatrix} 0 & 0 & d_{F,v}^X \end{bmatrix} \boldsymbol{M}(t)\boldsymbol{v}_F^x \tag{I.94}$$

$$Q_M^Y = \begin{bmatrix} d_{M,\beta}^Y & 0 & 0 \end{bmatrix} \boldsymbol{M}(t)\boldsymbol{\beta} + \begin{bmatrix} d_{M,v}^Y & 0 & 0 \end{bmatrix} \boldsymbol{M}(t)\boldsymbol{v}_M^y \tag{I.95}$$

$$Q_{yaw} = \begin{bmatrix} 0 & 0 & d_{M,\beta}^{yaw} \end{bmatrix} \boldsymbol{M}(t)\boldsymbol{\beta} + \begin{bmatrix} 0 & 0 & d_{M,v}^{yaw} \end{bmatrix} \boldsymbol{M}(t)\boldsymbol{v}_M^x \tag{I.96}$$

$$Q_{tilt} = \begin{bmatrix} 0 & d_{M,\beta}^{tilt} & 0 \end{bmatrix} \boldsymbol{M}(t)\boldsymbol{\beta} + \begin{bmatrix} 0 & d_{M,v}^{tilt} & 0 \end{bmatrix} \boldsymbol{M}(t)\boldsymbol{v}_M^x \tag{I.97}$$

The pitch actuator system is in general a system with complex dynamics and internal low level controllers. In this treatment we simply assume that the actuator dynamics are described by first order differential equations:

$$\begin{bmatrix} \tau_\beta & 0 & 0 \\ 0 & \tau_\beta & 0 \\ 0 & 0 & \tau_\beta \end{bmatrix} \dot{\boldsymbol{\beta}} + \boldsymbol{\beta} = \boldsymbol{\beta}_r \tag{I.98}$$

where τ_β is the time constant of the actuator dynamics and $\boldsymbol{\beta}_r$ is the pitch reference for the blades.

I.4.2 Linear model in multiblade coordinates

The tower and rotor dynamics described in the previous section are already linear and given in non-rotating coordinates. The dynamics in equations (I.85) and (I.86) will therefore be used directly.

The linear aerodynamics are trivially transformed to multiblade coordinates by the following relations

$$\bar{\boldsymbol{\beta}} = \boldsymbol{M}(t)\boldsymbol{\beta} \tag{I.99}$$

$$\bar{\boldsymbol{v}}_F^y = \boldsymbol{M}(t)\boldsymbol{v}_F^y \ , \quad \bar{\boldsymbol{v}}_F^x = \boldsymbol{M}(t)\boldsymbol{v}_F^x \tag{I.100}$$

$$\bar{\boldsymbol{v}}_M^y = \boldsymbol{M}(t)\boldsymbol{v}_M^y \ , \quad \bar{\boldsymbol{v}}_M^x = \boldsymbol{M}(t)\boldsymbol{v}_M^x \tag{I.101}$$

Transforming the pitch dynamics to multiblade coordinates we get

$$\begin{bmatrix} \tau_\beta & 0 & 0 \\ 0 & \tau_\beta & 0 \\ 0 & 0 & \tau_\beta \end{bmatrix} \dot{\bar{\boldsymbol{\beta}}} + \begin{bmatrix} 1 & 0 & 0 \\ 0 & 1 & \omega_{r,0}\tau_\beta \\ 0 & -\omega_{r,0}\tau_\beta & 1 \end{bmatrix} \bar{\boldsymbol{\beta}} = \bar{\boldsymbol{\beta}}_r \tag{I.102}$$

When inspecting the dynamic equations in multiblade coordinates we see that the dynamics affected by the symmetric (first) element of the multiblade pitch

reference and wind signals are decoupled from the dynamics affected by the asymmetric (second and third) elements of the multiblade pitch reference and wind signals. The for-aft tower dynamics and rotor dynamics are associated with the symmetric components. The side-side tower dynamics are associated with the asymmetric components.

Schematics of the dynamics affected by the symmetric components and the asymmetric components are shown in Fig. I.10 and Fig. I.11 respectively. $\boldsymbol{v_s}$ and $\boldsymbol{v_a}$ denote the symmetric and asymmetric components of the multiblade wind vectors. Note that integrators have been included to accumulate errors in rotational speed and yaw/tilt moment. These are included in the model for later use in the controller design to avoid bias from deterministic trends in the wind. For technical reasons the integral action is considered part of the model rather than part of the controller. However, the integral action can trivially be absorbed into the controller post-synthesis (See e.g. [27], pp. 450).

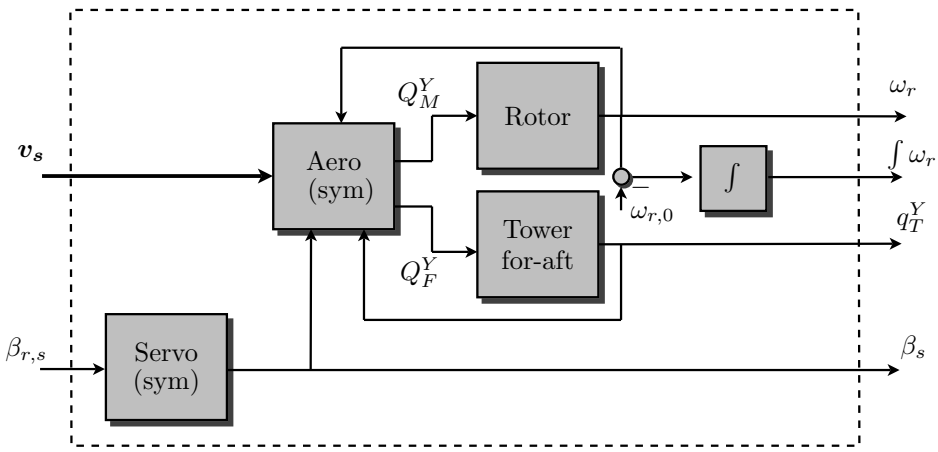

Figure I.10: Symmetric dynamics of multiblade wind turbine model

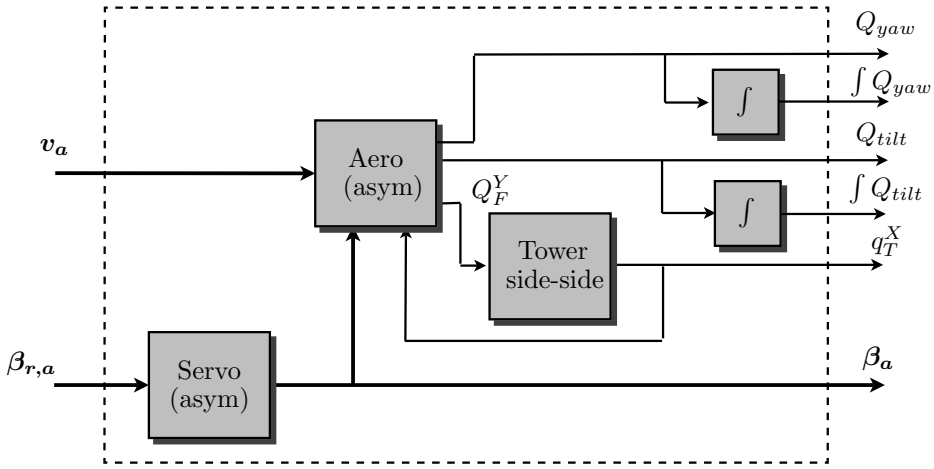

Figure I.11: Asymmetric dynamics of multiblade wind turbine model

I.4.3 Generalized model for control

As described in Sec. I.4.2 the dynamics of the system in multiblade coordinates are decoupled into two independent systems - one system pertaining to collective pitch control and one system pertaining to individual pitch control. We will take advantage of this separability in the controller design.

The actual models used in the controller design incorporated both the wind model as derived in Sec. I.3 and some tuning parameters (dynamic weights). We denote these generalized models by $\boldsymbol{P_s}$ and $\boldsymbol{P_a}$ for the symmetric and asymmetric dynamics respectively. The structures of the generalized models are equivalent. The generalized symmetric model $\boldsymbol{P_s}$ is depicted in Fig. I.12. If all *sym* are substituted with *asym* and all subscript s are substituted with a, the result is the structure of $\boldsymbol{P_a}$.

The disturbances $\boldsymbol{d_s}$ and $\boldsymbol{d_a}$ input to the generalized plants $\boldsymbol{P_s}$ and $\boldsymbol{P_a}$ consist of white noise input to the wind models and additionally inputs to a measurement noise model $\boldsymbol{W_{m,s}}$, $\boldsymbol{W_{m,a}}$. We have not pursued a model of the measurement noise, hence $\boldsymbol{W_{m,s}}$ and $\boldsymbol{W_{m,a}}$ are simply regarded as tuning parameters and their inputs interpreted as white noise.

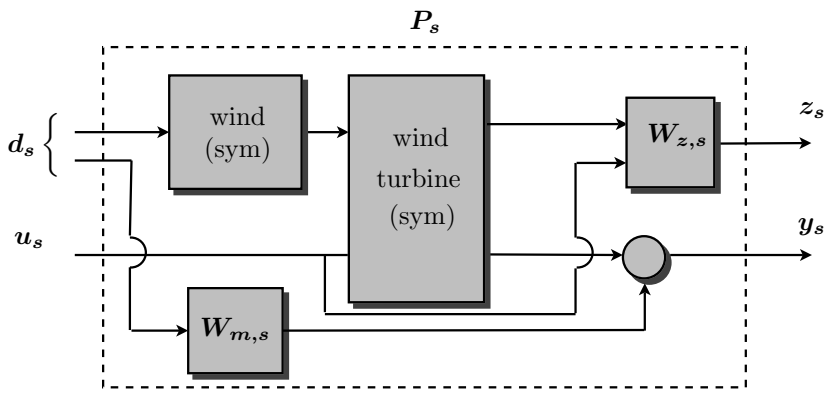

Figure I.12: Design model $\bar{\boldsymbol{P}}_{\boldsymbol{s}}$ for the collective pitch controller. The design model for the individual pitch controller has the same general form.

The control inputs to the generalized plants are the multiblade pitch signals:

$$\boldsymbol{u_s} = \beta_{r,s} \tag{I.103}$$

$$\boldsymbol{u_a} = \begin{bmatrix}\beta_{r,a1} & \beta_{r,a2}\end{bmatrix}^T \tag{I.104}$$

The outputs $\boldsymbol{z_s}$ (and $\boldsymbol{z_a}$) represent the signals which we are interested in controlling. They are weighted versions of actual signals present in the dynamics and given as:

$$\boldsymbol{z_s} = \boldsymbol{W_{z,s}} \begin{bmatrix}\dot{q}_T^Y & \omega_r & \int \omega_r & \beta_s & \beta_{r,s}\end{bmatrix}^T \tag{I.105}$$

$$\boldsymbol{z_a} = \boldsymbol{W_{z,a}} \begin{bmatrix}\dot{q}_T^X & Q_{yaw} & Q_{tilt} & \int Q_{yaw} & \int Q_{tilt} & \beta_{a1} & \beta_{a2} & \beta_{r,a1} & \beta_{r,a2}\end{bmatrix}^T \tag{I.106}$$

The weights $\boldsymbol{W_{z,s}}$ and $\boldsymbol{W_{z,a}}$ are tuning parameters in the controller design. The measurement signals in the setup are given as:

$$\bar{\boldsymbol{y}}_{\boldsymbol{s}} = \begin{bmatrix}\dot{q}_T^Y & \omega_r\end{bmatrix}^T + \begin{bmatrix}\mathbf{0} \\ \mathbf{W_{m,s}}\end{bmatrix} \bar{\mathbf{d}}_{\mathbf{s}} \tag{I.107}$$

$$\bar{\boldsymbol{y}}_{\boldsymbol{a}} = \begin{bmatrix}\dot{q}_T^X & Q_{yaw} & Q_{tilt}\end{bmatrix}^T + \begin{bmatrix}\mathbf{0} \\ \mathbf{W_{m,a}}\end{bmatrix} \bar{\mathbf{d}}_{\mathbf{a}} \tag{I.108}$$

where the noise terms have been described previously.

The generalized model for the total system $\bar{\boldsymbol{P}}$ consists of the decoupled dynamics of the symmetric and asymmetric models as shown in Fig. I.13.

Since the dynamics are decoupled, we can also separate the controller design. In the following the dynamic controller $\boldsymbol{K_s}$ is associated with symmetric dynamics

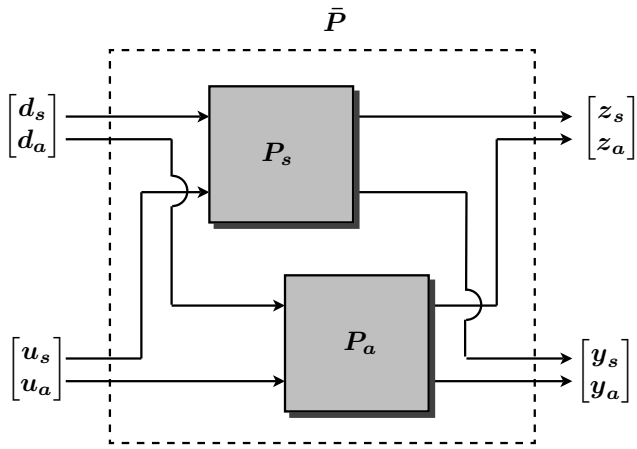

Figure I.13: Generalized model for controller design. The model is decoupled into the symmetric dynamics and the asymmetric dynamics

and $\boldsymbol{K_a}$ is associated with the asymmetric dynamics. The total controller for the multiblade system is:

$$\bar{\boldsymbol{K}} = \begin{bmatrix} \boldsymbol{K_s} & \\ & \boldsymbol{K_a} \end{bmatrix} \tag{I.109}$$

The closed loop system will hence be given by

$$\bar{\boldsymbol{P}}_{\boldsymbol{K}} = \mathcal{F}_l\left(\bar{\boldsymbol{P}}, \bar{\boldsymbol{K}}\right) \tag{I.110}$$

$$= \begin{bmatrix} \mathcal{F}_l(\boldsymbol{P_s}, \boldsymbol{K_s}) & \\ & \mathcal{F}_l(\boldsymbol{P_a}, \boldsymbol{K_a}) \end{bmatrix} \tag{I.111}$$

$$= \begin{bmatrix} \boldsymbol{P_{s,K}} & \\ & \boldsymbol{P_{a,K}} \end{bmatrix} \tag{I.112}$$

For the controller designs $\boldsymbol{K_s}$ and $\boldsymbol{K_a}$ we choose to use the $\mathcal{H}_2$ controller synthesis. The resulting controller minimizes the $\mathcal{H}_2$-norm of the closed loop transfer function. Optimality of the $\mathcal{H}_2$ controller has several interpretations in the time domain. For example, it minimizes the expected 2-norm of the performance signal when the disturbance is regarded as white noise. Since the stochastic wind model is driven by white noise, the $\mathcal{H}_2$ controller is the natural choice. The $\mathcal{H}_2$ controller can be realized as an LQG controller for the generalized plant description [17]. In state space the LQG controller consists of a linear quadratic optimal state feedback $\mathbf{F}$ and a Kalman filter with the associated Kalman gain $\mathbf{L}$ [13].

To synthesize the controllers, a specific choice of the weights $\boldsymbol{W}_{z,s}$,$\boldsymbol{W}_{z,a}$ and $\boldsymbol{W}_{m,s}$,$\boldsymbol{W}_{m,a}$ has been made. They are chosen as diagonal matrices and the

magnitude of elements reflects the objectives and relative levels of the signals. The elements are mostly static. The only exceptions are the elements in $\boldsymbol{W_{z,s}}$ and $\boldsymbol{W_{z,a}}$ associated with the pitch signals. These elements are high pass filters of the form:

$$\frac{(s+\alpha)^3}{(s+\beta)^3} \tag{I.113}$$

where $\beta > \alpha$. Including high-pass filtration will effectively cause the controller to minimize high frequency activity in the pitch signal.

Finally it is important to emphasize that the actual controller for the system is:

$$\boldsymbol{K}_{\psi(t)} = \boldsymbol{\mathcal{M}}_u^{-1}(\psi(t)) \begin{bmatrix} \boldsymbol{K_s} & \\ & \boldsymbol{K_a} \end{bmatrix} \boldsymbol{\mathcal{M}}_y(\psi(t)) \tag{I.114}$$

I.5 Simulations

In this section the controller design is illustrated in simulations. The model used in the simulation is a nonlinear version of the design model. More specifically the structural dynamics and actuator model are equivalent. However, the aerodynamics are nonlinear and calculated using the BEM method (without dynamic effects). The wind field is generated using the Veers method [26]. The underlying statistical properties are the same as those used for setting up the wind model in Sec. I.3.6. A grid size of 10×10 is used for the wind field. The wind realization at hub center is shown in Fig. I.14. A vertical linear wind shear has been added to the wind field. The deterministic wind profile is 14 m/s at the bottom at the rotor disc and 18 m/s at the top of the rotor disc. The mean wind speed is naturally 16 m/s. The wind turbine model is simple compared to state of the art wind turbine codes. Since this work is concerned with wind modeling it allows us to illustrate the main contribution without the additional overhead of a highly complex wind turbine model. The wind generation algorithm, however, is comparable to algorithms used together with complex wind turbine codes.

Three controllers have been synthesized with the $\mathcal{H}_2$ method. First and foremost a controller which we believe serves as a good trade-off between load attenuation and control activity. This controller will be denoted: *trade-off*. Based on this design a conservative controller and an aggressive controller has been designed. They have been obtained by simply changing the shape of the high-pass filters associated with the pitch signals.

The performance of the trade-off controller will be illustrated first. Fig. I.15 shows the rotational speed ω_r and the for-aft tower deflection speed $\dot{q}_T^Y$ of the

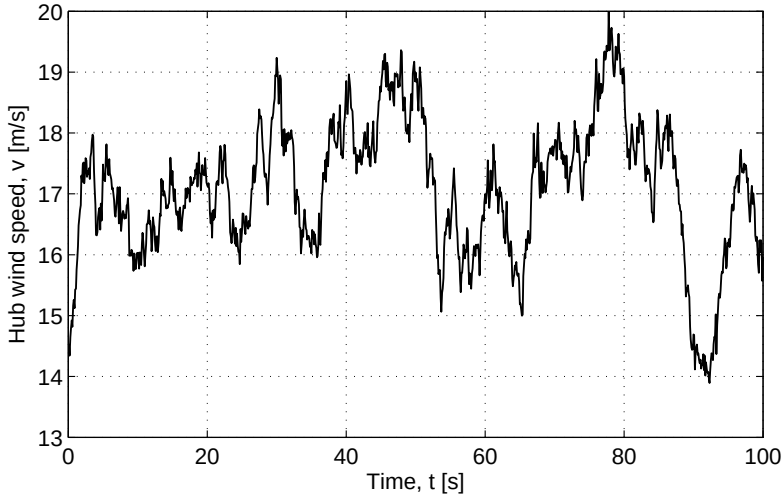

Figure I.14: Wind speed at hub center

controlled (trade-off) and uncontrolled system. The controller readily attenuates the effect of the wind which results in an almost constant rotational speed ω_r. The for-aft tower deflection speed $\dot{q}_T^Y$ is also attenuated to a certain extent. In the tuning of the design it was decided not to attenuate $\dot{q}_T^Y$ further, since this would cause too much high frequency pitch activity.

Fig. I.16 shows the tilt Q_{tilt} and yaw Q_{yaw} moments in the support of the blades. The side-side tower deflection speed is similarly shown in the figure. The deterministic shear comes across as a deterministic bias in the tilt moment Q_{tilt} of the open loop system. The yaw moment Q_{yaw} has a zero mean over time. As expected the pitch controller attenuates both the deterministic trend from the shear as well as the loads owing to the turbulent wind.

Attenuating the effect of the wind comes at the cost of high pitch activity. Fig. I.17 shows the blade pitch angle β_1 and speed $\dot{\beta}_1$ for the controlled system. For comparison, the trajectories are shown for control with and without individual pitch action. A notable increase in pitch speed is observed when including the individual pitch control loop. The design has been tuned such that the pitch speed does not increase above 10 rad/s. 10 rad/s is assumed to be the maximum pitch rate.

A conservative design or conversely a more aggressive design can easily be obtained by changing the weights in the design. The present design is easily made more conservative or aggressive by changing the shape of the high-pass filter.

Fig. I.18 shows the tilt moment Q_{tilt} for two such designs. Fig. I.19 shows the corresponding pitch for blade 1 and the pitch angle speed.

Fig. I.20 shows the power spectral density of the tilt moment Q_{tilt} when the system is controlled by the conservative, the aggressive and the first design (trade-off design). The power spectral densities reveal some interesting properties of the different controllers. The conservative controller primarily removes the constant deterministic trend (wind shear) but does not do much to attenuate the effect of the turbulence. The aggressive controller heavily attenuates both the 0P and the 3P effect as well as the deterministic shear. The chosen design (the trade-off controller) heavily attenuates the 0P effect and also attenuate the 3P effect to a certain extent.

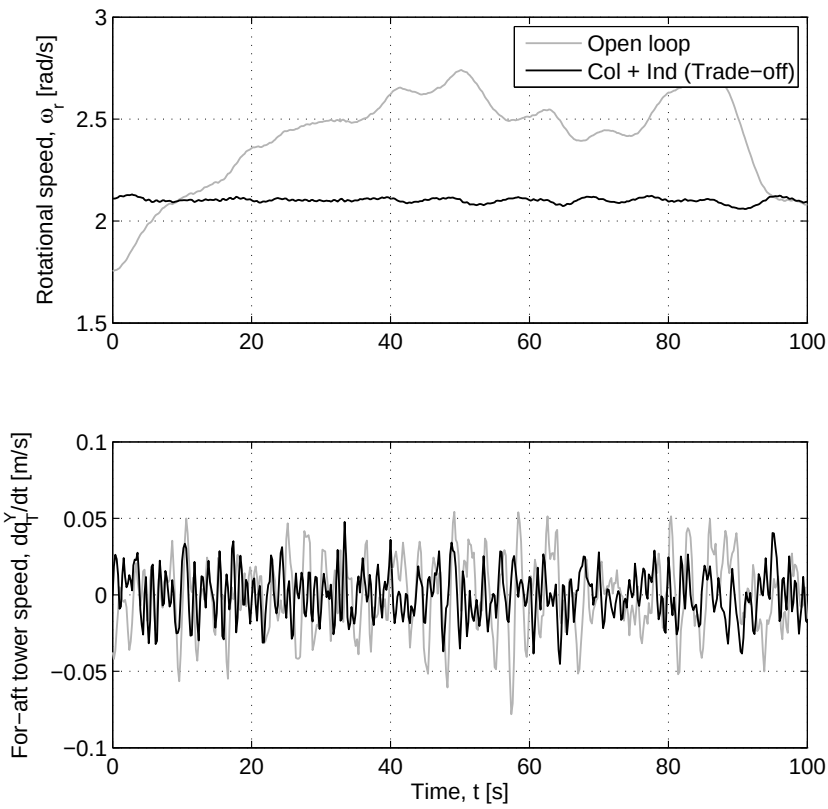

Figure I.15: Rotational speed ω_r and for-aft tower deflection speed $\dot{q}_T^Y$

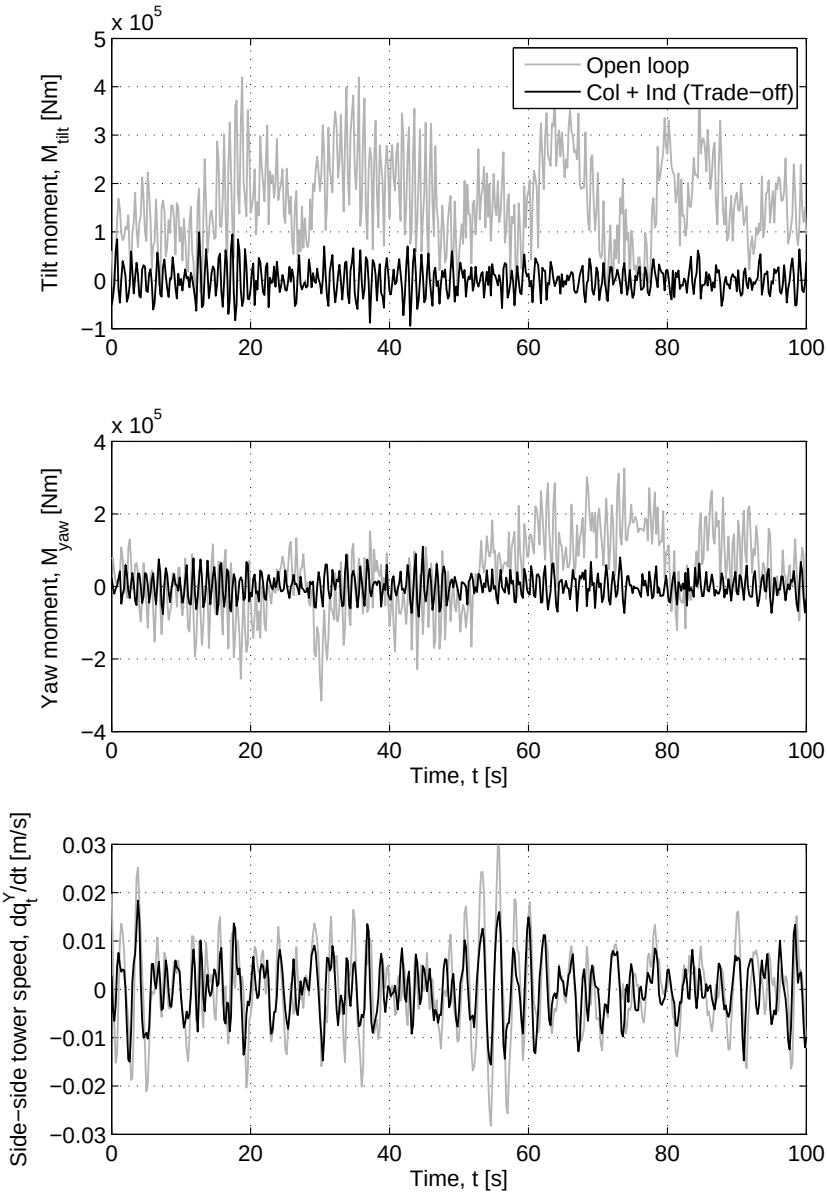

Figure I.16: Yaw moment Q_{yaw}, tilt moment Q_{tilt} and tower deflection speed $\dot{q}_T^X$

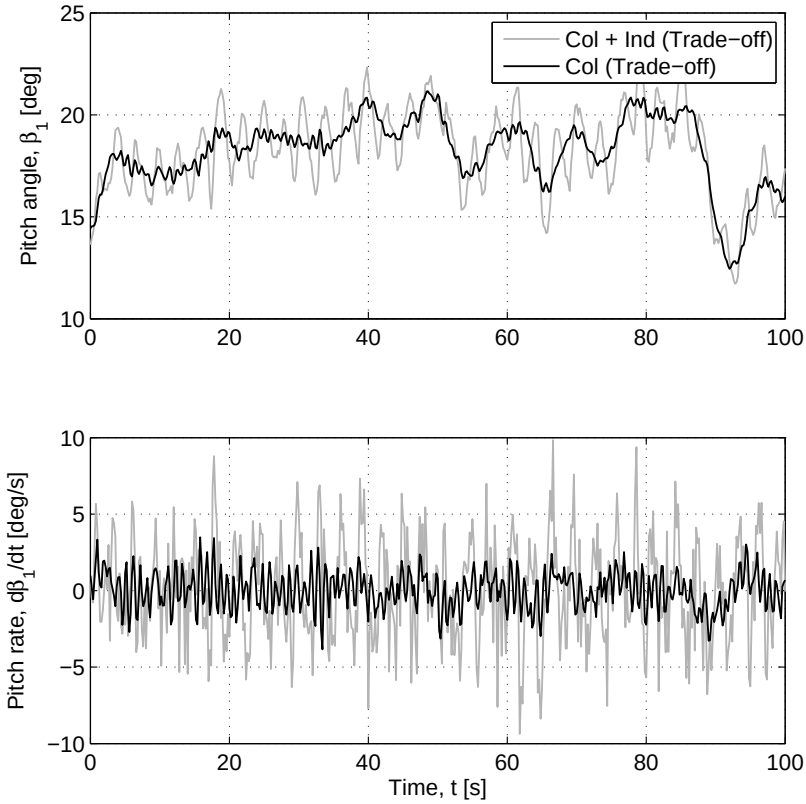

Figure I.17: Pitch angle β_1 and pitch angle speed $\dot{\beta}_1$

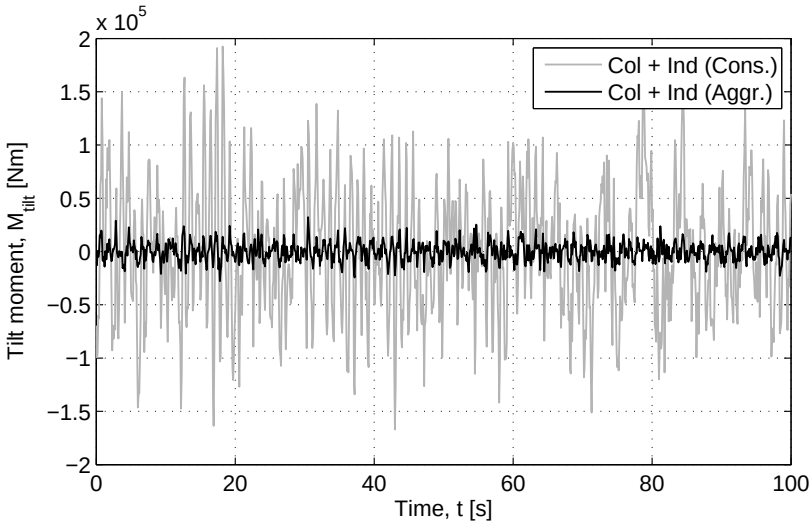

Figure I.18: Tilt moment Q_{tilt} a more conservative and a more aggressive controller

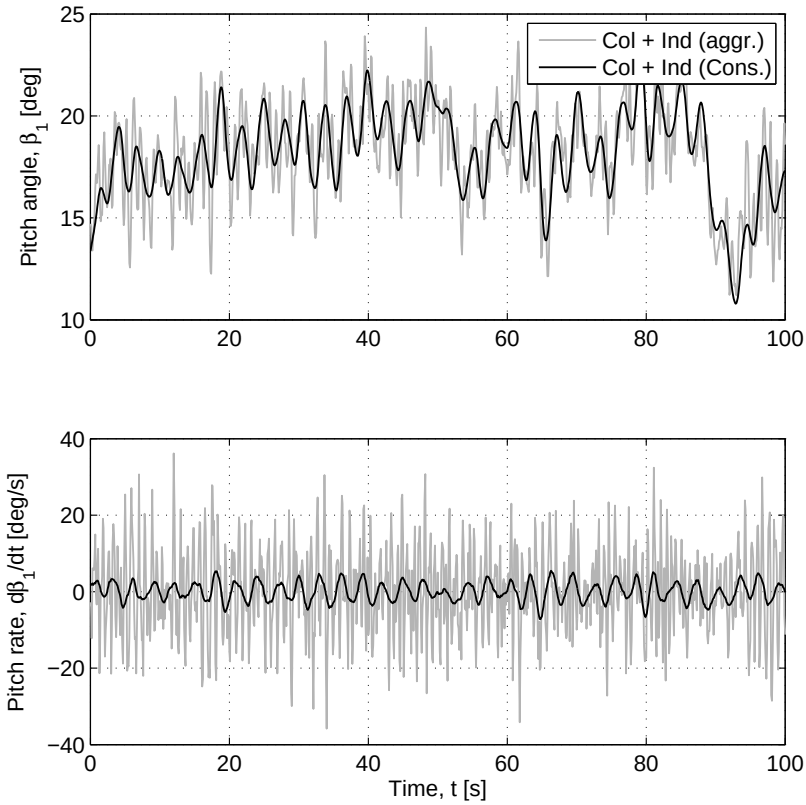

Figure I.19: Pitch β_1 and pitch speed $\dot{\beta}_1$ with the more conservative and a more aggressive controller

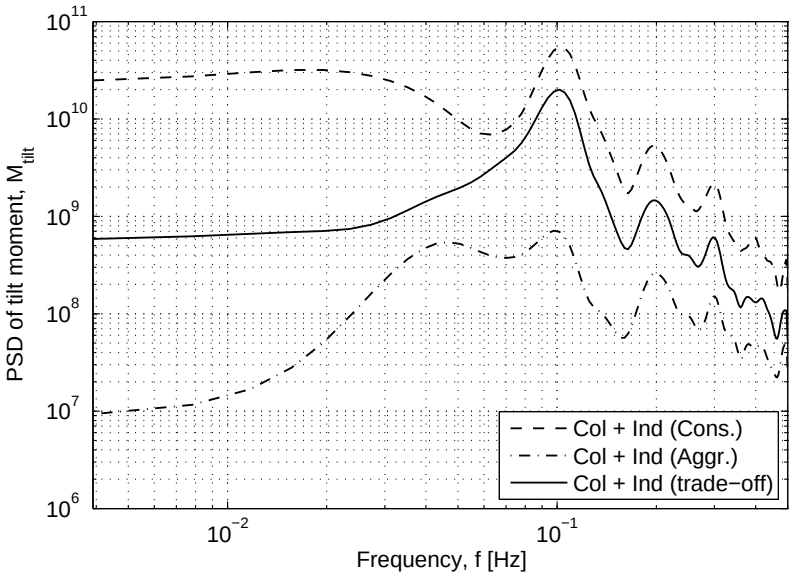

Figure I.20: Estimated power spectral density of tilt moment Q_{yaw} when controlled by the conservative, the aggressive and the trade-off design

I.6 Perspectives

The wind model itself can also be used for other purposes than control. Knowing the structure of the wind will allow for improved estimation of the wind turbine states/outputs. This can be useful in connection with model-based fault diagnosis in which the input-output data is used to detect changes in the model (usually using stochastic tests). Incorporating a stochastic model of the wind will probably reduce the number of faulty detections. The model can also prove useful in connection to short-term wind/load predictions which can be used e.g. by a supervisory controller.

I.7 CONCLUSION

In this paper we have illustrated how to set up a frequency domain model of the wind in multiblade coordinates. The model gives a meaningful description of both the turbulent wind (stochastic) and the constant wind profile (deterministic). The model captures both the symmetric and asymmetric forcing action of the wind as perceived by a wind turbine. From the point of view of control it was seen that the symmetric wind component relates to collective pitch control. Similarly the asymmetric wind components relate to individual pitch control. We showed that the spectral model can be used for controller synthesis by approximating the spectral description with linear systems; a stochastic system for the turbulent wind and a deterministic system for the constant wind profile. This model was used in a controller design based on the $\mathcal{H}_2$ synthesis method. Simulations illustrated strong attenuation of wind fluctuation in the frequency span emphasized by the control model. Consequently, the model seems very suitable for attenuating the harmonic effects caused by rotational sampling of the wind. However, care must be taken not to make an overly aggressive controller design.

Bibliography

[1] K.J. Åstrøm. *Introduction to stochastic control theory.* Academic Press New York, 1970.

[2] E.A. Bossanyi. Individual Blade Pitch Control for Load Reduction. *Wind Energy*, 6(2):119–128, 2003. DOI: 10.1002/we.76.

[3] E.A. Bossanyi. Wind turbine control for load reduction. *Wind Energy*, 6(3):229–244, 2003. DOI:10.1002/we.95.

[4] E.A. Bossanyi. Further load reductions with individual pitch control. *Wind Energy*, 8(4):481–485, 2005. DOI:10.1002/we.166.

[5] Tony Burton, David Sharp, Nick Jenkins, and Ervin Bossanyi. *Wind Energy Handbook.* Wiley, 2001.

[6] R.P. Coleman and A.M. Feingold. Theory og self-excited mechanical oscillations of helicopter rotors with hinged blade. Technical report, NACA, 1958. naca-report-1351.

[7] ECN. Website for turbu offshore.

[8] M.J. Grimble. Horizontal axis wind turbine control: comparison of classical, LQG and $\mathcal{H}_\infty$ designs. *Dynamics and Control*, 6(2):143–161, 1996. DOI:10.1007/BF02169534.

[9] M. Hansen. Aeroelastic stability analysis of wind turbines using an eigenvalue approach. *Wind Energy*, 7:133–143, 2004.

[10] M. O. L. Hansen. *Aerodynamics of Wind Turbines.* James & James, 2000.

[11] W. Johnson. *Helicopter Theory.* Princeton University Press, 1980.

[12] S. Kanev and T. G. van Engelen. Exploring the limits in individual pitch control. In *Proceedings of European Wind Energy Conference*, 2009.

[13] Huibert Kwakernaak and Raphael Sivan. *Linear Optimal Control Systems*. Wiley-Interscience, 1972.

[14] T.J. Larsen, H.A. Madsen, and K. Thomsen. Active load reduction using individual pitch, based on local blade flow measurements. *Wind Energy*, 8(1):67–80, 2005. DOI:10.1002/we.141.

[15] D.J. Leith and W.E. Leithead. Implementation of wind turbine controllers. *International Journal of Control*, 66(3):349–380, 1997.

[16] K. Selvam, S. Kanev, J.W. van Wingerden, T. van Engelen, and M. Verhaegen. Feedback-feedforward individual pitch control for wind turbine load reduction. *International Journal of Robust and Nonlinear Control*, 19(1):72–91, 2009. DOI:10.1002/rnc.1324.

[17] Sigurd Skogestad and Ian Postlethwaite. *Multivariable Feedback Control: Analysis and design*. John Wiley & Sons, 1996.

[18] P. Sørensen. Frequency domain modelling of wind turbine structures. Technical report, Risø National Laboratory, Roskilde, Denmark, 1994.

[19] K.A. Stol, W. Zhao, and A. D. Wright. Individual blade pitch control for the controls advanced research turbine (cart). *Journal of Solar Energy Engineering*, 128:498–505, November 2006. DOI:10.1115/1.2349542.

[20] S.C. Thomsen, H. Niemann, and N.K. Poulsen. Individual pitch control of wind turbines using local inflow measurements. *Proceedings of the 17th IFAC World Congress, IFAC'08*, pages 5587–5592, 2008.

[21] S.C. Thomsen, H. Niemann, and N.K. Poulsen. Stochastic wind turbine modeling for individual pitch control. In *Proceedings of the European Control Conference*, 2009.

[22] S.C. Thomsen and N.K. Poulsen. A disturbance decoupling nonlinear control law for variable speed wind turbines. In *Proceedings of the 15th Mediterranean Conference on Control and Automation*, pages 1268–1273, 2007.

[23] T. G. van Engelen. Design model and load reduction assessment for multi-rotational mode individual pitch control (higher harmonics control). In *Proceeding of European Wind Energy Conference*, 2006.

[24] T. G. van Engelen. Control design based on aero-hydro-servo-elastic linear model from turbu (ecn). In *Proceedings of European Wind Energy Conference*, 2007.

[25] T.G. van Engelen and J. van der Tempel. Frequency domain load calculation for offshore wind turbines. In *Proceedings of the European Wind Energy Conference*, London, UK, December 2004.

[26] Paul S. Veers. Three-dimensional wind simulation. Technical report, Sandia National Laboratories, 1988.

[27] K. Zhou, J.C. Doyle, and Glover K. *Robust and optimal control*. Prentice Hall, 1996.